

**DEVELOPMENT OF INSTRUMENTAL AND  
COMPUTATIONAL TOOLS FOR INVESTIGATION  
OF POLYMER FLAMMABILITY**

**by**

**Richard N. Walters**

A thesis submitted in partial fulfillment for the requirements of the degree of Doctor of  
Philosophy at the University of Central Lancashire (by Published Work)

**March 2013**

## STUDENT DECLARATION

I declare that while registered as a candidate for the research degree, I have not been a registered candidate or enrolled student for another award of the University or other academic or professional institution.

I declare that no material contained in the thesis has been used in any other submission for an academic award and is solely my own work.

I declare that this thesis has been composed by myself while being registered as a candidate for the degree of Doctor of Philosophy (PhD) to which this submission is made. I declare that I have participated fully in all joint publications submitted in the thesis. My participation included original ideas, working hypotheses, experimental designs, literature search, experimental work, analysis and interpretation of data, preparation and presentation of the data, writing, correcting and submission of manuscripts for publication purposes. Descriptions of my contribution to each manuscript are included in Appendix E.



Signature of Candidate.....

Doctor of Philosophy (PhD by Published Work)

Type of Award.....

School of Forensic & Investigative Sciences

School.....

## ABSTRACT

This thesis describes published work undertaken over the last 17 years. The main focus is the development and utilization of the microscale combustion calorimeter (MCC) and how it helps us understand the flammability of materials.

A reproducible way to quantitatively assess material flammability was needed. The simplest approach is based on the molecular structure of a material to determine which moieties influence the flammability. This approach is based on material properties that can be measured using small-scale thermal analysis methods such as Thermogravimetric Analysis (TGA), Differential Scanning Calorimetry (DSC), and the MCC. Properties such as thermal stability, heat of gasification, and heat of combustion provide key information about materials' flammability.

Tests such as LOI, UL-94 and other Bunsen burner type tests provide pass/fail type results. These types of tests are not quantitative and are dependent on physical properties and extrinsic parameters such as sample geometry and orientation. They do not provide a true measure of flammability, and formulations can be optimized to pass the test even though they are highly flammable.

A more quantitative approach is to use larger bench scale flammability tests such as cone calorimeter and Ohio State University (OSU) fire calorimeter. Although these tests are also dependent on the physical properties and test geometry, they measure properties such as burning rates, mass loss rates, and combustion efficiency under different imposed fire scenarios from which material properties can be derived.

The ultimate flammability test for a material is to subject it to a fire in a real-life scenario where other materials are present, a full-scale fire test. These tests can involve a single item or combinations of items. These tests are highly dependent on physical and material properties and are useful for making direct comparisons of one scenario to the next, for properties like flame spread and time to flashover.

Measurements have been made using all of the thermal analysis and fire test methodologies listed above. Correlations between the test methods have been drawn and the theory relating them derived. Predictive methods for estimating polymer

flammability from molecular structure have been formulated using a molar group contribution approach. Methods for predicting fire performance in the bench scale tests from the small scale test measurements have also been derived. Modelling the bench scale fire performance in the quantitative tests as well as determining a probability for the rating in the pass/fail type bench scale tests for a range of polymeric materials has been undertaken. This type of work in the small- and bench-scale has helped identify materials that perform well when subjected to the harshest fire conditions in the full-scale. The ultimate goal being to save lives by preventing deaths due to fire through the development of more fire-safe materials.

## TABLE OF CONTENTS

Title	i
Student Declaration	ii
Abstract	iii
Table of Contents	v
Acknowledgements	viii
List of Tables	ix
List of Figures	xiii
List of Symbols	xix
List of Manuscripts	xxiv
1. PRINCIPLE OF OPERATION	1
1.1 Pyrolysis Combustion Flow Calorimetry	2
1.2 Fuel Generation Rate	2
1.3 Heat Release Capacity	4
1.4 Condensed Phase Model	6
1.5 Gas Phase Model	7
1.6 Effect of Additives	10
1.7 Summary and Conclusions	13
2. INSTRUMENT CONSTRUCTION	14
2.1 Overview	15
2.2 Pyrolyzer	16
2.2.1 Mass Transfer	17
2.2.2 Sample Heating and Control	19
2.3 Combustor	23
2.3.1 Thermal Oxidation Kinetics	24
2.4 Microscale Combustion Calorimeter	28
2.4.1 Validation of Technique	33
2.5 Summary and Conclusions	34
3. MATERIAL PROPERTIES	36
3.1 Overview	37
3.2 Heat of Gasification	37

3.2.1	Heat Capacity	40
3.2.2	Heat of Melting	41
3.2.3	Heat of Decomposition	42
3.3	Heat of Combustion Measurements	46
3.3.1	Gross Heat of Combustion	47
3.3.2	Net Heat of Combustion	48
3.4	Heat of Combustion Calculations	49
3.4.1	O <sub>2</sub> Consumption	49
3.4.2	Heat of Formation	50
3.4.3	Molar Group Contributions to Heat of Combustion	55
3.4.3.1	Heat of Combustion Molar Group Contribution Theory	56
3.4.3.2	Sample Calculation	59
3.5	Heat Release Capacity	62
3.5.1	Molar Group Contributions to Heat Release Capacity	62
3.5.2	Heat Release Capacity Experimental	64
3.5.3	Calculation of Heat Release Capacity	67
3.6	Char Heat of Combustion	68
3.6.1	Oxidative Pyrolysis Combustion Flow Calorimetry	69
3.7	Summary and Conclusions	71
4.	MATERIAL STUDIES	73
4.1	Overview	74
4.2	Reactions / Processing	74
4.2.1	Viscosity and Processing	74
4.2.2	Epoxies	76
4.2.3	Cyanate Esters	78
4.2.4	Cyanate Ester / Epoxy Blends	81
4.3	Mechanical Properties	86
4.4	Thermal Analysis / Decomposition	88
4.4.1	Mechanisms	90
4.4.2	Cyanate Esters	93
4.4.3	Volatile Degradation Products	99
4.4.4	Cyanate Ester Epoxy Blends	102
4.5	Flammability	104
4.6	Ignitability	121

4.7 Combustion Products	124
4.8 Summary and Conclusions	128
<b>5. CORRELATIONS &amp; PREDICTIVE CAPABILITIES</b>	<b>129</b>
5.1 Non-Flaming Combustion	130
5.2 Flaming Combustion	130
5.2.1 Steady Burning	130
5.2.2 Unsteady Burning	132
5.3 Flammability	133
5.3.1 UL94	134
5.3.2 Oxygen Index	142
5.4 Fire Response	145
5.5 Fire Modelling	147
5.5.1 Model Parameterization	150
5.5.2 Model Set Up	154
5.6 Summary and Conclusions	163
<b>6. CONCLUSIONS &amp; FUTURE WORK</b>	<b>165</b>
6.1 Conclusions	166
6.2 Future Work	168
<b>REFERENCES</b>	<b>170</b>
<b>APPENDICES</b>	<b>188</b>
A. Combustion Data for Polymeric Materials	188
B. Heat Release Values from MCC	192
C. Cyanate Ester Heat Release Rates in Cone Calorimeter	204
D. Contribution to Science	207
E. Contribution to Each Manuscript	230
F. Background / Literature Review	236
<b>PUBLISHED WORKS</b>	<b>242</b>

## ACKNOWLEDGEMENTS

This thesis would not have been possible without the support of many people. First and foremost, I would like to thank my family, Angi, Lexi and Max, for their patience and affording me the time to dedicate to this work. I wish to express my gratitude to my supervisors, Anna Stec and T. Richard Hull for allowing me to pursue an advanced degree under them. Deepest gratitude are also due to the co-authors (listed below) of the published works that made this thesis possible, without whose knowledge and assistance in our work together, would not have been successful. I would also like to convey thanks to the Federal Aviation Administration and the University of Central Lancashire for providing the means to make this possible.

Richard E. Lyon

Stanislav I. Stoliarov

Michael L. Ramirez

Lauren M. Castelli

Sanjeev Gandhi

Edward P. Savitski

Sean B. Crowley

Stacey M. Hackett

## LIST OF TABLES

Table 1. Kinetic parameters determined experimentally and obtained from the literature [38] for the oxidation reaction of methane gas and polymer pyrolysis products.

Table 2. Net heats of combustion of non-charring polymer pyrolyzates by PCFC compared to oxygen bomb calorimeter values.

Table 3. Flammability parameters for thermoplastic materials obtained by PCFC. Heat release capacity, total heat release, char yield, and peak pyrolysis temperature and their repeatabilities are listed.

Table 4. Parameters describing the dependence of measured heat capacities on temperature where  $C_{LO}$  and  $C_{LI}$  are the slopes and y-intercept on the left of  $T_{trans}$  and  $C_{RO}$  and  $C_{RI}$  are the slopes and y-intercept on the right.

Table 5. Temperatures and heats of melting determined by DSC. Relative crystallinity was obtained by dividing the measured heat of melting by the literature value for a fully crystalline material [63].

Table 6. Temperatures and heats of decomposition determined by DSC. Literature values are also provided where available.

Table 7. Heats of gasification and components; integral heat capacity, heat of melting and heat of decomposition, as determined by DSC.

Table 8. Char yields at temperature,  $T_{char}$ , and char-weight-adjusted integral heats of gasification.

Table 9. Gross heat of combustion values for polymers measured by oxygen bomb calorimetry and calculated by a group contribution method and net heat of combustion values obtained by adjusting the gross for the heat of vaporization of water and calculated by oxygen consumption calorimetry.

Table 10. Comparison of experimental gross heats of combustion to literature values for several polymers [20].

Table 11. Structural groups and their molar contributions to the gross heat of combustion.

Table 12. Calculation of heat of combustion of BPA epoxy using molar group contributions.

Table 13. Structural Groups and their Molar Contribution to the Heat Release Capacity. (Molar group contributions derived from a single polymer are marked with an asterisk (\*) to indicate that these are not optimized values).

Table 14. Group contributions used in the calculation of the heat release capacity of bisphenol-A epoxy.

Table 15. Net heat of combustion of charring ( $\mu \neq 0$ ) and non-charring ( $\mu = 0$ ) polymers obtained by oxygen bomb calorimetry and oxidative pyrolysis-combustion flow calorimetry (oPCFC).

Table 16. Resins and hardeners used for comparing BPA to BPC epoxy and cyanate ester systems.

Table 17. Trade names, chemical formula and structures of cyanate ester monomers.

Table 18. Thermal analysis results for BPC cyanate ester - epoxy blends from DSC, TGA, and rheometer.

Table 19. Thermo-mechanical properties of thermoset epoxy resins cured using different co-polymer systems.

Table 20: Flexural strengths of thermoset structural composites from 3-point flex test.

Table 21. Thermal analysis results for BPA and BPC epoxy co-polymer systems from DSC, TGA and PCFC.

Table 22. Small-scale thermal analysis and flammability results from TGA and PCFC.

Table 23. Polycyanurate glass transition temperatures from the literature [85,95,96] and thermal properties from TGA measurements.

Table 24. Wavenumbers of the OCN group absorbance doublet for the volatile decomposition products.

Table 25. Fire and flammability data for BPA and BPC epoxies cured with different hardeners.

Table 26. Heat release data for thermoset polymer composites from the OSU calorimeter, 14 CFR 25.853(a-1), at 35-kW/m<sup>2</sup> irradiance.

Table 27. multiple-ply laminate heat release data from the cone calorimeter at 50 kW/m<sup>2</sup>.

Table 28. Flammability results from PCFC and OSU for BPC cyanate ester and epoxy polymers and reference materials.

Table 29. Net heat of complete combustion, specific heat release, heat release capacity, and char fraction for polycyanurates.

Table 30. Fire behavior and properties of polycyanurates in cone calorimeter at several different heat fluxes.

Table 31. Ignition properties of polycyanurates derived from cone calorimeter experiments.

Table 32. Cone calorimeter data for smoke obscuration and combustion product yields at several heat fluxes for polycyanurates.

Table 33. UL 94 rating of plastics,  $HRP$ ,  $T_{max}$ , and critical heat flux ( $CHF$ ).

Table 34. Reaction parameters for polycarbonate and polyvinylchloride decomposition.

Table 35. Physical properties of polycarbonate and polyvinylchloride material components.

Table 36. Summary of results of cone calorimetry experiments and simulations.

Appendix A. Combustion Data for Polymeric Materials

Appendix B. Heat Release Values from MCC

## LIST OF FIGURES

Figure 1. Flow diagram for pyrolysis-combustion flow calorimetry as it relates to flaming combustion.

Figure 2. PCFC with Pyroprobe pyrolyzer and heated pyrolysis chamber.

Figure 3. Effect of pyrolysis cell wall temperature on mass transfer efficiency of pyrolysis gases for PEEK, Kevlar, and polyethylene using a Pyroprobe with a heated interface.

Figure 4. Experimental setup for controlled heating of a sample in the MCC.

Figure 5. Temperature response of applying a constant voltage to a heater from cold start. Gray dots are experimental data. Black lines are results of the least-square fit with equation 31.

Figure 6. Dependencies of parameters of equation 31 on voltage. Circles are parameter values derived from experimental data. Black lines are the least square fits with equations 32 and 33.

Figure 7. PCFC combustor cross section and temperature distribution for a 900°C set-point.

Figure 8. Reaction time versus temperature for 99.5% combustion of methane gas and polymer pyrolysis products calculated from oxidation kinetic parameters.

Figure 9. Oxygen concentration of a stoichiometric (1:2) CH<sub>4</sub>:O<sub>2</sub> mixture in nitrogen exiting the MCC combustor at the indicated temperature with a residence time of 10 seconds.

Figure 10. Schematic drawing of the MCC showing heated zones and flow path.

Figure 11. Heat release rate histories of common polymers in MCC sorted along the z-axis by  $T_{max}$ .

Figure 12. Maximum specific  $HRR$ ,  $Q_{max}$ , versus heating rate,  $\beta$ , in Pyroprobe PCFC for 1 mg samples of PE, PS, PA66, PMMA, PBT, PPO, PC, POM, and PT.

Figure 13. Peak HRR normalized for heating rate versus heating rate for PE, HIPS, PMMA, POM, and FEP obtained in the MCC with a 2-5 mg sample.

Figure 14. Comparison of individual and average heat release capacities from three different laboratories for the 14 polymers in table 3.

Figure 15. Comparison of heat release capacities obtained by Pyroprobe PCFC at  $\beta = 260$  K/min and TGA-GC/MS at  $\beta = 10$  K/min.

Figure 16. DSC heat flow curves obtained for a sample of poly(methylmethacrylate). Endothermic is positive. (a) Unprocessed sample and baseline curves. (b) Sample heat flow derived from the data shown in (a) and cast to the units of heat capacity

Figure 17. Correlation plot of the calculated heats of combustion using oxygen consumption versus experimental net heats of combustion for 49 polymers (line is  $y = x$ ). Error bars shown are the 4.4% average relative deviation for the calculation.

Figure 18. Correlation plot of the calculated heats of combustion using group contributions versus experimental gross heats of combustion for 38 polymers (line is  $y = x$ ). Error bars shown are the 4.2% average relative deviation for the calculation.

Figure 19. Plot of the heat of combustion values calculated using molar group contributions versus the measured for 66 polymers and 78 small molecules.

Figure 20. Kinetic heat release rate data for several polymers measured in the Pyroprobe PCFC (horizontally shifted for clarity).

Figure 21. Heat release capacity values calculated using molar group contributions versus measured heat release capacities for 80 pure polymers.

Figure 22. Residual mass fraction and heat of combustion of pyrolysis gases versus temperature for test of polycarbonate in TGA PCFC at  $\beta = 20$  °C/min.

Figure 23. Specific HRR of polycarbonate versus time and temperature obtained by oPCFC (oxidation of gases in combustor and solid char in pyrolyzer are shown as separate processes).

Figure 24. Viscosity of several thermoset resins as a function of temperature obtained using parallel plate rheology.

Figure 25. Cyclotrimerization reaction of the cyanate ester (A) and the subsequent reaction with glycidylether (B) to form the oxazoline.

Figure 26. Cyanate ester polymerization reaction illustrating the cyclotrimerization to form the triazine linkage.

Figure 27. FT-IR cure monitoring of B-10 cyanate ester resin showing the disappearance of the cyanate ester and subsequent formation of the triazine.

Figure 28. DSC curves for blended BPC resins heated at 1°C/min under nitrogen showing energy and temperature for reactions.

Figure 29. IR spectra of uncured and cured 6:4 blend showing the cyanate ester, epoxy, triazine, and oxazoline bands.

Figure 30. Normalized infrared peak heights for the reactants and products of the 6:4 cyanate ester : epoxy blend.

Figure 31. Thermogravimetry data for DGEBA-MDA and DGEBC-MDA systems.

Figure 32. Thermal decomposition mechanism of chloral-based condensation polymers showing the evolution of HCl and char formation.

Figure 33. Idealized chemical structure of DGEBC reaction products with: a) BPC, and b) EMI. Potentially volatile fuel component (R group) enclosed in dashes.

Figure 34. Thermogravimetric data for the 9 polycyanurates.

Figure 35. Mass loss rate versus temperature for phenolic triazine thermoset resin.

Figure 36. Cyanate ester polymerization and thermal degradation reactions.

Figure 37. Temperature resolved FT-IR spectra of B-10 polycyanurate film during heating through decomposition.

Figure 38. Temperature resolved gas phase FT-IR spectra of B-10 polycyanurate volatile decomposition products.

Figure 39. Temperature resolved gas phase FT-IR spectra of BPC polycyanurate decomposition products.

Figure 40. TGA traces for the neat and blended BPC resins heated at 10°C/min under nitrogen.

Figure 41. Heat release rates of single-ply composite laminates in OSU calorimeter at 35 kW/m<sup>2</sup>.

Figure 42. Heat release rates of the multiple-ply composite panels in cone calorimeter at 50 kW/m<sup>2</sup> heat flux.

Figure 43. Pyroprobe PCFC heat release rates for the series of BPC epoxy-cyanate ester resin blends (shifted in time for clarity).

Figure 44. Heat release rate curves from the OSU calorimeter (heat release curves have been shifted along the Y-axis for clarity).

Figure 45. Pyroprobe PCFC heat release rate data for polycyanurates (horizontally shifted for clarity).

Figure 46. Heat release histories of polycyanurates at 50 kW/m<sup>2</sup> heat flux in cone calorimeter.

Figure 47. Time to ignition data versus external heat flux from the cone calorimeter for B-10 polycyanurate.

Figure 48. Soot yield and CO/CO<sub>2</sub> ratio versus combustion efficiency in flame for cyanate esters at different irradiances.

Figure 49. Flammability ( $\eta_c$  and UL 94 rating) of glass fiber-reinforced plastics versus fiberglass weight fraction.

Figure 50. Flammability ( $\eta_c$  and flame resistance) of aerospace epoxy versus phosphorus concentration for reactive phosphorus compounds.

Figure 51. Heat release capacity,  $\eta_c$ , and heat of combustion of hydrocarbon volatiles versus bromine concentration for DGEBA epoxy.

Figure 52. UL 94 rating versus heat release capacity  $\eta_c$  of polymers (NR = no rating in vertical test). The lower threshold for self-sustained ignition,  $\eta_c \approx 200$  J/g-K is shown as a vertical dashed line.

Figure 53. Flame resistance diagram showing the heat release capacity for flame extinction versus decomposition temperature. Upper abscissa indicates decomposition temperature range for generic plastics..

Figure 54. Probability of sustained ignition in UL94V test versus  $\eta_c$ ; solid line is equation 69 with  $\alpha_0 = -6$  and  $\alpha_1 = 1/67$ .

Figure 55. The probability (black line) and 68% confidence interval (gray lines) of a UL 94 V-0 rating versus heat release capacity.

Figure 56. LOI versus  $\eta_c$  for  $\chi\theta = 1$  and various  $T_{max}$ .

Figure 57. LOI versus  $\eta_c$  for  $T_{max} = 450^\circ\text{C}$  and various  $\chi\theta$ .

Figure 58. Peak HRR in cone calorimeter at  $50 \text{ kW/m}^2$  external flux versus heat release capacity in PCFC shows there is a definite trend.

Figure 59. Peak HRR in OSU versus heat release capacity in PCFC.

Figure 60. Results of TGA experiments and decomposition reaction modelling. The mass loss rates are normalized by the initial sample mass.

Figure 61. Heat release results of MCC experiments. The heat release rates are normalized by the initial sample mass ( $m_0$ ).

Figure 62. Six millimeter thick samples of PC (left) and PVC (right) burnt in the cone calorimeter at  $EHF_0 = 75 \text{ kW/m}^2$ . Both tests were stopped at about 200 s: the samples were removed from under the cone and photographed.

Figure 63. Results of 6 cone calorimetry experiments performed on each polymer under identical conditions at a heat flux of  $75 \text{ kW/m}^2$ .

Figure 64. Results of fitting experimental heat release rates in cone calorimeter with *PC\_char* and *PVC\_char* heat transfer parameters.

Figure 65. Comparison of model predictions with the results of cone calorimetry experiments performed at  $EHF_0 = 50 - 92 \text{ kW/m}^2$  on 3 - 9 mm thick samples.

Appendix C. Cyanate Ester Heat Release Rates in Cone Calorimeter

## LIST OF SYMBOLS

$A$	frequency factor or surface area
$\alpha$	radiation absorption coefficient
ABS	acrylonitrile-butadiene-styrene
ASTM	American Society for Testing and Materials
$\beta$	heating rate / constant rate of temperature rise
BPA	bisphenol A
BPC	bisphenol C
$c$	heat capacity
$^{\circ}\text{C}$	degrees Celsius
cc	cubic centimeter
CE	cyanate ester
CFR	Code of Federal Regulations
CFT	char forming tendency
cm	centimeter
$\text{cm}^{-1}$	wavenumber
$C_{mat}$	heat capacity of the starting material
$C_{prod}$	heat capacity of decomposition products
$CHF$	critical heat flux
$CHR$	critical heat release rate
DGEBA	diglycidylether of bisphenol-A
DGEBC	diglycidylether of bisphenol-C
$E$	Thornton's rule
$e$	Euler's number
$\varepsilon$	surface emissivity
$E_a$	activation energy
EHC	effective heat of combustion
$EHF$	external radiative heat flux
EMI	ethyl methyl imidazole
eq	equivalent
$F$	volumetric flow rate
FAA	Federal Aviation Administration
FEP	fluorinated ethylene-propylene

FR	flame retarded
FT-IR	Fourier transform infrared spectrometer
GC	gas chromatograph
GFRP	glass fiber reinforced plastics
$\gamma$	reflectivity
$H$	enthalpy
$H_c$	molar heat of complete combustion
$H_{dec}$	heat of decomposition
$H_g$	heat of gasification
$H_i$	the molar heat of combustion of component $i$
$H_{melt}$	heat of melting
$H_{polym}$	The heats of polymerization per mole
$H_{rxn}$	heat of reaction
$h_c$	net heat of combustion
$h_c^o$	specific heat of combustion
$h_{c,p}^o$	heats of complete combustion for polymer
$h_{c,\mu}^o$	heats of complete combustion for char
$h_{c,v}^o$	heat of combustion of evolved gases
$h_g$	heat required to gasify unit mass of the material
HIPS	high impact polystyrene
HOC	heat of combustion
HRR	heat release rate
Hz	frequency
$I$	laser beam intensity
$I_s$	incident radiative flux onto a material surface
ID	inner diameter
$\phi$	non-combustible fraction
J	Joule
K	Kelvin
$k$	thermal conductivity or extinction coefficient
$k_{app}$	apparent rate constant
$k_c$	global rate constant for combustion
$k_p$	rate constant for thermal decomposition
$L$	length / thickness

$L_g$	heat of gasification per unit mass of volatilized material
ln	natural logarithm
LOI	limiting oxygen index
$\lambda$	gas transfer coefficient
$n$	number of moles
$M$	molecular weight / molar mass
$m$	mass
$\dot{m}''$	peak mass loss rate
MCC	microscale combustion calorimeter
MDA	methylenedianiline
mg	milligram
MLR	mass loss rate
$MLR_{pk}$	peak mass loss rate
mm	millimeter
MS	mass spectrometer
$\dot{m}_s$	sample mass loss rate
NBS	National Bureau of Standards
$\eta_c$	heat release capacity
$\eta_g$	normalizing parameter
$N_i$	number of moles
NIST	National Institute of Standards and Technology
$\theta$	oxygen concentration or heat/mass transfer efficiency
oPCFC	oxidative pyrolysis-combustion flow calorimetry
OSU	Ohio State University fire calorimeter
Pa	Pascals
PA66	polyamide 66
PBT	polybutyleneterephthalate
PC	polycarbonate
PCFC	pyrolysis combustion flow calorimetry
PE	polyethylene
PEI	polyetherimide
PET	polyethyleneterephthalate
PMMA	polymethylmethacrylate
POM	polyoxymethylene

PP	polypropylene
PPO	polyphenyleneoxide
PPS	polyphenylenesulfide
PS	polystyrene
PVC	polyvinylchloride
PVDF	polyvinylidene fluoride
PT	phenolic triazine
$\Psi$	molar heat release capacity
$\Psi_i$	molar group contribution to heat release capacity
$Q$	combustion heat
$Q_c$	gross heat of combustion
$\dot{Q}_c$	kinetic heat release rate
$\dot{q}_{fl}''$	flame heat flux back to the surface
$\dot{q}_{rr}''$	heat lost from the surface due to re-radiation
$\dot{q}_{net}$	net heat flux
$\dot{q}_{ext}$	external radiant heat flux
$\dot{q}_{loss}$	heat lost to the environment by re-radiation and convection
$q_{ext}''$	external heat flux
$R$	gas constant
$r_0$	stoichiometric oxygen / fuel mass ratio
$\rho$	density
$s$	seconds
$\sigma$	Stefan–Boltzmann constant
$SEA$	specific extinction area
$SPR$	smoke production rate
STA	simultaneous thermal analyzer
$T$	temperature
$t$	time
$\tau$	response or reaction time
$T_a$	ambient temperature
TBBA	tetrabromobisphenol-A
$T_{dec}$	decomposition temperature
TETA	triethylenetetramine
$T_{final}$	final temperature

$T_g$	glass transition temperature
TGA	thermogravimetric analyzer
THR	total heat release
$T_{ign}$	ignition temperature
$t_{ign}$	time to ignition
$T_{init}$	initial temperature
$T_m$	melting points
$T_{max}$	maximum mass loss / fuel generation temperature
$T_{melt}$	melting temperature
$T_0$	initial temperature
$T_p$	maximum mass loss rate temperature
TRP	thermal response parameter
$T_{trans}$	transition temperature
TTI	time to ignition
UL94	Underwriters Laboratories vertical Bunsen burner test
$\mu$	mass fraction of char
V	Volt
$\nu$	inert filler / fiberglass fraction or convection coefficient
$V_f$	volumetric flow rate in the exhaust duct
VARTM	vacuum-assisted resin transfer molding
W	Watt
$\omega$	radiative heat transfer coefficient
$w$	weight fraction
$\chi$	extent of reaction or combustion efficiency
$\xi$	concentration
$\xi_g$	critical mass flux

## LIST OF MANUSCRIPTS

1. **R.N. Walters**, R.E. Lyon and S.M. Hackett, "Heats of Combustion of High Temperature Polymers," *Fire and Materials Journal*, 24, pp. 245-252, 2000.
2. R.E. Lyon, L.M. Castelli and **R.N. Walters**, "A Fire-Resistant Epoxy," DOT/FAA/AR-01/53, FAA Technical Report, 2001.
3. R.E. Lyon and **R.N. Walters**, "A Microscale Combustion Calorimeter," DOT/FAA/AR-01/117, FAA Technical Report, 2002.
4. M. Ramirez, **R.N. Walters**, E.P. Savitski, and R.E. Lyon, "Thermal Decomposition of Cyanate Ester Resins," *Journal of Polymer Degradation and Stability*, 78, pp. 73-82, 2002.
5. **R.N. Walters**, "Molar Group Contributions to the Heat of Combustion," *Fire and Materials Journal*, 26, pp. 131-145, 2002.
6. **R.N. Walters** and R.E. Lyon, "Molar Group Contributions to Polymer Flammability," *Journal of Applied Polymer Science*, 87, pp. 548-563, 2003.
7. **R.N. Walters** and R. E. Lyon, "Fire Resistant Cyanate Ester- Epoxy Blends," *Fire and Materials Journal*, 27, pp. 183-194, 2003.
8. R. Lyon and **R. Walters**, "Pyrolysis Combustion Flow Calorimetry," *Journal of Applied Pyrolysis*, 71, pp. 27-46, 2004.
9. R.E. Lyon, **R.N. Walters**, and S. Gandhi, "Combustibility of Cyanate Ester Resins," *Fire and Materials Journal*, 30, pp. 89-106, 2006.
10. R.E. Lyon, **R.N. Walters**, and S.I. Stoliarov, "A Thermal Analysis Method for Measuring Polymer Flammability", *Journal of ASTM International*, 3, 4, April 2006.

11. R.E. Lyon, **R.N. Walters** and S.I. Stoliarov, "Screening Flame Retardants for Plastics Using Microscale Combustion Calorimetry," *Polymer Engineering and Science*, 47, 10, pp. 1501-1510, 2007.
12. S.I. Stoliarov, **R.N. Walters** and R.E. Lyon, "A Method for Constant-Rate Heating of Milligram Sized Samples," *Journal of Thermal Analysis and Calorimetry*, 89, 2, pp. 367-371, 2007.
13. R.E. Lyon, **R.N. Walters** and S.I. Stoliarov, "Thermal Analysis of Flammability," *Journal of Thermal Analysis and Calorimetry*, 89, 2, pp. 441-448, 2007.
14. S.I. Stoliarov and **R.N. Walters**, "Determination of Heats of Gasification of Polymers Using Differential Scanning Calorimetry," *Polymer Degradation and Stability Journal*, 93, 422-427, 2008.
15. **R.N. Walters** and R.E. Lyon, "Flammability of Polymer Composites," DOT/FAA/AR-08/18, FAA Technical Report, May 2008.
16. S.I. Stoliarov, S. Crowley, **R.N. Walters** and R.E. Lyon, "Prediction of the Burning Rate of Charring Polymers," *Combustion and Flame*, 157, 11, pp. 2024-2034, 2010.

## CHAPTER 1

### PRINCIPLE OF OPERATION

## 1.1 PYROLYSIS COMBUSTION FLOW CALORIMETRY

The rate at which heat is released by a burning material is the single most important parameter determining its hazard in a fire, particularly in an enclosed space such as a building, a ship, or an aircraft cabin [1-3]. Several different bench scale methods have been developed for measuring heat release rate during flaming combustion of materials, products, and components [4,5]. These bench scale fire calorimetry methods require replicate samples of the order of a hundred grams each and the results are highly dependent on the ignition source [6], sample thickness [7], sample orientation [8], ventilation [9], and edge conditions [8], all of which combine to make the test data configuration-dependent, and to obscure the effect of material properties and composition on burning behavior.

A dynamic method for evaluating the combustibility of milligram-sized solid samples is described. Pyrolysis-combustion flow calorimetry (PCFC) separately reproduces the solid state and gas phase processes of flaming combustion in a non-flaming test by rapid controlled pyrolysis in an inert gas stream, followed by high temperature oxidation (combustion) of the pyrolyzate in excess oxygen. The rate at which the sample releases its heat is calculated from the oxygen consumed. The maximum rate of heat release that is normalized for sample mass and heating rate has the physical significance of a material property. This depends only on the chemical composition of the polymer and is a good predictor of fire behavior and flammability. PCFC is the process by which a material is thermally degraded and the gaseous products are evaluated for flammability. The microscale combustion calorimeter (MCC) is a stand-alone test device that utilizes the PCFC process. Both the processes of PCFC and the construction of the MCC are described here.

## 1.2 FUEL GENERATION RATE

Pyrolysis-combustion flow calorimetry measures the rate at which the heat of combustion of the fuel gases are generated by a solid during a controlled pyrolysis experiment in an inert gas stream. The fuel gases are mixed with excess oxygen and combusted (oxidized) at high temperature. The instantaneous heat of combustion of the flowing gas stream is measured by oxygen consumption calorimetry. The rate at which combustion heat  $Q$  is liberated per unit time  $t$  in the PCFC or in a fire is limited by the

fuel generation rate of the thermally decomposing solid. Thus, the heat release rate  $dQ/dt$  is proportional to the mass generation rate of volatile fuel or to the mass loss rate of the solid

$$\dot{Q}_c(t) \equiv \frac{dQ_c(t)}{dt} = h_{c,v}^o(t) \frac{dm_v(t)}{dt} = -h_{c,v}^o(t) \frac{dm_s(t)}{dt} \quad (1)$$

where the proportionality factor  $h_{c,v}^o$  (J/g) is the enthalpy (heat) of complete combustion of the volatile pyrolysis products of mass  $m_v$ , and  $m_s$  is the instantaneous residual mass of solid. In a fire, volatiles are generated anaerobically at the surface of the material over a range of temperatures and a distribution of molecular weights and atomic compositions are produced [10], so that in general  $h_{c,v}^o$  varies over the mass loss history and cannot be treated as a constant as in equation 1. In many cases low molecular weight organic and inorganic (e.g., HCl, SO<sub>x</sub>) species are cleaved from the polymer backbone and released in the initial stages of fuel generation followed by higher molecular weight organic compounds in the intermediate and latter stages [10,11]. For materials which form a carbonaceous char during the fuel generation process, the instantaneous atomic composition of the volatiles will necessarily differ from the atomic composition of the original material [12], with hydrogen being evolved in a secondary, high temperature decomposition step [13], leaving a carbonaceous residue. Although the C-H bond is stronger than the C-C bond, H is evolved before C, leaving char. Consequently, a constant heat of combustion for the volatile fuel which is equal to the heat of combustion of the solid,  $h_c$ , so cannot be assumed except for a few cases, e.g., polymers which thermally depolymerize (unzip) exclusively to monomer (e.g., polymethylmethacrylate, polyoxymethylene, poly ( $\alpha$ -methylstyrene) or to a single, known species. Thus,  $h_{c,v}^o(t)$  must be determined continuously during the course of the fuel generation process to obtain  $\dot{Q}_c(t)$  from the mass loss rate. Continuous determination of  $h_{c,v}^o$  during fuel generation is time consuming so average [14,15] or instantaneous [16] values of  $h_{c,v}^o$  have been used instead.

Thornton [17] made the experimental observation that the net heat of complete combustion of typical organic molecules per mole of oxygen consumed is relatively constant at  $E = 419 \pm 19 \text{ kJ/mol-O}_2$  or  $13.1 \pm 0.6 \text{ kJ/g-O}_2$ , and is essentially independent of the chemical composition of the combusted material. Sussot *et al.* [18], Huggett

[19], and Babrauskas [20] later confirmed this result for a wide range forest products, chemical compounds, and organic polymers, thereby establishing oxygen consumption as the preferred method for determining heat released in flaming combustion. Thus, to a good approximation ( $\pm 5\%$ ) the net heat of complete combustion of the volatile degradation products, regardless of chemical composition, is

$$m_v(t)h_{c,v}^o(t) = E\Delta m_{O_2}(t) \quad (2)$$

where  $\Delta m_{O_2}(t)$  is the mass consumption of diatomic oxygen. Substituting the time derivative of equation 2 into equation 1

$$\dot{Q}_c(t) \equiv \frac{dQ_c(t)}{dt} = \frac{-h_{c,v}^o(t) dm_s(t)}{dt} = E\Delta\dot{m}_{O_2}(t) \quad (3)$$

shows that the instantaneous heat release rate of the solid  $\dot{Q}_c(t)$  (Watts) resulting from complete and instantaneous combustion of the volatile decomposition products can be determined from the product of the mass loss rate and heat of combustion of the fuel, or more simply from the mass consumption rate of  $\Delta\dot{m}_{O_2}(t) = \dot{m}_{O_2}^0 - \dot{m}_{O_2}(t)$ . Equation 3 shows that the rate at which heat is released by combustion of the fuel gases during controlled polymer thermal degradation can be obtained by measuring the mass of oxygen consumed, and this result is independent of the composition of the fuel. The total heat of combustion of the volatiles (Joules) after the pyrolysis process is complete, as the rate of oxygen consumption returns to zero is simply the time integral of Equation 3

$$Q_c = \int_0^{\infty} \dot{Q}_c(t)dt = E \int_0^{\infty} \Delta\dot{m}_{O_2}(t)dt \quad (4)$$

### 1.3 HEAT RELEASE CAPACITY

Although the laboratory measurement of non-flaming heat release and heat release rate by PCFC have been described, the relationship of these quantities to material properties remains to be demonstrated. It has been shown that the fuel generation process of a combustible material in a fire is anaerobic [21,22] so that the methodology of analytical pyrolysis should be applicable to the study of the behavior of materials in fires. In

particular, the maximum fractional mass loss rate of a polymer, which thermally decomposes completely in a single-step to volatile fuel gases and a residue fraction  $\mu$  when heated at a constant rate of temperature rise  $\beta$ , is [21,22]

$$-\frac{1}{m_0} \frac{dm}{dt} \Big|_{\max} = (1-\mu) \frac{\beta E_a}{eRT_p^2} \quad (5)$$

where  $E_a$  is the global activation energy for pyrolysis,  $T_p$  is the temperature of maximum mass loss rate, and  $e$ ,  $R$  are the natural number and gas constant, respectively. Multiplying equation 5 by the heat of combustion of the fuel gases gives the maximum specific heat release rate of the solid

$$\dot{q}_c^{\max} = \frac{\dot{Q}_c^{\max}}{m_0} = (1-\mu) h_{c,v}^o \frac{\beta E_a}{eRT_p^2} = h_{c,s}^o \frac{\beta E_a}{eRT_p^2} \quad (6)$$

where  $h_{c,s}^o = (1-\mu)h_{c,v}^o$  is the heat of combustion of the fuel gases per unit initial mass of solid  $m_0$  and  $h_{c,v}^o$  is the heat of combustion of the volatiles. The maximum specific heat release rate (equation 6) contains only  $\beta$  and material properties which depend on the chemical composition of the material. Normalizing  $\dot{q}_c$  for heating rate gives a time- and rate-independent material flammability property  $\eta_c$  which has the units and significance of a heat [release] capacity [23],

$$\eta_c \equiv \frac{\dot{q}_c^{\max}}{m_0} = \left[ \frac{(1-\mu)h_{c,v}^o E_a}{eRT_p^2} \right] = \frac{E\rho F}{\beta m_0} \left( \theta + \tau \frac{d\theta}{dt} \right) \Big|_{\max} \propto \frac{h_{c,s}^o}{h_g} \quad (7)$$

where  $F$  is the volumetric flow rate,  $\rho$  is the gas stream density,  $\theta$  is the measured oxygen concentration and  $\tau$  is the response time of the instrument, which is proportional to the combustibility ratio [9],  $\frac{h_{c,s}^o}{h_g}$ , where  $h_g$  is the heat required to gasify unit mass of the material. The heat release capacity is a true material property in that it depends only on thermodynamic state variables ( $h_{c,s}^o, h_g$ ), is independent of sample size and heating rate, is calculable from polymer structure using additive molar group contributions [23], and can be measured by different methods [16].

## 1.4 CONDENSED PHASE MODEL

The burning of a condensed phase material (e.g., a solid polymer) produces volatile fuel species, and possibly a solid carbonaceous char or ash, under anaerobic conditions [24,25]. The material at the burning surface is heated at a rate that is the product of the surface temperature gradient and the surface recession velocity, and is typically of the order of a few degrees Kelvin per second [21,22]. The simplest approach to the process of volatile fuel generation at the burning polymer surface is described by a single-step, anaerobic thermal decomposition reaction [21,22,26-33],



where species  $P$ ,  $F$ , and  $C$  represent the polymer ( $P$ ) and its fuel gases ( $F$ ) and solid thermal decomposition products ( $C$ ), respectively. The mass loss/fuel generation rate of a polymer at a burning surface can be described by single-step, first-order thermal decomposition kinetics [22]

$$-\frac{dm}{dt} = k_p(m - m_c) = k_p(m - \mu m_0) \quad (9)$$

where  $m$  is the instantaneous mass of polymer,  $m_c$  is the mass of char remaining after pyrolysis,  $m_0$  is the initial mass, and  $\mu = m_c/m_0$  is the constant mass fraction of char. The rate constant for thermal decomposition at temperature  $T$  is

$$k_p = A \exp\left[-\frac{E_a}{RT}\right] \quad (10)$$

in terms of the frequency factor  $A$ , global activation energy  $E_a$ , and gas constant  $R$ . If the sample is thermally decomposed at a constant heating rate  $dT/dt = \beta$ , the independent variable is transformed from time to temperature, and equation 9 can be integrated to approximate the fraction of the initial mass remaining at temperature  $T$  [22],

$$\frac{m(T)}{m_0} = \mu + (1 - \mu)e^{-\gamma} \quad (11)$$

where the exponent  $y = (ART^2 \exp[-E_a/RT]) / \beta(E_a + 2RT)$  has complex temperature dependence. The specific mass loss rate at temperature  $T$  for a constant heating rate  $\beta$  is the time derivative of equation 11,

$$\frac{-1}{m_0} \frac{dm}{dt} = (1 - \mu) k_p e^{-y} \quad (12)$$

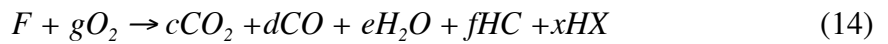
Equation 12 has a maximum value for  $\mu \neq 1$  [22],

$$-\frac{1}{m_0} \frac{dm}{dt} \Big|_{\max} = \frac{\beta(1 - \mu)}{eRT_{\max}^2 / E_a} = \frac{\beta(1 - \mu)}{\Delta T_p} \quad (13)$$

where  $T_{\max}$  is the temperature at maximum mass loss/fuel generation rate and  $\Delta T_p = eRT_{\max}^2 / E_a$  is the characteristic temperature interval over which pyrolysis occurs [22,34].

## 1.5 GAS PHASE MODEL

The reaction of volatile fuel  $F$  with oxygen in the gas phase can yield complete ( $CO_2$ ,  $H_2O$ ,  $HX$ ) and incomplete ( $CO$ ,  $HC$ ) combustion products depending on the conditions, i.e.,



where  $X$  is a halogen,  $HX$  is a halogen acid, and  $HC$  is a gaseous hydrocarbon.

Rarely is the stoichiometric oxygen / fuel ratio known in advance, and combustion is never 100% complete during the burning of polymers because of kinetic and diffusion limitations in the gas phase. In equation 14,  $g = a + b/2 + c/2$ , and the rate of fuel consumption by oxidation (assuming the second order kinetics) is

$$-\frac{d[F]}{dt} = k_c [F][O_2] \quad (15)$$

where  $[F]$  and  $[O_2]$  are the molar concentrations of fuel and oxygen, respectively, in the gas phase, and  $k_c$  is the global rate constant for combustion. For combustion in a large excess of oxygen where  $[O_2] \approx [O_2]_0$  is approximately constant, equation 15 becomes

$$-\frac{d[F]}{dt} = \{k_c [O_2]_0\} [F] = k_{app} [F] \quad (16)$$

$k_{app} = [O_2]_0 k_c$  is an apparent rate constant for fuel combustion. Equation 16 is solved immediately for the isothermal fuel concentration at time  $t$ , and  $k_{app}$  is a constant.

$$\frac{[F]}{[F]_0} = 1 - \chi = e^{-k_{app}t} \quad (17)$$

Where  $\chi = \chi(t, T)$  is the extent of reaction expressed as the change in fuel concentration  $\Delta[F]$  at elapsed time  $t$ , temperature  $T$ , divided by the change in fuel concentration for complete reaction  $\Delta[F]_0$ . The relationship between  $\chi$  and the oxygen consumed by combustion follows directly from equation 14.

$$\chi = \chi(t, T) = \frac{\Delta[F]}{\Delta[F]_0} = \frac{g\Delta[O_2]}{g\Delta[O_2]_0} = \frac{\Delta[O_2](t, T)}{\Delta[O_2](\max)} \quad (18)$$

If oxygen is present in large excess and there is sufficient time and temperature for complete combustion, then  $\chi = 1$ ,  $[F] = 0$  and fuel  $F$  is quantitatively converted to  $CO_2$ ,  $H_2O$ , and possibly  $HX$ . For complete combustion, the amount of oxygen consumed is uniquely related to the fuel composition,  $F = C_c H_h O_m N_n X_x$ ,



The stoichiometric oxygen / fuel mass ratio  $r_0$  is readily calculated from equation 19 for fuels of known composition and is in the range  $r_0 = 2.0 \pm 1.5$  for the majority of organic compounds [20]. The heat of complete combustion of organic gases and liquids  $h_{c,v}^0$  (J/g-fuel) divided by the stoichiometric mass ratio is essentially constant and independent of the type of fuel [17-19]

$$E = \frac{h_{c,v}^0}{r_0} = 13.1 \pm 0.7 kJ / g - O_2 \quad (20)$$

This observation became the basis for oxygen consumption calorimetry [35], whereby measurement of the mass of oxygen consumed from the combustion atmosphere is used to deduce the amount of heat released during the burning of plastics and products [36,37]. Equation 18 is valid only for complete combustion, i.e., equation 17.

Multiplying the specific mass loss rate of a thermally decomposing solid by the heat of combustion of the evolved gases  $h_{c,v}^0$ , assuming complete combustion, and invoking the oxygen consumption principle (equation 20) gives the specific heat release rate (W/g-sample) by oxygen consumption [38]

$$\dot{Q}(t) = \frac{-h_{c,v}^0}{m_0} \frac{dm}{dt} = -\frac{E}{m_0} \frac{dr_0 m}{dt} = \frac{\rho E F}{m_0} [\Delta O_2](t) \quad (21)$$

In equation 21,  $\rho$  and  $F$  are the oxygen density and volumetric flow rate of the gas stream, respectively, and  $[\Delta O_2](t)$  is the change in the volume fraction of oxygen in the gas stream due to combustion at time,  $t$ . The specific heat of combustion of the sample is the time integral of  $Q(t)$

$$h_c^0 = (1 - \mu)h_{c,v}^0 = \int_0^{\infty} \dot{Q}(t) dt = \frac{\rho E}{m_0} \int_0^{\infty} F[\Delta O_2](t) dt \quad (22)$$

If the sample is small ( $\approx 5$  mg) and heated at a constant rate of temperature rise  $\beta$  such that thermal equilibrium with the heat source is maintained, then according to equations 17, 21, and 22, the maximum value of the specific heat release rate in terms of oxygen consumption is

$$\dot{Q}_{\max} = \left. \frac{-h_{c,v}^0}{m_0} \frac{dm}{dt} \right|_{\max} = \frac{\beta h_c^0}{\Delta T_p} = \frac{\rho E F}{m_0} [\Delta O_2]_{\max} \quad (23)$$

Dividing equation 23 by  $\beta$  yields the flammability parameter,  $\eta_c$  [23,35], Which has the units and significance of a heat (release) capacity [21-23,40-42].

$$\eta_c = \frac{\dot{Q}_{\max}}{\beta} = \frac{h_c^0}{\Delta T_p} = \frac{\rho E F}{\beta m_0} [\Delta O_2]_{\max} \quad (24)$$

The heat release capacity  $\eta_c$  is comprised of thermal stability and combustion properties ( $h_c^0, \mu, E_a, T_{max}$ ) and is measurable by oxygen consumption calorimetry [39].

$$\eta_c = \frac{h_c^0}{\Delta T_p} = \frac{\dot{Q}_{max}}{\beta} \left[ \frac{\beta}{\beta_0} \right] \quad (25)$$

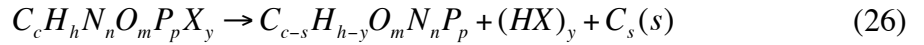
Equation 25 shows that the heat release capacity,  $\eta_c$ , is the average amount of heat released by combustion of the pyrolysis gases per degree of temperature rise over the pyrolysis interval.  $\eta_c$  is defined at a specific heating rate ( $\beta_0$ ). However, it can be calculated from the data obtained at a different heating rate ( $\beta$ ) using equation 25. Within a range of heating rates of small scale thermal analysis equipment, where there are no thermal gradient / diffusion issues, the heat release capacity obtained should be independent of heating rate  $\beta$ . For a polymer that decomposes by a first order (single step) process, the heat release capacity is seen to be a particular function of thermal stability ( $E_a, T_{max}$ ) and combustion ( $\mu, h_{c,v}^0$ ) properties, each of which is known to be separately calculable from additive molar group contributions [13,43,44]. Consequently,  $\eta_c$  should be (and is) calculable from additive molar group contributions [42] which is described in more detail here in Chapter 3, Material Properties.

## 1.6 EFFECT OF ADDITIVES

Flame-retardant chemicals are added to plastics to reduce flammability in at least three ways [45].

Inert fillers replace combustible mass with noncombustible mass to reduce the amount of fuel available for burning.

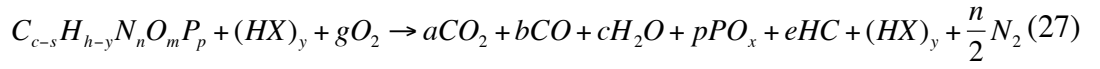
Condensed-phase active flame-retardants promote solid-state chemical reactions that produce carbonaceous char at the expense of volatile fuel. The char also acts as a mass and thermal diffusion barrier. The anaerobic solid-state pyrolysis reactions that produce carbonaceous char,  $C_s$ , from a hydrocarbon plastic or compound containing halogen  $X = F, Cl, Br, I$  or heteroatoms  $P = P, S, Si$  are



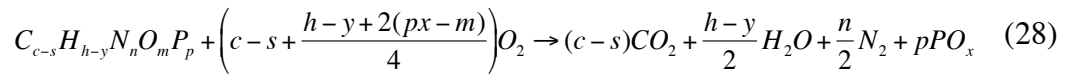
The first two terms on the right-hand side of equation 26 are idealized chemical formula for the volatile thermal decomposition products that enter the diffusion flame, mix with oxygen, and react to form complete and incomplete combustion products and liberate heat. The  $C_s$  term on the right hand side of equation 26 represents the moles of carbonaceous (solid) char remaining after pyrolysis. If  $\mu$  is the mass fraction of char and  $\nu$  is the mass fraction of inert filler, the non-combustible fraction is  $\phi = \mu + \nu$ , and the combustible / fuel fraction is  $1 - \phi$ . Among the mechanisms by which condensed phase flame-retardants act to reduce flammability is char swelling at the burning surface, which insulates the underlying solid from the heat of the flame [45].

An expression for the relative efficiency of heat and mass transfer at the solid surface is  $\theta = (1 - \phi)^a$ , where  $a$  is an empirical constant that depends on the mechanism of action of the condensed phase flame-retardant. Because  $\theta$  is the relative efficiency of heat and mass transfer at the surface, it must be a positive number, but there is no restriction on the sign or magnitude of the exponent  $a$ . For example, inert fillers such as minerals, chopped glass fibers, and nanometer-scale particles have 5–10 times higher thermal conductivity than polymers; so, a non-charring polymer containing these fillers at  $\phi = \nu$  would have  $\theta = (1 - \nu)^a > 1$ . The “wick effect” that is thought to cause an increase in flammability at low mass fraction  $\nu$  of fiberglass [46] and a reduced time-to-ignition are described by  $a < 0$ . Conversely, an unfilled ( $\nu = 0$ ), non-charring ( $\mu = 0$ ) polymer with or without a non-conducting filler would have  $\phi \approx 1$ , while a charring polymer would have  $\theta < 1$ , and those exhibiting intumescence (volumetric expansion of a char layer) would have  $\theta \ll 1$ . The heat / mass transport efficiency  $\theta$  is a lumped, empirical parameter in the analyses to follow. Thus, the concept of  $\theta$  will be important to correlate flame test results, but its functional form will not.

Gas-phase active flame-retardants inhibit chemical reactions in the flame between the volatile hydrocarbons and oxygen so that combustion is incomplete and less heat is available to sustain burning. The chemical reaction of the volatile compounds from equation 26 with oxygen in the flame proceeds according to the generalized combustion reaction



The right-hand side of equation 27 contains complete ( $CO_2$ ,  $H_2O$ ,  $HX$ ) as well as incomplete (carbon monoxide /  $CO$ , unburned hydrocarbons and soot /  $HC$ , and oxidized heteroatom /  $PO_x$ ) combustion products. The  $CO_2/CO$  ratio (mole ratio,  $a/b$  in equation 27) is a measure of the completeness of the combustion process. Complete (100%) combustion is only achieved under laboratory conditions, under which, the amount of oxygen consumed is uniquely related to the fuel composition



The stoichiometric oxygen / fuel mass ratio  $r_0$  is readily calculated for complete combustion (equation 28) for fuels of known composition, and is in the range  $r_0 = 2.0 \pm 1.5$  for the majority of organic compounds [20]. The heat of combustion of organic gases, liquids, and solids,  $h_c^o$  (J/g-fuel) divided by the stoichiometric mass ratio is essentially constant and independent of the type of fuel, i.e.  $h_c^o / r_0 = constant = 13.1 \pm 0.7$  MJ/kg- $O_2$  [17,19]. This observation became the basis for oxygen consumption calorimetry [35], whereby measurement of the mass of oxygen consumed from the combustion atmosphere is used to deduce the amount of heat released during the burning of materials and products [19,35],

$$h_c^o = (13.1 \text{ kJ/g-}O_2) \left( \frac{\text{mass of } O_2 \text{ consumed}}{\text{mass of fuel burned}} \right) \quad (29)$$

Equation 29 applies only to complete combustion (i.e., equation 28). For incomplete combustion as occurs in diffusion flames (e.g., flammability / flame tests), the effective heat of combustion ( $HOC$ ) is less than  $h_c^o$  in the ratio  $\chi = HOC/h_c^o \leq 1$ , where  $\chi$  is the extent of reaction, or combustion efficiency. Flaming combustion efficiency under well-ventilated conditions ranges from  $\chi \approx 1$  for hydrocarbon plastics to about  $\chi \approx 0.3$  for halogen-containing plastics [47].

The MCC does not sense the effect of gas phase flame retardants when run under standard conditions [48]. The inert fillers dilute the sample and therefore the amount of

fuel that is available for burning. Condensed phase flame retardants often work by providing a barrier at the sample surface, preventing the volatile fuel from readily escaping. The small scale of the MCC and geometry of heating from all sides may prevent this mechanism. Only additives that change the degradation chemistry by creating more char show any effect in the MCC. Gas phase flame retardants do not have a chance to inhibit the flame in the MCC because it is a non-flaming test, operating by forced oxidation of the volatiles at high temperatures in an excess of oxygen. Future work, where lower combustion temperatures are evaluated, will hopefully show and provide a quantitative measure of gas phase flame retardant activity.

## 1.7 SUMMARY AND CONCLUSIONS

The processes by which a material degrades and its gaseous decomposition products burn was examined. PCFC is a test methodology by which a sample is thermally degraded and the volatile decomposition products oxidized to completion in an attempt to indicate the potential fire hazard of a material. Fuel generation rates are calculated from mass loss measurements and pyrolysis kinetics are derived from this. A condensed phase model was derived to describe the production of evolved fuel over a specified pyrolysis interval. The gas phase model was derived that explains the fuel composition and reaction chemistry with oxygen. This reaction with oxygen is the basis for PCFC. Heat release rates are determined from the composition of the volatile decomposition products. Combustion reaction rates are used to relate this data to physical and material properties that comprise the heat release capacity.

## CHAPTER 2

### INSTRUMENT CONSTRUCTION

## 2.1 OVERVIEW

Figure 1 is a schematic diagram showing how the component processes of flaming combustion are reproduced in pyrolysis-combustion flow calorimetry. The apparatus is based on Susott's *et al.* original concept [12,18,49] of linear programmed heating of milligram samples in an inert (non-oxidizing) atmosphere to separate the processes of char formation and gas phase combustion that normally occur in a fire. In the present device the sample is heated using a linear temperature program and the volatile thermal degradation products are swept from the pyrolysis chamber by an inert gas and combined with excess oxygen in a tubular furnace at flame temperatures to force complete non-flaming combustion (oxidation) of the fuel. Combustion products, H<sub>2</sub>O, and acid gases are scrubbed from the gas stream and the transient heat release rate is calculated from the measured flow rate and oxygen concentration after correcting for flow dispersion.

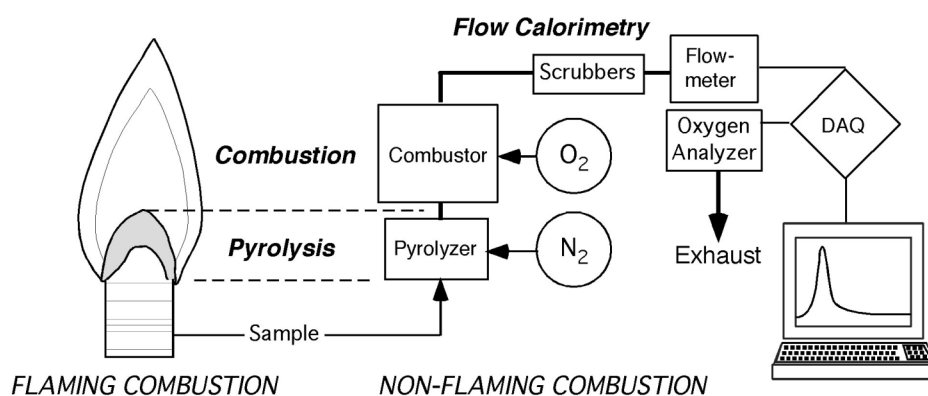


Figure 1. Flow diagram for pyrolysis-combustion flow calorimetry as it relates to flaming combustion.

The maximum (peak) value of the PCFC heat release rate normalized for the initial sample mass and heating rate is a material flammability parameter with units of heat [release] capacity (J/g-K) which depends only on chemical composition of the sample and is proportional to the burning rate of the material in a fire. Time-integration of the PCFC heat release rate gives the heat of complete combustion of the pyrolysis gases, while the char yield is measured by weighing the sample before and after the test. If the pyrolysis is conducted in air, so that no char remains after the test, time-integration of

the oxygen consumption signal gives the net heat of complete combustion of the solid as would be determined in a high pressure oxygen bomb calorimeter [50].

A constant rate of temperature rise (ramp) is used to heat the sample to a temperature which is well above the thermal decomposition range of typical combustible solids. The ramp program forces complete thermal decomposition of most combustible solids and the heat release rate has physical significance in terms of material properties. Selecting a hold temperature on the pyrolyzer which corresponds to a particular fire environment (heat flux), but which is within the normal temperature range of the polymer thermal decomposition, discriminates between materials with regard to heat resistance but not fire resistance, since in general, the fire heat flux is not known *a priori*. Therefore, in order to obtain an unambiguous measure of the capacity of a combustible material to release heat in a fire, the standard pyrolysis-combustion (micro heat release rate) test involves heating the sample at a constant rate (60 K/min, typically) to a temperature at least 50°C above the maximum decomposition temperature of the material to effect complete pyrolysis. The volatile pyrolysis products are generated during the temperature ramp and are swept from the pyrolyzer by nitrogen gas flowing at 80 cm<sup>3</sup>/min to which 20 cm<sup>3</sup>/min of pure oxygen is added at the inlet of the combustor. Combustion gases are scrubbed to remove water and acid gases (if any) and the gas stream passes through a flow meter and oxygen analyzer. The heat release rate, heat release capacity, and total heat of combustion are calculated and displayed. The sample container is weighed after the test to determine the mass of sample residue.

## 2.2 PYROLYZER

Initial studies utilized a commercial thermogravimetric analyzer (Perkin Elmer TGA 7) to pyrolyze the polymer samples [14,15]. This design was unsuccessful due to condensation of the thermal decomposition products in the TGA cell and heated transfer line. Smearing of the output signal (heat release rate) was also observed because of dilution of the pyrolysis gases with nitrogen in the large mixing volume of the TGA cell. Moreover, the maximum heating rate capability of the TGA (100-200 K/min) was well below the heating rates in fires which can be as high as several hundred degrees per minute [21]. For these reasons, the next version, a temperature-controlled pyrolysis chamber, was designed which could be continuously purged with gas, coupled directly to the combustion furnace, and accept a commercial probe pyrolyzer (Pyroprobe

1000/2000, CDS Analytical) to gasify the sample. This arrangement provided consistent temperature and minimum dead-volume with the probe in place for the experiment as shown in figure 2. The probe pyrolyzer body is 6.4 mm in diameter and contains a 3 mm diameter, 25 mm long platinum resistance coil which heats the sample at a constant rate in the range  $\beta = 20 \times 10^{-3}$  to  $20 \times 10^3$  K/s. At the highest heating rate the temperature history of the sample approximates a step change to a preset temperature and in this mode can be used to study the isothermal pyrolysis kinetics of liquids and solids by pulsed heating [51].

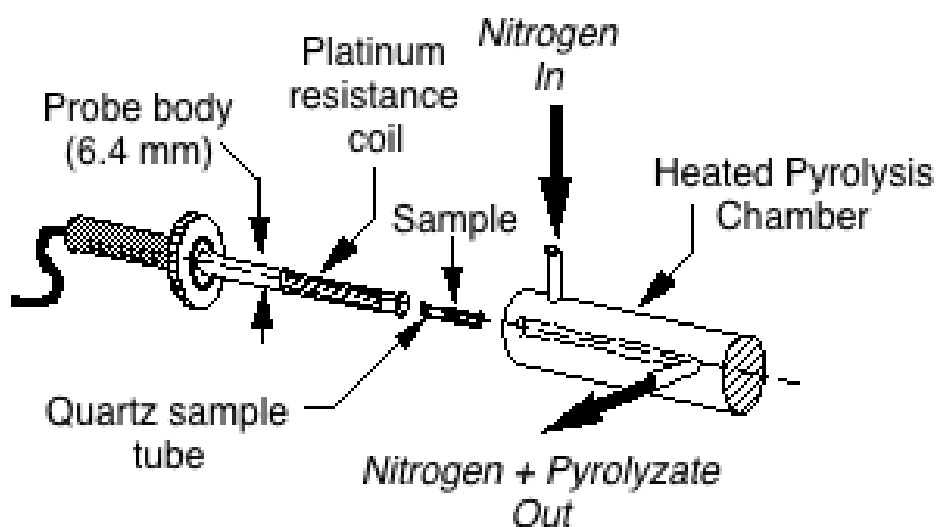


Figure 2. PCFC with Pyroprobe pyrolyzer and heated pyrolysis chamber.

### 2.2.1 Mass Transfer

Mass transfer efficiency from the heated pyrolysis chamber to the combustor was studied for a few polymers (polyethylene, polyetheretherketone and Kevlar™) to determine the minimum temperature necessary to maintain all of the pyrolysis products in the gaseous state entering the combustor. Mass transfer efficiency was calculated as the ratio of the time-integrated heat release rate (total heat of combustion) of the pyrolysis gases at cell temperature  $T$ , i.e.,  $h_{c,s}^0(T)$  to the maximum value obtained in the experiments, i.e., mass transfer efficiency  $h_{c,s}^0(T)/h_{c,s}^0(\text{max})$ . The results of these studies are plotted in figure 3 as the mass transfer efficiency versus pyrolysis chamber temperature. Figure 3 shows that high molecular weight thermal degradation products are generated during pyrolysis which vaporize at temperatures approaching the

decomposition temperature of the polymer. The highest transfer efficiency was obtained close to the decomposition of the material. If the heated interface temperature was too high the sample would start to decompose prior to the start of the test, thereby reducing the transfer efficiency. If the temperature is too low, then volatiles condense. Loss of these low volatility fuel products by condensation between the pyrolyzer and combustor significantly reduces the peak heat release rate and total heat release unless the pyrolysis chamber temperature is held to within a few degrees of the 1% weight loss temperature of the sample. The transfer efficiency for polyethylene was complete because the material does not leave any char and the measured total heat release values were the same as the heat of combustion obtained in a bomb calorimeter. PEEK and Kevlar™ transfer efficiencies could not be validated with another technique because both samples leave a large char fraction when thermally decomposed. It was determined that this was the best system configuration to transfer the most evolved gases from polymer pyrolysis for the Pyroprobe PCFC.

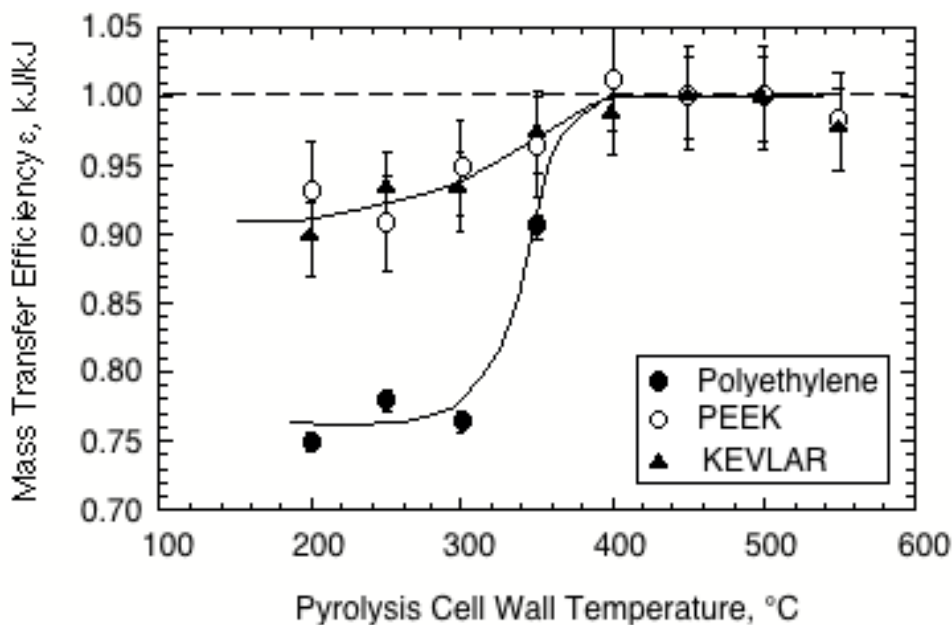


Figure 3. Effect of pyrolysis cell wall temperature on mass transfer efficiency of pyrolysis gases for PEEK, Kevlar, and polyethylene using a Pyroprobe with a heated interface.

A mass flow controller measures and controls the flow of pure (99.99%) nitrogen at 80 cm<sup>3</sup>/min into the heated pyrolysis chamber to provide an anaerobic pyrolysis environment. Volatile pyrolysis products are swept out of the pyrolysis manifold and

20 cm<sup>3</sup>/min of pure (99.99%) oxygen is metered into, and mixed with, the nitrogen-pyrolyzate stream prior to entering the combustor. The pyrolysis chamber is held slightly below the decomposition temperature of the sample, as determined in a separate TGA experiment at moderate (10-20 K/min) heating rate, to prevent condensation of high molecular weight decomposition products on the walls of the chamber.

The present version of the MCC integrates the pyrolyzer with the combustor, eliminating any transfer lines, by using a single continuous furnace tube with two independently controlled heaters. This eliminates any heated manifolds and cold spots associated with transferring volatile decomposition products.

A new method for constant-rate heating, based on a semi-empirical mathematical expression relating sample temperature, heating rate, and electric power supplied to the furnace was developed. In this method, a single thermocouple is used to monitor the temperature of a sample and control its heating rate. According to the comparative analysis described below, the linearity of the sample temperature versus time curves obtained using this method in combination with a simple furnace setup is the same as the linearity of the curves generated by modern commercial thermogravimetric analyzers.

### 2.2.2 Sample Heating and Control

Heating a small (1-10 mg) sample of material at a constant heating rate (typically, 0.1-1.0 °C/s) is a technique that is used widely in thermal analysis and pyrolysis experiments [52,53]. The constant-rate heating is usually achieved by employing a furnace equipped with a resistive heating element. The temperature of the element is monitored by a thermocouple and controlled by a proportional integral derivative (PID) controller [52,54]. The controller manipulates electric power supplied to the element in order to keep its temperature as close as possible to the programmed temperature, which is a linear function of time. A separate thermocouple is used to monitor the temperature of a sample, which is usually placed in the middle of the furnace.

A schematic of the setup used in the heating experiments is shown in figure 4. A ceramic tube (1.5 mm thick wall) with a nichrome wire tightly spiraled around the outside served as a furnace. This tube was enclosed in a metal box (approximately 10 x

10 x 12 cm). The tube was continuously purged with 80 cm<sup>3</sup>/min of nitrogen. A small ceramic cup (about 5 mm in diameter and 0.5 mm thick walls) was used as a sample container. The cup was placed on a ceramic post located on the axis of the tube. A type K thermocouple was built into the post. The bead of the thermocouple was in direct contact with the bottom of the sample cup. Direct electric current generated by a programmable power supply was used to heat the furnace. A PC equipped with a data acquisition board and custom software [55] was used to control the power supply output and read temperature of the thermocouple.

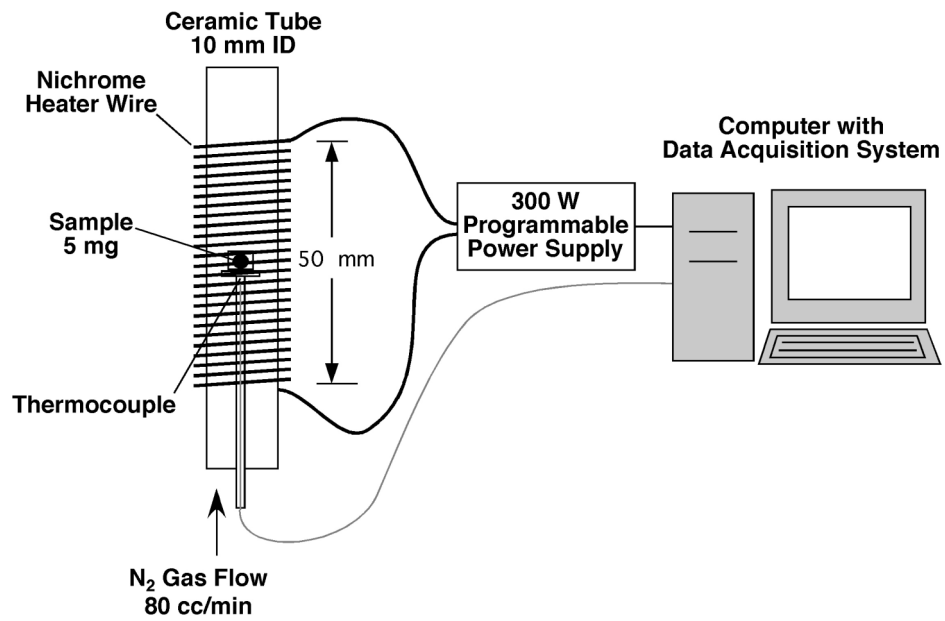


Figure 4. Experimental setup for controlled heating of a sample in the MCC.

Temperature histories obtained by application of constant voltages to the furnace are shown in figure 5. The sample container used in these measurements was empty. It is apparent from the shape of the curves that they can be described by an exponential-rise function,

$$T = B - Ae^{-kt}, \quad (30)$$

where  $B$ ,  $A$ , and  $k$  are adjustable parameters and  $t$  is time. The results of the least-square fit of the experimental data with this function are presented in figure 5.

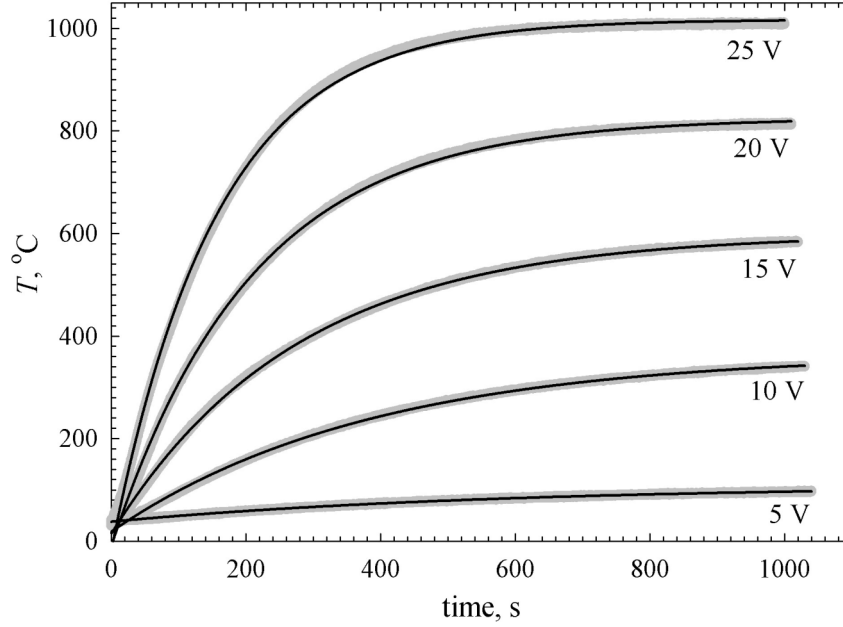


Figure 5. Temperature response of applying a constant voltage to a heater from cold start. Grey lines are experimental data. Black lines are results of the least-square fit with equation 31.

Differentiation of equation 30 with respect to time, and subsequent expression of the result in terms of temperature, yield a linear relation between the temperature and heating rate:

$$\frac{dT}{dt} = k \{ Ae^{-kt} \} = k \{ B - T \} = kB - kT. \quad (31)$$

The form of equation 31 indicates that the system under consideration is a lumped-heat-capacity system, which describes the functional form of the temperature relationship and frequently used to describe transient heat conduction [56]. The  $kB$  product and  $k$  are two parameters that depend on the voltage applied to the furnace. The values of these parameters (obtained from the fit of the constant-voltage temperature histories) are plotted with respect to the voltage,  $U$ , in figure 6. As demonstrated by the graphs, these dependencies can be captured by second-order polynomials:

$$kB = b_0 + b_1U + b_2U^2, \quad (32)$$

$$k = k_0 + k_1U + k_2U^2. \quad (33)$$

Substitution of these polynomial expressions into equation 31 yields a quadratic equation:

$$\{b_2 - k_2T\}U^2 + \{b_1 - k_1T\}U + \left\{b_0 - k_0T - \frac{dT}{dt}\right\} = 0. \quad (34)$$

The positive root of this equation,

$$U = \frac{-\{b_1 - k_1T\} + \sqrt{\{b_1 - k_1T\}^2 - 4\{b_2 - k_2T\}\left\{b_0 - k_0T - \frac{dT}{dt}\right\}}}{2\{b_2 - k_2T\}}, \quad (35)$$

is an expression of the voltage in terms of the temperature and heating rate. This expression provides us with the means to calculate the voltage that needs to be applied to the furnace in order to heat a sample, which is currently at temperature  $T$ , at the rate  $\frac{dT}{dt}$ , provided the change in temperature and voltage is small with respect to time.

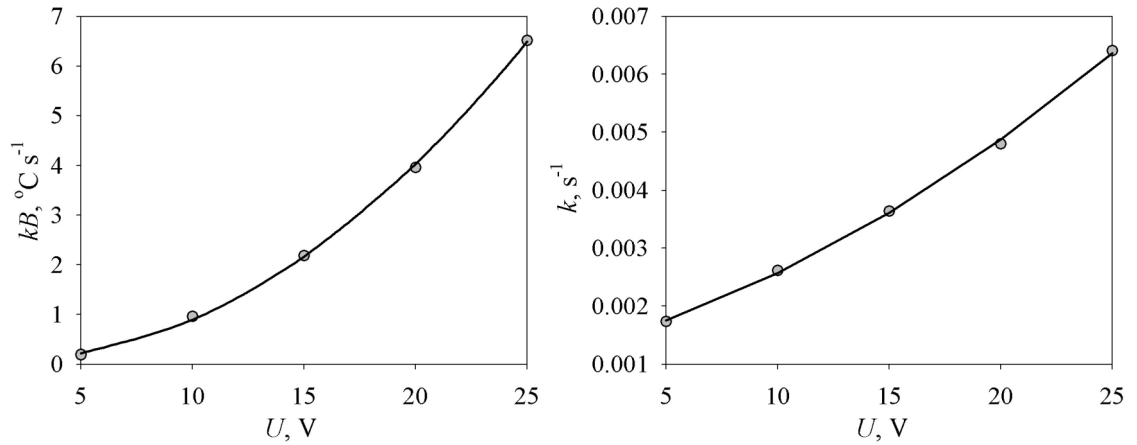


Figure 6. Dependencies of parameters of equation 31 on voltage. Circles are parameter values derived from experimental data. Black lines are the least square fits with equations 32 and 33.

The applicability of equation 35, which is subsequently referred to as control expression, to heating rate control is based on the assumption that  $kB$  and  $k$  parameters of equation 31 depend only on the voltage applied to the furnace and are insensitive to the rate of change of this voltage with time. It is further assumed that the presence of a sample does not have a significant effect on the heating process. The mass of the furnace and sample holder are much greater than that of the sample so it does not have an impact on heating the system. The range of heating rates and temperatures covered by the control expression is, to a large degree, determined by the range of voltages used in the generation of constant-voltage temperature histories.

The present method is a promising alternative to the traditional constant-rate heating approach. Application of this method to a simple furnace setup has resulted in the level of heating rate stability that matches the heating rate stability of modern thermogravimetric analyzers as determined experimentally in laboratories at the Federal Aviation Administration (FAA) and the National Institute of Standards and Technology (NIST). This method is currently employed in the new version of the MCC where the heat of combustion, heat release capacity, and ignition temperature of materials using milligram-sized samples [34,38] is measured.

### 2.3 COMBUSTOR

The initial combustor used for the PCFC was a coiled, 5 meter length of 6.35 mm outside diameter Inconel tubing having a wall thickness of 0.89 mm, a coiled length of 24 cm, and an outer coil diameter of 5 cm as shown in cross section in figure 7. The coiled combustion tube is contained in a ceramic furnace capable of maintaining a maximum temperature of 1200°C. The Inconel tubing in the ceramic heater are surrounded with 5 cm of ceramic fiber insulation and a 3.4 mm thick cylindrical aluminum shell. The combustion tube length was selected to provide a residence time of approximately 60 seconds at a volumetric flow rate of 100 cm<sup>3</sup>/min in order to completely oxidize the pyrolyzate stream. Published studies of the oxidation of the products of flaming combustion showed that a residence time of 60 seconds at 1000°C was required to completely oxidize the largest size soot particles observed in real fires [57]. However, gaseous pyrolysis products and fire gases should be completely (>99%) oxidized in less than a millisecond at the nominal 900°C combustor temperature, as

deduced from high temperature oxidation kinetics of methane [58] and volatile polymer pyrolysis products [59].

The temperature distribution along the length of the Inconel tubing coil was measured using a shielded thermocouple probe positioned at several locations along the inside surface of the coil with nitrogen flowing through the coil at 100 cm<sup>3</sup>/min. These experiments were repeated for various set point temperatures. A nearly symmetric temperature distribution about the coil midpoint location,  $x = 0$ , was observed (figure 7) at the nominal 900°C set point. Temperature distributions for set point temperatures from 500 to 1000°C were similar.

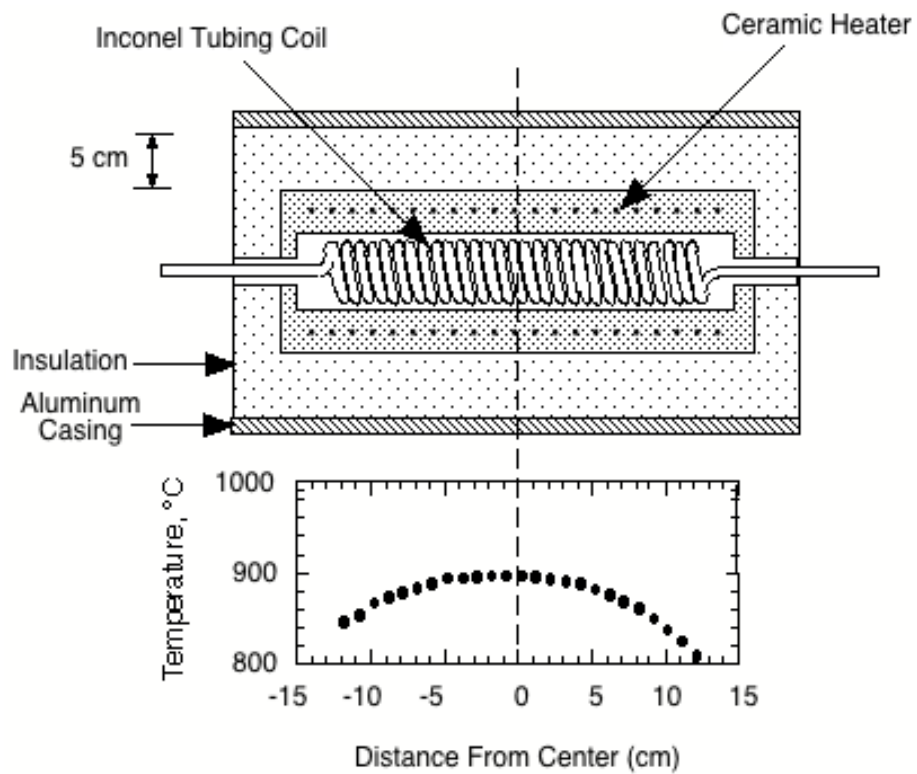


Figure 7. PCFC combustor cross section and temperature distribution for a 900°C set-point.

### 2.3.1 Thermal Oxidation Kinetics

Experiments were also conducted in which the purge gas was methane (8.3 cm<sup>3</sup>/min) and nitrogen (75 cm<sup>3</sup>/min) and the oxygen flow rate was 16.7 cm<sup>3</sup>/min, so that the molar ratio of oxygen/fuel was stoichiometric, i.e.,  $[O_2] / [CH_4] = 2$ . The combustor

temperature was slowly cycled between 25° and 950°C so that the temperature of the  $CH_4 / O_2 / N_2$  gas mixture did not change significantly during the 10-second residence time in the combustor. The oxidized gas stream was analyzed for residual oxygen to compute the extent of reaction as a function of combustor temperature for a residence time of 10 seconds.

Experimental results for  $A = A_c [O_2]_0$  and  $E_a$  from thermal oxidation studies of methane (Methane 1) and the pyrolyzates of PMMA and polypropylene (PP), are listed in table 1. Also listed in table 1 are values of  $A$  and  $E_a$  obtained from the literature for methane (Methane 2) [58] as well as the pyrolysis products of some common hydrocarbon polymers [59].

Table 1. Kinetic parameters determined experimentally and obtained from the literature [38] for the oxidation reaction of methane gas and polymer pyrolysis products.

Polymer	$E_a$ (kJ/mol)	$A$ ( $s^{-1}$ )	Temperature Range (K)
Methane 1	241	$10^{12}$	1020-970
Methane 2	230	$10^{10}$	1000-2000
PMMA 1	62	$10^4$	725-973
PMMA 2	130	$10^7$	773-898
Polypropylene	94	$10^5$	607-656
Polybutadiene	91	$10^5$	800-945
Polyisoprene	75	$10^4$	825-975
Ethylene-propylene rubber	133	$10^8$	800-975
PC/ABS blend	188	$10^{10}$	800-975

The minimum residence time in the combustor at temperature  $T_c$  for any degree of oxidation can be calculated using first order rate law kinetics. If the oxidation reaction of the fuel gases in the presence of excess oxygen is required to be 99.5% complete by the time the gas stream exits the combustor, then the minimum residence time  $\tau_r$  in the combustor at temperature  $T_c$  is

$$\tau_r = \frac{-\ln(1-0.995)}{A \exp[-E_a/RT_c]} = \frac{5.3}{A \exp[-E_a/RT_c]} \quad (36)$$

Equation 36 is plotted in figure 8 as reaction time  $\tau_r$  versus temperature for the materials and kinetic parameters in table 1. Figure 8 shows that for all the fuels examined, thermal oxidation is 99.5% complete in 1 second at 1000°C, or in 10 seconds at 900°C, without the use of a catalyst. These results are significantly different from the 50 seconds at 1000°C claimed by Babrauskas *et al.* [57] to be necessary for complete thermal oxidation of fire gases containing soot particles using a platinum catalyst.

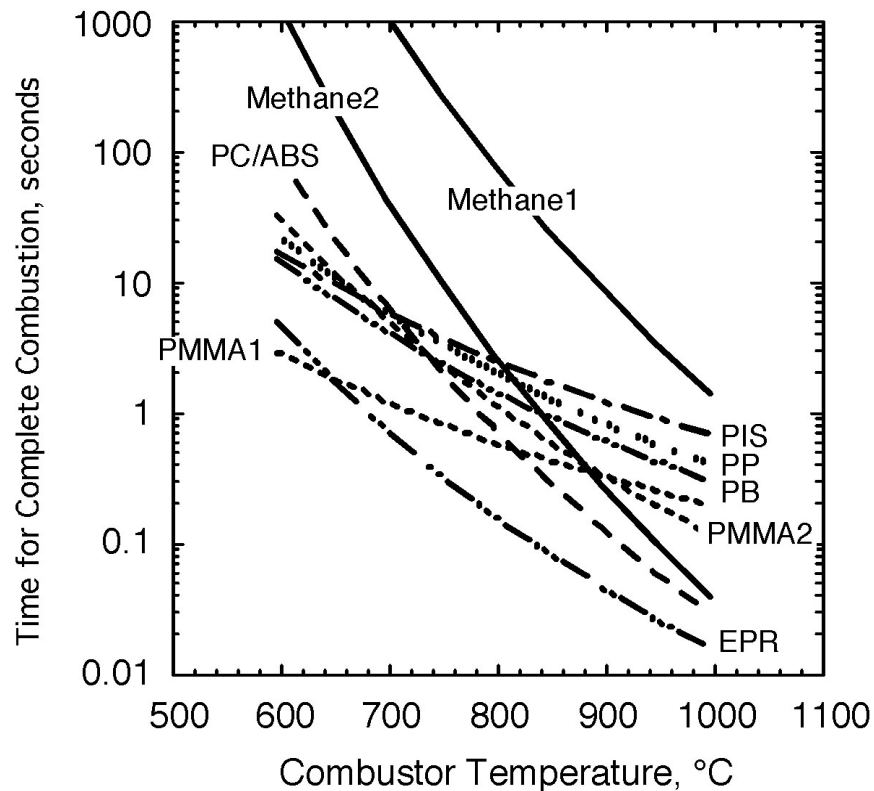


Figure 8. Reaction time versus temperature for 99.5% combustion of methane gas and polymer pyrolysis products calculated from oxidation kinetic parameters.

The results of combustor temperature cycling experiments for the stoichiometric mixture of methane and oxygen in nitrogen are shown in figure 9, as the final oxygen concentration of the combustion stream versus the combustor temperature over the range 500-900°C. It is apparent that the oxygen concentration goes to zero, i.e., all the oxygen (and methane) is consumed during the 10-second residence time in the combustor at temperatures between 775 and 800°C. This result is in general agreement

with the data in figure 8 with the exception of Methane 1. The absence of any residual oxygen in the stoichiometric reaction with methane shows that oxygen is not rate limiting under the conditions of these experiments.

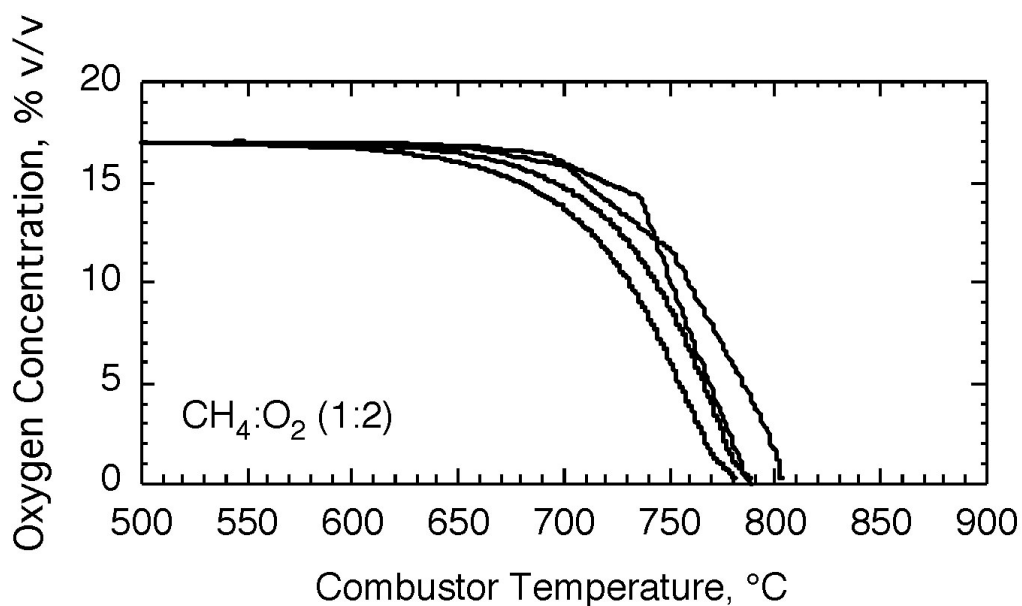


Figure 9. Oxygen concentration of a stoichiometric (1:2)  $\text{CH}_4:\text{O}_2$  mixture in nitrogen exiting the MCC combustor at the indicated temperature with a residence time of 10 seconds.

Table 2 lists the heats of combustion of the pyrolysis products (monomers and oligomers) of non-charring polymers measured in the MCC for a residence time of 10 seconds at 900°C in the combustor. Also listed in table 2 are heats of complete combustion of the same polymers obtained by adiabatic, high-pressure, oxygen bomb calorimetry [44,60]. The excellent agreement between PCFC and oxygen bomb calorimetry confirms complete (100%) combustion of typical polymer pyrolysis products in 10 seconds at 900°C in excess oxygen.

Table 2. Net heats of combustion of non-charring polymer pyrolyzates by PCFC compared to oxygen bomb calorimeter values.

Polymer	ASTM D 2015 (kJ/g)	PCFC (kJ/g)	Relative Deviation (%)
Polyethylene	43.3	43.5 ±0.1	0.5
Polystyrene	39.8	39.4 ±0.5	-1.0
Polymethylmethacrylate	24.9	25.0 ±0.1	0.4
Polyoxymethylene	15.9	16.0 ±0.1	0.6

## 2.4 MICROSCALE COMBUSTION CALORIMETER

These earlier designs were used as a learning experience and abandoned for the present single tube design where the pyrolyzer and combustor are adjacent on a single tube as shown in figure 10. The method is implemented as a stand-alone device or as an evolved gas accessory attached to a TGA. In the stand-alone apparatus, 1-5 milligram samples are heated to up to 1000°C at a heating rate of 1°C/s (typically) in a stream of nitrogen flowing at 80 cm<sup>3</sup>/min. The volatile thermal degradation products are swept from the pyrolyzer by the nitrogen purge gas and mixed with 20 cm<sup>3</sup>/min of pure oxygen prior to entering the combustor, held at 900°C. After exiting the combustor, the gas stream passes over anhydrous calcium sulfate (Drierite) to remove moisture and acid gases prior to passing through a mass flow meter and oxygen analyzer to calculate the HRR by oxygen consumption.

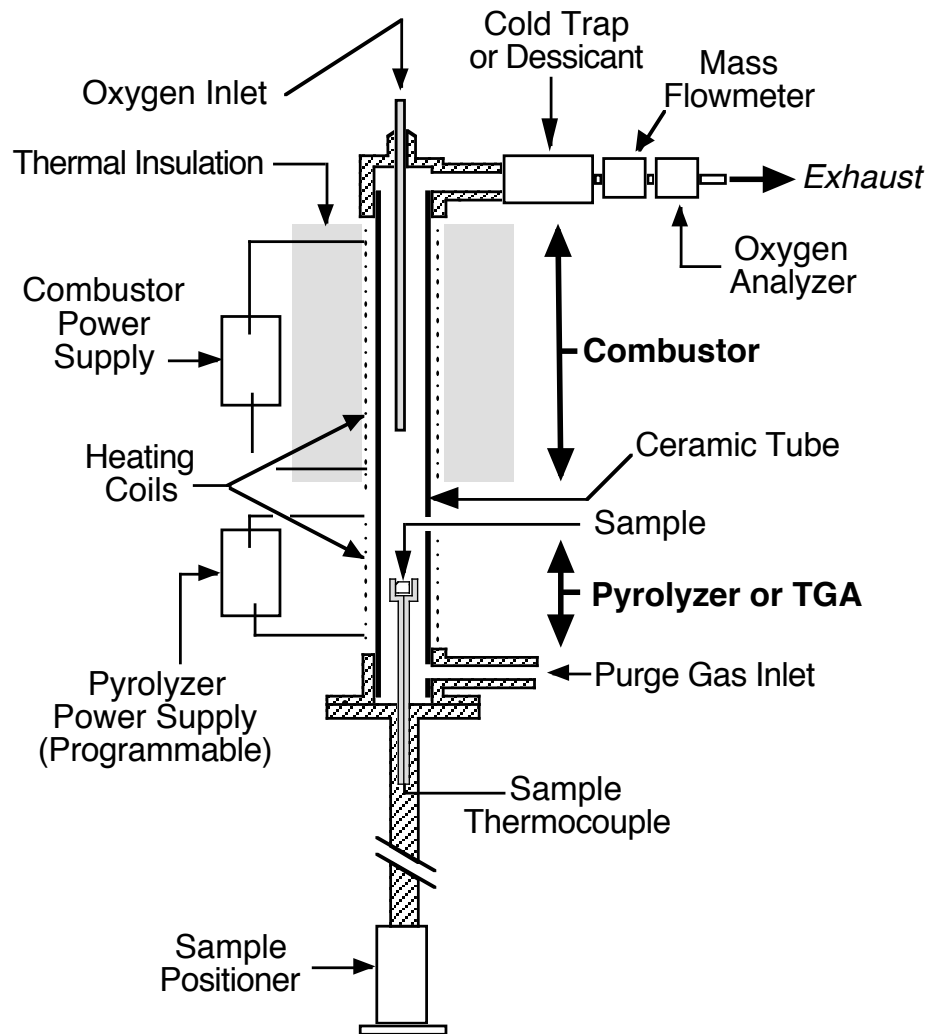


Figure 10. Schematic drawing of the MCC showing heated zones and flow path.

Figure 11 shows experimental data for the normalized heat release rate  $Q/\beta$  versus temperature for polyoxymethylene (POM), polymethylmethacrylate (PMMA), polyvinylchloride (PVC), polyethyleneterephthalate (PET), polyamide 66 (PA66), acrylonitrile-butadiene-styrene (ABS), polypropylene (PP), polyvinylidene fluoride (PVDF), polyethylene (PE), fluorinated ethylene-propylene (FEP), polyetherimide (PEI), polyphenylenesulfide (PPS), and polycarbonate (PC) measured by PCFC. Tests were performed at a heating rate of 1 K/s using a combustor residence time of 10 seconds at 900°C. The data in figure 11, which is sorted from front to back by the maximum mass loss rate temperature  $T_{max}$ , shows, along the z-axis, that  $\eta_c (Q_{max}/\beta)$  varies widely in magnitude and temperature for common polymers.

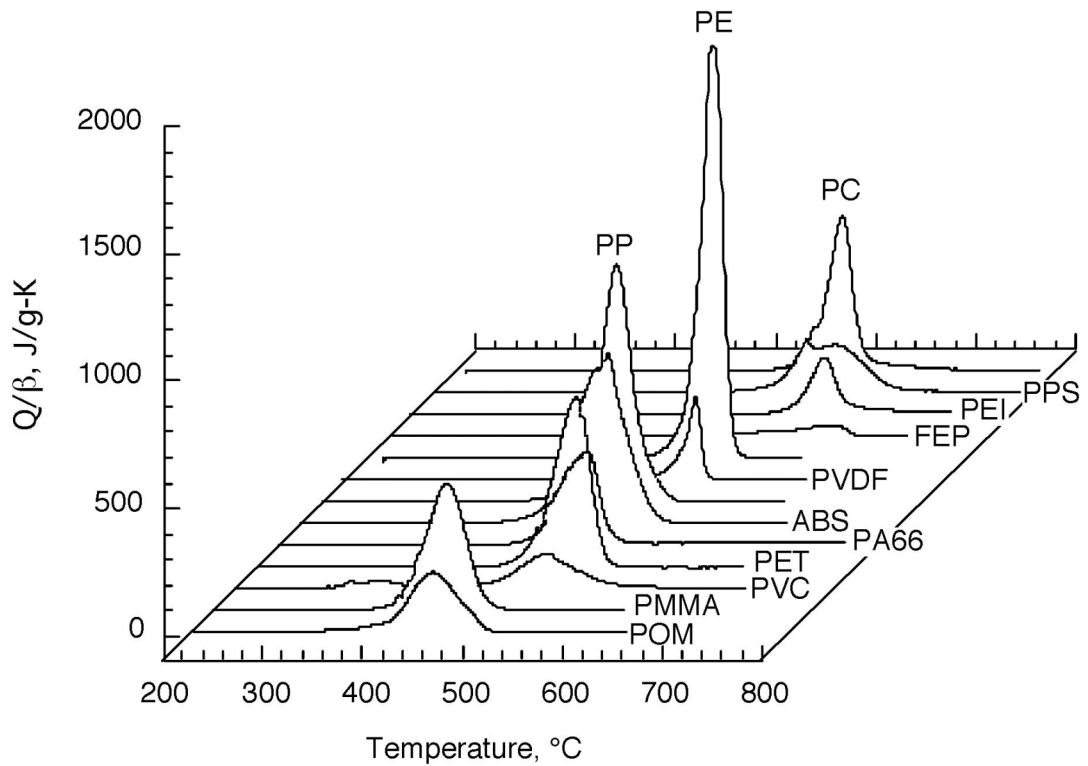


Figure 11. Heat release rate histories of common polymers in MCC sorted along the z-axis by  $T_{max}$ .

Figure 12 is a plot of the maximum specific HRR  $Q_{max}$  versus heating rate for milligram samples of PE, polystyrene (PS), PA66, PMMA, polybutyleneterephthalate (PBT), PET, polyphenyleneoxide (PPO), PC, POM, and phenolic triazine (PT). This data was obtained using 1 mg samples with the Pyroprobe PCFC. The weak dependence of  $Q_{max}/\beta$  on  $\beta$  is illustrated in figure 13, which shows these data for PE, high-impact polystyrene (HIPS), PMMA, POM, and FEP obtained using 2 - 5 mg samples in the MCC.

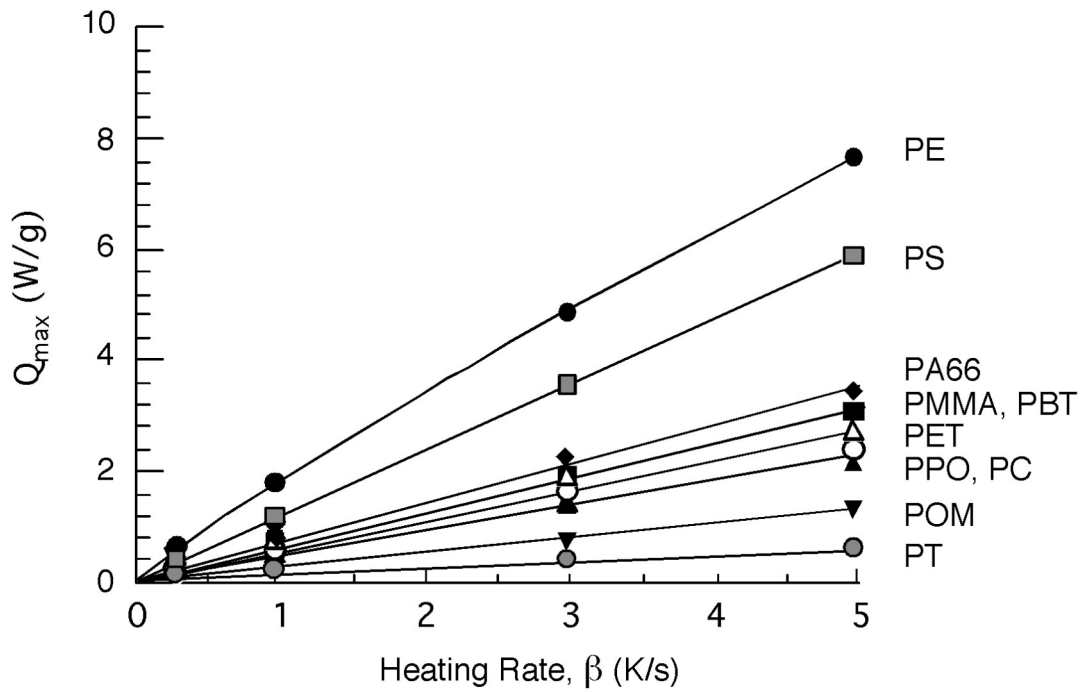


Figure 12. Maximum specific  $HRR$ ,  $Q_{max}$ , versus heating rate,  $\beta$ , in Pyroprobe PCFC for 1 mg samples of PE, PS, PA66, PMMA, PBT, PPO, PC, POM, and PT.

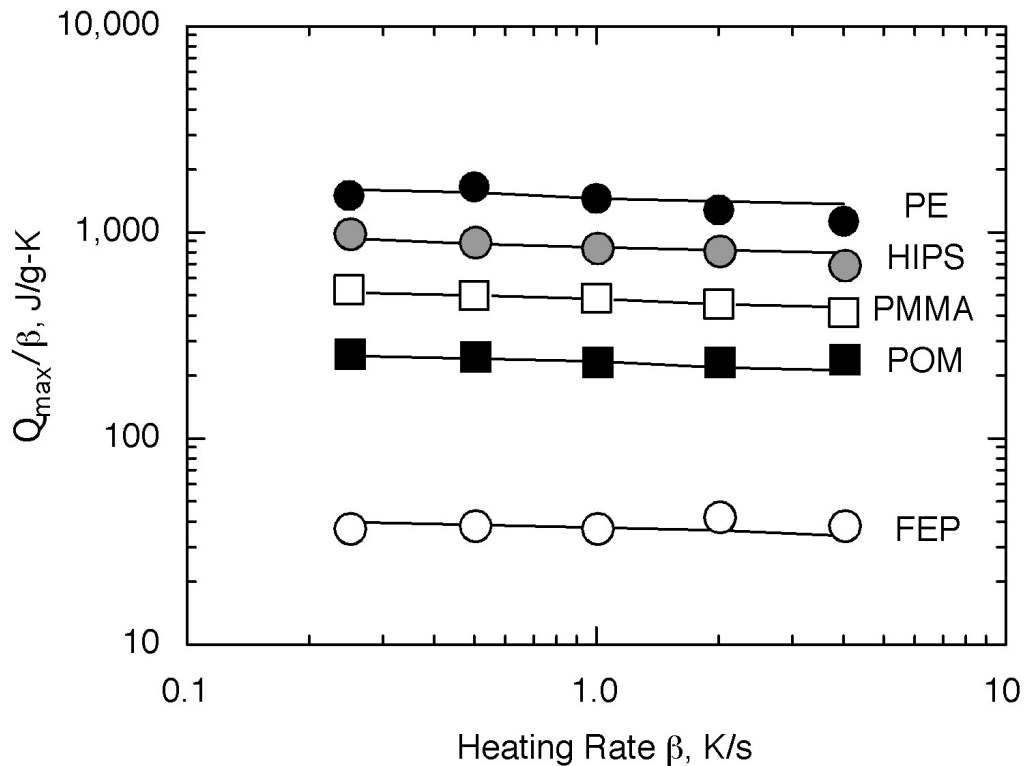


Figure 13. Peak HRR normalized for heating rate versus heating rate for PE, HIPS, PMMA, POM, and FEP obtained in the MCC with a 2-5 mg sample.

The repeatability (intra-laboratory variation) of measurements made in the laboratory in the apparatus of figure 10 is indicated by the data in table 3, which lists mean values and one standard deviation for triplicate determinations of heat release capacity ( $\eta_c$ ), total heat released by combustion of volatile fuel ( $h_{c,v}^0$ ), char yield ( $\mu$ ), and heat release, or pyrolysis, temperature ( $T_p$ ) of some of the commercial polymers whose HRR histories are shown in figure 11. Repeatability estimated from the average coefficient of variation for the data in table 3 is better than 5% (i.e., the average relative deviation from the mean is less than 5%). The reproducibility (inter-laboratory variation) of measurements for these same polymers obtained using the apparatus of figure 10 is about 10%, as demonstrated graphically in figure 14, which is a plot of individual  $\eta_c$  from each of three different laboratories versus the average  $\eta_c$  for the three laboratories.

Table 3. Flammability parameters for thermoplastic materials obtained by PCFC. Heat release capacity, total heat release, char yield, and peak pyrolysis temperature and their repeatabilities are listed.

Polymer	$\eta_c$ (J/g-K)	$h_{c,v}^0$ (kJ/g)	$\mu$ (%)	$T_p$ (°K)
HDPE	1486 ± 20	43.5 ± 0.1	0.1 ± 0.1	504 ± 1
PP	1130 ± 24	43.2 ± 0.2	0.0 ± 0.0	483 ± 1
HIPS	859 ± 4	37.8 ± 0.1	2.5 ± 0.2	452 ± 1
PA66	623 ± 34	29.4 ± 0.1	1.0 ± 0.1	475 ± 2
ABS	581 ± 14	37.0 ± 0.2	6.2 ± 0.3	454 ± 1
PC 2	539 ± 26	20.4 ± 0.2	22.5 ± 0.8	547 ± 2
PC 1	484 ± 13	20.4 ± 0.1	23.2 ± 0.2	545 ± 3
PMMA	475 ± 6	24.9 ± 0.1	0.0 ± 0.0	393 ± 2
PET	357 ± 16	16.8 ± 0.7	12.6 ± 1.5	459 ± 3
POM	267 ± 19	16.2 ± 0.0	0.0 ± 0.0	398 ± 6
PPS	248 ± 27	15.7 ± 0.1	44.0 ± 0.6	535 ± 1
PEI	201 ± 7	9.3 ± 0.2	51.3 ± 0.3	565 ± 1
PVC	129 ± 3	10.8 ± 0.2	18.8 ± 0.1	467 ± 4
FEP	57 ± 1	4.1 ± 0.0	0.0 ± 0.0	589 ± 1

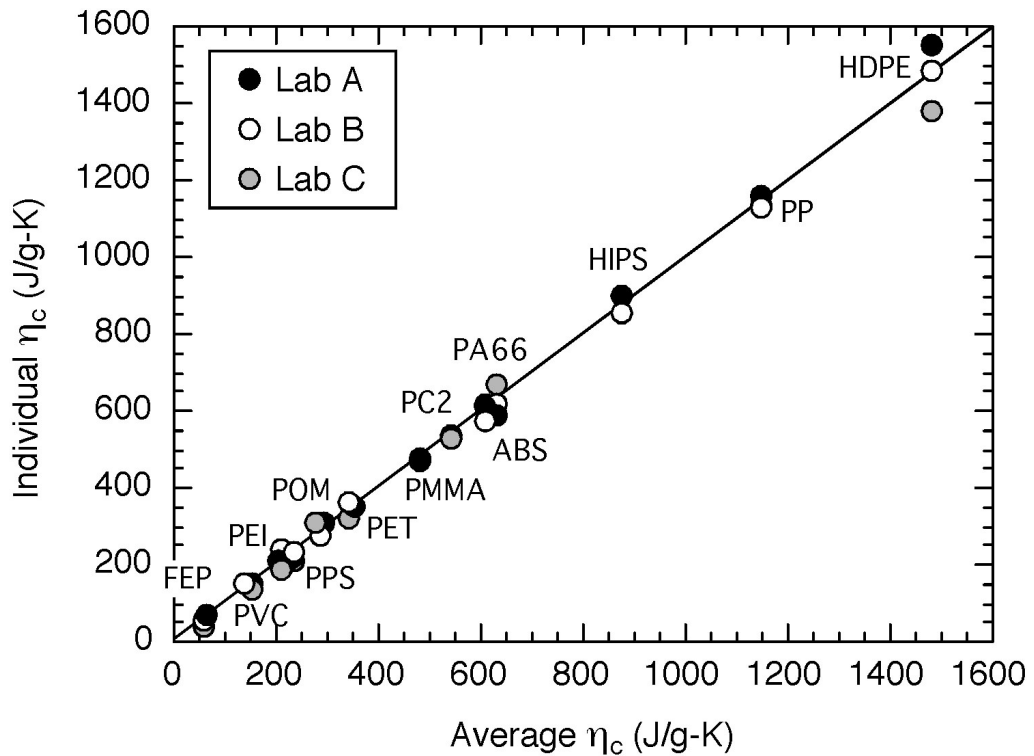


Figure 14. Comparison of individual and average heat release capacities from three different laboratories for the 14 polymers in table 3.

Using a TGA as the pyrolyzer was revisited using an instrument with a small internal volume and lower heating rates. Experiments were also conducted in which the combustor was attached to the furnace of a TGA (STA-851e, Mettler-Toledo) to thermally oxidize the evolved pyrolysis gases. Three to five samples of each polymer were tested. The HRR data were synchronized with the sample temperature by subtracting the transit time of the gases from the pyrolyzer (PCFC) or TGA furnace (STA) to the oxygen analyzer.

#### 2.4.1 Validation of Technique

To validate the PCFC method, the heat release capacities of 15 polymers, measured by PCFC, were compared to those measured for the same samples using a TGA coupled to a gas chromatograph (GC) and mass spectrometer (MS) to determine the fuel species [16,61,62]. In the TGA-GC/MS method of determining  $\eta_c$ , the thermal decomposition products at maximum mass loss rate were sampled, separated, and analyzed by GC/MS, and the resulting data used to compute the heat of complete combustion of the fuel gases  $h_{c,v}^0$  from their known or calculated heats of combustion and relative abundance

(mass fraction). The heat of combustion so determined is multiplied by the maximum value of the fractional mass loss rate, measured in the TGA at a constant heating rate (e.g., 10 K/min), to obtain the heat release capacity. The heat release capacities normalized to  $\beta = 1$  K/s measured by PCFC and TGA-GC/MS on samples of the same polymer are plotted on the ordinate and abscissa, respectively, in figure 15. The proximity of the data to the equivalence line indicates an accuracy of about  $\pm 16\%$  for  $\eta_c$  obtained by PCFC versus TGA-GC/MS, which is comparable to the experimental uncertainty of the TGA-GC/MS method.

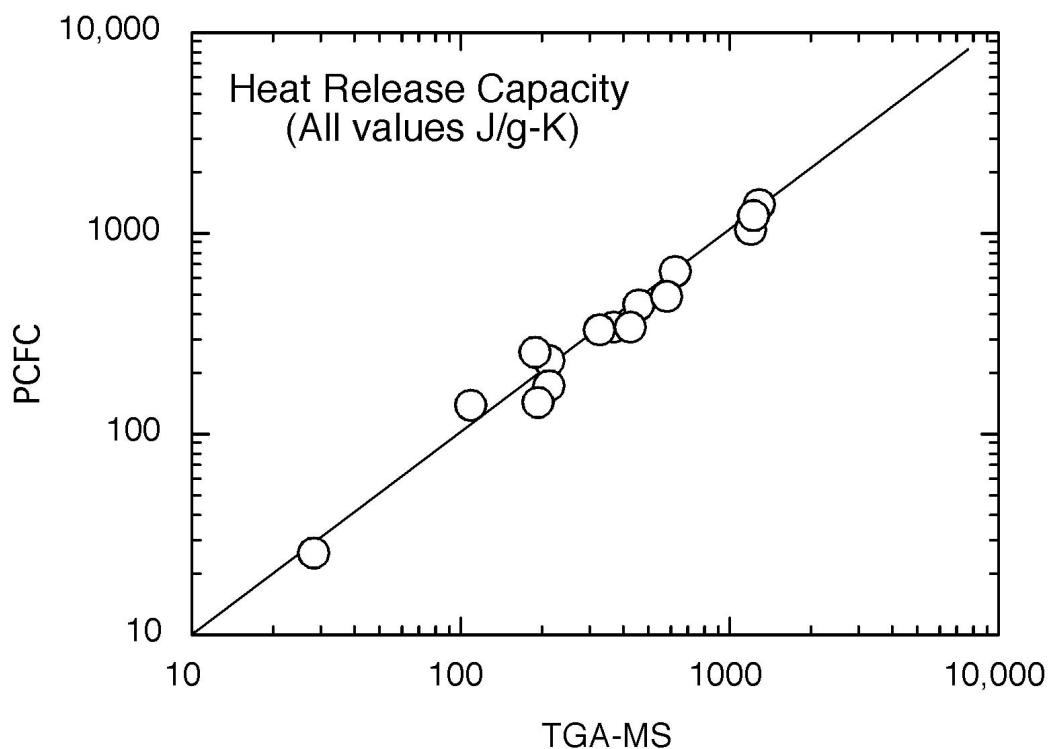


Figure 15. Comparison of heat release capacities obtained by Pyroprobe PCFC at  $\beta = 260$  K/min and TGA-GC/MS at  $\beta = 10$  K/min.

## 2.5 SUMMARY AND CONCLUSIONS

The development of PCFC and the MCC was an iterative process. The two main processes, pyrolysis and combustion, evolved through trial and error. The pyrolyzer initially started with ballistic heating of a 1 mg sample. Eventually it was determined that controlled, linear heating of a larger sample provided the most repeatable results. The pyrolyzer also developed from having a separate sample heater and heated interface to having the interface become the sample heater. Algorithms were developed to

control the heater with a single thermocouple method. Controlled sample heating coupled with plug flow enabled the oxygen and subsequent heat release rate to be synchronized with the temperature.

The combustor was initially a coiled tube with a long residence time to ensure the oxidation of any soot particles that may be formed during the polymer pyrolysis. Oxidation kinetic studies were performed with the coiled combustor on gases and polymer decomposition products. It was found that only a couple seconds were required to oxidize the volatile thermal decomposition products. A smaller combustor with a residence time of less than 10 seconds was developed. This new combustor design, incorporated with the new pyrolyzer in a single tube design, eliminated transfer lines and spawned the modern MCC.

Once the concept of PCFC was established, it had to be validated. Alternate methodologies were used to generate comparable results to independently verify the measurements. The PCFC was validated and several more MCC units were made. Once the MCC was in several different laboratories, tests for the repeatability and reproducibility could be performed. Good intra- and inter-laboratory results proved the PCFC concept to be a robust method for analyzing samples for their potential fire threat.

## CHAPTER 3

### MATERIAL PROPERTIES

### 3.1 OVERVIEW

For the purpose of fire and flammability, there are properties that are linked to the molecular structure of materials. These properties are used to describe material events through mathematical relationships. Material properties of interest, examined in this study, are used to characterize thermal stability and flammability properties. These small scale investigations of materials are then used to predict their role in full scale fires.

### 3.2 HEAT OF GASIFICATION

The heat of gasification ( $H_g$ ) is a thermodynamic quantity that is equal to the amount of energy required to gasify unit mass of material at a constant pressure.  $H_g$  depends on the initial temperature of material ( $T_{init}$ ) and final temperature of its gasification products ( $T_{final}$ ).  $H_g$  also depends on the composition of the products, which may potentially depend on the temperature history. Unfortunately, even for the most common polymers, the exact composition of the gasification products is usually unknown, is dependent on the pyrolysis conditions, and very difficult to measure. As a first order approximation, it is assumed that the composition is not affected by the rate at which material is heated.

The heat of gasification can be presented as a sum of contributions of heat capacity and heats of processes that occur when material is gasified:

$$H_g = \int_{T_{init}}^{T_{dec}} C_{mat} dT + H_{melt} + H_{dec} + \int_{T_{dec}}^{T_{final}} C_{prod} dT \quad (37)$$

$C_{mat}$  and  $C_{prod}$  are temperature dependent heat capacities of the material and products of its thermal decomposition.  $H_{melt}$  is the heat of melting.  $H_{dec}$  is the heat of decomposition, which also includes the heat of vaporization of volatiles formed during the decomposition. The decomposition and vaporization occur at  $T_{dec}$ . Samples are heated throughout decomposition, and for materials that char, it is assumed that the heat capacity of the char,  $C_{prod}$ , is the same as the starting material,  $C_{mat}$ . Therefore equation 37 can be simplified by assuming that  $C_{prod} \approx C_{mat}$ :

$$H_g = \int_{T_{init}}^{T_{final}} C_{mat} dT + H_{melt} + H_{dec} \quad (38)$$

Taking into account that an initial material and its decomposition products have identical elemental composition and similar chemical structures, this is a reasonable assumption. Furthermore, for most of the polymers, thermal decomposition occurs within a range of temperatures that is only 100-200°C wide, which means that  $T_{dec}$  and  $T_{final}$  are close. This makes  $C_{prod}$  contribution to  $H_g$  relatively small. It should be noted, however, that in the case of materials that decompose to produce a high yield of solid residue (char), the heat capacity of the residue may still play an important role in the pyrolysis or combustion.

The assumption of  $C_{prod} \approx C_{mat}$  has one more significant implication. The heat of decomposition becomes a temperature independent quantity (because of the conservation of energy). Thus, within this framework, the heat of gasification is a function defined by two material-specific constants,  $H_{melt}$  and  $H_{dec}$ , and temperature dependent heat capacity.

A methodology for determining parameters of this function using power-compensation differential scanning calorimetry has been developed and applied to a set of 10 non-charring and charring polymers. The results of the measurements have been verified against literature data. These parameters were used to obtain integral values of the heats of gasification for heating materials from room temperature through their decomposition. For most of the polymers studied, the contributions to the integral heats from heat capacity and melting were found to be approximately equal to the contributions from decomposition and vaporization.

The heat flow measurements were performed using a Perkin-Elmer DSC 7 with a flow-through cover. The sample and reference enclosures were ventilated with ultra high purity nitrogen at the rate of 35 cm<sup>3</sup>/min. The measurements were performed within 40 - 600°C temperature range.

The part of the DSC heat flow that is not associated with a sample, baseline heat flow, can be evaluated by performing an empty-sample-pan experiment at the same heating rate ( $dT/dt$ ). However, we found that the baseline changed significantly from experiment to experiment (even after many hours of equilibration). This instability was attributed to heat loss terms. Fortunately, the heat loss contribution can be evaluated during a DSC run by stopping the temperature ramp and measuring the heat flow at constant temperature ( $dT/dt = 0$ ).

In this study, this approach was used to measure heat loss contributions in both sample and empty-sample-pan (or baseline) experiments. The heating program consisted of  $5^{\circ}\text{C}/\text{min}$  temperature increases separated by 5 min long isothermal regions. The temperatures of the regions, which were  $100 - 350^{\circ}\text{C}$  apart, were selected carefully to make sure that the sample did not undergo any phase transition or decomposition during the isotherms. The heat loss contributions were assumed to have a linear dependence on temperature between measurement points and were subtracted from DSC heat flow curves. Subsequently, heat-loss-corrected baseline was subtracted from the corresponding heat-loss-corrected sample curve to obtain the sample heat flow dependence on temperature. The sample heat flow was divided by the heating rate and initial sample mass to cast it to the units of heat capacity. An example of unprocessed sample and baseline heat flow curves and resulting sample heat flow curves are shown in figure 16.

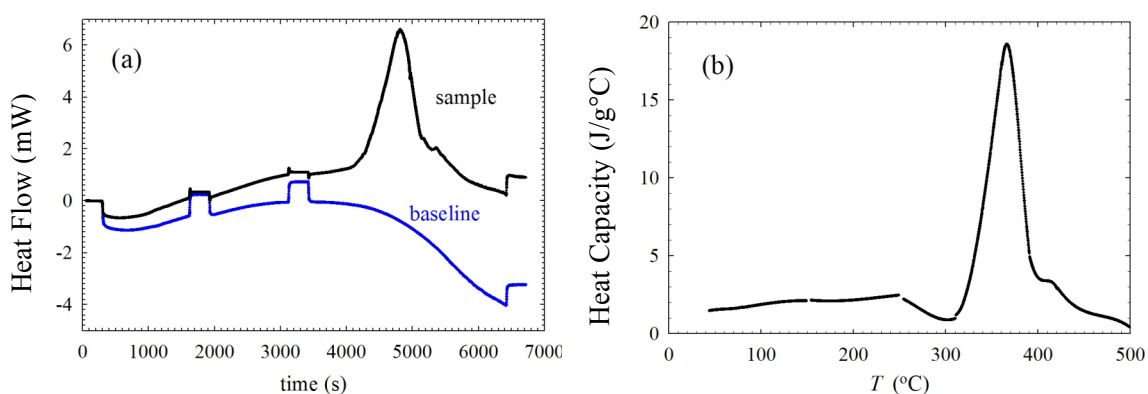


Figure 16. DSC heat flow curves obtained for a sample of poly(methylmethacrylate). Endothermic is positive. (a) Unprocessed sample and baseline curves. (b) Sample heat flow derived from the data shown in (a) and cast to the units of heat capacity

Several sample sizes, heating rates, and sample container configurations were tested. 2-4 mg samples heated at 5°C/min yielded the most reproducible results. The samples were cut into thin flat squares, placed into an aluminum pan, and covered by an aluminum lid, bent at approximately 135°. Small gaps between the lid and pan walls ensured that volatile decomposition products can escape readily. An empty aluminum pan with a bent lid was used as a reference. In the case of the samples containing halogens (i.e., samples of poly(vinylidene fluoride) and poly(vinyl chloride)), several experiments were performed using graphite pans with bent gold-covered copper lids. This was done to insure that potential chemical interactions of the decomposition products with container surfaces did not factor in the measured heat flows. Thermogravimetric analyses were performed using a Perkin-Elmer TGA 7.

The polymers used in this study were provided in the form of large (approximately 2 x 1 m) sheets, which were about 6 mm thick. The need for such large quantities arose from planned bench-scale flammability tests on the same materials.

### 3.2.1 Heat Capacity

Four DSC experiments, each consisting of a baseline and sample run, were performed for every polymer. Temperature dependencies of heat capacities were obtained by simultaneous least-square fitting of all four sample heat flow curves. Straight line fits (slope and intercept) of the data up to their glass transition with additional straight line fits after the transition were performed to describe the heat capacity behavior. The resulting parameters are given in table 4 where  $C_{LI}$  and  $C_{RI}$  are the slopes and  $C_{LO}$  and  $C_{RO}$  are the y-intercepts. The subscripts L and R refer to the equations of the line to the left and right of the glass transition temperature,  $T_{trans}$ . Taking into account that the structures of the materials used in these studies are not identical, the agreement is reasonable.

Table 4. Parameters describing the dependence of measured heat capacities on temperature where  $C_{LO}$  and  $C_{LI}$  are the slopes and y-intercept on the left of  $T_{trans}$  and  $C_{RO}$  and  $C_{RI}$  are the slopes and y-intercept on the right.

Polymer	$C_{LO}$ (J/g-°C)	$C_{LI}$ (J/g-°C <sup>2</sup> )	$T_{trans}$ (°C)	$C_{RO}$ (J/g-°C)	$C_{RI}$ (J/g-°C <sup>2</sup> )
poly(methylmethacrylate)	1.01	0.00858	130	1.78	0.00240
poly(oxymethylene)	1.11	0.00811	165	1.34	0.00275
polyethylene	1.41	0.00896	134	1.76	0.00508
polypropylene	1.38	0.01013	158	2.15	0.00247
polystyrene	1.10	0.00644	148	1.91	0.00072
polyamide 6,6	1.66	0.00573	262	2.41	0.00056
poly(ethylene terephthalate)	0.97	0.00453	253	1.72	0.00086
bisphenol A polycarbonate	1.05	0.00377	147	1.68	0.00134
poly(vinylidene fluoride)	0.98	0.00558	167	0.76	0.00467
poly(vinyl chloride)	0.42	0.01080	78	1.40	0.00091

### 3.2.2 Heat of Melting

Table 5 contains temperatures and heats of melting obtained by averaging of the data from individual sample heat flow curves. The uncertainties in  $\Delta H_{melt}$  are  $\pm 1$  standard deviation of the data. The temperatures of melting ( $T_{melt}$ ), which were assumed to correspond to the maxima of the melting peaks, are in good agreement with the melting points listed in reference [63]. The degrees of crystallinity, which were evaluated as the ratio of the measured heat of melting and the heat of melting of a fully crystalline polymer (see table 6), were also found to be within the expected ranges [63,64].

Table 5. Temperatures and heats of melting determined by DSC. Relative crystallinity was obtained by dividing the measured heat of melting by the literature value for a fully crystalline material [63].

Polymer	$T_{melt}$ (°C)	$\Delta H_{melt}$ (J/g)	$\Delta H_{melt.crystal}^*$ (J/g)	Relative Crystallinity (%)
poly(methylmethacrylate)	no melting peak observed			
poly(oxymethylene)	165	141 ±4	325	43
polyethylene	134	218 ±18	292	75
polypropylene	158	80 ±4	207	39
polystyrene	no melting peak observed			
polyamide 6,6	262	55 ±5	190	29
poly(ethylene terephthalate)	253	37 ±3	140	26
bisphenol A polycarbonate	no melting peak observed			
poly(vinylidene fluoride)	167	47 ±2	98	48
poly(vinyl chloride)	no melting peak observed			

\* The heat of melting of a fully crystalline polymer from reference [63]

### 3.2.3 Heat of Decomposition

The data on decomposition are summarized in table 6. While each material decomposed over a range of temperatures, a single characteristic temperature ( $T_{dec}$ ) corresponding to the maximum of the decomposition peak was recorded. Poly(vinyl chloride) was the only material that, according to a thermogravimetric analysis, had two distinct mass loss steps. The data in table 6 show results for each of these steps. As is the case with the data on melting, both  $T_{dec}$  and  $\Delta H_{dec}$  are averages of the values determined from individual sample heat flow curves. The uncertainties in  $\Delta H_{dec}$  are ±1 standard deviation.

Table 6. Temperatures and heats of decomposition determined by DSC. Literature values are also provided where available.

Polymer	$T_{dec}$ (°C)	$\Delta H_{dec}$ (J/g)	$\Delta H_{dec.lit}^*$ (J/g)
poly(methylmethacrylate)	366	870 ±200	800
poly(oxymethylene)	369	2540 ±300	--
polyethylene	478	920 ±120	670
polypropylene	447	1310 ±70	630
polystyrene	427	1000 ±90	820
polyamide 6,6	438	1390 ±90	560
poly(ethylene terephthalate)	433	1800 ±80	--
bisphenol A polycarbonate	499	830 ±140	--
poly(vinylidene fluoride)	475	2120 ±250	--
poly(vinyl chloride)	276	170 ±170	--
	475	540 ±390	--

\* The heat of decomposition from reference [65]

In general, there are no well established values for the heats of decomposition of polymers. One exception is poly(methylmethacrylate) for which  $\Delta H_{dec}$  can be calculated from the heat of polymerization and heat of vaporization of the monomer [65]. The calculated value, 800 J/g, compares favorably with the result of the present study, 870 J/g. Table 6 also contains the heats of decomposition measured by Frederick and Mentzer [65] using a heat flux DSC (a somewhat less direct technique that requires a calibration curve to convert measured temperatures to heat flow). Their heats of decomposition of poly(methylmethacrylate) and polystyrene are close to those obtained in this work. However, in the case of polypropylene and polyamide 6,6, their values are much lower. This could be due to several factors including the measured heat capacities and heats of melting being higher than the literature [63]. The materials themselves were not exactly the same as evidenced by the measured glass transition temperature of 262°C for polyamide 6,6 as compared to the literature [63] value of 50°C.

The parametric description of  $C_{mat}$  together with  $\Delta H_{melt}$  and  $\Delta H_{dec}$  can be used within the framework of a pyrolysis or combustion model to describe the thermal behavior of a

material. These parameters can also be substituted into equation 38 to obtain an integral value for the heat of gasification for specific initial and final temperatures. The values of  $\Delta H_g$  for  $T_{init} = 25^\circ\text{C}$  and  $T_{final} = T_{dec}$  are given in table 7 ( $T_{final} = 475^\circ\text{C}$  was used for poly(vinyl chloride)). This table also lists all contributions to the heats of gasification including the values of heat capacity integral (sensible heat).

$$\int_{T_{init}}^{T_{final}} C_{mat} dT = C_{L0}(T_{trans} - T_{init}) + \frac{C_{L1}}{2}(T_{trans}^2 - T_{init}^2) + C_{R0}(T_{final} - T_{trans}) + \frac{C_{R1}}{2}(T_{final}^2 - T_{trans}^2) \quad (39)$$

Note that the integration from  $T_{init} = 25^\circ\text{C}$  to  $T_{final} = T_{dec}$  involves extrapolation of the heat capacity dependencies beyond the temperature ranges of the fitted experimental data. This, together with the way in which parameters of these dependencies were obtained, made evaluation of the uncertainties in the sensible heat difficult. For simplicity, it was assumed that, for all polymers, these uncertainties are equal to the average relative uncertainty of  $\Delta H_{melt}$  and  $\Delta H_{dec}$ , which was found to be  $\pm 16\%$ . Absolute values of these uncertainties are given in table 7. Table 7 also contains uncertainties in the integral value of  $\Delta H_g$ , which were calculated by propagating errors [66] from the sensible heat,  $\Delta H_{melt}$ , and  $\Delta H_{dec}$ .

Table 7. Heats of gasification and components; integral heat capacity, heat of melting and heat of decomposition, as determined by DSC.

Polymer	$\int_{25^{\circ}\text{C}}^{T_{dec}} C_{mat} dT$ (J/g)	$\Delta H_{melt}$ (J/g)	$\Delta H_{dec}$ (J/g)	$\Delta H_g^{25^{\circ}\text{C}-T_{dec}}$ (J/g)
poly(methylmethacrylate)	740 ±120	0	870 ±200	1610 ±230
poly(oxymethylene)	690 ±110	141 ±4	2540 ±300	3370 ±320
polyethylene	1370 ±220	218 ±18	920 ±120	2510 ±250
polypropylene	1150 ±180	80 ±4	1310 ±70	2540 ±190
polystyrene	800 ±130	0	1000 ±90	1800 ±160
polyamide 6,6	1050 ±170	55 ±5	1390 ±90	2500 ±190
poly(ethylene terephthalate)	730 ±120	37 ±3	1800 ±80	2570 ±140
bisphenol A polycarbonate	910 ±150	0	830 ±140	1740 ±210
poly(vinylidene fluoride)	910 ±150	47 ±2	2120 ±250	3080 ±290
poly(vinyl chloride)	710 ±110	0	710 ±430*	1420 ±440

\* The sum of the heats of decomposition obtained for 2 decomposition steps

Some of the polymers used in this study did not vaporize completely and left a considerable amount of post-decomposition residue (char). The char yields ( $\mu$ ) and the temperatures at which they were measured ( $T_{char}$ ) are given in table 8 (this information was obtained from thermogravimetric analyses performed using the same heating programs as that used in the corresponding DSC experiments). The last column in table 8,  $L_g$ , is the integral heat of gasification (specified in table 7) that was renormalized per unit mass of volatilized material; i.e.,  $L_g = \Delta H_g / (1-\mu)$ . This quantity is frequently used in fire protection engineering calculations to assess material's response to external heat flux [67].

Table 8. Char yields at temperature,  $T_{char}$ , and char-weight-adjusted integral heats of gasification.

Polymer	$\mu$ (wt. fraction)	$T_{char}$ (°C)	$L_g$ (J/g)
poly(methylmethacrylate)	0	--	1610 ±230
poly(oxymethylene)	0	--	3370 ±320
polyethylene	0	--	2510 ±250
polypropylene	0	--	2540 ±190
polystyrene	0.03	550	1860 ±160
polyamide 6,6	0.03	500	2580 ±200
poly(ethylene terephthalate)	0.15	530	3020 ±160
bisphenol A polycarbonate	0.24	575	2290 ±280
poly(vinylidene fluoride)	0.38	600	4970 ±470
poly(vinyl chloride)	0.20	600	1780 ±550

### 3.3 HEAT OF COMBUSTION MEASUREMENTS

Oxygen consumption calorimetry measures the heat released by the burning of volatile polymer decomposition products [21], the net heat of complete combustion of which can be written

$$\Delta h_{c,v}^0 = \frac{\Delta h_{c,p}^0 - \mu \Delta h_{c,\mu}^0}{1 - \mu} \quad (40)$$

where  $\Delta h_{c,v}^0$ ,  $\Delta h_{c,p}^0$ , and  $\Delta h_{c,\mu}^0$  are the heats of complete combustion for the volatiles, polymer and char respectively and  $\mu$  is the char fraction. The effective heat of combustion,  $\Delta h_c^{eff}$ , is obtained by multiplying equation 40 by the combustion efficiency in the flame,  $\chi$ ,  $\Delta h_c^{eff} = \chi \Delta h_{c,v}^0$ . The heat of combustion of the volatile fraction can differ significantly from that of the polymer and the char, so polymer heats of combustion should not be used to calculate flaming combustion efficiency of materials.

New polymers with extremely low heat release rate in fires are being developed. Typically these materials tend to be char forming, thermally-stable polymers containing

a high degree of chemical bond unsaturation, aromaticity, and the heteroatoms—nitrogen, sulfur, silicon, phosphorus, and oxygen. The original work for the oxygen consumption principle was based on hydrocarbon polymers [19,68]. The objective of the present work was to measure and document the heats of combustion of some commercial, pre-commercial, and research polymers containing heteroatoms on the assumption that their decomposition products would also contain heteroatoms. The accuracy of the universal value of 13.1 kJ of heat per gram of O<sub>2</sub> for combustion thermally-stable, char-forming polymers and their decomposition products could then be determined. The heats of complete combustion of forty nine polymers were measured by the standard experimental procedure for determining gross and net calorific value using adiabatic oxygen bomb calorimetry and compared to the results of two different thermochemical calculations of the heat of combustion based on oxygen consumption, and, group additivity of the heats of formation of products and reactants. An additional theory was developed using molar group contributions to the heat of combustion.

### 3.3.1 Gross Heat of Combustion

The gross heat of combustion was measured in an oxygen bomb calorimeter (Model 1341, Plain Jacket Oxygen Bomb Calorimeter, Parr Instrument Co., Moline, Illinois) according to a standard procedure, ASTM D2382-88 [50]. A weighed sample of approximately 1 gram is placed inside a calibrated adiabatic bomb calorimeter with 1 milliliter of deionized water. A Chromel (chromium nickel alloy) wire is connected to the two electrodes in the pressure vessel (bomb) and placed in contact with the sample for ignition. The bomb is then assembled, sealed and purged twice by pressurizing to 0.5 MPa with pure (99.99%) oxygen then venting. The vessel is then pressurized with pure oxygen to 2.0 MPa for the test and placed inside a bath containing 2 liters of water in an insulated jacket. A motorized stirrer is placed inside the water bath to circulate the water around the bomb creating a uniform temperature. The temperature of the water is measured using a precision thermistor (Omega Model 5831A). The equilibrium temperature of the bath prior to the test is recorded as the initial temperature,  $T_0$ , in the experiment. The sample is then ignited by passing an electric current through the Chromel wire causing the sample to burn to completion in the high pressure oxygen. The temperature of the water bath rises a few degrees Celsius above the initial temperature, typically, and reaches a maximum value,  $T_{max}$ , which is recorded. The bath

temperature then slowly decreases due to convective heat losses to the environment. The gross heat of combustion of the hydrocarbon polymers was calculated from the sample mass,  $m$ , and the difference between the initial and maximum bath temperature,  $\Delta T_{max} = (T_{max} - T_0)$ , after correcting for the heat of combustion of the wire. Three replicates are performed for each sample.

For samples containing atoms besides C, H, and O, combustion products in addition to  $\text{CO}_2$  and  $\text{H}_2\text{O}$  are formed and corrections must be made for the heat of formation and / or heat of solution of these compounds. An ignition correction ( $e_1$ ) is made for the heat contribution from burning the nickel chromium alloy fuse wire. The wire is weighed before and after combustion and the weight loss is multiplied by the heat of combustion of the alloy, 5.8576 kJ/g, to calculate the ignition energy,  $e_1$ . A correction for the heat of product formation ( $e_2$ ) and heat of solution of the products ( $e_3$ ) is required for samples which contain elements other than carbon, hydrogen, and oxygen. A pH titration is performed to determine the heats of formation and solution (in water) of the additional products, typically mineral acids. In practice the bomb is rinsed with distilled water and the acidic washings are titrated with 0.1 M NaOH to the appropriate pH break point using a bench top pH meter (Orion Model 611). Some of the acids formed are HF,  $\text{HNO}_3$ ,  $\text{H}_3\text{PO}_4$ , or  $\text{H}_2\text{SO}_4$  depending on the element(s) in the sample. The number of moles of mineral acid formed during combustion are calculated from the stoichiometric endpoint multiplied by the energy of formation of the relevant compound to calculate the heat of formation,  $e_2$ , and heat of solution,  $e_3$ , corrections for the acids formed [69]. The gross heat of combustion,  $Q_c$ , is then calculated as

$$Q_c = (C \Delta T_{max} - e_1 - e_2 - e_3) / m \quad (41)$$

The average standard error for this technique is 0.51 kJ/mol.

### 3.3.2 Net Heat of Combustion

There are no direct methods for measuring the net heat of combustion which is the gross heat of combustion minus the latent heat of vaporization of the water produced during the reaction. The net or lower heat of combustion is relevant to flaming combustion where water is in the gaseous state at flame temperatures of  $\approx 1000$  K. As a result, the

latent heat of water at 298 K is subtracted from the gross heat of combustion because this amount of heat is required to maintain the combustion product water in the gaseous state. The gross heat of combustion measured by the procedure stated above is corrected for the heat of vaporization of the water formed during the combustion to give the net heat of combustion,  $\Delta h_c$ , using the relation in equation 42 as described by Babrauskas [20].

$$\Delta h_c = Q_c - 21.96w_H \quad (42)$$

where  $w_H$  is the weight fraction of hydrogen in the sample and  $\Delta h_c$ ,  $Q_c$  are in kJ/g.

### 3.4 HEAT OF COMBUSTION CALCULATIONS

#### 3.4.1 Oxygen Consumption

Several approaches have been taken to calculate the heat of combustion based on the molecular structure of a material [43,70,71]. Oxygen consumption is a commonly used method for calculating the heat of combustion from known chemical structures [17] and for measuring heat release rates in flaming combustion tests [19,72]. Another method for obtaining the heat of combustion is by using the heat of formation of the products and the reactants [13,73,74]. These different methods have been examined [60] and found to agree to within  $\pm 5\%$ .

Heats of combustion calculated from oxygen consumption rely on the empirical observation that a wide range of organic compounds, including polymers, have approximately the same heat of complete combustion per gram of diatomic oxygen consumed

$$E = \Delta h_c \left[ \frac{n_p M_p}{n_{O_2} M_{O_2}} \right] = \frac{\Delta h_c}{r_o} = 13.1 \pm 0.7 \text{ kJ/g-O}_2 \quad (43)$$

where  $\Delta h_c$  is the net heat of complete combustion of the sample with all products in their gaseous state,  $n_p$  and  $M_p$  are the number of moles and molecular weight of the molecule or polymer repeat unit, respectively,  $n_{O_2}$  is the number of moles of  $O_2$

consumed in the balanced thermochemical equation, and  $M_{O_2} = 32$  g/mol is the molecular weight of diatomic oxygen. In equation 43, the quantity  $r_o = [n_{O_2}M_{O_2} / n_pM_p]$  is the stoichiometric oxygen-to-fuel mass ratio. This calculation was performed for polymers in several studies [19,60] to determine  $E$  from known atomic compositions and measured heats of combustion. Inverting equation 43 shows that the net heat of complete combustion of a polymer is simply calculated if the atomic composition of the polymer is known so that the balanced thermochemical reaction equation can be written.

$$\Delta h_c = E \left[ \frac{n_{O_2}M_{O_2}}{n_pM_p} \right] = Er_o \quad (44)$$

### 3.4.2 Heat of Formation

The calculation of the heat of the combustion can also be carried out using the principle of molar additivity of the heats of formation of the combustion products and reactants [13]. The concept is derived from the fact that enthalpy ( $H$ ) is a state function and therefore its change in any process is independent of the path from reactants to products. Thus, the overall enthalpy of a reaction is simply the sum of the enthalpies of the component reactions. In practice, the heat of combustion of the reaction can be calculated by subtracting the heat of formation of the products from the heat of formation of the reactants

$$\Delta h_c = \sum_i n_p \Delta h_{f,p}^0 - \sum_i n_r \Delta h_{f,r}^0 \quad (45)$$

where  $p$  and  $r$  denote products and reactants, respectively, in the standard state at temperature, 298 K. For polymeric reactants the molar heat of formation can be estimated from the tabulated molar contributions of the chemical groups which constitute the monomer or repeat unit.

Although the heat/enthalpy of combustion is a negative (exothermic) quantity, positive (absolute) values are listed in the following tables and figures for convenience. Appendix A is a compilation of all of the polymeric materials tested listed by chemical and/or common name, abbreviated name, and Chemical Abstracts Service (CAS) registry numbers where available. Trade names and manufacturer or sample source are

listed in Appendix A along with atomic composition of the polymer repeat unit. The gross heat of combustion ( $Q_c$ ), net heat of combustion ( $\Delta h_c$ ), and the net heat of combustion divided by the oxygen-to-fuel mass ratio ( $\Delta h_c/r_o$ ) are listed for each polymer. Values for  $Q_c$  are averages of triplicate determinations  $\pm 1$  standard deviation. When no standard deviation is shown,  $Q_c$  is the result of a single test.

The quantity,  $E = \Delta h_c/r_o$  is the heat released by combustion per unit mass of oxygen consumed in a fire where all combustion products are in their gaseous state. An accurate and representative value of  $E$  is thus important for calculating the heat released during flaming combustion of polymers from oxygen consumption measurements. Values for  $E$  from the present work are listed in the last column of Appendix A for comparison to the universal value used in oxygen consumption fire calorimetry,  $E = 13.1$  kJ of heat released per gram of diatomic oxygen ( $O_2$ ) consumed.

Table 9. Gross heat of combustion values for polymers measured by oxygen bomb calorimetry and calculated by a group contribution method and net heat of combustion values obtained by adjusting the gross for the heat of vaporization of water and calculated by oxygen consumption calorimetry.

	Polymer	Bomb Calorimeter Gross (kJ/g)	Group Contribution Gross (kJ/g)	Bomb Calorimeter Net (kJ/g)	Oxygen Consumption Net (kJ/g)
1	Polyoxymethylene	17.39	18.20	15.93	13.97
2	Polytetrafluoroethylene	6.68	7.57	6.68	8.38
3	Polyvinylalcohol	23.31	26.20	21.31	23.82
4	Polyethylene	47.74	46.00	44.60	44.91
5	Polydimethylsiloxane	19.53	N/A	17.75	16.99
6	Polypropylene	45.80	46.00	42.66	44.91
7/8	Polymethylmethacrylate	26.81	27.50	25.05	25.15
9/10	Poly(1,4-phenylenesulfide)	29.01	30.80	28.20	27.17
11	Poly(2,6-dimethyl-1,4-phenyleneoxide)	34.21	34.70	32.75	33.19
12	Polystyrene	43.65	41.30	41.96	40.31
13	Polyethyleneterephthalate	24.13	24.10	23.22	21.83
14	Epoxy novolac	31.37	32.06	29.73	34.93
15	Poly(1,4-phenyleneethersulfone)	25.42	25.70	24.66	22.59
16	Poly(1,4-butanediol terephthalate)	27.91	26.90	26.71	24.77
17	Poly(hexamethyleneadipamide)	30.90	32.80	28.76	30.61
18	Poly(etherketone)	31.07	31.45	30.17	29.94
19	Poly(benzoyl-1,4-phenylene)	38.35	35.90	37.37	33.77
20	Poly(p-phenylene benzobisoxazole)	29.18	29.00	28.62	25.98
21	Poly(m-phenyleneisophthalamide)	26.45	29.30	25.53	27.30
22	Aramid-arylester copolymer	25.27	29.30	24.35	27.30
23	Poly(p-phenyleneterephthalamide)	26.92	29.30	26.00	27.30
24	Poly(amideimide)	24.97	26.75	24.31	24.61
25	Poly(acrylonitrile-butadiene-styrene)	39.84	39.43	38.07	38.24
26	Bisphenol E Cyanate Ester	29.38	N/A	28.38	28.58
27/28	Polycarbonate of bisphenol-A	31.30	31.20	30.09	29.71
29	Hexafluorobisphenol A Cyanate Ester	18.71	N/A	18.25	19.55
30	Bisphenol-A Cyanate Ester	29.92	N/A	28.81	29.40
31	Bisphenol-A Epoxy	32.50	33.50	30.94	30.79
32/33	Poly(etheretherketone)	31.28	31.50	30.37	29.84
34	Tetramethylbisphenol F Cyanate Ester	31.23	N/A	29.94	30.82
35	Poly(etherketoneketone)	31.15	31.50	30.27	30.04
36	Polybenzimidazole	31.65	33.40	30.79	31.30
37	Polyimide	26.03	26.30	25.45	24.14
38/39	Phenol Novolac Cyanate Ester	29.63	N/A	28.79	28.00
40	Bisphenol M Cyanate Ester	34.39	N/A	33.06	32.82
41/42	Polysulfone	30.46	31.20	29.37	28.93
43	Poly(bisphenol-A/aniline) benzoxazine	34.89	35.80	33.46	34.03
44	Polyhexafluorobisphenol-A-TPPO	26.50	N/A	25.74	25.26
45/46	Polyetherimide	29.33	30.00	28.44	28.32
47	Polyester of HBA-HNA	26.54	26.81	25.80	25.47
48	Polyethylenenaphthylate	25.92	N/A	25.01	25.09
49	XU-71787	33.64	N/A	32.14	35.44

Table 9 lists experimental values for the gross and net heats of combustion measured in the present study by oxygen bomb calorimetry. The fourth column in table 9 lists the gross heats of combustion calculated from molar group additivity of the heats of formation according to the method described. Column 5 lists the net heats of combustion calculated from the gross heat of combustion using equations 42 and 44. Column 6 of table 9 lists the net heats of combustion calculated from oxygen consumption with the universal value,  $E = 13.1 \text{ kJ/g-O}_2$ . Data for identical polymers from different sources have been combined in tables 9 and 10. The values for the heats of combustion calculated using the oxygen consumption and group contribution methods are very close to the experimental values obtained from bomb calorimeter experiments. Also, values for the gross heat of combustion that were obtained experimentally show good agreement to literature values [20] for the same material.

Table 10. Comparison of experimental gross heats of combustion to literature values for several polymers [20].

Polymers	$Q_c$ (kJ/g) (Present Study)	$Q_c$ (kJ/g) [Ref. 20]
Polycarbonate of bisphenol-A	31.3	31.0
Polyethylene	47.7	46.2
Polyethyleneterephthalate	24.1	22.2
Polyhexamethyleneadipamide	30.9	29.6
Polymethylmethacrylate	26.8	26.6
Polyphenyleneoxide	34.2	34.6
Polypropylene	45.8	46.4
Polystyrene	43.7	42.5
Polyvinylalcohol	23.3	25.0

Figure 17 is a plot of the net heats of combustion calculated from oxygen consumption *versus* experimental net heats of combustion obtained from oxygen bomb calorimetry in table 10. The average relative deviation for the oxygen consumption technique for estimating the net heat of combustion was found to be  $\pm 4.4\%$  (shown by the error bars in figure 17).

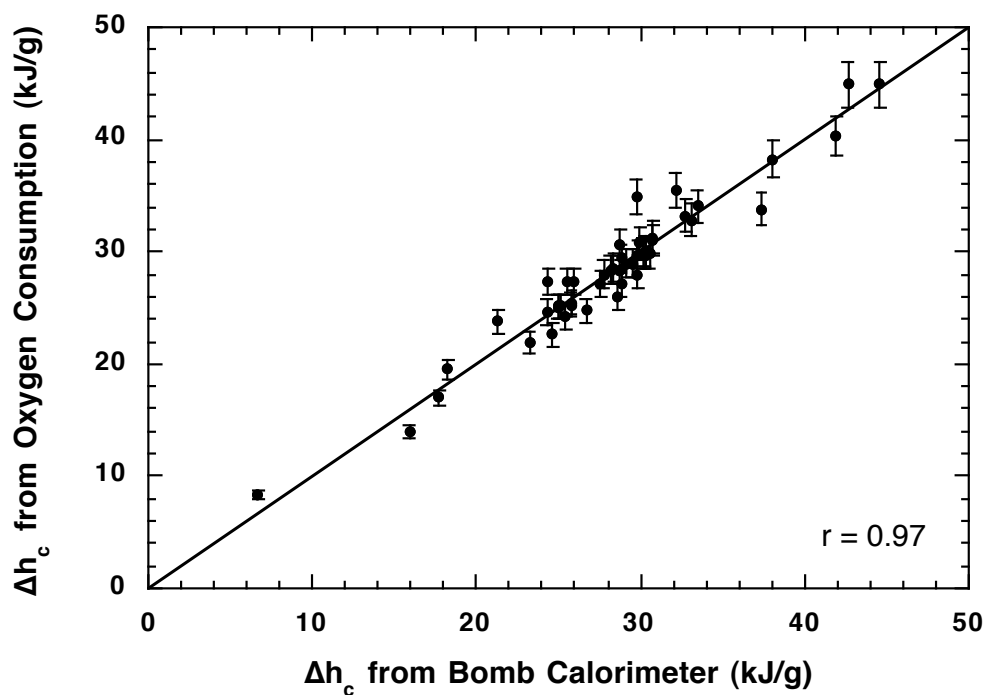


Figure 17. Correlation plot of the calculated heats of combustion using oxygen consumption versus experimental net heats of combustion for 49 polymers (line is  $y = x$ ). Error bars shown are the 4.4% average relative deviation for the calculation.

Figure 18 is a plot of the gross heats of combustion calculated from group additivity of the heats of formation *versus* experimental gross heats of combustion obtained from oxygen bomb calorimetry in table 10. The average relative deviation for the group contribution technique for estimating the gross heat of combustion was found to be  $\pm 4.2\%$  (shown by the error bars in figure 18).

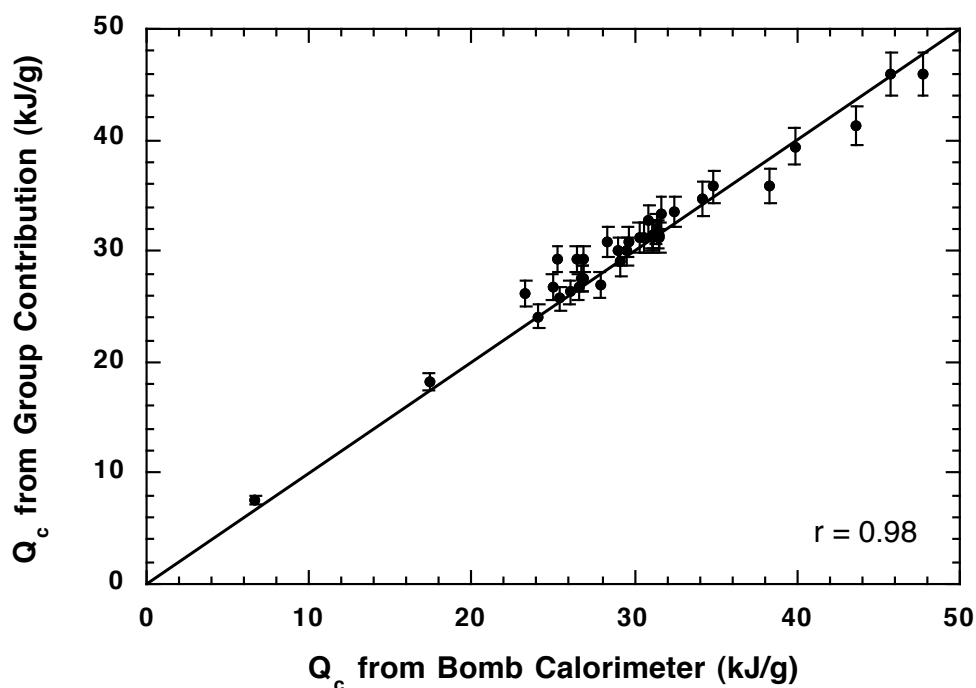


Figure 18. Correlation plot of the calculated heats of combustion using group contributions versus experimental gross heats of combustion for 38 polymers (line is  $y = x$ ). Error bars shown are the 4.2% average relative deviation for the calculation.

### 3.4.3 Molar Group Contributions

The additivity of molar group contributions to the physical and chemical properties of materials is the basis of an empirical methodology for relating chemical structure to properties [43,70,71]. The early work in this area focused on calculating heats of combustion from the individual atoms comprising small molecules. However, performing calculations for large (polymer) molecules based on the interactions of the individual atoms can prove to be very difficult. A simpler approach to correlating polymer chemical structure with properties is to group the atomic contributions into characteristic structural elements (e.g.,  $-\text{CH}_3$ ), determine the value of the group contribution to the property of interest parametrically, and add these group contributions according to their mole fraction in the polymer repeat unit. This method has been used to relate the chemical structure of polymers to their thermal, chemical, optical, and mechanical properties, as well as flammability, with excellent results [43,70,71].

Other methods involve compiling structural group contributions and correction factors for their adjacent bonds [75]. This method for deriving the heat of combustion is very accurate but difficult to perform and is only applicable to linear hydrocarbon molecules. A simpler, more accurate method has been developed for calculating the heat of combustion under standard conditions using molar group additivity.

#### 3.4.3.1 Heat of Combustion Molar Group Contribution Theory

An empirical approach was taken to derive values for the structural group contributions to the heat of combustion. This simple approach does not take into account interactions between the structural groups that are defined here. The molar heat of complete combustion  $\Delta H_c$  is a thermodynamic property and should be calculable from the molar group contributions of the structural components. Assume that there is a molar heat of combustion,  $H$ , with units of kJ/mol, in which each chemical group  $i$  in the polymer contributes according to its mole fraction,  $n_i$ , in the repeat unit,

$$H = \sum_i n_i H_i \quad (46)$$

with  $H_i$ , the molar heat of combustion of component  $i$ . Since,

$$n_i = \frac{N_i}{\sum_i N_i} \quad \text{and} \quad M_o = \sum_i n_i M_i = \frac{\sum_i N_i M_i}{\sum_i N_i} \quad (47)$$

where  $N_i$  and  $M_i$  are the number of moles and molar mass, respectively, of group  $i$  in the polymer having repeat unit of molar mass  $M_o$ , the heat of combustion can be expressed on a mass basis.

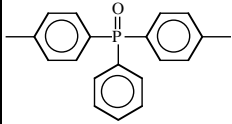
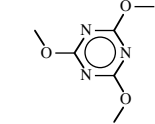
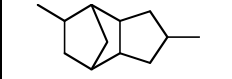
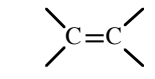
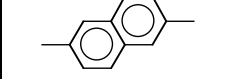
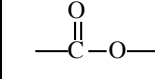
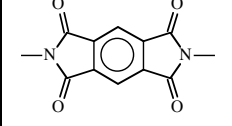
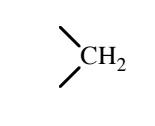
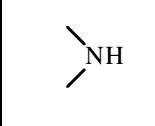
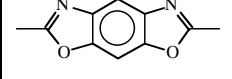
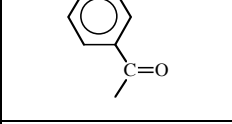
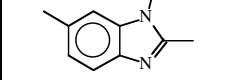
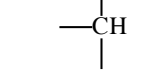
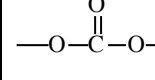
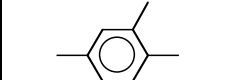
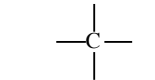
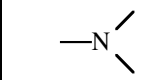
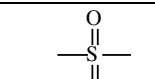
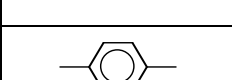
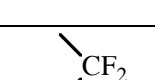
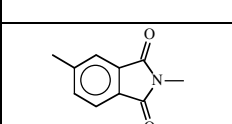
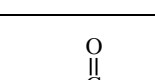
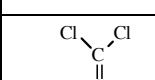
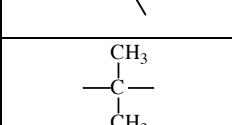
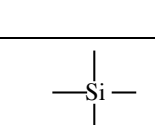
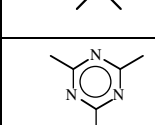
$$\Delta H_c = \frac{H}{M_o} = \frac{\sum_i n_i H_i}{\sum_i n_i M_i} = \frac{\sum_i N_i H_i}{\sum_i N_i M_i} \quad (48)$$

In practice, the largest chemical groups listed in the table 11 are used to calculate the heat of combustion of the molecule. The sum of the molar group contributions is

divided by the molecular weight of the molecule or polymer repeat unit to yield the specific heat of combustion.

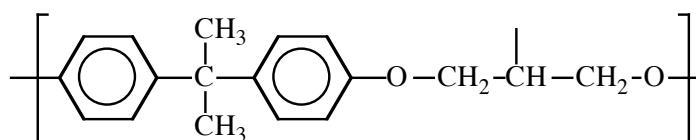
Measured heat of combustion values for 66 polymers [60] and 78 small molecules [20,76] with known chemical structure have been used to generate the additive molar group contributions in table 11. The molar group contributions were obtained by treating the  $H_i$  as adjustable parameters in the linear system of equations for materials with known chemical structures and measured  $\Delta H_c$ . The optimization calculation continued until the sum of the squares of the relative error between the measured  $\Delta H_c$  and calculated values was a minimum. The calculation converged rapidly to the unique  $H_i$  listed in table 11 which were independent of initial estimates. Molar group contributions derived from a single material are marked with an asterisk (\*) to indicate that these are not optimized values. Measured and calculated heats of combustion for the 66 polymers and 78 small molecules are plotted against one another in figure 19.

Table 11. Structural groups and their molar contributions to the gross heat of combustion.

Structural Group, <i>i</i>	$H_i$ (kJ/mol)	Structural Group, <i>i</i>	$H_i$ (kJ/mol)	Structural Group, <i>i</i>	$H_i$ (kJ/mol)
	9845*		939	—CF <sub>3</sub>	213
	4955*		781	—H	190
	4889	—CH <sub>3</sub>	775		112
	4343*		670		77
	3964*	—C≡N	548	—NO <sub>2</sub>	0
	3725*	—CH <sub>2</sub> -O—	522*	—Cl	-43
	3444*		518		-78*
	3186		431		-100
	3130		338	—OH	-108
	2871		328	—O—	-132
	2746	—S—	311	—F	-230
	2653		259		NA
	2294		219		NA

### 3.4.3.2 Sample Calculation

Table 12 shows an example of the thermochemical calculation of the heat of combustion from additive molar group contributions for a ring-opening polymerization of the diglycidyl ether of bisphenol A (BPA epoxy). This polymer has the repeat unit structure



The polymer repeat unit is comprised of six basic chemical groups and the heat of combustion is calculated from the associated  $N_i$ ,  $M_i$ , and  $H_i$  as follows.

Table 12. Calculation of heat of combustion of BPA epoxy using molar group contributions.

Structural Group, $i$	$N_i$	$M_i$ (g/mol)	Group Value, $H_i$ (kJ/mol)	$N_i M_i$ (g)	$N_i H_i$ (kJ)
	1	12.011	431	12.011	431
	1	13.0189	518	13.0189	518
	2	14.0268	670	28.5036	1340
	2	15.0347	775	30.0694	1550
	2	76.0976	2653	152.1952	5306
	2	15.9994	-132	31.9988	-264
			Sum:	267.7969	8881

The molar heat of combustion, obtained by summing the group contributions according to their mole fraction is then divided by the molar mass of the repeat unit to give the heat of combustion in units of kJ/g. The predicted value of 33.16 kJ/g compares well with the measured value of 32.50 kJ/g for this particular polymer.

$$\Delta H_c = \frac{\sum_i N_i H_i}{\sum_i N_i M_i} = \frac{8881 \text{ kJ}}{267.797 \text{ g}} = 33.16 \text{ kJ / g}$$

Molecules that can be described by several different group combinations should use the largest groups listed for calculating the heat of combustion.

Since the molar group contributions are derived from experimental data they should correlate well with measured heats of combustion. In fact, calculated and measured heats of combustion for over 140 compounds agree to within an average relative deviation of  $\pm 2.5\%$ .

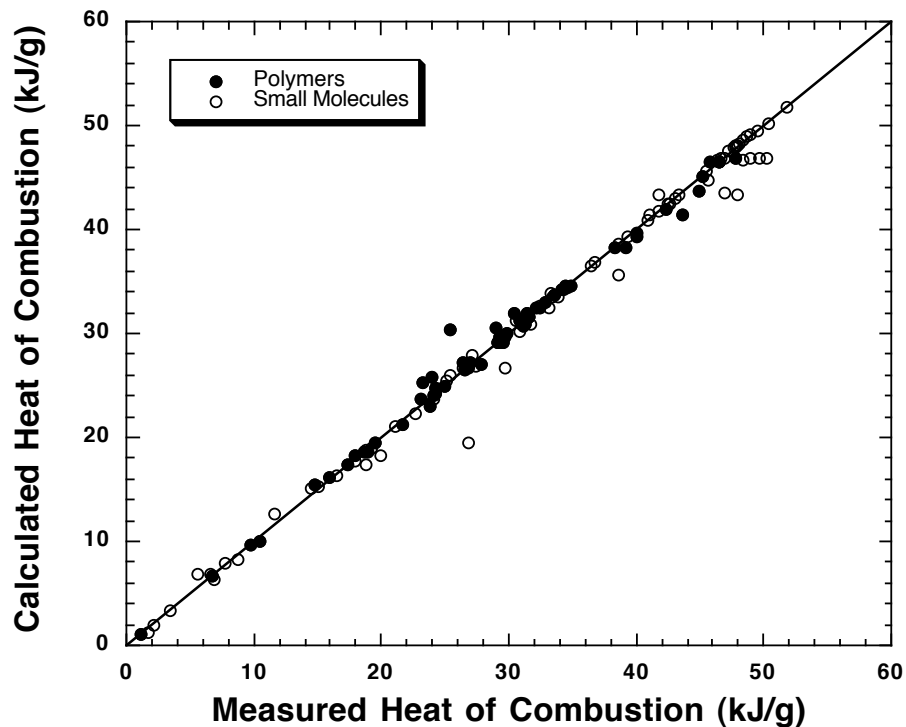


Figure 19. Plot of the heat of combustion values calculated using molar group contributions versus the measured for 66 polymers and 78 small molecules.

Re-evaluation of the constant used for calculating the heat release rates of burning polymers based on oxygen consumption has been updated to include high performance plastics. A value of  $E = 13.10 \pm 0.78 \text{ kJ/g-O}_2$  was found for the net heat of combustion per gram of diatomic oxygen consumed from the data for all of the polymers in

Appendix A (n = 48). Included are the halogenated, phosphorus-, sulfur-, and, nitrogen-containing materials. The mean  $E$  value from this study is identical to the universal value used in oxygen consumption calorimetry, although the coefficient of variation of 6.0 percent is somewhat higher than the 5 percent usually reported for oxygen consumption calorimetry. Regardless, the uncertainty in  $E$  is significantly lower than the reported 15 percent uncertainty in peak heat release and mass loss rates in oxygen consumption fire calorimetry measurements [77] and will not be a factor in the accuracy of a heat release rate test.

Thermochemical calculations to estimate the net heat of combustion from the stoichiometric amount of oxygen consumed in a complete combustion reaction are simple to perform if the atomic composition of the polymer is known *a priori*. The average relative deviation of the experimental and calculated heats of combustion from oxygen consumption thermochemistry, using  $E = 13.1 \text{ kJ/g-O}_2$ , is 4.4 percent for all of the polymers in table 9 (n = 48).

Thermochemical calculations for estimating the gross heat of combustion from heats of formation of products and reactants for the polymers listed in table 5 have an average relative deviation of 4.2 percent from the experimental (bomb) values (n = 38). Excluded from the comparison were the 6F-ETPP polymer, polydimethylsiloxane, polyethylenenaphthylate, XU-71787 and other cyanate esters for which the group contributions for the phosphine oxide, siloxane, naphthyl, norbornene, and cyanurate, respectively, were unknown or unavailable. Thus, thermochemical calculations of the gross heat of combustion from molar group additivity of the heats of formation of products and reactants achieves better accuracy than calculations based on oxygen consumption for the polymers examined in this study. This is not surprising since the group contributions to the heats of formation used in this study were originally determined from the gross heats of combustion of materials with known composition.

Additive molar contributions to the gross heat of complete combustion for 37 structural groups have been determined from data for 66 polymers and 78 small molecules with known chemical structure. The group contribution method improves upon previous techniques by providing a simpler and more accurate method for calculating the heat of combustion of chemical compounds.

### 3.5 HEAT RELEASE CAPACITY

Prerequisite to any structure-property correlation is the ability to identify and reproducibly measure the intrinsic property of interest. In the area of polymer flammability, no single material property has correlated with fire performance, nor does any test measure fire performance unambiguously because burning rate, ignitability, flammability, and heat release rate are not intrinsic properties. Rather, they are extrinsic quantities resulting from the reaction of a macroscopic polymer sample to a severe thermal exposure. Because the sample size in a flammability or fire test is orders of magnitude larger than the chemical process zone [6,26,27], where the burning takes place, heat- and mass-transfer dominate the fire response. Thus, an intrinsic material property for use by scientists in designing fire-resistant polymers is not obtainable from standard fire or flammability tests. The heat release capacity [21-23], has been identified which appears to be a good predictor of the fire response and flammability of polymers. A stand-alone method for directly measuring the heat release capacity has been reported [14,78,79].

#### 3.5.1 Molar Group Contributions to Heat Release Capacity

The solid-state thermochemistry of flaming combustion [21-23] reveals a material fire parameter that has the units (J/g-K) and significance of a heat (release) capacity, expressed previously in terms of the measured quantities in equations 24 and 25.

$$\eta_c = \frac{h_c^0(1 - \mu)E_a}{eRT_p^2} \quad (49)$$

The heat release capacity,  $\eta_c$ , is a combination of thermal stability and combustion properties, each of which is known to be calculable from additive molar group contributions [13]. The component material properties are the heat of complete combustion of the pyrolysis gases,  $h_c^0$  (J/g); the weight fraction of solid residue after pyrolysis or burning,  $\mu$  (g/g); the global activation energy for pyrolysis,  $E_a$  (J/mole); and the temperature at the peak mass loss rate,  $T_p$  (K), in a linear heating program at constant rate,  $\beta$  (K/s). The constants in equation 49 are the natural number  $e$  and the gas constant  $R$ . Equation 49 shows the heat release capacity to be a particular function of

thermal stability and combustion properties, each of which is known to be calculable from additive molar group contributions [13]. Consequently,  $\eta_c$  itself is a material property, should be calculable from the same (or similar) molar groups as the component properties as long as there are no interactions between the chemical structural units. Proceeding with this assumption of group additivity, and the postulate that for a polymer repeat unit of molar mass  $M$  there is a molar heat release capacity  $\Psi$  with units of J/mol-K whose functional form is equation 49 but with the thermal stability and combustion properties written as molar quantities,  $H$ ,  $V$ ,  $E$  and  $Y / M$  in place of  $h_c^o$ ,  $(1-\mu)$ ,  $E_a$  and  $T_p$ , respectively. If each chemical group  $i$  in the polymer adds to the component molar properties according to its mole fraction  $n_i$  in the repeat unit

$$\Psi = \frac{HV E}{eR (Y/M)^2} = \frac{\left(\sum_i n_i H_i\right) \left(\sum_i n_i V_i\right) \left(\sum_i n_i E_i\right)}{eR \left(\sum_i n_i Y_i / M_i\right)^2} \quad (50)$$

with  $H_i$ ,  $V_i$ ,  $E_i$ ,  $Y_i$ , and  $M_i$  the molar heat of combustion, mole fraction of fuel, molar activation energy, molar thermal decomposition function [13], and molar mass of component  $i$ , respectively. Expanding the summations in equation 50 and retaining only the non-interacting terms for which  $i = j = k \dots$  (i.e., neglecting terms containing products and quotients with mixed indices)

$$\Psi = \sum_i n_i \frac{H_i V_i E_i}{eR (Y_i/M_i)^2} = \sum_i n_i \Psi_i \quad (51)$$

Equation 51 shows that there is a molar group contribution to the heat release capacity  $\Psi_i$  that adds according to its mole fraction in the repeat unit of the polymer. If  $N_i$  and  $M_i$  are the number of moles and molar mass, respectively, of group  $i$  in the polymer having repeat unit molar mass  $M$

$$n_i = \frac{N_i}{\sum_i N_i} \quad \text{and} \quad M_o = \sum_i n_i M_i = \sum_i \frac{N_i}{\sum_i N_i} M_i$$

then the heat release capacity on a mass basis is

$$\eta_c = \frac{\Psi}{M} = \frac{\sum_i n_i \Psi_i}{\sum_i n_i M_i} = \frac{\sum_i N_i \Psi_i}{\sum_i N_i M_i} \quad (52)$$

Equations 50 through 52 provide the physical basis for an additive heat release capacity function, but the values of the molar contributions of chemical groups must be derived empirically (i.e., experimentally). To this end, the heat release capacities of more than 200 polymers with known chemical structure have been measured using the measurement technique described below and these experimental values have been used to generate over 40 group contributions [80,81].

### 3.5.2 Experimental Determination of Heat Release Capacity

A pyrolysis-combustion flow calorimeter [14,78,79] was used for all experiments. The quantities measured in the test are the kinetic heat release rate  $\dot{Q}_c$  (W/g); the heat release capacity  $\eta_c$  (J/g-K) calculated from the peak kinetic heat release rate and the linear heating rate of the sample; the total heat released by complete combustion of the pyrolysis gases  $h_c^0$  (J/g); and the residual mass fraction  $\mu$  (g/g) after the test.

Pyrolysis-combustion flow calorimeter (PCFC) data for the kinetic heat release rate of polyethylene (PE), polypropylene (PP), polystyrene (PS), an acrylonitrile-butadiene-styrene terpolymer (ABS), polymethylmethacrylate (PMMA), polyethyleneterephthalate (PET), polyetheretherketone (PEEK), and polybenzimidazole (PBI) are shown in figure 20, horizontally shifted for clarity. Dividing the maximum kinetic heat release rate (W/g) measured during the test (peak height in figure 20) by the constant sample heating rate ( $\beta = 4.3$  K/s in these tests) gives the heat release capacity of the polymer in units of J/g-K. Figure 20 illustrates the range of heat release values obtained for different materials. A higher peak HRR and total HR translates to a material being more flammable in a fire. The linear polymers with aliphatic structures tend to be the most flammable. As the aromaticity and conjugation of the polymer structure increases, the thermal stability increases, and the amount of fuel available decreases. High performance polymers with highly aromatic polymer backbones show the highest thermal stability and lowest flammability.

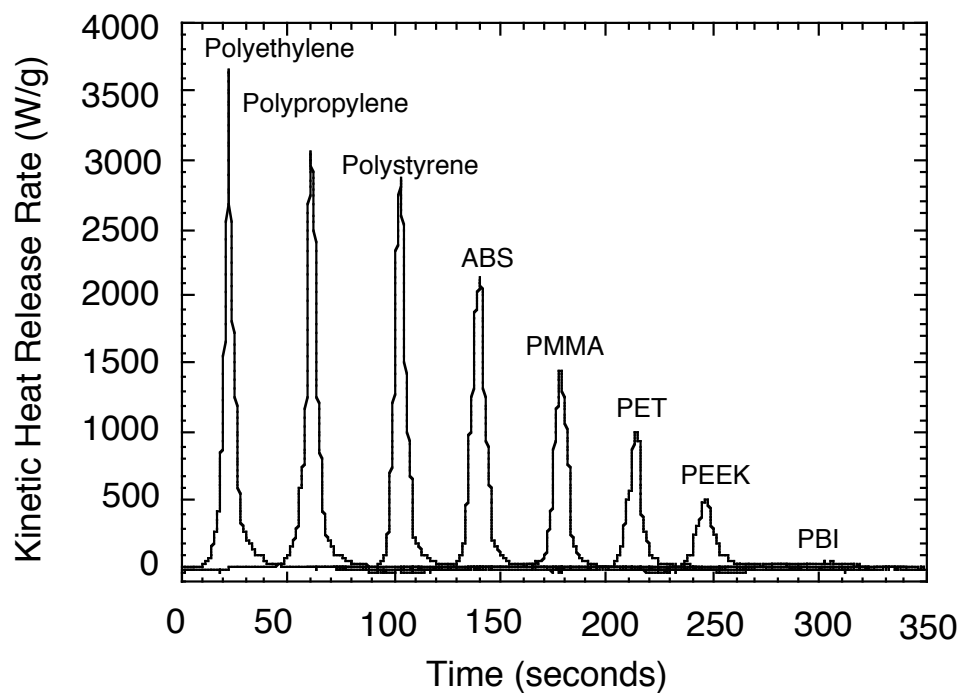


Figure 20. Kinetic heat release rate data for several polymers measured in the Pyroprobe PCFC (horizontally shifted for clarity).

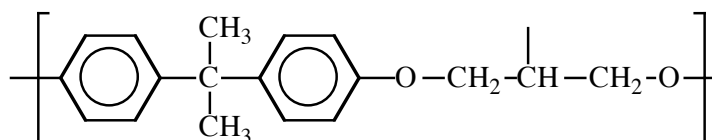
Measured heat release capacities for more than 100 polymers with known chemical structure are shown in Appendix B. This data has been used to generate the group contributions shown in table 13. The molar group contributions were obtained by treating the  $\Psi_i$  as adjustable parameters in the linear system of equations (equation 52) for polymers with known chemical structures and measured  $\eta_c$ . The optimization calculation continued until the sum of the squares of the relative error between the measured  $\eta_c$  and the value calculated from group contributions was a minimum. The calculation converged rapidly to the unique  $\Psi_i$  listed in table 13 which were independent of initial estimates.

Table 13. Structural groups and their molar contribution to the heat release capacity. (Molar group contributions derived from a single polymer are marked with an asterisk (\*) to indicate that these are not optimized values).

Group	Contribution (kJ/mol-K)	Group	Contribution (kJ/mol-K)	Group	Contribution (kJ/mol-K)
	118*		7.7		-20.0
	74.0		4.18		-22.0
	68.4		1.9		-22.1
	53.2		-0.23		-23.3*
	30.6		-8.7		-34.7
	28.9		-10.9*		-36.0*
	28.8		-11.6		Pendant: -39.1 Backbone: -13.5
	28.3		-13.8		-43.0*
	26.6		-13.9*		-50.0
	22.5		-15.0		-53.5*
	16.7		-17.7		-66.7
	14.2		-18.0		-74.0
	9.95		-18.9*		-76.7
	8.0		-19.8		

### 3.5.3 Calculation of Heat Release Capacity

The following example illustrates the calculation of heat release capacity from molar group contributions for a diglycidylether of bisphenol A (BPA epoxy) cured by anionic ring opening polymerization. This polymer has the repeat unit chemical structure



The polymer repeat unit is comprised of six basic chemical groups and the heat release capacity is calculated from the associated  $N_i$ ,  $M_i$ , and  $\Psi_i$  for these groups listed in table 14. First, the molar heat release capacity is obtained by summing the group contributions according to their mole fraction in the repeat unit.

Table 14. Group contributions used in the calculation of the heat release capacity of bisphenol-A epoxy.

Chemical Group, $i$	$N$	$M_i$ (g/mol)	$\Psi$ (kJ/mol-K)	$N_i M_i$ (g/mol)	$N_i \Psi$ (kJ/mol-K)
	1	12	30.0	12	30.0
	1	13	32.0	13	32.0
	2	14	14.0	28	28.0
	2	15	23.0	30	46.0
	2	76	28.2	152	56.4
	2	16	-9.0	32	-18.0
			Sum:	267	174.4

Dividing the molar heat release capacity by the molar mass of the repeat unit gives the heat release capacity on a mass basis in units of J/g-K.

$$\eta_c = \frac{\Psi}{M} = \frac{\sum_i n_i \Psi_i}{\sum_i n_i M_i} = \frac{\sum_i N_i \Psi_i}{\sum_i N_i M_i} = \frac{174.4 \text{ kJ/mole-K}}{267 \text{ g/mole}} = 653 \text{ J/g-K}$$

The predicted value of 653 J/g-K compares favorably with the measured value of 657 J/g-K for this polymer as determined in this study.

Figure 21 is a plot of calculated versus measured heat release capacities for 80 polymers for which optimized  $\Psi_i$  were determined. The correlation coefficient between measured and predicted heat release capacities is  $r = 0.96$  and the average relative error is  $\pm 15\%$ .

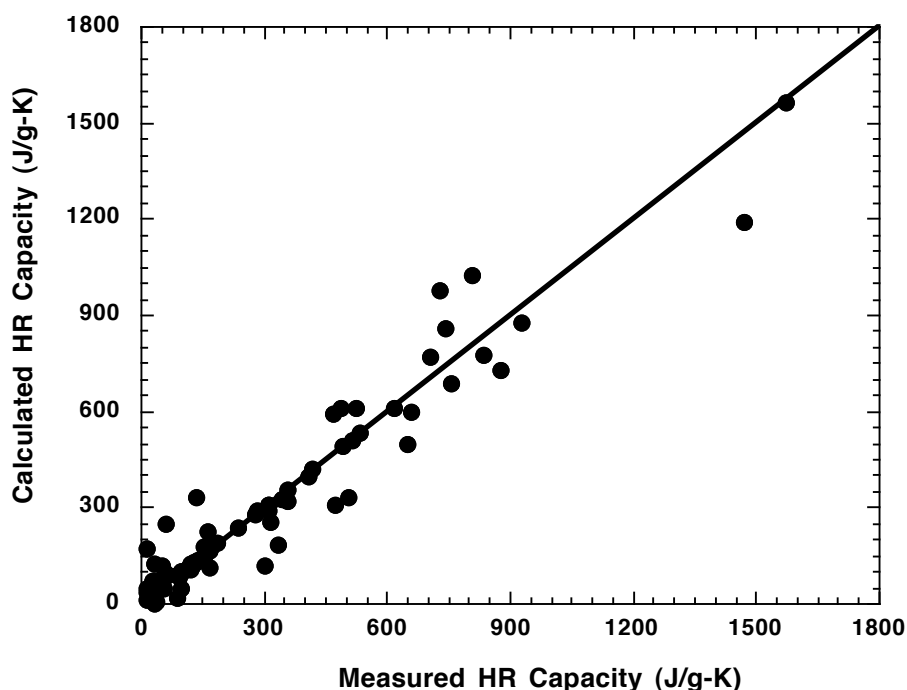


Figure 21. Heat release capacity values calculated using molar group contributions versus measured heat release capacities for 80 pure polymers.

### 3.6 CHAR HEAT OF COMBUSTION

Experimental data for thermal oxidation of the pyrolysis gases evolved from PC in the TGA at a heating rate  $\beta = 20 \text{ K/min}$  is shown in figure 22. Residual mass plotted on the left ordinate shows that thermal decomposition begins at about  $450^\circ\text{C}$ , and that 24% of the original mass is left as char at the end of the experiment ( $700^\circ\text{C}$ ). The heat of

combustion of the thermal decomposition products is obtained by dividing the specific HRR,  $Q(t)$ , by the specific mass loss rate ( $m_0^{-1} dm/dt$ ) at each time  $t$  during the test. Figure 22 shows that the  $h_{c,v}^0$  values ranged from 20 - 25 kJ/g for the primary decomposition step at  $535^\circ \pm 25^\circ\text{C}$  generating monomer fragments (phenol, bisphenol, diphenylcarbonate) and a solid primary char [82-84]. The primary char decomposes in a second step to a carbon-rich solid over a broad temperature range with the evolution of methane gas [84], which is consistent with the data in figure 22 showing that the heat of combustion of the gases evolved between  $550^\circ - 700^\circ\text{C}$ , is on the order of methane ( $h_{c,v}^0 = 50 \text{ kJ/g}$ ).

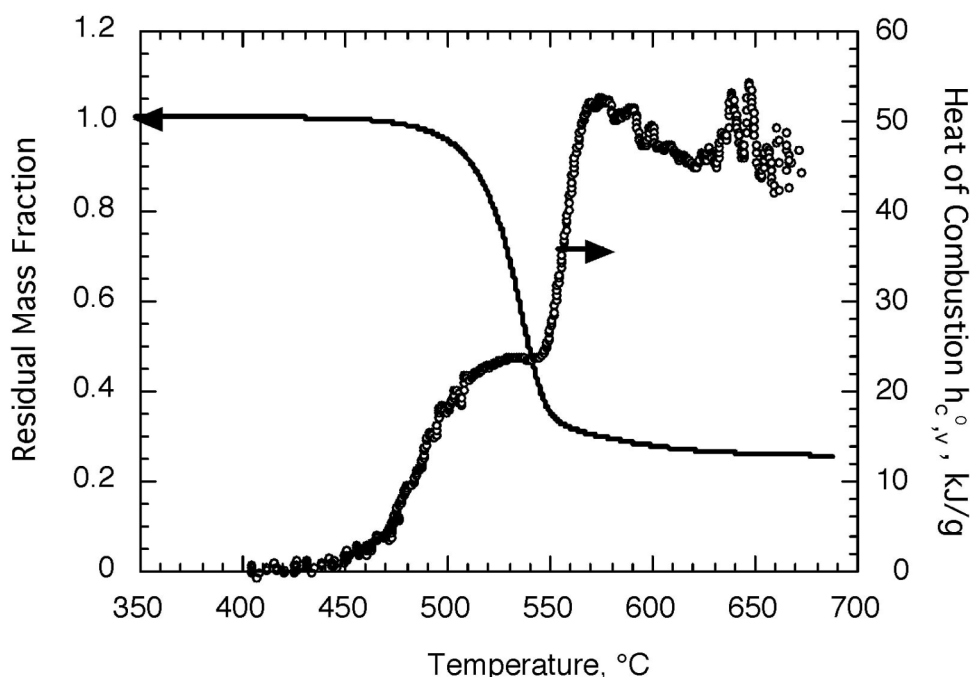


Figure 22. Residual mass fraction and heat of combustion of pyrolysis gases versus temperature for test of polycarbonate in TGA PCFC at  $\beta = 20^\circ\text{C}/\text{min}$ .

### 3.6.1 Oxidative Pyrolysis Combustion Flow Calorimetry

Figure 23 shows experimental data from oxidative pyrolysis-combustion flow calorimetry (oPCFC) in the apparatus of figure 10 for a 1 mg sample of polycarbonate at  $\beta = 5 \text{ K/s}$ . Oxidation of the sample gases in the combustor and the delayed oxidation of the solid char in the pyrolyzer during an air purge are shown as separate processes. The area under the  $Q(t)$  versus time curve is the net heat of complete combustion of polycarbonate,  $H_c^0 = 29.1 \text{ kJ/g}$  in this case. Table 15 compares data for the net heat of

combustion of several polymers obtained by oxygen bomb calorimetry [17,20] and oPCFC. The accuracy of the oPCFC method, characterized by the average relative deviation of its results from the corresponding oxygen bomb calorimetry measurements, is about 3%. This has been shown to give comparable results for a sample size of a couple milligrams for the oPCFC compared to a sample size of 1 gram for the oxygen bomb calorimeter tests. This method is a good way to estimate the net heat of combustion when limited material is available.

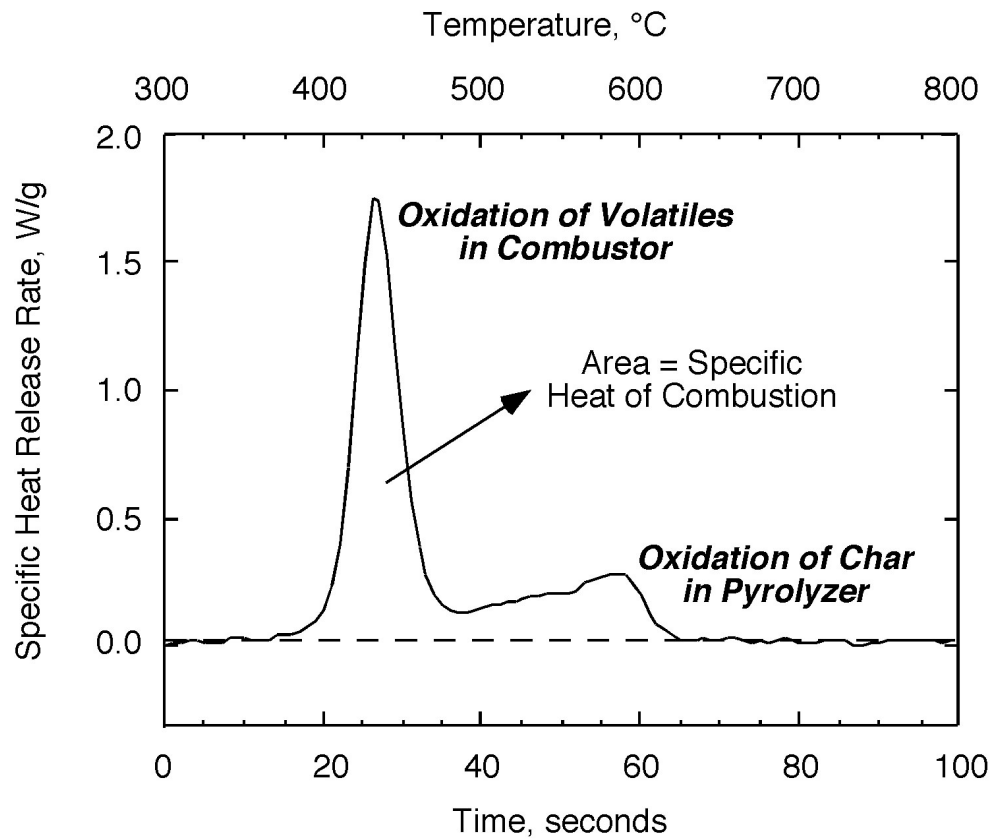


Figure 23. Specific HRR of polycarbonate versus time and temperature obtained by oPCFC (oxidation of gases in combustor and solid char in pyrolyzer are shown as separate processes).

Table 15. Net heat of combustion of charring ( $\mu \neq 0$ ) and non-charring ( $\mu = 0$ ) polymers obtained by oxygen bomb calorimetry and oxidative pyrolysis-combustion flow calorimetry (oPCFC).

Polymer ( $\mu$ , kg/kg)	ASTM D 2015 (MJ/kg)	oPCFC (MJ/kg)	Relative Deviation (%)
Polyethylene (0)	43.3	43.5	0.5
Polystyrene (0)	39.8	39.4	-1.0
Polymethylmethacrylate (0)	24.9	25.0	0.4
Polyoxymethylene (0)	15.9	16.0	0.6
Polybutyleneterephthalate (0.02)	26.7	26.3	-1.5
Polyethyleneterephthalate (0.13)	21.8	23.2	6.4
Polycarbonate (0.23)	29.8	29.1	-2.3
Polyaramide fiber (0.36)	27.8	28.1	1.1
Polyetheretherketone (0.47)	30.2	30.9	2.3
Phenolic Triazine (0.67)	29.8	29.5	-1.0

### 3.7 SUMMARY AND CONCLUSIONS

Material properties are essential to characterize flammability performance. These values are also needed for use in thermochemical calculations and for modelling flammability. Test methodologies to generate values that describe the solid state processes as well as the gas phase processes were discussed.

Heats of gasification were determined by DSC where the heat capacity, heat of melting and heat of decomposition were summed to provide a value for a material. This value describes the amount of energy it takes to gasify a material, thereby providing the fuel for a fire.

Values for the heat of combustion were measured. Thermochemical calculations that predict the heat of combustion were explored and a new, simple molar group contribution method was derived. In addition the  $E$  value, widely used in fire science testing, was re-examined for materials that contain hetero-atoms other than carbon and

hydrogen. It was found that the already established value was applicable to all modern organic polymers and small molecules.

The heat release capacity was examined as a material property. It was shown that the quantity can be calculated from thermal stability and combustion properties. A group contribution method for calculating this quantity was derived. A fairly good correlation between the measured and calculated values was shown which further justifies the heat release capacity as a material property.

The heat of combustion is a material property that is widely used in fire and flammability calculations. An alternate method of PCFC was examined where the sample is degraded in air instead of nitrogen. This method does not leave a carbonaceous char and values obtained are similar to those obtained using oxygen bomb calorimetry. In addition to providing an alternate method for obtaining the heat of combustion, values for the amount of fuel retained in the char can be calculated when coupled with the traditional PCFC method.

## CHAPTER 4

### MATERIAL STUDIES

## 4.1 OVERVIEW

This chapter is a compilation of material studies for thermosetting polymer systems. Evaluations consist of characterizing the liquid resins for processability using rheology and differential scanning calorimetry. The cure chemistry was examined using DSC, and infrared spectroscopy. Mechanical properties were evaluated using rheology and mechanical testing. Thermal analysis was performed using TGA, rheology, infrared analysis, and MCC. Flammability testing was performed using cone calorimetry, OSU, bomb calorimetry, and MCC.

Materials examined in these studies fall into several groups. Epoxy systems with copolymers and catalysts were evaluated. A series of cyanate esters were also evaluated. Cyanate esters are of interest due to their facile-processing characteristics and addition cure mechanism that produces no volatiles [85]. They are also of interest due to their high strength, thermal stability, and high char yield when burned [86-90]. Combinations of epoxies with cyanate esters were also examined. Chlorinated versions of the epoxies and cyanate esters and their blends are also included in the studies. Chlorinated versions of these polymers are desirable for applications where extreme fire resistance is required. Blending the resins allows for customization of properties such as glass transition temperature, mechanical properties, and adhesion while reducing the cost. Several other commercial and experimental samples were included for baseline values and for comparison.

Samples were tested as neat resins, cured in plaques. Composite panels were made in single ply configurations as well as multi layered structural panels. Single-layer specimens (lamina) for fire testing were prepared by hand lay-up. Structural laminates were fabricated from liquid resins and woven glass fabric by hand lay-up or vacuum-assisted resin transfer molding (VARTM).

## 4.2 REACTIONS / PROCESSING

### 4.2.1 Viscosity and Processing

Isothermal viscosities of liquid resins were measured as the complex viscosity on a rheometer (RDA II, Rheometrics) using 50-mm (2-inch) parallel plates with a 0.5-mm

(0.020-inch) gap at a strain of 10% in dynamic time sweep mode at 1 Hz at different set-point temperatures in the range of 25° to 100°C.

Resin viscosities varied over a wide range. Several common resins were tested for comparison to literature values and were found to be within the reported ranges [91]. The BPACE and the BPCCE resins are crystalline at room temperature and have melting points of 92° and 75°C, respectively, as determined by differential scanning calorimetry (DSC). Once the resin is melted, it remains liquid until a nucleation site is introduced. The recrystallization of the BPACE is rapid and exothermic, while the BPCCE is slow, on the order of days. The liquid resins have very different viscosities. The BPACE has a very low viscosity, while the BPCCE is fairly viscous at room temperature. Figure 24 shows a plot of the resin viscosity as a function of set point temperature.

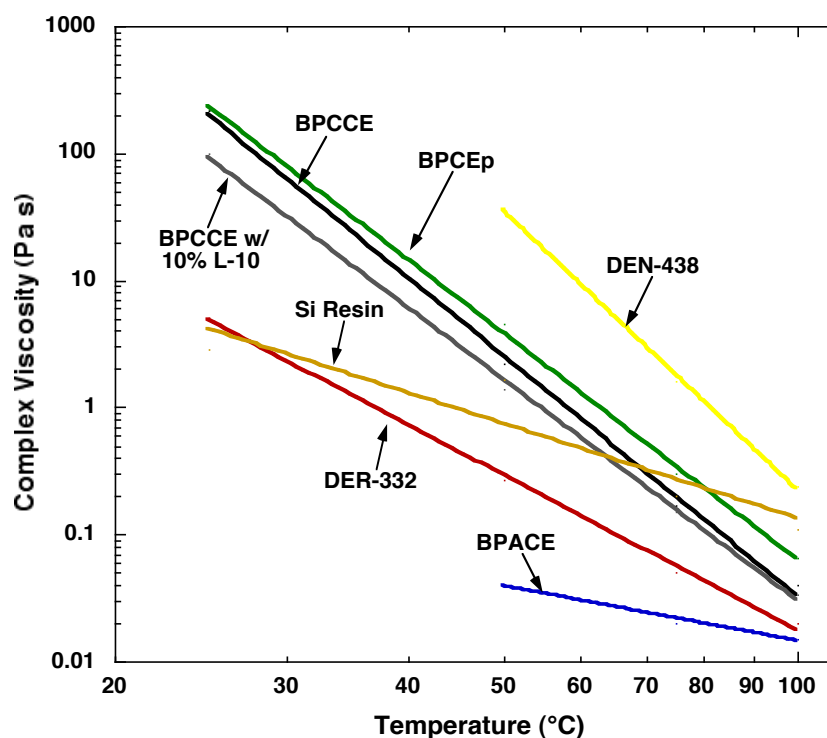


Figure 24. Viscosity of several thermoset resins as a function of temperature obtained using parallel plate rheology.

The viscosity of the BPCCE fell in the middle of the resins tested. Adding 10 percent of bisphenol F cyanate ester (L-10, Vantico) reduced the viscosity of the BPCCE by more than a factor of two. Values for the viscosity of the BPACE at 25°C could not be

obtained due to the sample recrystallizing, and the viscosity of the novolac epoxy resin (DEN-438) at 25°C was too high and was out of the range of the transducer. An experimental silicone resin was tested without the addition of the hardener to prevent curing during the test.

#### 4.2.2 Epoxies

The DGEBC and DGEBA epoxies were polymerized by four different mechanisms:

- 1) Anionic ring opening polymerization using catalytic amounts of 2-ethyl-4-methylimidazole.
- 2) Addition polymerization with aliphatic (triethylenetetramine) and aromatic (4,4'-methylenedianiline) amines.
- 3) Catalyzed phenolic cure with the parent phenols (bisphenols A and C).
- 4) The dicyanate ester resin derived from bisphenol C.

Table 16. Resins and hardeners used for comparing BPA to BPC epoxy and cyanate ester systems.

	Trade name [CAS Registry No.]	Supplier	Equiv. Weight (g/eq)
<b>EPOXY RESINS</b>			
diglycidylether of bisphenol-A (DGEBA)	DER-322 [001675-54-3]	Dow Chemical	174
diglycidylether of bisphenol-C (DGEBC)	RD-98-238 [N/A]	Ciba Specialty Chemicals	208
	XPR-1015 [N/A]	Pacific Epoxy Polymers	209
<b>HARDENERS</b>			
2-ethyl-4 methyl-imidazole (2,4-EMI)	Imicure 24 [931-36-2]	Air Products and Chemicals	N/A
triethylenetetramine (TETA)	DEH-24 [000112-24-3]	Dow Chemical	24
4,4'-methylenedianiline (MDA)	Curithane 103 [101-77-9]	Acros	102
4,4'-isopropylidenediphenol (BPA)	Bisphenol A [80-05-7]	Sigma Chemical	114
1,1-dichloro-2,2-bis(4- hydroxyphenyl)ethylene (BPC)	Bisphenol C RD98-237 [14868-03-2]	Ciba Specialty Chemical	141
cyanate ester of bisphenol- C (CEBPC)	RD-98-228 [N/A]	Ciba Specialty Chemical	165

Epoxies (DGEBA and DGEBC) were warmed to melting and the curing agents added and mixed until homogeneous. The resin-hardener mixture was then poured into preheated molds and cured in a forced convection oven to make thermal, mechanical, and flammability test samples, or was hand impregnated into E-glass fabric (0.22-mm thick, 6781 S. Glass “Grieger” weave 8HS 8.95oz/sq yd, BGF Industries Inc.) and cured in a Carver press under contact pressure to make single-ply glass lamina for heat release rate testing in fire calorimeters. The formulations and cure schedules were as follows.

2-Ethyl-4-methyl imidazole: Two parts by weight of EMI-24 per hundred parts resin (phr) was added to each of the DGEBA and DGEBC epoxies and samples were cured at 100°C for 16 hrs and 150°C for 2 hours.

Triethylenetetramine: DEH-24 was added to DGEBA (14.0 phr) and DGEBC (13.5 phr) at 85°C and the samples cured in an oven at 50°C for 16 hours followed by 3 hours at 150°C.

4,4'-Methylenedianiline: MDA was added to DGEBA (58.6 phr) and DGEBC (56.4 phr) and samples cured at 100°C for 16 hours, 125°C for 2 hours, and 175°C for 16 hours.

Bisphenols A and C: Bisphenol A (66 phr) was added to DGEBA with 2% triphenylphosphine catalyst. Bisphenol C (78 phr) was added to DGEBC epoxy and 2 % w/w triphenylphosphine was added as a catalyst. Both formulations were cured 16 hours at 150°C and 24 hours at 200°C.

Cyanate ester of bisphenol C: The cyanate ester of bisphenol C (CEBPC) was added at 40 mole percent (53 phr) to the DBEBC epoxy and cured for 1 hour at 100°C and 16 hours at 175°C.

The heats of polymerization per mole of epoxide,  $\Delta H_{polym}$ , obtained by the DSC. The measured exothermic heat of polymerization of the DGEBC and DGEBA per mole of epoxide group is  $\Delta H_{polym} = 86 \pm 13$  kJ/mol for the EMI, TETA, MDA, BPA/BPC hardeners. This value is in the range  $\Delta H_{polym} = 106 \pm 20$  kJ/mol [92] reported for epoxide reactions. The heat of polymerization of the CEBPC hardener,  $\Delta H_{polym} = 120$  kJ/mole-epoxide, is significantly higher than for the other hardeners because of the heat

liberated by the cyclotrimerization reaction of the cyanate ester to form the cyanurate ring and the subsequent cyanurate-epoxy reaction to form the oxazoline [93] as shown in figure 25. Another method described by Bauer and Bauer [94] suggests a rearrangement of the cyanurate to the isocyanurate followed by its cleavage and subsequent reaction with the glycidylether to form an oxazolidone.

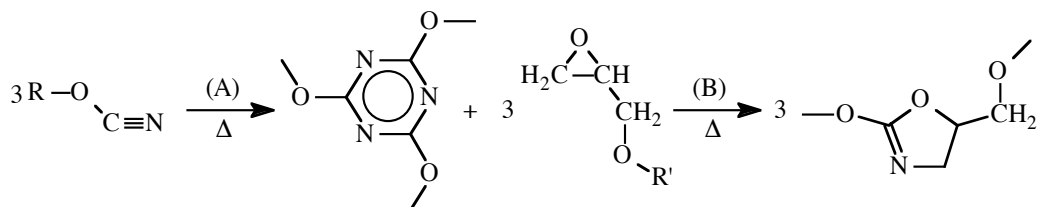
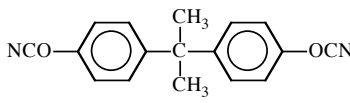
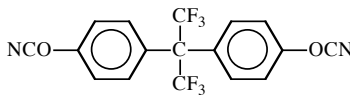
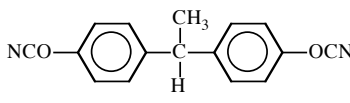
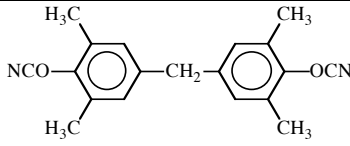
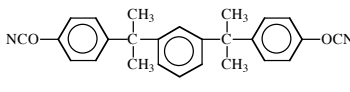
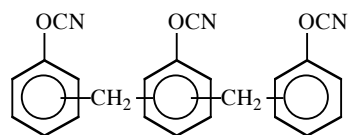
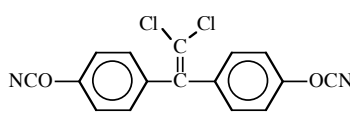
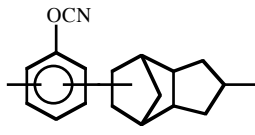
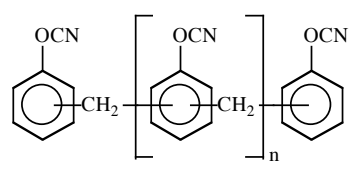


Figure 25. Cyclotrimerization reaction of the cyanate ester (A) and the subsequent reaction with glycidylether (B) to form the oxazoline.

#### 4.2.3 Cyanate Esters

Table 17 is a list of the cyanate ester monomers along with their trade name, atomic formula, and chemical structure. Five of the resins are difunctional cyanate esters derived from bisphenols, while two of the resins are multifunctional resins derived from phenol novolacs. All of the cyanate ester resins were used as received from the manufacturer without modification, purification, or catalysts. With the exception of the bisphenol C (BPC) cyanate ester, which is a research monomer at present, all of the resins examined in this study are commercial materials. The BPC polycyanurate was included in this study because of its unusually high fire resistance [95,96] and because the dichloro-diphenyl-ethylene unit linking the cyanurate rings is quantitatively converted to char and hydrogen chloride during pyrolysis [97], isolating the role of the cyanurate ring in thermal degradation. Solid polycyanurate samples were obtained from cyanate ester monomers (see figure 18) by polymerization in a forced air convection oven at 100°C for 30 minutes, 150°C for 30 minutes, 200°C for 60 minutes, and 250°C for 3 hours as per the manufacturer's recommended temperature program [98]. Phenol novolac cyanate esters were post-cured at 300°C for an additional 30 minutes.

Table 17. Trade names, chemical formula and structures of cyanate ester monomers.

Trade Name	Chemical Designation [CAS Reg. No.]	Formula	Structure
AroCy B-10	Bisphenol-A Cyanate Ester [1156-51-0]	$C_{17}H_{14}O_2N_2$	
AroCy F-10	Hexafluorobisphenol-A Cyanate Ester [32728-27-1]	$C_{17}H_8O_2N_2F_6$	
AroCy L-10	Bisphenol-E Cyanate Ester [47073-92-7]	$C_{16}H_{12}O_2N_2$	
AroCy M-10	Tetramethylbisphenol-F Cyanate Ester [101657-77-6]	$C_{19}H_{18}O_2N_2$	
AroCy XU-366	Bisphenol-M Cyanate Ester [127667-44-1]	$C_{26}H_{24}O_2N_2$	
AroCy XU-371	Phenol Novolac Cyanate Ester [P88-1591]	$C_{23}H_{15}O_3N_3$	
AroCy RD98-228	Bisphenol-C Cyanate Ester BPC = [14868-03-2]	$C_{16}H_8N_2O_2Cl_2$	
AroCy XU- 71787.02L	Dicyclopentadienyl- bisphenol Cyanate Ester [119505-06-5]	$C_{17}H_{17}NO$	
Primaset PT-30 PT-60 PT-90	Novolac Cyanate Ester n=1 [Ass. No. 160817] n=4 [Ass. No. 160817] n=7 [153191-90-3]	$C_{23}H_{15}O_3N_3$ $C_{47}H_{30}N_6O_6$ $C_{71}H_{45}N_9O_9$	

Polycyanurates are addition cured thermoset polymers that exhibit good [87-89,99] to outstanding [95,96] fire resistance. Because the ignition and fire resistance of solid polymers are governed by short term thermal stability and anaerobic degradation chemistry [13,21,22,24], the following study was conducted to understand these processes in polycyanurates. Polycyanurates are formed when three cyanate ester monomers containing the  $-O-CN$  functional group undergo a thermally initiated cyclotrimerization (addition) reaction [85,100] to form a six-member oxygen-linked triazine ring (cyanurate) as illustrated in figure 26.

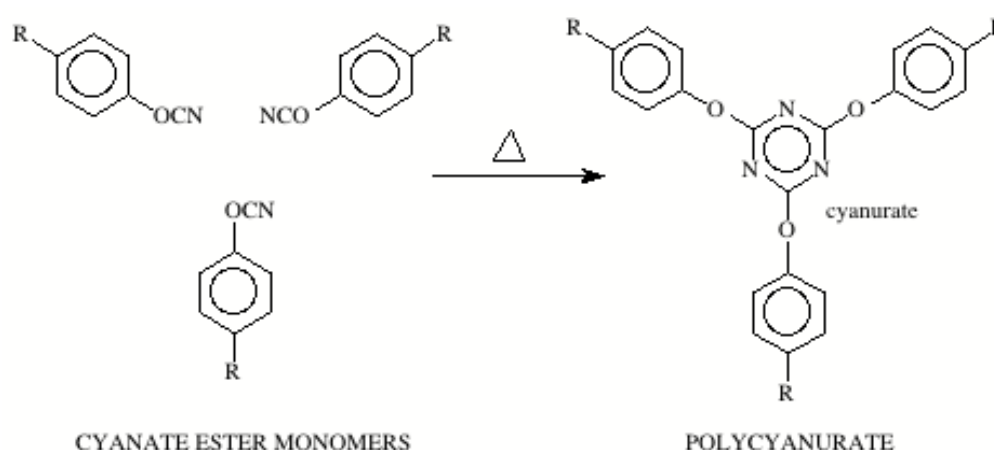


Figure 26. Cyanate ester polymerization reaction illustrating the cyclotrimerization to form the triazine linkage.

The cyanurate is a thermally stable crosslink that is responsible for the high mass loss temperature ( $450^{\circ}\text{C}$ ) of these thermosets. Polycyanurates derived from phenol novolac cyanate esters have a high glass transition temperature  $T_g > 350^{\circ}\text{C}$  approaching their thermal decomposition temperature [98,99,101]. In addition to having high thermal stability, polycyanurates form a carbonaceous char during burning that protects the underlying material and further enhances fire resistance [102,103]. Because cyanate ester resins polymerize by an addition reaction, no volatiles or by-products are produced during cure which can cause voids and subsequent loss of strength in the final product [98].

Figure 26 shows the chemistry of the cyanate ester polymerization to polycyanurate. The characteristic absorption bands of the  $-O-CN$  cyanate ester functional group are observed in the infrared spectrum between  $2200\text{-}2300\text{ cm}^{-1}$  [85,104]. The band is

usually split into a doublet or triplet of partially resolved peaks depending on the chemical environment of the cyanate ester. When the absorption appears as a doublet, the peaks are typically separated by approximately  $38\text{ cm}^{-1}$ . The polymerization (curing) of cyanate ester resins can be followed by monitoring the disappearance of the cyanate ester absorbance bands and/or the corresponding increase in the absorbance bands of the triazine ring near  $1360$  and  $1570\text{ cm}^{-1}$  [85,105] as illustrated in figure 27 for the polymerization of a solvent-cast film of B-10.

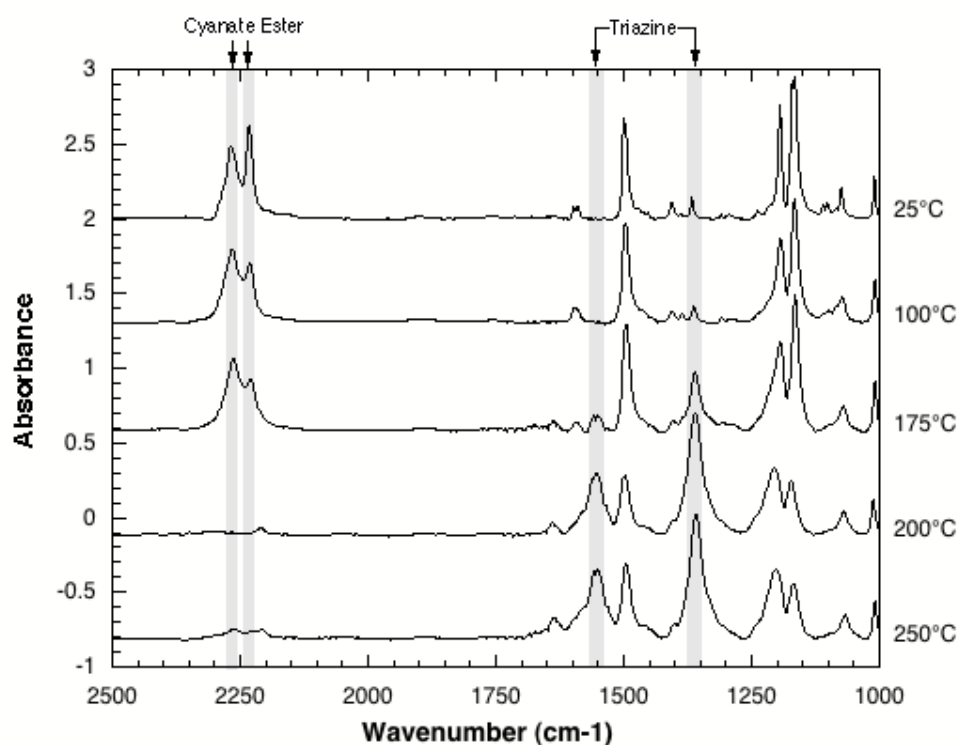


Figure 27. FT-IR cure monitoring of B-10 cyanate ester resin showing the disappearance of the cyanate ester and subsequent formation of the triazine.

The cyclotrimerization reaction occurs between  $150$  and  $200^\circ\text{C}$  for this heating program ( $20^\circ\text{C}/\text{min}$ ) as indicated by the disappearance of the cyanate ester bands at  $2200$ - $2300\text{ cm}^{-1}$  and the appearance of  $1370$  and  $1565\text{ cm}^{-1}$  triazine peaks. The polymerization can go to completion (100% reaction of cyanate ester groups) only at temperatures above the glass transition (vitrification) temperature of the polycyanurate, which for these materials ranges from  $192^\circ\text{C}$  for XU-366 to  $>350^\circ\text{C}$  for PT-30 and XU-371.

#### 4.2.4 Cyanate Ester Epoxy Blends

The chemistry of the BPA cyanate ester-epoxy systems has been examined and documented [85,106-108]. Several reactions occur in the systems that are being evaluated. Upon heating, several cyanate ester functional groups will undergo a cyclotrimerization reaction to form a triazine linkage [85,109,110]. The epoxide functionality also reacts with other epoxide groups to form a polyether. Also, the epoxide reacts with the triazine to form a five membered oxazoline ring [85,107]. Each of these reactions occur in varying amounts depending on the ratio of the blend. Evidence supporting these reactions will be discussed.

Blended samples of the cyanate ester and epoxy were prepared in ratios ranging from 0 to 100 mole percent. The initial screening required a small sample blend and only 1 gram of each blend was prepared. The reported functionality of the supplied resins were used to calculate the weight needed of each component for all of the formulations. The resins were supplied as solids and had to be warmed gently to produce a liquid with low viscosity. Melting points were determined experimentally by using DSC. Once the resins were melted, they would remain liquid for several days before recrystallizing into a solid. Formulated samples were weighed as solids, heated to the melting temperature and held there until completely melted. Once the samples were liquid, they were easily mixed and cooled prior to analysis. Blended liquid samples were then used for DSC and Fourier Transform-Infrared Spectroscopy (FT-IR) analysis. The remaining unreacted resin was then cured for additional analysis. Thermogravimetric analysis and pyrolysis-combustion flow calorimetry were used to determine the thermal stability and flammability. Samples were cured in an oven and were sampled periodically to determine the extent of cure.

The DSC (Perkin Elmer DSC 7) was used to determine the melting points,  $T_m$ , of the neat resins and the heat of reaction,  $\Delta H_{rxn}$ , for all the resin systems. For the melting point determination, approximately 3 mg of the neat sample was put in an open pan, weighed, placed in the DSC purged with nitrogen. The samples were then heated from 30°C at 5°C/min until the melting endotherm was observed. The DSC was also used for examining the heat of reaction of the blended resin systems. Approximately 3 mg of sample was placed in an aluminum pan, weighed and sealed in a press. The sealed pan was then placed inside the DSC and the sample heated at several different heating rates from 100° to 250°C. Two runs were performed on each sample for the determination of the heat of reaction. The first run was for obtaining the heat of reaction. The second

was for obtaining a baseline with the same shape and magnitude as the sample run. Heats of reaction were determined by integrating the sample curve after subtracting it from the baseline.

The melting points determined by DSC were  $75^{\circ} \pm 2^{\circ}\text{C}$  for the BPCCE and  $91^{\circ} \pm 4^{\circ}\text{C}$  for the BPCE. The heats of reaction were also determined by DSC. One peak was obtained for each of the neat resins (not shown or designated in figure 28) and two peaks were obtained for each of the blends as shown in figure 28. The two large exotherms were observed for the BPC blends in the DSC, and infrared spectroscopy was used to assign reactions to the measured heat flow which will be discussed later. The homopolymers of the BPA and BPC epoxy did not react on their own like the cyanate ester, and had to be cured with an imidazole catalyst (2-ethyl-4-methyl imidazole) [111-113]. It was found that the BPC epoxy cured at a much lower temperature,  $90^{\circ}\text{C}$ , whereas the BPA epoxy with the same amount of catalyst did not cure until over  $200^{\circ}\text{C}$ . The peak heat flow temperatures for the two large exotherms and total heats of reaction for the BPC polymers are shown in table 18.

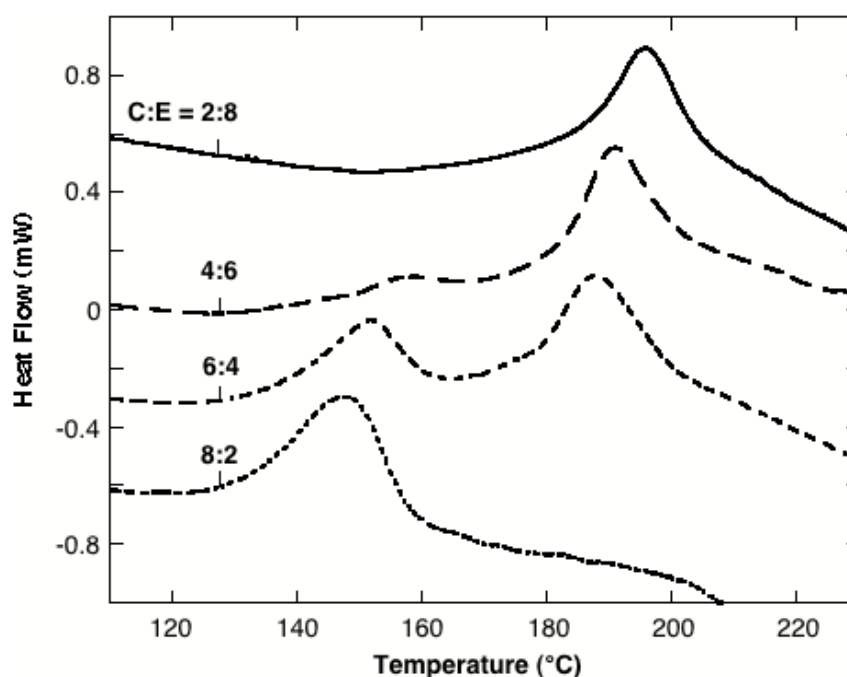


Figure 28. DSC curves for blended BPC resins heated at  $1^{\circ}\text{C}/\text{min}$  under nitrogen showing energy and temperature for reactions.

A rheometer (Rheometrics RDA2) was used to determine the glass transition temperature,  $T_g$ , of the blends. Rectangular test strips measuring 1 cm x 3 cm were cut from single layer glass laminates, described later, for the analysis. The composite strips were placed in a torsion fixture for the rheometer and tested under oscillatory conditions. Samples were subjected to a dynamic temperature ramp and heated in air at 5°C/min from 30°C until the transition was observed. A frequency of 1 Hz was used with a strain setting of 0.35%.

Table 18. Thermal analysis results for BPC cyanate ester - epoxy blends from DSC, TGA, and rheometer.

Sample	DSC			TGA			Rheometer
	$T_C$ (°C)	$T_E$ (°C)	$\Delta H_{rxn}$ (J/g)	Onset (°C)	$T_p$ (°C)	Char Yield (%)	$T_g$ (°C)
BPCCE	198	NA	270	460	479	55.8	247
8:2	147	199	450	335	352	53.9	242
6:4	151	188	612	341	346	52.3	226
4:6	157	191	375	347	350	47	206
2:8	162	196	333	377	381	41.4	153
BPCE	NA	91*	243	360	363	45.5	189

\* BPCE was cured with an imidazole catalyst.

The FT-IR was used to monitor the extent of reaction and to evaluate the cure chemistry. Thin films of the neat and blended resins were cast on salt plates prior to their cure for spectral analysis. The salt plates were then placed in a convection oven and the resins cured slowly. Spectra consisting of 32 scans at a resolution of 2  $\text{cm}^{-1}$  were taken periodically during the cure to monitor the extent of reaction and determine what bands were appearing/ disappearing. All of the samples were heated until the bands for the reactants completely disappeared, indicating completion of the cure. Additional sets of experiments were performed in the sample compartment of the FT-IR where the resins were cured in a heated transmittance cell. Liquid resin was placed between two salt plates and placed in the heated block assembly of a H2AT2 cell (Hot One-CIC Photonics Inc.). The sample was then heated from 100° to 300°C at 2°C/min. Spectra were taken every 2 minutes to obtain complementary data for some of the experiments from the DSC. Several bands were monitored for reactant consumption and product formation in the infrared. The bands for the reactive cyanate ester functionality are located at 2270  $\text{cm}^{-1}$ . Bands for the epoxide located at 915  $\text{cm}^{-1}$  and

3000  $\text{cm}^{-1}$  are also clearly visible. The triazine ring has a strong absorbance at 1565  $\text{cm}^{-1}$  and the oxazoline has an absorbance at 1608  $\text{cm}^{-1}$ . These bands were monitored to determine the extent of cure for all of the samples.

Figure 29 highlights the bands of interest for the reactants and products. The products being monitored are the cross-linking bonds that are formed by the cyanate ester cyclotrimerizing to form the triazine linkage, the epoxide reacting with another to form a polyether, and the epoxy reacting with the cyanate ester to form the oxazoline linkage.

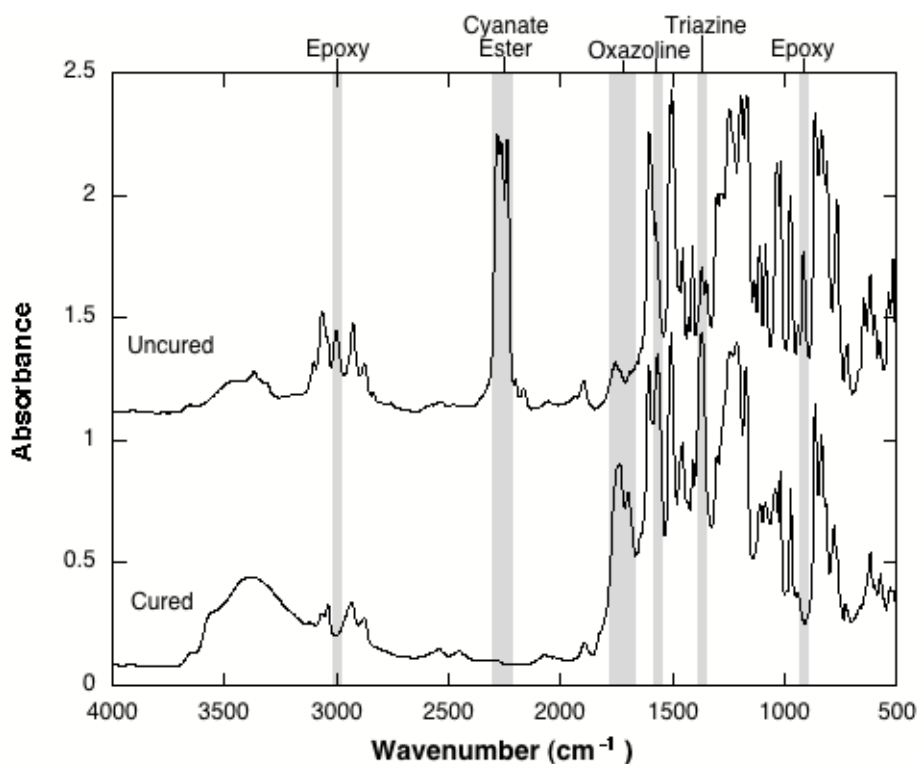


Figure 29. IR spectra of uncured and cured 6:4 blend showing the cyanate ester, epoxy, triazine, and oxazoline bands.

The reactant and product bands were monitored as a function of temperature for the 6:4 cyanate to epoxy blend in the sample compartment of the FT-IR. The peak heights were monitored as a function of temperature to analyze the chemistry of the reactions. Figure 30 shows the progress of the reaction. Initially it was thought that the epoxy and cyanate ester reacted with each other to form the oxazoline. The cyanate ester reacts first to form the six-membered triazine ring. This reaction proceeds at a much lower temperature than the neat cyanate ester. This is due to  $-\text{OH}$  groups formed by the ring

opening of the epoxy which catalyzes the cyanate reaction [114,115]. Once the triazine is generated, it reacts with the epoxy to form the five-membered oxazoline. The maximum rate of epoxy consumption was observed after almost all of the cyanate ester had been consumed. Work has already been done to determine the mechanism for the reaction. The literature in references 92 and 93 suggested several mechanisms for the cyanate ester-epoxy systems, including a rearrangement within the network structure to form an oxazolidinone. Another mechanism suggests the reaction of the oxirane ring with the triazine to form the oxazoline [85,107,108] as shown in figure 30.

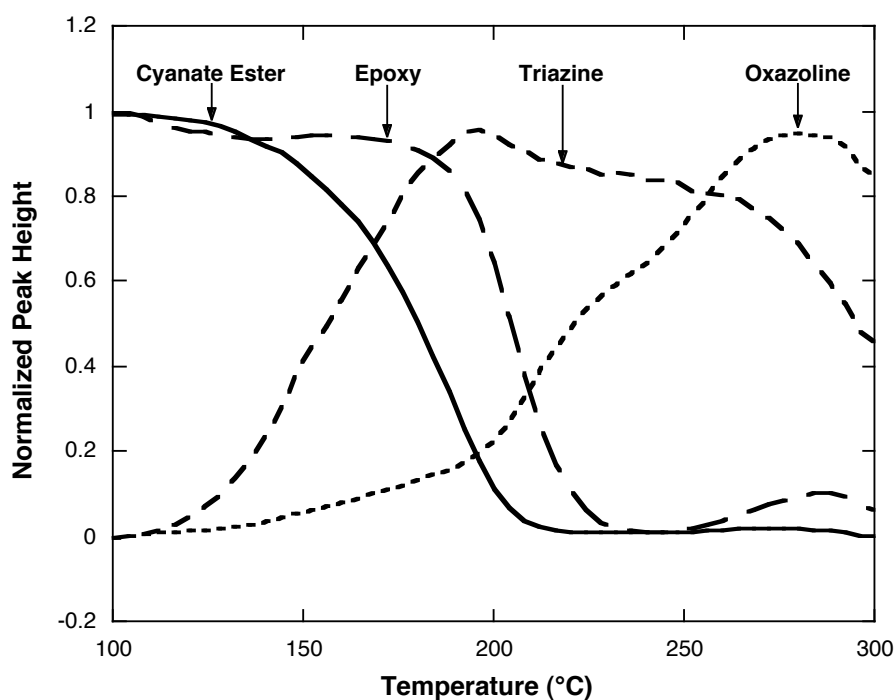


Figure 30. Normalized infrared peak heights for the reactants and products of the 6:4 cyanate ester : epoxy blend.

#### 4.3 MECHANICAL PROPERTIES

Thermal and mechanical properties of the DGEBA and DGEBC systems are listed in table 19. Due to limited quantities of DGEBC available the compressive moduli and strength could not be determined for CEBPC cured systems, while the compressive properties of the DGEBA-BPA and DGEBC-BPC systems were not tested because of poor sample quality. However, Table 19 shows that the glass transition temperatures, shear moduli, and Young's moduli of the DGEBC systems tested are similar to their DGEBA analogs, and typical of epoxies in general [92,116].

Table 19. Thermo-mechanical properties of thermoset epoxy resins cured using different co-polymer systems.

HARDENER	EPOXY DGEb-	Glass Transition Temperature, $T_g$ (°C)	Shear Modulus (GPa)	Young's Modulus (GPa)	Yield Strength (MPa)
EMI-24	A	113	1.10	2.08	111
	C	122	1.10	1.95	123
TETA	A	131	1.15	1.73	107
	C	87	0.82	2.01	96
MDA	A	112	1.25	2.52	118
	C	110	1.38	2.71	123
BPA	A	105	1.05	—	—
BPC	C	—	—	—	—
CEBPC	C	206	—	—	—

Flexural strength and stiffness of composite laminates were determined in three-point bending on a universal testing machine (Model 4400, Series 1125, Instron Corporation) using a 5-kN load cell according to ASTM D 790-95a [117]. Sample dimensions of the bars used for all the flexural tests measured approximately 6 by 12 by 150-mm (0.24 by 0.47 by 6-inch). Dimensions for the aerospace epoxy composite were approximately 3 by 12 by 150-mm (0.12 by 0.47 by 6-inch). The three-point bend fixture had rollers with a 6-mm radius, and the span length was set to 100-mm. A crosshead speed of 2.8-mm/min (0.11-inch/min) was used for all tests. Five duplicate tests were performed for each sample to obtain an average value.

Flexural testing results, according to ASTM D 790-95a for the 18-ply laminates, are shown in table 20. All values listed are the average of five duplicate tests, unless otherwise indicated. All the samples tested had similar flexural strengths. Sample failures occurred by a combination of tension and compression except for the resin-rich sample of BPC epoxy, which failed by shear. The aerospace composite sample was tested as-received from the manufacturer at a thickness of 3 mm and having carbon fiber reinforcement. All the other samples had a thickness of approximately 6 mm and continuous glass fiber reinforcement. Mechanical testing showed the flexural strengths of the BPA and BPC polymer systems were similar.

Table 20: Flexural strengths of thermoset structural composites from 3-point flex test.

Resin	Yield Stress (MPa)	Yield Strain (%)	Flexural Modulus (GPa)
Aerospace Epoxy*	795.7	1.83	46.7
BPA Epoxy	622.4	2.31	28.8
BPA CE	571.3	1.84	31.7
BPC CE	519.6	2.22	26.0
BPAE + MDA	502.0	1.63	31.8
BPC Epoxy**	486.1	2.10	24.8
Silicone Resin	222.5	1.14	23.5

\*Sample was tested as received in 3-mm thickness

\*\*Result from a single test due to a limited amount of sample

#### 4.4 THERMAL ANALYSIS / DECOMPOSITION

Table 21 lists the heats of polymerization per mole of epoxide,  $\Delta H_{polym}$ , obtained by DSC, as well as the decomposition temperature,  $T_p$ , and char yield,  $\mu$ , of the epoxy formulations obtained by TGA. Also listed in Table 21 are the heat release capacity,  $\eta_c$ , heat of combustion of the fuel gases per original mass of polymer,  $h_c$ , and pyrolysis residue,  $\mu$  at 900°C obtained by pyrolysis-combustion flow calorimetry (PCFC). Results show the heats of polymerization reactions are close when comparing the BPA to the BPC version of a polymer system. The TGA showed BPC versions of the polymer systems degraded at lower temperatures but left significantly more char. Also the PCFC showed a considerable reduction in the heat release capacity for the BPC polymers. Samples were heated to higher temperatures in the PCFC which would account for the systematically lower char yields when compared to the TGA.

Table 21. Thermal analysis results for BPA and BPC epoxy co-polymer systems from DSC, TGA and PCFC.

HARDENER	EPOXY DGEB-	DSC	TGA		PCFC		
		$\Delta H_{polym}$ (kJ/mol)	$T_p$ (°C)	$\mu$ (%)	$\eta_c$ (J/g-K)	$h_c$ (kJ/g)	$\mu$ (%)
EMI-24	A	72	460	11	833	25	5
	C	83	420	44	487	10	36
TETA	A	92	400	8	655	26	4
	C	78	350	30	577	15	23
MDA	A	94	425	18	641	26	8
	C	111	310	39	261	16	32
BPA	A	83	450	10	858	27	1
BPC	C	76	330	44	153	11	39
CEBPC	C	120	350	47	291	8	42

Figure 31 shows thermogravimetric data for the DGEBA and DGEBC epoxies cured with MDA. The principle mass loss event for the DGEBC-MDA system begins at lower temperature than for the DGEBA-MDA system but continues over a much broader temperature range, and more char is produced.

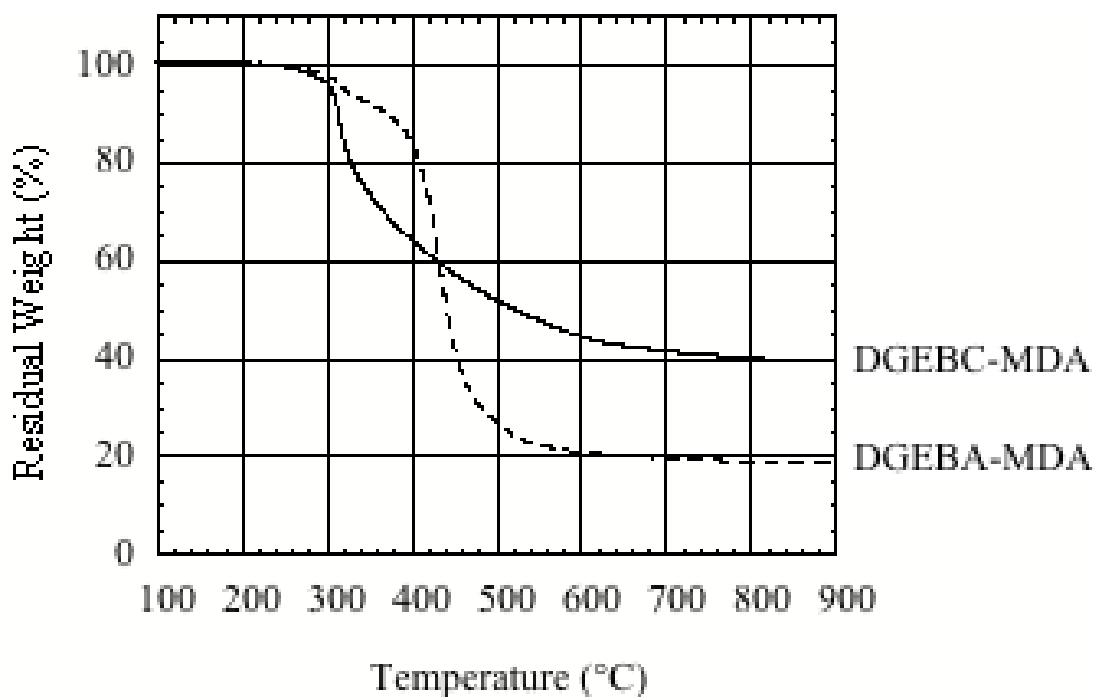


Figure 31. Thermogravimetry data for DGEBA-MDA and DGEBC-MDA systems.

#### 4.4.1 Mechanisms

Table 21 shows that lower thermal stability ( $T_p$ ), lower heat of combustion of the fuel gases ( $h_c$ ), and higher char yield ( $\mu$ ) are characteristic of the DGEBC materials relative to DGEBA. High char yields ( $\geq 30\%$ , w/w) are usually associated with thermally-stable aromatic structures in the polymer backbone. In the case of the DGEBC systems these aromatic structures are generated in situ as a product of the unique thermal degradation chemistry of the dichloroethylidene linkage. Reasonably good agreement between the TGA and PCFC char yields,  $\mu$ , is observed despite the weighing error associated with removing the sample from the PCFC apparatus to make the measurement. The DGEBC systems had consistently lower heat release capacities,  $\eta_c$ , and total heat release,  $h_c$ , than did the DGEBA systems.

Figure 32 shows a proposed decomposition mechanism of the DGEBC materials [118]. Thermal degradation is thought to proceed via a dichlorostilbene intermediate to yield two moles of hydrochloric acid and diphenylacetylene in the polymer backbone. The diphenylacetylene undergoes a strong exothermic reaction  $\Delta H = 75 \text{ kJ/mol}$  [118-120] liberating fuel gases R and forming a solid polyaromatic char in near-quantitative yield. According to this degradation scheme the only volatile degradation products are the noncombustible mineral acid HCl and the R group linking the dichloroethylidene moiety to the polymer backbone. Consequently, the fuel value of the polymer is determined by the heat of combustion of the R group and its tendency to volatilize in a fire.

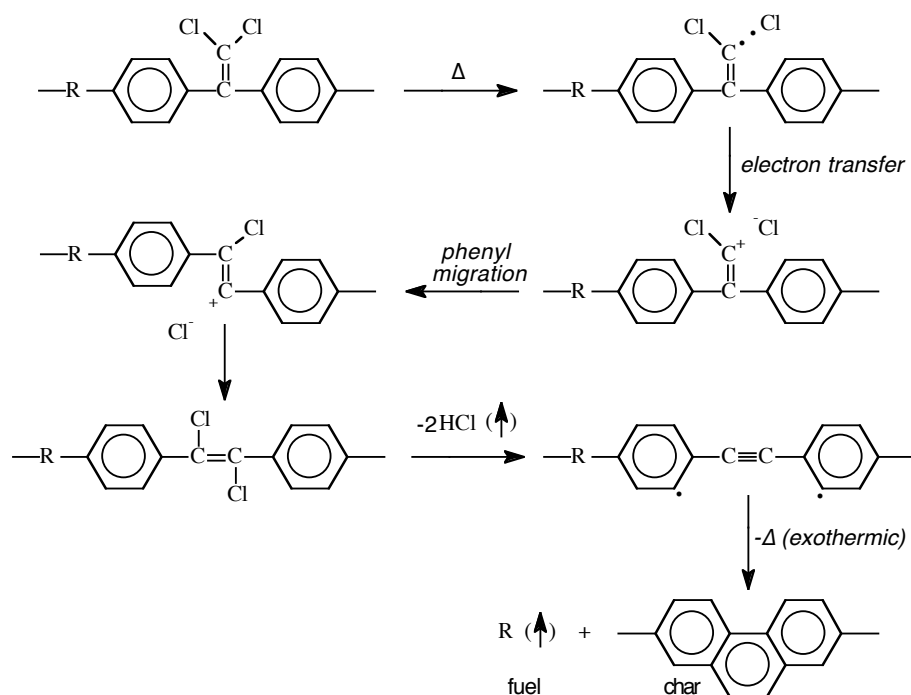


Figure 32. Thermal decomposition mechanism of chloral-based condensation polymers showing the evolution of HCl and char formation.

It has been found that when the backbone R group has a low heat of combustion such as when R= carbonate [121], or cyanate [93,118], or is readily incorporated in the char, e.g., R= phthalate [121], the heat release rate and flammability of the polymer is greatly reduced. In the present case, R is the reaction product of the glycidyl ether with itself (EMI-24 cure), an aliphatic amine (TETA), aromatic amine (MDA), bisphenol (A or C), or the dicyanate ester (CEBPC), so the fuel value of the decomposition products should be equal to the heat of combustion of the volatile fraction of these groups. The data in table 21 is consistent with the thermodynamics of the proposed dichloroethylidene degradation mechanism in that both the char yield,  $\mu$ , and the measured heat of combustion of the fuel gases,  $h_c$ , per unit initial mass of compound are roughly equal to the values calculated from the aliphatic portions of the molecule not contained in the dichloroethylidene moiety. By way of example, the R groups for the DGEBC reaction with bisphenol C ( $\text{R} = \text{C}_3\text{H}_6\text{O}_3$ ) and EMI-24 ( $\text{R} = \text{C}_3\text{H}_5\text{O}_2$ ), which differ only by a hydroxyl ( $-\text{OH}$ ), are shown in Figure 33a and 33b enclosed in the dashed lines. Assuming the volatile fuel compositions are  $\text{R} = \text{C}_3\text{H}_6\text{O}_3$  and  $\text{R} = \text{C}_3\text{H}_5\text{O}_2$  for the DGEBC-BPC and DGEBC-EMI systems, respectively, the calculated heats of combustion and char yields are  $h_c \approx 7 \text{ kJ/g-compound}$  and  $\mu \approx 35\text{-}40\%$ , in qualitative agreement with the measured values listed table 21. The backbone phenyl groups of the

methylenedianiline hardener are largely incorporated into the DGEBC-MDA char as deduced from the fact that the experimental char yield ( $\mu = 39\%$ ) is significantly higher than the theoretical value calculated assuming a volatile aliphatic glycidylamine fuel group ( $\mu = 28\%$ ).

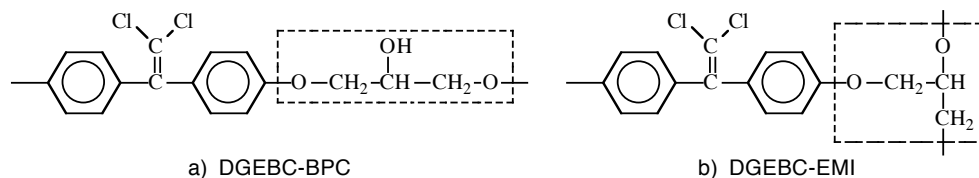


Figure 33. Idealized chemical structure of DGEBC reaction products with: a) BPC, and b) EMI. Potentially volatile fuel component (R group) enclosed in dashes.

The presence of the hydroxyl group in the phenolic (BPC) cure lowers the heat release capacity and flaming heat release rate of the epoxies relative to the ring-opening polymerization (EMI-24) cure mechanism, possibly as a result of dehydration and transient crosslinking reactions of the hydroxyl group at high temperature. The thermal stability ( $T_p$ ) of the dichloroethylidene moiety in the amine- and phenolic-cure DGEBC systems is  $50^\circ\text{C}$  lower than for the DGEBC-EMI chain homopolymerization ( $T_p = 420^\circ\text{C}$  in table 21) or linear BPC-based thermoplastics, e.g., BPC-polycarbonate,  $T_p \approx 450^\circ\text{C}$  [118-121]. The lowered thermal stability of the dichloroethylidene moiety in the addition-cured systems is due to the presence of hydrogen atoms in unreacted phenol, amine, or hydroxyl groups (bond dissociation energy  $\approx 360\text{--}430$  kJ/mol) [122] which are more labile than the aromatic ring hydrogen (bond dissociation energy  $\approx 464$  kJ/mol) [110] of the backbone phenyl groups. The labile hydrogen in the addition-cured DGEBC facilitates HCl elimination by the dichloroethylidene moiety so that the major mass loss event occurs at lower temperatures, i.e.,  $T_p \approx 350^\circ\text{C}$  versus  $T_p \approx 450^\circ\text{C}$  for the linear thermoplastic BPC-polycarbonate.

Thermogravimetry shows the effect on thermal stability with the substitution of the dichloroethene for the isopropylidene group in the epoxy and cyanate ester. Both the onset and peak decomposition temperatures are lowered with the inclusion of the dichloroethyl group, as shown in table 22. However, there is a boost in the char yield and a decrease in rate of heat release and the heat of combustion of the evolved gases as found by PCFC, also shown in table 22. The BPCCE is among the least flammable of

the materials in this study and of the many polymers that have been tested by PCFC [123].

Table 22. Small-scale thermal analysis and flammability results from TGA and PCFC.

Resin	TGA – 10°C/min			PCFC		
	Onset (°C)	$T_p$ (°C)	Char (%)	HR Capacity (J/g-K)	Total HR (kJ/g)	Char (%)
BPC Epoxy	342	345	46.8	766	6.2	39.9
BPAE + MDA	373	384	16.2	618	23.8	12.7
BPA Epoxy	411	432	9.5	502	24.8	7.1
BPA CE	428	440	41.9	341	14.8	42.4
Aerospace Epoxy*	374	403	73.3	96	6.8	72.2
Silicone Resin	490	543	77.4	85	8.9	77.5
BPC CE	422	437	55.1	10	1.2	61.5

\*Composite used in analysis

#### 4.4.2 Cyanate Esters

A thermogravimetric analyzer (Perkin Elmer TGA 7) was used to study the anaerobic mass loss processes accompanying thermal degradation of cured samples. The TGA cell was purged for 20 minutes with flowing nitrogen (100 cm<sup>3</sup>/min) after which the sample was heated from 200 to 900°C at a constant rate of 10°C/minute.

Figure 34 shows thermogravimetric data for the nine samples between 300 and 900°C. Figure 35 shows the mass loss rate (derivative of the TGA) data for the PT-30 polycyanurate and the deconvolution of that data using an asymmetric double sigmoidal peak fit to isolate the individual mass loss processes that occur during heating. The data reveals that the polycyanurates thermally decompose in two steps with the major mass loss event beginning at about 450°C as reported [85,124-126]. Thermogravimetric studies of polycyanurates in air have indicated that thermo-oxidative degradation proceeds via rapid hydrolysis of the ether oxygen bond between the phenyl and triazine rings in the presence of moisture at temperatures of 350-420°C [124-126]. Purely thermal degradation under anaerobic conditions is claimed at higher temperature ( $\geq$

450°C) via homolytic cleavage of the hydrocarbon backbone over a narrow temperature range (450-500°C) independent of the chemical structure of the linking groups between the cyanurate rings [124-126]. The present study extends these previous thermogravimetric studies of polycyanurate thermal degradation to include infrared analysis of the solid and gaseous pyrolysis products.

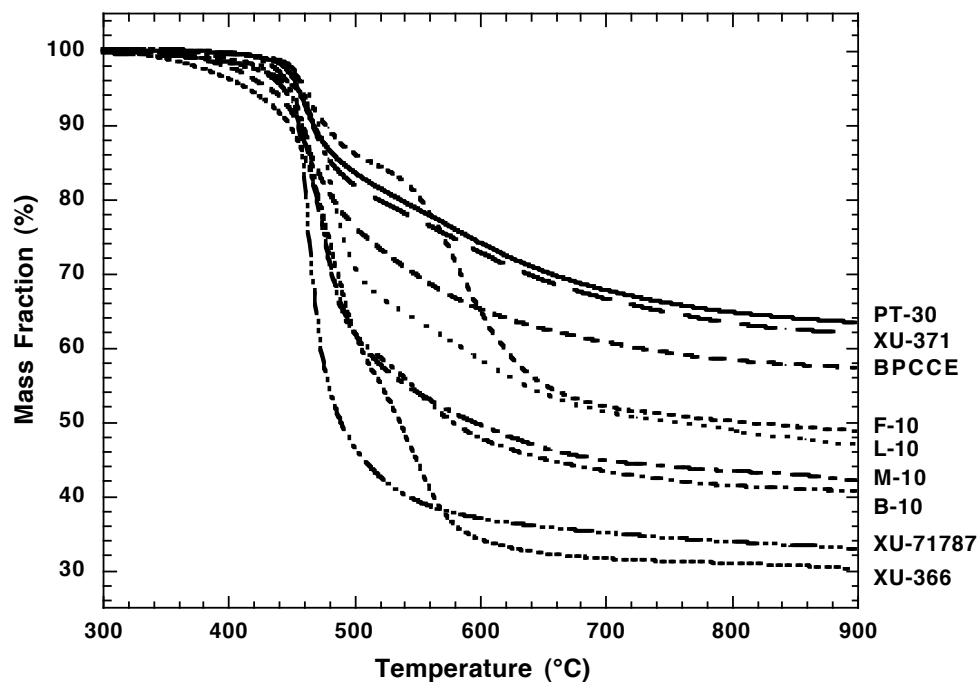


Figure 34. Thermogravimetric data for the 9 polycyanurates.

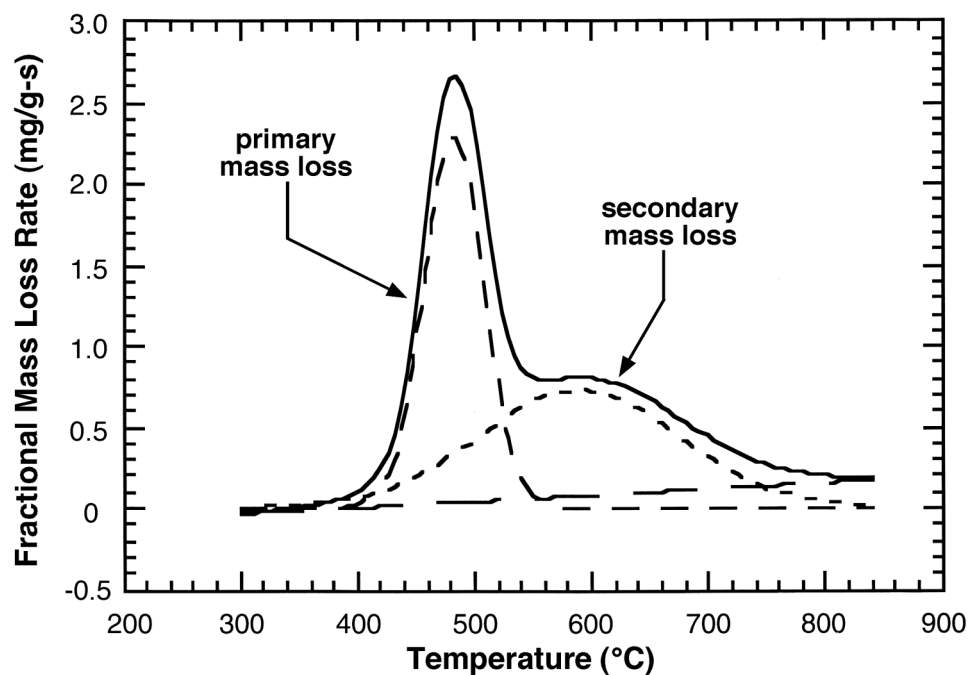


Figure 35. Mass loss rate versus temperature for phenolic triazine thermoset resin.

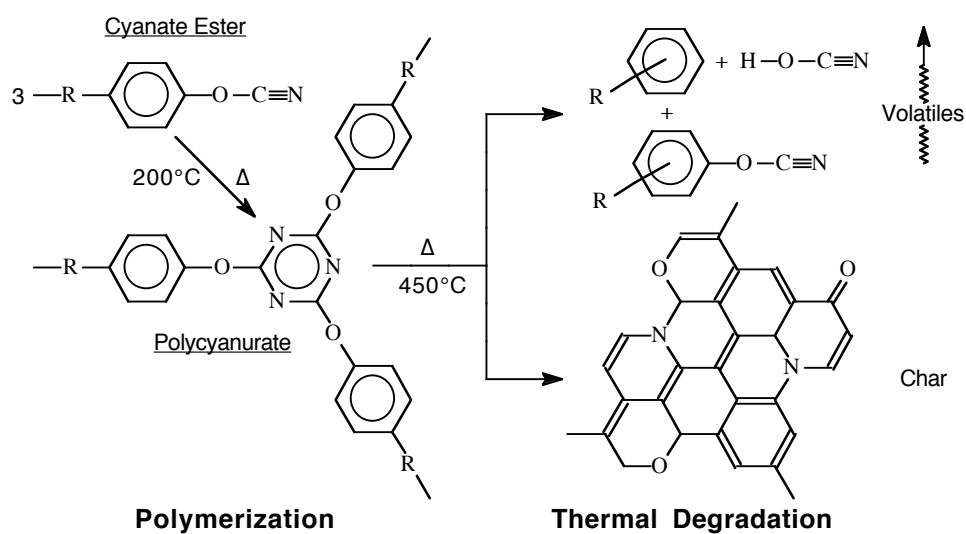


Figure 36. Cyanate ester polymerization and thermal degradation reactions.

Table 23 shows the temperature at 5% weight loss, the temperature at maximum mass loss rate, the char yield at 900°C, and the reported [85,95,96] glass transition temperatures. Note that the 5% weight loss temperatures ( $448 \pm 7$  °C) and the peak mass loss rate temperatures ( $468 \pm 8$  °C) are relatively insensitive to monomer chemical structure for the nine polycyanurates tested. Conversely, the char yield is sensitive to

the chemical structure of the monomer and increases with glass transition temperature and in rough proportion to the mole fraction of unsaturated carbon-carbon bonds.

Table 23. Polycyanurate glass transition temperatures from the literature [85,95,96] and thermal properties from TGA measurements.

Sample	Glass Transition Temperature (°C)	5% Weight Loss Temperature (°C)	Peak Mass Loss Rate Temperature (°C)	Char Yield at 900°C (%)
XU-366	192	439	482	31
XU-71787	244	447	463	33
B-10	257	443	468	39
M-10	252	443	471	41
L-10	258	455	479	47
F-10	270	453	465	49
BPCCE	275	441	461	56
XU-371	> 350	454	461	62
PT-30	> 350	457	462	63
Average:		448	468	47
Standard Deviation:		± 7	± 8	± 12

The char yield of polymers has been empirically related to the char forming tendency CFT of the individual chemical groups comprising the polymer repeat unit by Van Krevelen [13,24] who conducted anaerobic pyrolysis experiments on over 100 polymers [24]. In particular, the char forming tendency is an additive molar quantity that is defined as the amount of char per structural unit divided by 12 (the atomic weight of carbon), i.e., the amount of carbon equivalents in the char per structural unit. The char forming tendency of the cyanurate can be calculated by Van Krevelen's method using the reported char forming tendencies of the chemical groups comprising the backbone of the cyanate ester monomers and the char yields of the polycyanurates reported in table 23. The individual results for the char forming tendency of the cyanurate (OCN)<sub>3</sub> calculated from the TGA data are: B-10, CFT = 6 carbon equivalents per structural unit; L-10, CFT = 7 c-eq./unit; XU-366, CFT = 8 c-eq./unit); M-10, CFT = 8 c-eq./unit); and PT-30, CFT = 9 c-eq./unit. The average value of the char forming tendency from these separate determinations is: CFT = 8 ± 1 carbon equivalents per

cyanurate, meaning that on average, 8 carbon-equivalent atoms are incorporated into the char for each 3-carbon cyanurate. Consequently, most of the nitrogen and oxygen in the cyanurate ring are also incorporated into the char, but at an efficiency that is 2-3 times higher than fused-aromatic heterocycles such as benzimides, benzimidazoles, and phenylquinoxalines [13,24]. Alternatively, the cyanurate could be interacting with other structural groups to increase their char forming tendency during the process of thermal degradation— in which case the assumption of molar group additivity (non interacting groups) is invalid.

The incorporation of oxygen and nitrogen into the char as deduced from molar group calculations is supported by elemental analyses of the polycyanurates chars recovered after flaming combustion in a fire calorimeter. Fire chars are formed under similar conditions as nitrogen-purged TGA chars because in flaming combustion the char reaches several hundred degrees Celsius and the thermal degradation process in the pyrolysis layer is anaerobic because atmospheric oxygen is consumed by the flame [22,22]. Consequently, fire and TGA chars should (and do) have comparable mass fraction [21,22] and composition. Elemental analysis, as determined by an independent laboratory, of the virgin PT-30 polycyanurate gives  $C_{23}H_{15}O_3N_3$  for the repeat unit composition ( $C_{23}H_{15}O_3N_3$  from structural formula) versus  $C_{23}H_7O_{2.7}N_{1.4}$  for the fire char. Similarly, the virgin BPC polycyanurate has measured (or from structural formula) atomic composition  $C_{16}H_8O_2N_2Cl_2$  versus  $C_{16}H_3O_{1.3}N_{1.3}$  for the char. Chlorine is absent from the BPC polycyanurate fire char because all of the chlorine is evolved as hydrogen chloride during thermal degradation. In summary, analysis of the chars from pyrolysis and burning shows that about 2/3 of the original oxygen and nitrogen in the polycyanurate remains in the char after anaerobic thermal degradation, with 1/3 leaving as volatile species.

A temperature-programmable cell (The Hot-One, CIC Photonics) positioned in the beam of a Fourier transform infrared (FT-IR) spectrometer (Magna 550 FT-IR, Nicolet Instruments) was used to collect infrared spectra of thin films cast from acetone solution during or after polymerization. Samples were heated between 25°C and 675°C in a nitrogen purge at a constant heating rate of 10°C/min. The temperature of the film was monitored using a thermocouple in contact with the sample. The FT-IR spectra of the films were obtained using 32 scans at a resolution of 4 cm<sup>-1</sup>. Figure 37 contains a series

of solid film infrared spectra of B-10 polycyanurate during heating at 10°C/min to 675°C under nitrogen.

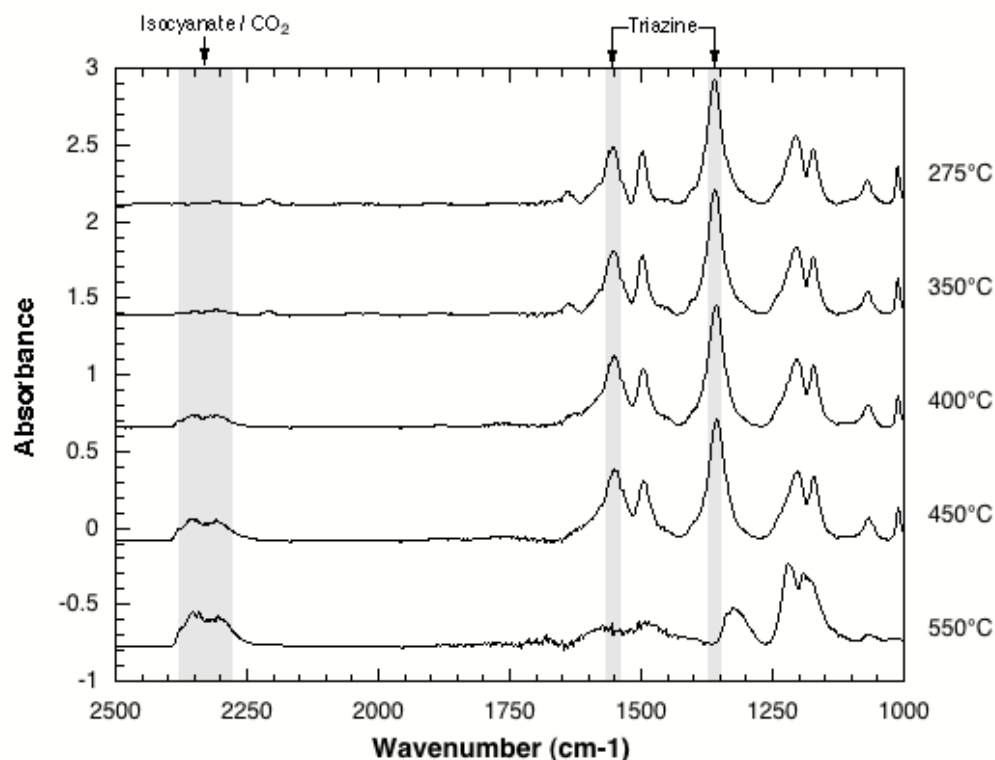


Figure 37. Temperature resolved FT-IR spectra of B-10 polycyanurate film during heating through decomposition.

The infrared spectra of all of the polycyanurate films during thermal degradation are similar. There are no major changes in the solid film infrared spectra of the polycyanurates at temperatures below 400°C indicating that very little thermal degradation has occurred. Above 400°C the 1570  $\text{cm}^{-1}$  triazine band of the cyanurate ring decreases rapidly while a 2280  $\text{cm}^{-1}$  absorbance band, tentatively assigned to isocyanate in the solid and/or carbon dioxide gas in the cell, increases in intensity over the same temperature interval, reaching a maximum at 475°C. This pattern suggests thermal isomerization of the cyanurate to isocyanate [127]. Above 475°C the 2280  $\text{cm}^{-1}$  band decreases again probably because of the elimination of hydrocyanic acid (HOCN). A common model for the degradation of the cyanurate involves the production of the volatile compounds CO, CO<sub>2</sub>, HCN, and ammonia [85,109,124,128]. In present study it appears that the first step in the solid degradation process involves isomerization of cyanurate to isocyanate which subsequently reacts with moisture to form carbamates that can further hydrolyze to carbamic acid, an unstable intermediate that spontaneously

decomposes to CO<sub>2</sub> and ammonia [127]. Above 440°C weight loss begins in earnest and all of the infrared absorption bands for the solid decrease in intensity uniformly until only the optically black [129] char remains.

#### 4.4.3 Volatile Degradation Products

A commercial probe pyrolyzer (Pyroprobe 2000, CDS Analytical), heated gas cell (Pyroscan/IR, CDS Analytical) and Fourier transform infrared spectrometer (Magna 550 FT-IR, Nicolet Instruments) were used to obtain gas phase infrared spectra of the volatile polycyanurate decomposition products. The pyrolysis probe-gas cell arrangement allows solid samples to be thermally decomposed directly in the FT-IR beam so that infrared spectra of the gaseous decomposition products are obtained instantaneously. In the experiments, approximately 15 mg of sample in a quartz tube (3-mm outside diameter x 12-mm long) was placed in the heating coil of the probe pyrolyzer which was then inserted into a heated gas cell with a working volume of 20 cm<sup>3</sup>. The gas cell was maintained at 200°C and purged with nitrogen at a flow rate of 20 cm<sup>3</sup>/min for 20 minutes prior to, and continuously during, the experiment in which samples were heated from 200 to 1000°C at a constant heating rate of 20°C/min. One spectrum (16 scans, 4 cm<sup>-1</sup> resolution, gain 1.0) was collected each minute of the heating program in synchronization with the cell turnover time.

Analysis of the gas phase thermal decomposition products by pyrolysis-FT-IR shows no absorption bands at 1570 and 1360 cm<sup>-1</sup> indicating that the volatile thermal degradation products contain no triazine as shown in figures 38 and 39 for the B-10 and BPC cyanate esters, respectively. In contrast, the -OCN group is present in the volatile decomposition products evolved between 435 – 450°C as evidenced by the appearance of an absorption doublet at 2290 and 2250 cm<sup>-1</sup>. Also detected in the infrared spectrum are phenols, methane, ammonia, and carbon dioxide.

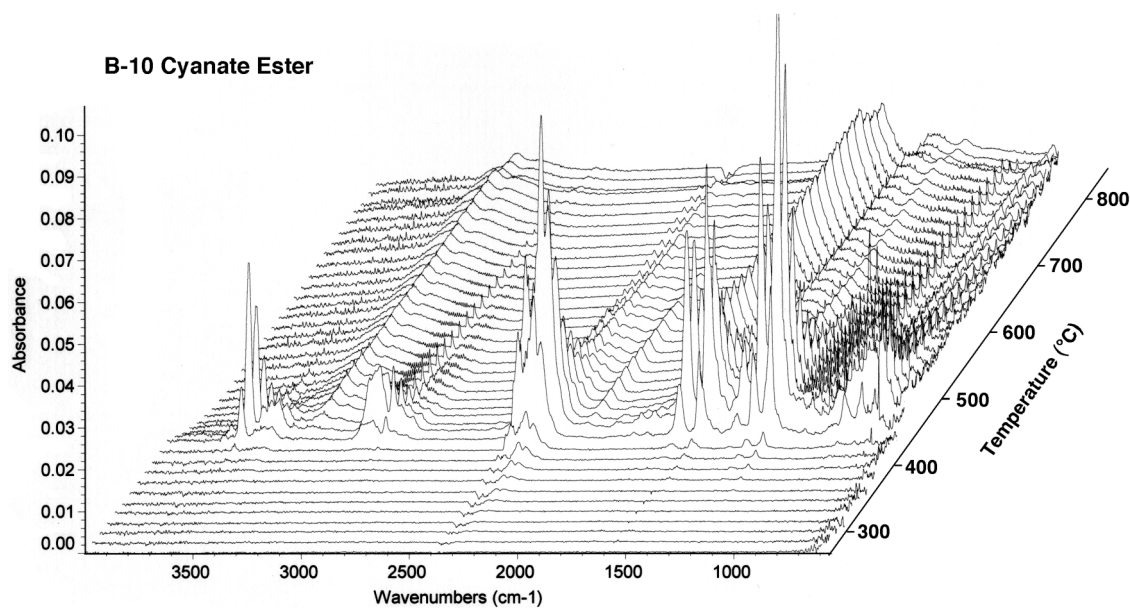


Figure 38. Temperature resolved gas phase FT-IR spectra of B-10 polycyanurate volatile decomposition products.

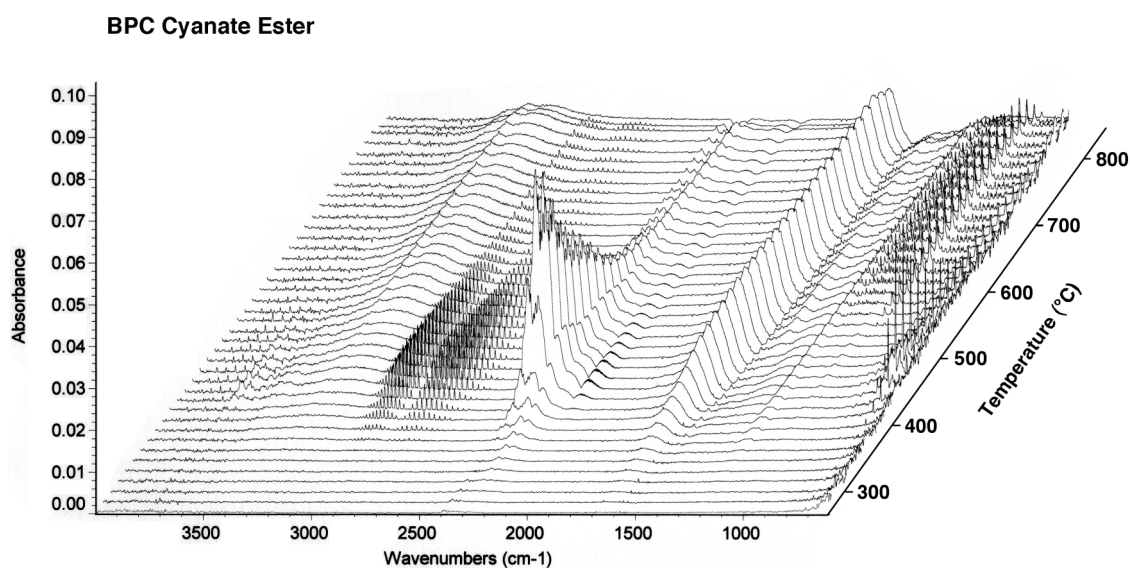


Figure 39. Temperature resolved gas phase FT-IR spectra of BPC polycyanurate decomposition products.

Table 24 lists the wavenumbers of the infrared absorbance doublets for the volatile decomposition products of each of the polycyanurates. All are within the 2200-2300  $\text{cm}^{-1}$  range and are separated by  $38 \text{ cm}^{-1}$ .

Table 24. Wavenumbers of the OCN group absorbance doublet for the volatile decomposition products.

Polycyanurate	$n_1$ ( $\text{cm}^{-1}$ )	$n_2$ ( $\text{cm}^{-1}$ )	$D_n$ ( $\text{cm}^{-1}$ )
XU-366	2282	2251	31
XU-71787	2283	2245	38
B-10	2282	2252	30
M-10	2290	2260	40
L-10	2287	2250	37
F-10	2283	2251	32
BPCCE	2286	2245	41
XU-371	2289	2251	38
PT-30	2288	2257	31

The gas phase bands are shifted slightly in frequency from those of the solid film of figure 37. The presence of an ether oxygen stretching band at  $1264 \text{ cm}^{-1}$  in some of the gas phase spectra indicates that the -OCN group is connected to a carbon atom. The presence of  $\text{CO}_2$  is indicated by the absorption peaks at  $2360$  and  $1339 \text{ cm}^{-1}$ . When the PT-30 pyrolysis gas spectrum is corrected for  $\text{CO}_2$  absorption by spectral subtraction, the doublet centered around  $2270 \text{ cm}^{-1}$  persists, indicating that its origin is probably the -OCN group. Also manifest in the gas phase decomposition product spectrum is the multiplet around  $3520 \text{ cm}^{-1}$  which is most likely due to amines, isoureas, or melamine derivatives [127]; the C-N band that appears at  $1172 \text{ cm}^{-1}$ ; and the aromatic and substituted benzene bands at  $1513 \text{ cm}^{-1}$ , and in the  $900\text{-}600 \text{ cm}^{-1}$  range, respectively. Aromatic amines, isoureas, and melamine derivatives can result from carbamate decomposition [130]. Further evidence of this reaction is the presence of characteristic absorption bands for phenolics near  $3740$  and  $3654 \text{ cm}^{-1}$ , since phenolics can be generated by aryl carbamates [130].

Analogously, the literature illustrates the thermal decomposition behavior of cyanuric acid which results in quantitative generation of hydrocyanic acid [130,131]. With this in mind it is logical that the polycyanurates, which are the esters of cyanuric acid, would exhibit similar thermal degradation reactions to yield the cyanate ester group but at higher temperature due to the increased thermal stability imparted by the phenyl ring.

In addition to the lack of triazine bands in the gas phase spectra the scanning experiments indicate that the generation of the aryl cyanates and other products by the solid during heating is rather continuous throughout the temperature range until the production of alkenic structures absorbing at 965 and 930  $\text{cm}^{-1}$  due to secondary decomposition processes in the char above 600°C. It is possible that earlier investigators missed detecting the aryl cyanate degradation fraction because gas transport temperatures were too low to maintain volatility of these species.

#### 4.4.4 Cyanate Ester Epoxy Blends

The observed mass loss onset temperatures for the liquid BPCCE and BPCE resins were 252° and 299°C, respectively. The weight loss curves for the reacted solid resins are presented in figure 40. It was found that several characteristics of the TGA trace correlated with the molar formulation ratio. A summary of these trends is presented in table 18. The amount of weight lost in the major decomposition step, as well as the char yield, correlated with the formulation ratio. Values obtained for all blends fell between those from the BPCCE and BPCE, with the exception of the 2:8 blend. A decrease in the onset temperature and an increase in the peak pyrolysis temperature was observed for the 2:8 blend. All of the tests were reproduced to confirm these observations.

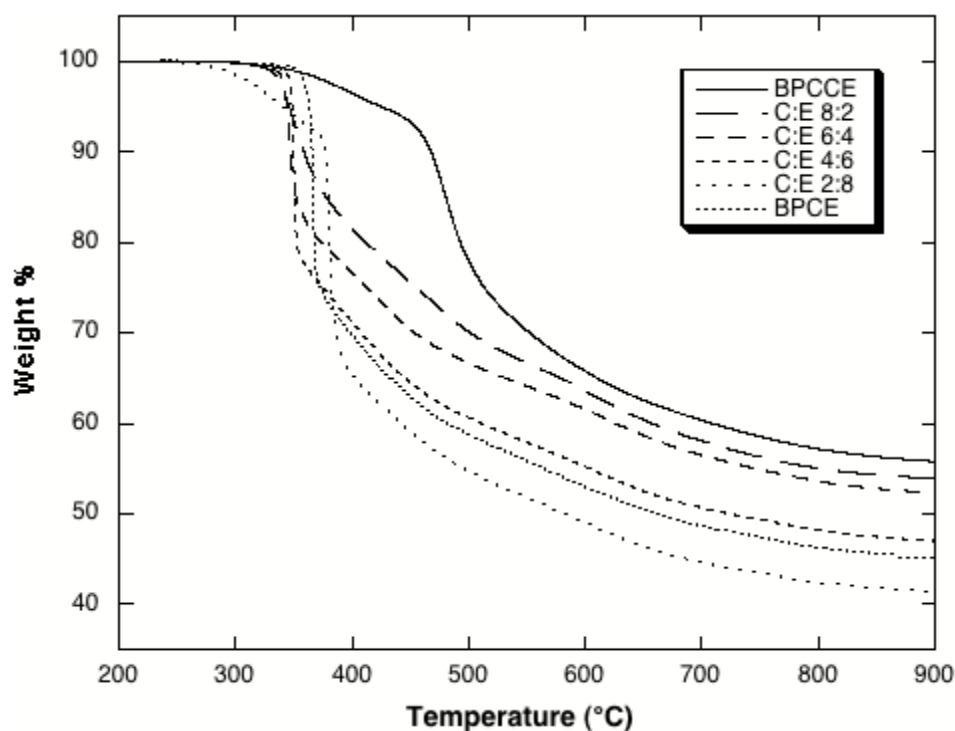


Figure 40. TGA traces for the neat and blended BPC resins heated at 10°C/min under nitrogen.

The decomposition mechanism and products for a BPC polycarbonate have been identified by Ramirez [118]. He found that the dichloroethylene group, between the two phenyl rings, rearranges to form stilbenes and acetylenes, releasing hydrogen chloride (HCl) as a degradation product at about 400°C. The presence of labile hydrogen as -OH in the BPC epoxy systems lowers the degradation temperature to around 350°C. The decomposition mechanism and products for the triazine ring have been identified by Ramirez and Schimp, respectively [88,90,128]. In their studies they found the triazine ring depolymerizes regenerating the -OCN functionality at around 475°C. This is illustrated by the neat BPCCE in figure 40. The neat BPCE and the formulated samples all had the major decomposition step occur around 350°C. It is believed that the oxazoline degrades first, along with the chlorine abstraction. There is a high weight percent of chlorine (18-21%) in the BPC polymers. Loss of the chlorine, as HCl, could account for almost all of the weight lost in the major decomposition step. An initial infrared analysis of the gas phase decomposition products from the BPC cyanate ester and epoxy blends under vacuum was performed. The gas phase spectra show ammonium chloride, and CO<sub>2</sub> generated early, followed by HCl, phenol and -OCN in the major decomposition step (~350°C). The presence of CO<sub>2</sub> and ammonium

chloride, containing both nitrogen and hydrogen, infers the oxazoline is the source of these products. Ammonia, methane, and CO were observed in the gas phase later in the decomposition (>550°C).

The glass transition temperatures of the blends are presented in table 18. The BPCCE was found to have a  $T_g$  of 247°C and the BPCE a  $T_g$  of 189°C. The blended resins  $T_g$  fell between the two values for the neat resins with the exception of the 2:8 BPCCE:BPCE which was considerably lower.

#### 4.5 FLAMMABILITY

An OSU (Ohio State University) calorimeter was used to evaluate the flammability of the cyanate ester-epoxy blends under standard conditions [132] according to 14 CFR 25.853 a-1. The OSU is a bench scale fire calorimeter that requires a 15 cm x 15 cm sample which is mounted vertically. After thermal equilibration in a holding chamber, samples are rapidly exposed to a 35 kW/m<sup>2</sup> heat flux with a pilot flame impinging on the sample surface. The OSU also has a gas burner above the sample which aids in the combustion of the evolved gases. The stock OSU calorimeter determines flammability by measuring the temperature rise of the effluent gas stream which is the convective component of the heat release. Samples were tested as single-ply glass lamina prepared by using a hand lay-up technique, as routinely used to screen resins for fire performance [133,134]; or structural laminates prepared by VARTM, as required by the Navy [135]; or obtained from suppliers.

Table 25 lists the UL94 V ranking, limiting oxygen index (LOI), peak heat release rate, and total heat release in flaming combustion according to 14 CFR 25.853 a-1 [132].

Table 25. Fire and flammability data for BPA and BPC epoxies cured with different hardeners.

HARDENER	EPOXY DGEBC-	Peak Heat Release Rate (kW/m <sup>2</sup> )	Total Heat Release (kW-min/m <sup>2</sup> )	LOI (% O <sub>2</sub> )	UL94
EMI-24	A	109	42	19-20	B
	C	50	26	27-28	B
TETA	A	144	67	21-22	B
	C	70	32	—	—
MDA	A	82	46	27-28	B
	C	44	32	—	V-0
BPA	A	71	49	20-22	B
BPC	C	30	19	35-36	V-0
CEBPC	C	34	18	—	—

The fire behavior and flammability of an epoxy resin derived from 1,1-dichloro-2,2-bis(4-hydroxyphenyl)ethylene (i.e., diglycidylether of bisphenol-C, DGEBC) was measured and found to be significantly better than bisphenol-A epoxy for each of the five systems compared in the study. All but one of the DGEBC systems passed the Federal Aviation Administration requirement for the maximum heat release of large-area aircraft cabin materials 14 CFR 25.853 a-1 [132] and exhibited UL94 V-0 behavior with aromatic (MDA, BPC) hardeners. By way of comparison, none of the DGEBA systems passed the FAA heat release requirement or exhibited self extinguishing characteristics in the UL94 V test. The BPC epoxies showed a large increase in their oxygen index when compared to the BPA versions, where available for comparison. The thermal and mechanical properties of DGEBC and DGEBA systems were virtually identical.

The cone calorimeter (ASTM E 1354) [36] was used to test fire performance per MIL-STD-2031 [136] at radiant heat fluxes ranging from 25 to 100 kW/m<sup>2</sup>. MIL-STD-2031 fire response parameters include the peak and average heat release rates (kW/m<sup>2</sup>) and the time to ignition (seconds) as well as the type and amount of combustion gases produced at a 25 kW/m<sup>2</sup> incident heat flux.

The BPCCE composites showed very good fire performance when compared to the BPACE and epoxy panels. The BPCCE easily passed the required 65 kW/m<sup>2</sup> peak HRR at 5 minutes and the 65-kW-min/m<sup>2</sup> total heat release in 2 minutes (65 / 65) as both single- and 18-ply laminates while the epoxies did not, as shown in table 26. The single-ply samples showed good response and separation in the test. A range of peak heat release values were obtained with the lowest being the two BPC materials and the silicone resin.

Table 26. Heat release data for thermoset polymer composites from the OSU calorimeter, 14 CFR 25.853 a-1, at 35-kW/m<sup>2</sup> irradiance.

Resin	Single-Ply Lamina			Multiple-Ply Laminates		
	Peak HRR (kW/m <sup>2</sup> )	2-min Total HR (kW-min/m <sup>2</sup> )	Char* (%)	Peak HRR (kW/m <sup>2</sup> )	2-min Total HR (kW-min/m <sup>2</sup> )	5-min Total HR (kW-min/m <sup>2</sup> )
BPAE + MDA	88	26	5.6	216	-11	350
BPA Epoxy	111	44	1.9	168	-13	324
Aerospace Epoxy	NA	NA	NA	146	83	342
BPA CE	72	28	16.3	139	-18	171
BPC Epoxy	48	28	14.1	102	-3	201
BPC CE	13	13	26.8	11	-13	-14
Silicone Resin	33	12	NA	0	-0.6	-1

\*Char yield based on resin fraction

Figure 41 shows the heat release rates for the first 3 minutes of the 14 CFR 25.853 [132] test. The BPCCE has near-zero peak heat release rate and negligible heat release. The silicone resin also performed very well in the single-ply configuration. The char yield listed in column 4 of table 26 is based on the resin fraction of the composite and was obtained by subtracting the weight of the glass from the sample weight measured before and after the test. The aerospace composite was received as a cured laminate and could not be tested in the single-ply configuration.

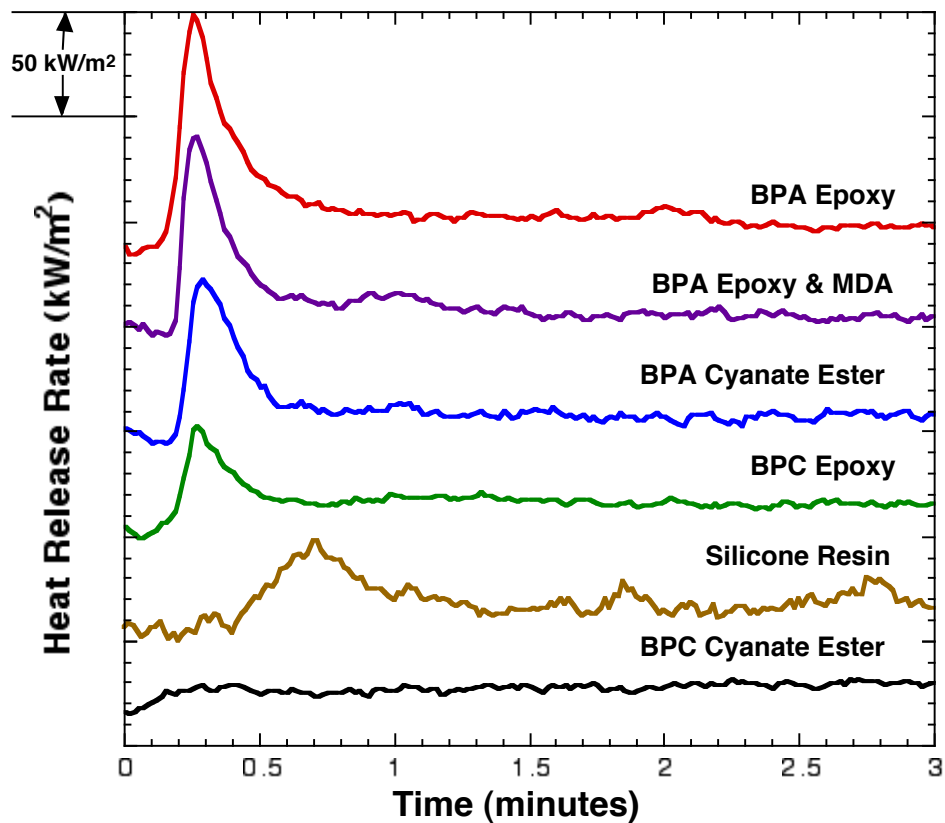


Figure 41. Heat release rates of single-ply composite laminates in OSU calorimeter at 35 kW/m<sup>2</sup>.

All the multi-ply composite laminates showed good performance early in the test up to about 2 minutes. After that, the impinging pilot flame ignited all the samples, excluding the BPCCE and silicone resin. Once the samples ignited, they burned readily for the remainder of the test. The values for the 18-ply polymer composites in table 26 are the 14 CFR Part 25 values for maximum heat release rate during the first 5 minutes and the average heat release during the first 2 minutes, as listed in 14 CFR 25.853 a-1 [132]. The last column of data is the 5-minute total heat release. This shows that after the samples ignited at around 2 minutes they released a considerable amount of heat. The long delay to ignition can be attributed to the sample thickness. Single-ply samples tested in the OSU were less than 0.5-mm thick, whereas the structural composite panels were around 6-mm thick and therefore took longer to reach the ignition temperature. The 2-minute average is expressed as a negative number because the samples remove heat from the system before ignition. This is due to the OSU measuring heat release by a temperature rise method. Although all the structural composite samples, except for

the aerospace composite, passed the 2-minute average HRR requirement, all but the BPCCE and silicone resin failed the criteria for the peak HRR within 5 minutes.

Laminates were tested in the cone calorimeter at a radiant heat flux of 50 kW/m<sup>2</sup>. The results from these tests are shown in table 27.

Table 27. Multiple-ply laminate heat release data from the cone calorimeter at 50 kW/m<sup>2</sup>.

Resin	Peak HRR (kW/m <sup>2</sup> )	Avg. HRR (kW/m <sup>2</sup> )	Total HR (MJ/m <sup>2</sup> )	<i>t</i> <sub>ig</sub> (s)	Char* (%)
Aerospace Epoxy	302	182.0	29.3	61	NA
BPA Epoxy	155	77.5	36.4	102	24.5
BPA CE	118	24.2	13.3	129	52.1
BPAE + MDA	107	77.9	33.6	110	40.0
BPC Epoxy	77	51.0	26.9	74	44.3
Silicone Resin	74	47.9	23.0	259	82.7
BPC CE	8	-2.4	0.3	NI	62.4

\*Based on resin fraction of composite

All the samples ignited and burned completely at a 50-kW/m<sup>2</sup> heat flux with the exception of the BPCCE, as shown in figure 42. The BPCCE had no ignition (NI) during the 10-minutes exposure to the radiant heat flux. There was some variation in the results due to non-uniformity of each sample; however, the burning character of each material was completely different. The BPA epoxy ignited and burned steadily for about 4 minutes with a large flame that gradually went out. The BPA / MDA epoxy sample ignited, burned with a steady increase in the heat release rate, then decreased. The BPC epoxy ignited, burned steadily, then rapidly increased, shooting flames out the sides of the holder and up and around the cone heater. The flames rapidly died down and the sample continued to flicker until about nine minutes into the test. The BPACE ignited and burned steadily through small jets distributed uniformly over the surface, then gradually decreased until it flickered and eventually extinguished at 8 minutes into the test. The BPCCE sample sat there and gradually turned black with slight off-gassing above and eventually below the sample holder. The average heat release rate of the BPCCE is expressed as a negative number due to the sample not igniting and

evolving mostly noncombustible gases. The results in table 27 for peak HRR correspond to the first peak after ignition. Peaks occurring later in the test, for some materials, were larger due to heat re-radiating from the back of the samples as the thermal wave passed through them. The BPC epoxy performance has to be weighted when compared to the others due to a 7 to 15% larger resin fraction in the resulting composite. Its high flammability can be attributed to the large aliphatic groups between aromatic rings. Since there was a limited supply of the BPC epoxy, only one sample was prepared and tested. The silicone resin took almost 5 minutes to ignite and burned steadily with a low heat release rate until it diminished and self-extinguished about 10 minutes later. The aerospace composite ignited in about 1 minute, burned rapidly for about 2 minutes and self-extinguished within 5 minutes.

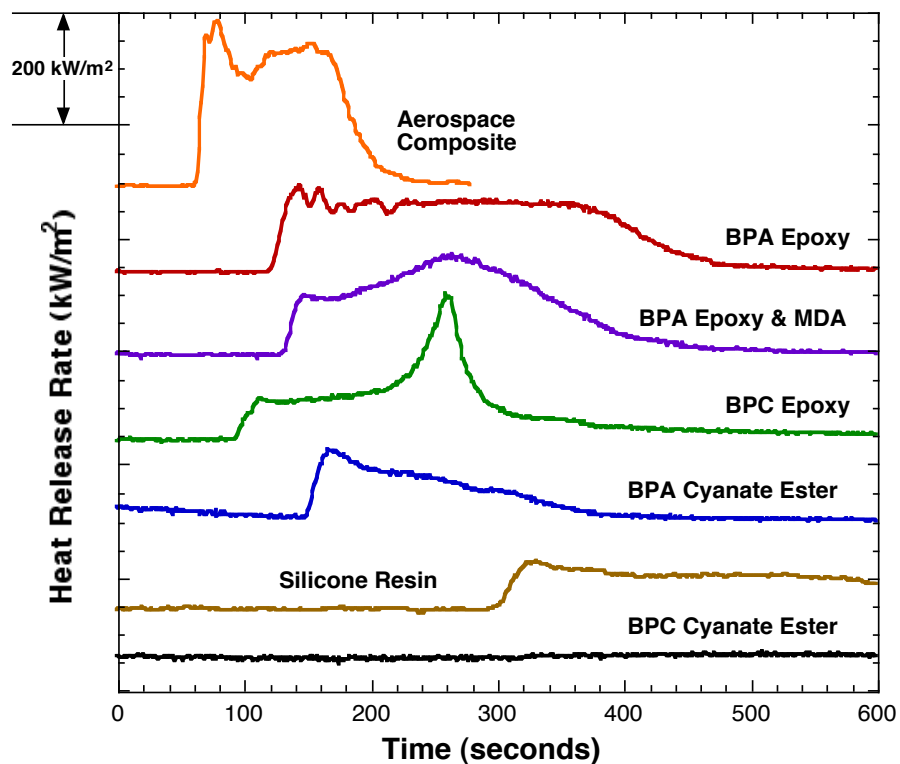


Figure 42. Heat release rates of the multiple-ply composite panels in cone calorimeter at  $50 \text{ kW/m}^2$  heat flux.

The BPCCE structural composites were also tested at  $75$  and  $100 \text{ kW/m}^2$  heat fluxes. The results for the peak heat release rate and the time to ignition were almost identical to those obtained by Koo *et al.* [137]. Results at  $100 \text{ kW/m}^2$  for the time to ignition was 145 seconds, and the peak heat release rate was  $48.1 \text{ kW/m}^2$ . The BPCCE samples

performed better under a 100-kW/m<sup>2</sup> heat flux than the other samples at a 50 kW/m<sup>2</sup> heat flux. The residual BPCCE samples still retained some strength after the 100 kW/m<sup>2</sup> test.

It has been demonstrated that high flexural strengths, similar to those of epoxies, can be achieved with the bisphenol-C cyanate ester when prepared using vacuum-assisted resin transfer molding. This study showed the BPCCE glass fiber-reinforced laminates to have comparable mechanical properties to epoxy resin laminates in contrast to previous results.

The BPCCE resin satisfies the fire performance requirements for both large surface area decorative panels in commercial aircraft and structural polymer composites for Navy ships and submarines as an unmodified resin containing no fillers or additives to reduce flammability, improve mechanical properties, or enhance processing characteristics.

Trends in the measured heat release rates (*HRR*) of the blends were observed. The heat release capacity measured in the non-flaming test show a decrease in the heat release capacity with an increasing cyanate concentration as shown in figure 43. The microscale calorimeter results are summarized in table 28. A large reduction in the peak *HRR* of the BPC epoxy systems was observed with the addition of as little as 20 percent cyanate ester. The peak rate of heat release and the total heat release increase when there is an increase in the epoxy concentration. It is believed that the large aliphatic portion of the epoxy is responsible for the increasing heat release rate. Increasing aromatic group concentration reduces the heat release rate by providing less fuel and more char, typically. The shape of the heat release curves for the BPCCE and the blends were all similar with a sharp peak followed by a low, broad peak, indicating several steps in the decomposition as evidenced by TGA. The neat BPCE had a single, sharp peak which indicates a single step decomposition. The presence of ammonium chloride in the gas phase IR spectra indicates a large amount of hydrogen which could account for the sharp heat release peak observed in this test.

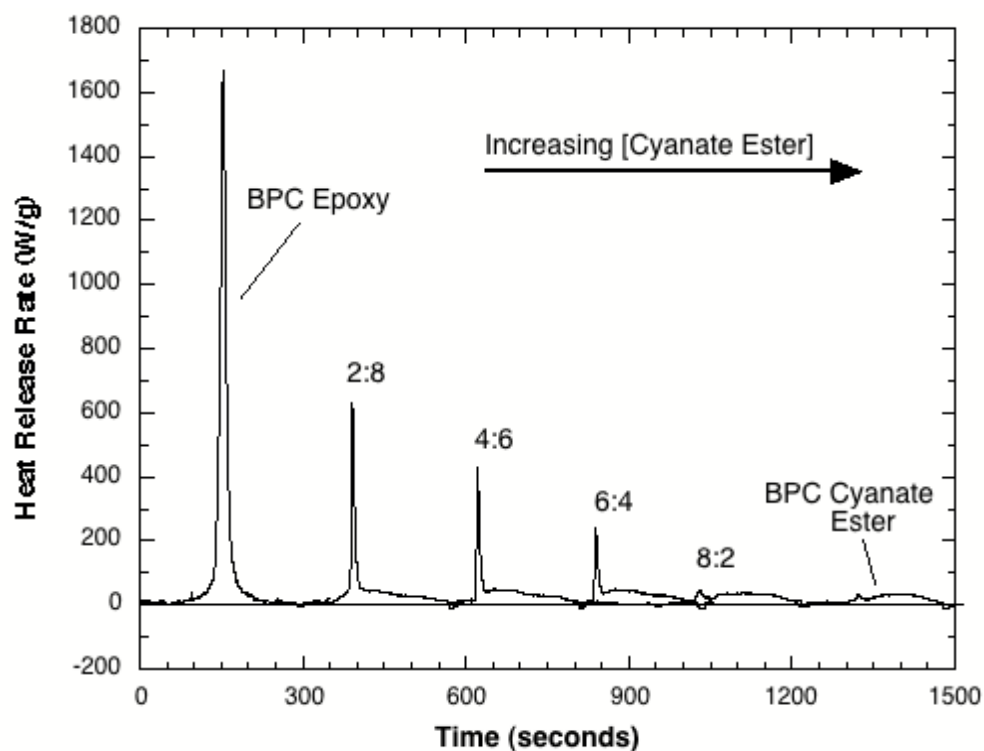


Figure 43. Pyroprobe PCFC heat release rates for the series of BPC epoxy-cyanate ester resin blends (shifted in time for clarity).

Definite trends were observed in the flammability behavior of the BPC polymer blends as shown in figure 44. The peak heat release rate and the 2-minute-total heat release increased with an increase in epoxy concentration. Only a single test was performed on each of the neat and blended resins due to a limited supply of the BPC resins. All of the materials tested in this study passed the FAA 65 / 65 flammability requirements [132] for large surface area components with the exception of the BPA epoxy.

Table 28. Flammability results from PCFC and OSU for BPC cyanate ester and epoxy polymers and reference materials.

Sample	PCFC			OSU		
	HR Capacity (J/g-K)	Total HR (kJ/g)	Char Yield (%)	Peak HR (kW/m <sup>2</sup> )	2 min Total HR (kW-min/m <sup>2</sup> )	Char Yield <sup>†</sup> (%)
BPCCE	13	4	59	14	13	27
8:2	13	5	53	18	18	30
6:4	149	6	52	30	15	22
4:6	291	8	42	34	18	16
2:8	393	9	33	32	22	14
BPCE	506	10	36	49	27	14
BPACE	283	18	36	NA	NA	NA
BPAE	657	26	4	110	44	2
Phenolic	NA	NA	NA	23	21	14

<sup>†</sup> Char yield is based on resin fraction of the composite panel.

The high thermal stability, increased char, and low heat of combustion of the evolved gases contribute to the low flammability of the BPC polymers. The BPC polymers were found to have a high concentration of HCl in the products of combustion. It is well known that halogens quench flaming reactions by scavenging free radicals. It is also well known that HCl is thermally stable and does not react with oxygen in a combustion reaction and does not contribute to the heat release of the material. The epoxy is more flammable than the cyanate ester due to the increased aliphatic content in the reacted networks. However, there is a considerable reduction in the measured heat release of the BPC epoxy when compared to the BPA epoxy. This demonstrates the effect that substituting one group in the polymer backbone has on the polymer flammability.

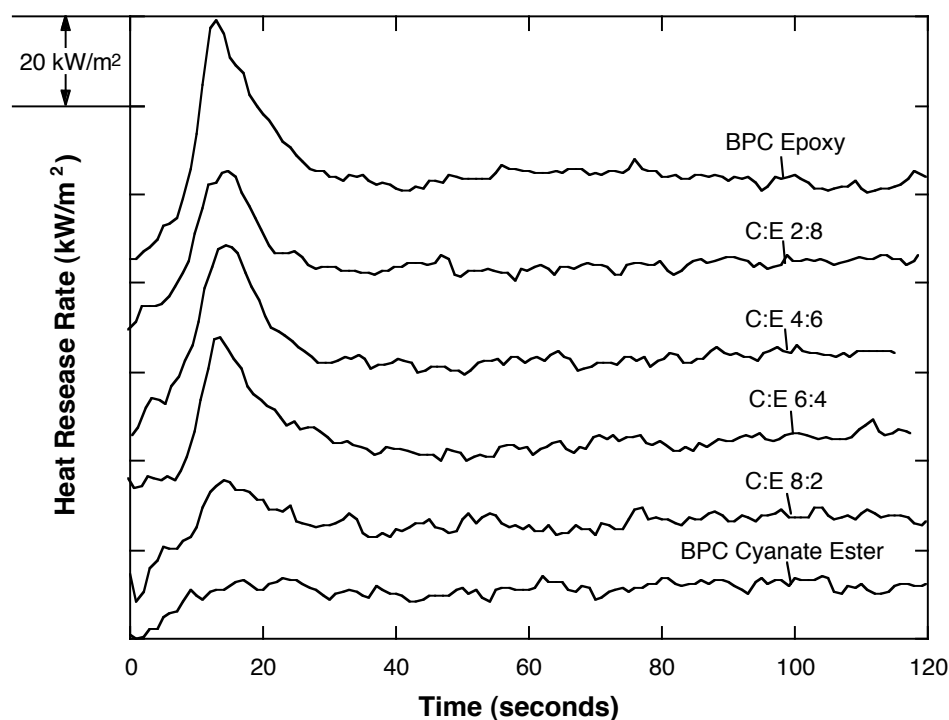


Figure 44. Heat release rate curves from the OSU calorimeter (heat release curves have been shifted along the Y-axis for clarity).

The char yields from the two flammability tests did not correlate well due to the different sample environments. Pyrolysis in the microscale calorimeter is completely anaerobic. Conditions in the OSU are only anaerobic at the sample surface when the sample is burning. If the sample does not ignite or ceases to burn, it is subjected to the radiant heat flux and an impinging flame, for the duration of the test. The high-volumetric flow rate of air sweeping over the sample surface at elevated temperatures causes oxidative pyrolysis and a lower char yield.

Although the heat release rate of the samples with a high epoxy formulation ratio were not as low as was hoped, one must keep in mind that these are unmodified resins that have passed the FAA heat release requirement of a maximum of  $65 \text{ kW/m}^2$  peak and  $65 \text{ kW-min/m}^2$  total. Additives and fillers can be used to optimize the flammability performance as well as other properties such as the glass transition temperature and toughness. These studies were beyond the scope of the current work and may be examined in the future.

The epoxy and cyanate ester derived from bisphenol-C show improved heat release rates relative to their bisphenol A (BPA) versions. Low-fuel content, high char yields, and halogen inclusion in the polymer structure all contribute to the low heat release rate of these materials. The blended resins showed a rule of mixtures increase in the heat release rate with increasing epoxy concentration. These materials show promise as a candidate for inclusion in commercial aircraft. All of the fabricated lamina of the BPC cyanate ester and epoxy had a good surface finish and passed Title 14 Code of Federal Regulations Part 25.853 (a-1) [132].

Extensive work was done on the flammability of cyanate esters. Almost all of the neat resins were tested at four different heat fluxes in the cone calorimeter (shown in Appendix C). Additional analysis and extrapolations from the flammability data could be made that could not be done with the other materials listed in this chapter.

Values for the gross heat of combustion for the cyanate esters were obtained with an oxygen bomb calorimeter (Parr Instrument Model 1341) using the American Society for Testing and Materials (ASTM) standard test method D 2382-88 [50].

The gross and net heats of complete combustion of the polycyanurates from oxygen bomb calorimetry are listed in table 29. Excluding the halogen-containing polymers F-10 and RD98-228, the net heats of combustion fall within the relatively narrow range 28.6-34.4 kJ/g. The net heat of complete combustion of the polycyanurate  $h_{c,p}^0$  is, on average, about 20% greater than the net heat of combustion of the volatile degradation products,  $h_{c,v}^0$  determined by pyrolysis combustion flow calorimetry. The disparity between the heats of combustion of the polymer and its fuel gases is the result of partitioning of degradation products into nitrogen (N) and oxygen (O) enriched volatile fuel and N, O depleted carbonaceous char during thermal degradation (see figure 36). The Code of Federal Regulations as

$$h_{c,v}^0 = \frac{h_{c,p}^0 - \mu h_{c,u}^0}{1 - \mu} \quad (53)$$

The last column of table 29 are the net heats of complete combustion of the char calculated with equation 53 from  $h_{c,p}^0$ ,  $h_{c,v}^0$  and  $\mu$  for each polycyanurate. It is seen that

$h_{c,\mu}^0$  increases with the carbon/hydrogen content of the polymer. The char fraction or pyrolysis residue increases from 27% to 65% in rough proportion to the aromatic content of the monomer backbone as predicted from group contributions to the char forming tendency of polymers [13]. The pyrolysis residue is in reasonable agreement with the char yield after flaming combustion measured in the cone calorimeter.

Table 29. Net heat of complete combustion, specific heat release, heat release capacity, and char fraction for polycyanurates.

Material	Oxygen Bomb		PCFC				Calculated
	$h_{c,p}^0$ gross (kJ/g)	$h_{c,p}^0$ net (kJ/g)	$Q_c$ (kJ/g)	$\eta_c$ (J/g-K)	Char Fraction	$h_{c,v}^0$ (kJ/g)	$h_{c,\mu}^0$ (kJ/g)
B-10	29.92	28.81	17.6	283	0.36	27.6	31.0
F-10	18.71	18.25	4.6	62	0.43	8.1	31.7
L-10	29.38	28.38	14.7	316	0.42	25.3	32.6
M-10	31.23	29.94	17.4	280	0.35	26.9	35.1
XU-366	34.39	33.06	22.5	239	0.26	30.6	39.4
XU-371	28.76	27.77	9.1	88	0.59	21.9	31.9
XU-71787	33.64	32.14	20.1	493	0.27	27.6	43.6
PT-30	30.65	29.81	9.9	122	0.52	20.6	38.0
RD98-228	22.25	21.72	4.2	24	0.53	9.0	33.0

Figure 45 shows specific heat release rate data for the polycyanurates obtained in the pyrolysis-combustion flow calorimeter. The data have been horizontally shifted from the reference XU-71787 data in 200 second increments for clarity. The maximum value of the heat release rate for each polycyanurate was divided by the sample heating rate (4.3 K/s) to compute the heat release capacity listed in table 30 along with the total heat release (area under the curve) and the char residue after the test. Polycyanurates with the highest heat release capacity and total heat release (XU-71787 and XU-366) had the highest aliphatic hydrocarbon content and fuel value. Increasing aromatic hydrocarbon content over the series: B-10, L-10, M-10, PT and XU-371 resulted in increased char yield, lower heat release capacity, and lower total heat release. The halogen-containing polycyanurates F-10 and RD98-228 exhibit high char yield and low heat of combustion of the fuel gases  $h_{c,v}^0$  and so had the lowest heat release capacity and total heat release.

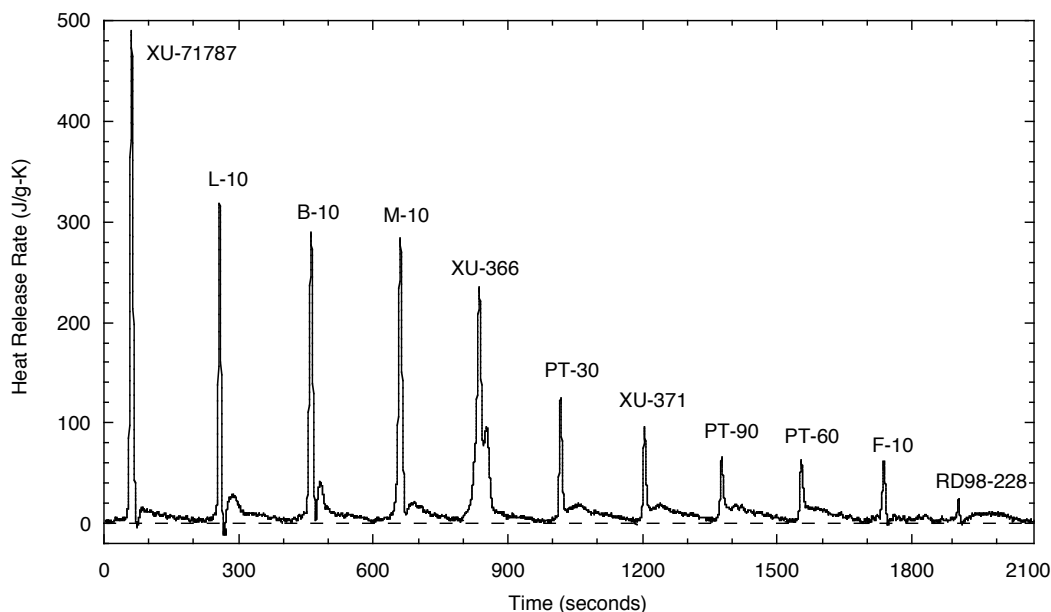


Figure 45. Pyroprobe PCFC heat release rate data for polycyanurates (horizontally shifted for clarity).

The heat release rate (HRR), mass loss rate, smoke density, and combustion gases for the cyanate esters were measured in a cone calorimeter. The cold wall external radiant heat flux was set at 35, 50, 75, and 100 kW/m<sup>2</sup> using a Schmidt-Boelter heat flux gage. A spark igniter located 2.5 cm above the sample surface was kept in place until stable flaming combustion was observed. The smoke extinction coefficient  $\kappa$  (1/m) was calculated from attenuation of the He-Ne laser beam intensity  $[I/I_0]$  over path length  $L$  (m) in the exhaust duct as,  $\kappa = (1/L) \ln[I/I_0]$ .

Square samples (100 x 100 x 6.4 mm) of each material were tested in a horizontal orientation with the retainer edge frame as per ASTM E1354 [36] for materials with tendency for swelling. The time to sustained ignition ( $t_{ig}$ ), heat release rate (HRR), total heat release (THR), mass loss rate (MLR), and effective heat of combustion (EHC) were measured for each material at each external irradiance level.

Figure 46 shows heat release rate histories for all of the polycyanurates at an external flux of 50 kW/m<sup>2</sup> with the exception of F-10 which did not sustain burning at that flux. The heat release rate curves are vertically shifted for clarity. The top four curves are data for the polycyanurates of monomers containing more than two reactive cyanate

ester groups (i.e., functionality,  $f > 2$ ) PT-30/60/90 and XU-371. These  $f > 2$  polycyanurates showed an initial peak in heat release rate at ignition followed by a decrease in HRR as the char layer forms and increases in thickness preventing the escape of pyrolysis (fuel) gases generated below the surface. A second heat release rate peak is observed for  $f > 2$  polycyanurates about a minute after the ignition peak that corresponds to a catastrophic fracture of the charred surface and the instantaneous release of pressurized pyrolysis gases formed at depth [138].

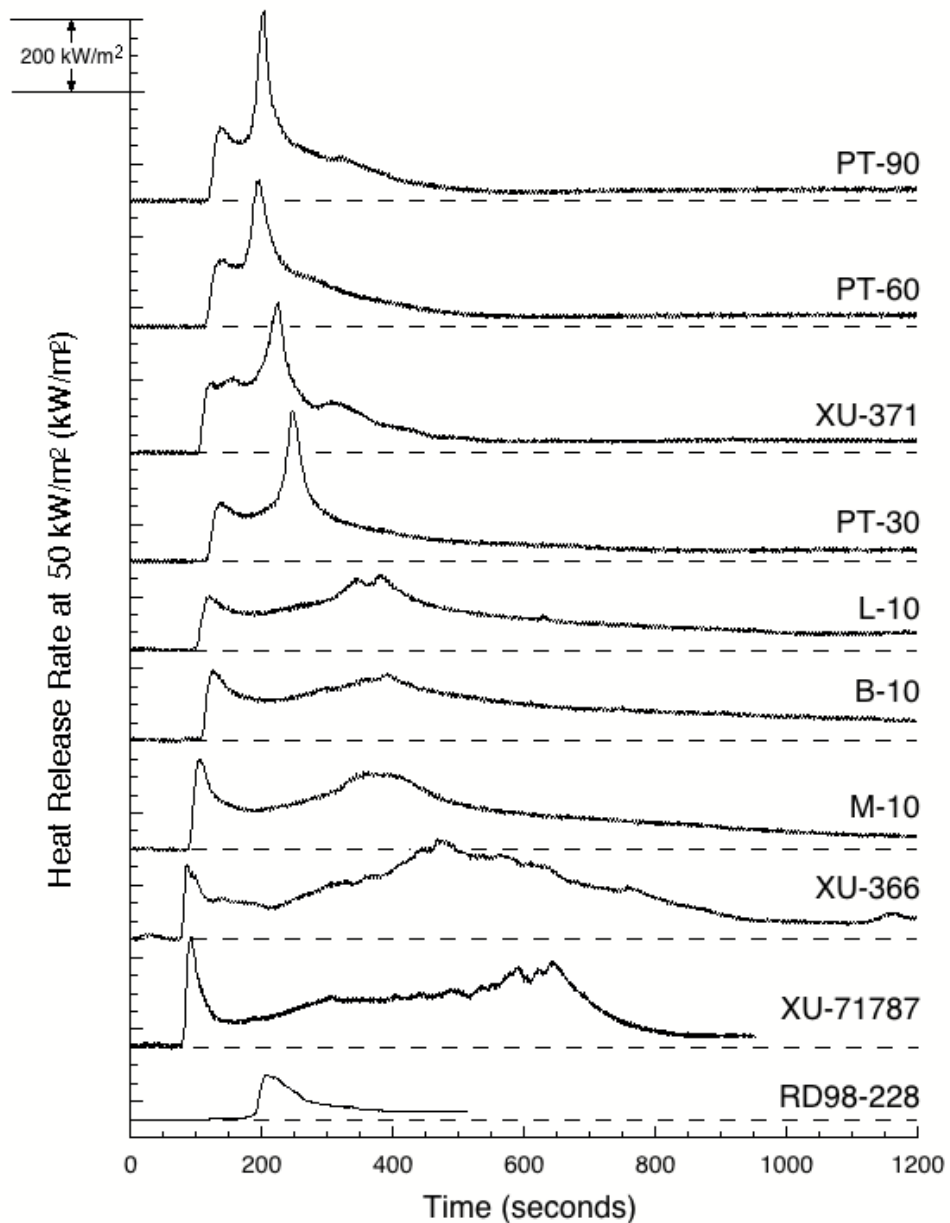


Figure 46. Heat release histories of polycyanurates at  $50 \text{ kW/m}^2$  heat flux in cone calorimeter.

The heat release rate histories of the polycyanurates of the difunctional ( $f = 2$ ) cyanate ester monomers L-10, B-10, M-10, XU-366, XU-71787, and RD98-228 are the lower six curves in figure 46. These  $f = 2$  polycyanurates show the same initial heat release rate peak at ignition as do the polycyanurates from the  $f > 2$  monomers. However, with the exception of RD98-228 the secondary heat release rate peak is broad and lower than the peak at ignition and occurs much later in the heat release history. The broad secondary HRR peak of the  $f = 2$  polycyanurates corresponds to char swelling and the generation of numerous small fissures in the char surface that gradually release the pyrolysis gases formed at depth. The absence of catastrophic char fracture during the burning of polycyanurates from  $f = 2$  monomers may be due to their lower char yield ( $35 \pm 7\%$ ) compared to the multifunctional resins ( $56 \pm 5\%$ ) and/or greater char permeability to pyrolysis gases. The  $f > 2$  polycyanurates have a lower molecular weight between cyanurate rings (higher crosslink density) [13] than those from  $f = 2$  resins, which could explain their higher char yield and the brittle fracture of their char during burning.

Yields of carbon monoxide and carbon dioxide per unit mass loss during flaming combustion ( $\text{kg-CO}_x/\text{kg-mass loss}$ ) were calculated from the instantaneous mass flow rates of the gases ( $\text{kg/s}$ ) divided by the sample mass loss rate  $\dot{m}_s$  ( $\text{kg/s}$ ). Specific smoke extinction area,  $SEA$  ( $\text{m}^2/\text{kg}$ ) is calculated during the test from the volumetric flow rate in the exhaust duct  $V_f$  ( $\text{m}^3/\text{s}$ ), the extinction coefficient  $k$  ( $1/\text{m}$ ) and mass loss rate of the sample as  $SEA = kV_f / \dot{m}_s$ . Extinction area is related to the number and size of smoke particles produced, with higher extinction area causing greater attenuation of the laser beam intensity in the test and, in principle, greater obscuration in a fire. Instantaneous smoke production rate,  $SPR$  ( $\text{m}^2/\text{s}$ ), is calculated as the product of the extinction coefficient and the volumetric flow rate in the exhaust duct divided by the sample surface area  $A$ ,  $SPR = kV_f / A$ . The smoke production rate, like the mass loss rate, tends to track the heat release rate fairly closely. The mass of soot generated per unit mass of burned sample ( $\text{kg/kg}$ ) was measured for the entire duration of the test by diverting 0.2% of the exhaust duct flow through a 47 mm diameter micro fiberglass collection filter using a mass flow controller and weighing the filter before and after the test.

Table 30 lists flaming combustion parameters extracted from that data for the polycyanurates. Listed in table 30 are the time-to-ignition ( $t_{ign}$ ), the maximum heat

release rate at ignition, i.e., the first peak in the HRR curves ( $HRR_{pk}$ ), the average heat release rate ( $HRR_{av}$ ) and the total heat released ( $THR$ ) over the entire 20 minute duration of the test, the peak mass loss rate ( $MLR_{pk}$ ), and the effective heat of combustion ( $EHC$ ) at each of the incident heat fluxes. The heat of gasification per unit mass of volatile fuel ( $L_g$ ) in column 8 of table 30 is obtained from the slope of a plot of peak heat release rate versus external heat flux which is a value called the heat release parameter ( $HRP$ ). The  $EHC$  divided by the  $HRP$  yields the heat of gasification. Values of  $L_g$  in parentheses are the result of only two peak mass loss rate, heat flux data pairs in table 30.

During the cone calorimeter tests the exposed face of the material began gasifying soon after exposure to the radiant heat flux. Ignition of gaseous fuel emerging from the exposed surface occurred 1-2 minutes into the test followed by surface charring, char cracking, and the development of porosity. The times to ignition for the polycyanurates were comparable at a particular heat flux with the exception of the halogenated F-10 and RD98-228 cyanate esters which were significantly longer. In case of the fluorinated polycyanurate F-10 there was no sustained ignition at 35 or 50 kW/m<sup>2</sup>.

Table 30. Fire behavior and properties of polycyanurates in cone calorimeter at several different heat fluxes.

Material	Heat Flux (kW/m <sup>2</sup> )	$t_{ig}$ (s)	$HRR_{pk}$ (kW/m <sup>2</sup> )	$HRR_{av}$ (kW/m <sup>2</sup> )	$THR$ (MJ/m <sup>2</sup> )	$MLR_{pk}$ (g/m <sup>2</sup> -s)	$L_g$ (MJ/kg)	$EHC$ (MJ/kg)
B10	35	171	166	92	93	8.3	4.0	25.5
	50	98	195	111	118	11.4		26.0
	75	40	246	157	160	22.3		27.5
	100	26	272	150	101	28.2		24.6
F10	35	NI	—	—	—	—	(3.0)	—
	50	(90)	—	—	—	—		—
	75	41	53	60	82	16.8		16.9
	100	27	78	45	53	25.2		9.8
L10	35	151	96	65	56	7.3	5.1	20.2
	50	88	149	104	102	10.3		26.0
	75	40	183	139	126	17.5		25.9
	100	22	204	145	100	19.6		24.1
M10	35	159	305	117	97	18.7	3.5	26.9
	50	69	251	125	117	10.0		27.1
	75	24	280	169	133	17.6		24.3
	100	19	338	173	112	35.5		25.1
PT30	35	202	179	71	46	19.8	5.0	19.1
	50	96	166	88	78	27.6		21.7
	75	40	118	112	83	34.8		21.2
	100	19	138	126	74	35.1		20.2
XU366	35	—	—	—	—	—	(2.2)	—
	50	69	202	149	152	11.0		28.4
	75	32	279	229	186	22.5		29.3
	100	—	—	—	—	—		—
XU371	35	203	204	68	42	20.9	(2.9)	17.5
	50	93	210	99	83	26.0		20.6
	75	41	231	123	79	27.0		20.9
	100	23	248	127	76	27.0		21.4
XU71787	35	167	244	55	51	12.98	4.4	24.9
	50	67	304	113	96	16.23		28.2
	75	32	378	172	165	24.6		28.6
	100	20	415	166	126	26.8		27.7
RD98-228	35	294	57	19	5.4	20	5.3	3.1
	50	189	124	45	13	17.6		3.5
	75	139	177	67	16	20.7		4.0
	100	129	186	57	19	32		4.1

## 4.6 IGNITABILITY

According to the thermal (heat transfer limited) theory of ignition [139], the time-to-ignition ( $t_{ign}$ ) for a semi-infinite thickness of material having ignition temperature  $T_{ign}$  experiencing a net heat flux  $\dot{q}_{net}$  is

$$t_{ign} = \frac{\pi}{4} k\rho c \left[ \frac{T_{ign} - T_0}{\dot{q}_{net}} \right]^2 \quad (54)$$

where  $k$ ,  $\rho$ , and  $c$  are the thermal conductivity, density, and heat capacity of the material, respectively. The net heat flux,  $\dot{q}_{net}$  is equal to the external radiant heat flux,  $\dot{q}_{ext}$  minus the heat lost to the environment at temperature  $T_0$  by re-radiation and convection  $\dot{q}_{loss}$ , i.e.,

$$\dot{q}_{net} = \dot{q}_{ext} - \dot{q}_{loss} \quad (55)$$

In practice the ignition time is found to depend on the ventilation conditions, ignition source, heat of combustion of the fuel value of the gases, etc. From equations 54 and 55

$$\frac{1}{\sqrt{t_{ign}}} = \frac{\dot{q}_{ext}}{\sqrt{\frac{\pi k\rho c}{4}(T_{ign} - T_0)}} - \frac{\dot{q}_{loss}}{\sqrt{\frac{\pi k\rho c}{4}(T_{ign} - T_0)}} \quad (56)$$

Equation 56 applies if  $L > 2(\alpha t_{ign})^{1/2}$ , where  $L$  is the sample thickness and  $\alpha = k/\rho c$  is the thermal diffusivity. In the present study  $L = 6.4$  mm and  $\alpha = 10^{-7}$  m<sup>2</sup>/s (typically) so ignition times,  $t_{ign} \leq L^2/4\alpha \approx 2$  minutes are valid for use with equation 56. Thus, fire calorimeter data for time-to-ignition for the polycyanurates at the higher external heat fluxes can be analyzed to extract an average value of the product  $k\rho c$  that represents the thermal resistance (inertia) of a material to external heating over the temperature range from ambient to ignition. Figure 47 is ignition data from table 30 for the B-10 polycyanurate plotted according to equation 56. The reciprocal slope of the line in figure 47 equals  $(T_{ign}-T_0)(\pi k\rho c/4)^{1/2} = (\pi/4)^{1/2} TRP$ , where  $TRP = (T_{ign}-T_0)(k\rho c)^{1/2}$  is referred to as the thermal response parameter, values for which have been tabulated for many common polymers and composites [9]. If the ignition temperatures of the

polycyanurates are equal to their decomposition temperatures measured in laboratory thermogravimetric analyses [90], then  $k\rho c$  can be computed from the measured thermal response parameter. Table 31 lists the measured thermal response parameter  $TRP$  and ignition (onset decomposition) temperature for each of the polycyanurates along with the thermal inertia ( $k\rho c$ ) calculated from these data. The  $TRP$  values are at the high end of the range reported for common polymers  $200\text{--}700 \text{ kW}\cdot\text{s}^{1/2}/\text{m}^2$  [9] because of the relatively high decomposition temperature of the polycyanurates [90]. However, when  $T_{ign}$  is accounted for in the calculation of the thermal inertia most of the  $k\rho c$  values of the polycyanurates are in the range of common, unfilled polymers,  $k\rho c \approx 1.0 \pm 0.2 \text{ kJ}^2/\text{m}^4\cdot\text{s}\cdot\text{K}^4$  [62]. The exceptions are the halogen-containing polycyanurates F-10 and RD98-228 which should have similar thermal properties to the other polycyanurates but instead exhibit experimental  $k\rho c$  values that are significantly higher, perhaps due to gas phase combustion inhibition not considered in the thermal (heat transfer limited) criterion for ignition (i.e., equation 56).

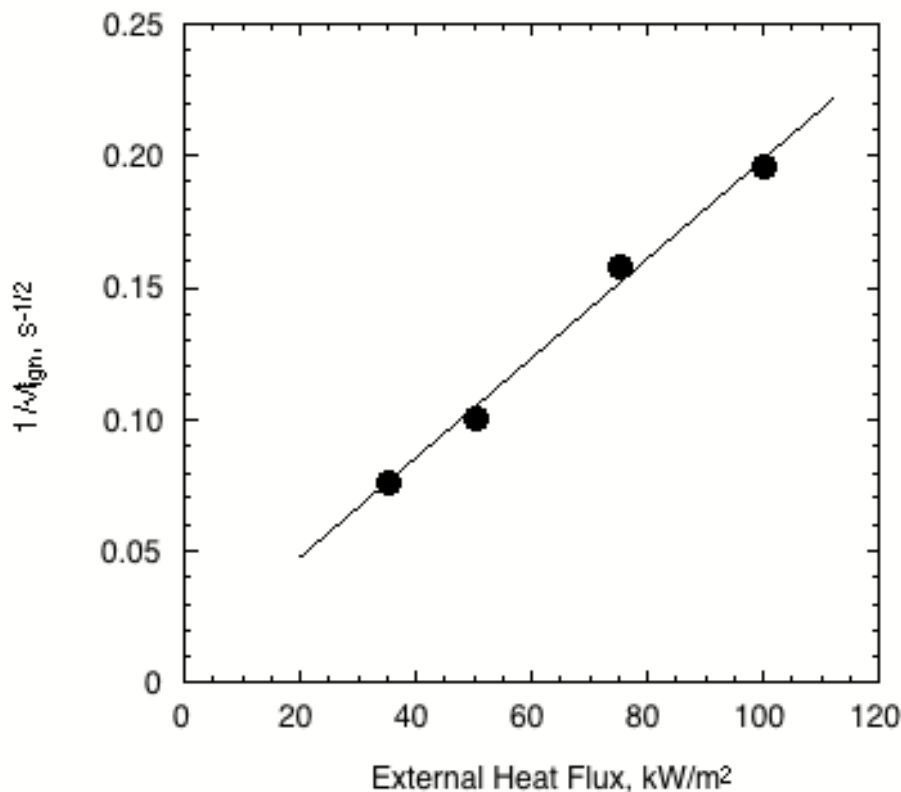


Figure 47. Time to ignition data versus external heat flux from the cone calorimeter for B-10 polycyanurate.

Table 31. Ignition properties of polycyanurates derived from cone calorimeter experiments.

Material	$T_{ign}$ (°C)	$TRP$ (kW-s <sup>1/2</sup> /m <sup>2</sup> )	$k\rho c$ (kJ <sup>2</sup> /m <sup>4</sup> -s-K <sup>4</sup> )
B-10	468	596	1.8
F-10	465	649	2.2
L-10	479	553	1.5
M-10	471	469	1.1
PT-30	462	463	1.1
XU-366	482	500	1.2
XU-371	461	531	1.5
XU-7178	463	508	1.3
RD98-228	461	705	2.6

Solid materials generate gaseous fuel when the total heat absorbed by the solid is sufficient to raise the temperature of the material to the thermal decomposition temperature, break primary chemical bonds in the polymer to make fuel fragments, and vaporize the resulting fuel fragments. This is the heat of gasification per unit mass of solid polymer,  $h_g$ . The heat of gasification determined from mass loss rate measurements,  $L_g$  in table 30, is the heat per unit mass of volatile fuel and it is obtained as the reciprocal slope of a plot of the peak mass loss rate ( $\dot{m}''$ ) versus external heat flux ( $\dot{q}_{ext}''$ ) assuming

$$\dot{m}'' = \frac{\dot{q}_n''}{L_g} = \frac{\dot{q}_{ext}'' + \dot{q}_{fl}'' - \dot{q}_{rr}''}{L_g} \quad (57)$$

where  $\dot{q}_{fl}''$  is the flame heat flux back to the surface and  $\dot{q}_{rr}''$  is the heat lost from the surface due to re-radiation. The char yields  $\mu$  and  $L_g$  in tables 30 and 32 can be used to calculate the heat of gasification per unit mass of polycyanurate,  $h_g = (1-\mu)L_g = 2.5 \pm 0.7$  kJ/g typical of synthetic polymers [21]. The narrow range of  $h_g$  indicates that the latent heats, bond breaking energies, and heats of vaporization of the degradation products that comprise  $h_g$  are similar for these polycyanurates, as would be expected based on their similar chemical composition and thermal degradation temperature.

## 4.7 COMBUSTION PRODUCTS

Table 32 lists data at 35, 50, 75, and 100 kW/m<sup>2</sup> radiant heat flux for the products of flaming combustion, i.e., the smoke yield in terms of specific extinction area, carbon monoxide (CO) and carbon dioxide (CO<sub>2</sub>) yields, soot yield, and the residual mass (char) fraction after the test. The combustion efficiency in the flame  $\chi$  is calculated as the ratio of the effective heat of flaming combustion (EHC in table 30) to the heat of complete combustion of the fuel gases ( $h_{c,y}^0$  in table 29), i.e.,  $\chi = EHC/h_{c,y}^0$ . The reported values for the combustion efficiency and combustion products are cumulative values for the entire test duration. Product yields are per unit mass of sample consumed. Char yield is expressed per unit initial mass of sample. The data in table 32 (with the exception of F-10) for soot yield, CO, and CO<sub>2</sub> (the latter quantities expressed as the ratio CO/CO<sub>2</sub>) are plotted versus combustion efficiency in figure 48.

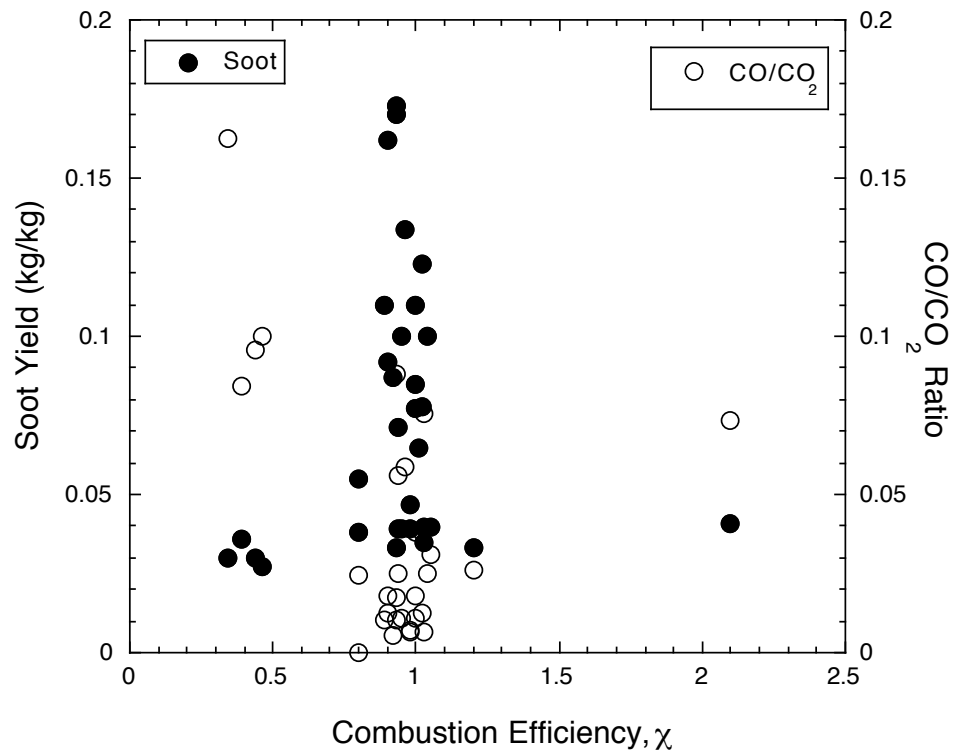


Figure 48. Soot yield and CO/CO<sub>2</sub> ratio versus combustion efficiency in flame for cyanate esters at different irradiances.

High soot yield and CO/CO<sub>2</sub> ratios are usually indicative of incomplete combustion in the flame. The data in table 32 plotted in figure 48 show that, in general, the CO/CO<sub>2</sub> ratio increases as the combustion efficiency decreases as would be expected for well-ventilated flaming combustion. However, soot yield appears to be largely independent of the combustion efficiency in the flame and depends instead on the chemical structure of the polymer. Soot yields were highest for the polycyanurates with pendent methyl (–CH<sub>3</sub>) groups B-10, M-10, and XU-366. It is seen that  $\chi$ , the soot yields, and the CO/CO<sub>2</sub> ratio are relatively independent of the applied external heat flux. Some errors are associated with the measurements which would account for combustion efficiencies greater than 1 and samples exhibiting both high combustion efficiencies and high soot yields. Also, these values are tabulated from averages over a range of burning behavior for a single material during a test.

Table 32. Cone calorimeter data for smoke obscuration and combustion product yields at several heat fluxes for polycyanurates.

Material	Heat Flux (kW/m <sup>2</sup> )	SEA (m <sup>2</sup> /kg)	CO (kg/kg)	CO <sub>2</sub> (kg/kg)	Soot Yield (kg/kg)	Combustion Efficiency, $\chi$	Char (%)
B10	35	583.7	0.01	1.87	0.087	0.92	48.7
	50	440.5	0.10	1.78	0.071	0.94	24.8
	75	683.2	0.04	2.20	0.085	1.00	19.1
	100	783.2	0.02	1.94	0.110	0.89	22.5
F10	75	54.6	0.14	1.91	0.041	2.1	16.0
	100	77.8	0.03	1.15	0.033	1.2	32.7
L10	35	522.9	0.04	1.65	0.055	0.80	61.5
	50	452.5	0.15	1.98	0.035	1.03	33.0
	75	540.6	0.08	2.10	0.078	1.02	27.0
	100	705.2	0.02	1.80	0.100	0.95	30.2
M10	35	723.6	0.07	1.84	0.077	1.00	53.3
	50	709.6	0.00	0.00	0.065	1.01	29.0
	75	771.3	0.02	1.61	0.092	0.90	23.6
	100	924.3	0.03	1.71	0.173	0.93	35.4
PT30	35	312.8	0.01	0.96	0.033	0.93	70.2
	50	235.9	0.05	1.61	0.040	1.05	56.9
	75	320.7	0.01	1.58	0.040	1.03	53.2
	100	395.6	0.01	1.49	0.047	0.98	50.5
XU371	35	345.7	0.00	0.91	0.038	0.80	70.3
	50	233.3	0.04	1.59	0.039	0.94	53.8
	75	305.7	0.00	0.00	0.039	0.95	54.8
	100	353.6	0.01	1.41	0.039	0.98	50.8
XU366	50	960.1	0.17	1.93	0.170	0.93	20.9
	75	906.6	0.12	2.04	0.134	0.96	17.0
XU71787	35	863.17	0.033	1.86	0.162	0.90	73
	50	747.72	0.024	1.93	0.123	1.02	58
	75	627.32	0.052	2.07	0.10	1.04	28
	100	767.72	0.02	1.85	0.11	1.00	43
RD98-228	35	123.0	0.039	0.240	0.030	0.34	62.0
	50	70.0	0.036	0.426	0.036	0.39	46.0
	75	97.0	0.036	0.376	0.030	0.44	55.0
	100	222.3	0.025	0.250	0.027	0.46	48.8

The high average flaming combustion efficiency for the polycyanurates calculated from all of the test data  $\chi = 0.93 \pm 0.3$  is consistent with the extremely low concentrations of hydrogen cyanide (3 ppm), carbon monoxide (207 ppm), and  $\text{NO}_x$  (3 ppm) in fire gases measured for these materials in fire calorimeters [85] and the low NBS smoke evolution ( $D_s = 1.7$ ) [85]. The anomalous combustion efficiencies calculated for the fluorinated cyanate ester F-10 ( $\chi > 1$ ) suggest that the effective heat of combustion listed in table 30 may include non-flaming heat of char oxidation (smoldering) which dominates the latter portion of the test after flame extinction as shown in Appendix C.

Halogen-containing polymers usually exhibit relatively high levels of incomplete combustion products such as CO and soot if they burn vigorously. However, the F-10 and RD98-228 polycyanurates barely support flaming combustion so their CO and soot yields as well as the specific extinction area for these halogen-containing polymers are comparable to, or lower than, the other polycyanurates because of the absence of gas phase combustion. The apparent contradiction between combustion product yields and combustion efficiency for RD98-228 is in fact consistent with the thermal degradation mechanism of this polycyanurate, which produces small amounts of low- and non-combustible gases (HCl, HOCN, CO, and  $\text{CO}_2$ ) and a large amount of char during pyrolysis [90]. The RD98-228 polycyanurate when used as a matrix resin for structural composites is the only conventionally-processed thermosetting polymer reported [137,140] to have passed all of the fire performance requirements for use on Navy submarines [136].

The combustibility of polycyanurates derived from a variety of cyanate ester monomers was studied in an attempt to correlate the chemical structure of these materials with their fire behavior. The effects of chemical composition were evidenced in the ignitability, burning behavior, and combustion efficiency in the flame. The halogen-containing polycyanurates were difficult to ignite and had extremely low heat release rates while soot production and carbon monoxide yields were comparable to, or lower than, the hydrocarbon materials.

#### 4.7 SUMMARY AND CONCLUSIONS

Extensive material studies on the thermal and flammability properties of thermoset resin systems were performed. Epoxy and cyanate ester resins were of particular interest in these studies due to their reaction chemistries and their good thermal, mechanical, and flammability properties.

Raw material properties and reaction chemistries for processing were examined using rheology, infrared spectroscopy and differential scanning calorimetry. It was demonstrated that cyanate esters and chlorinated (BPC) versions of epoxy and cyanate ester resins showed comparable processability and reaction temperatures. Strengths of the cured resin systems were shown to be in the range of the common baseline materials.

Thermal decomposition reactions were monitored using thermogravimetric analysis, infrared spectroscopy of both the solid and gas phase, and pyrolysis combustion flow calorimetry. Chlorinated versions of epoxy and cyanate esters showed similar decomposition temperatures but had a large difference in their heat release rates and amount of char residue. The BPC polymers showed a reduction in the peak and total heat release rates by a factor of two when compared to the BPA versions. Char yields were increased by a factor of two to four. This can be attributed to the decomposition mechanism cyclizing to form char instead of cleaving to produce volatiles.

Flammability studies were performed using cone and OSU calorimetry. Neat resins as well as structural composites were tested for flammability. Trends in the heat release rates that correlate with chemical structures were seen. Materials with more aromaticity and higher cross-link densities had lower heat release rates and higher char yields. Also, comparison of the BPA and BPC polymer systems showed the same trends as the thermal analysis results. The BPC had lower heat release rates due to the decomposition mechanism in addition to the release of non-flammable volatile decomposition products. Fire response parameters that provide information on the ignitability of a material were generated from series of tests at several heat fluxes in the cone calorimeter.

## CHAPTER 5

### CORRELATIONS & PREDICTIONS

## 5.1 NON-FLAMING COMBUSTION (PCFC)

A science-based screening method for flammability should be rapid, accurate, capable of measuring material/combustion properties, and be indicative of the results of fire and flame tests. Pyrolysis-combustion flow calorimetry or microscale combustion calorimetry was developed to satisfy these measurement criteria [34,141]. The MCC method separately reproduces the gas phase and condensed phase processes of flaming combustion and forces them to completion in a single, quantitative test using milligram-sized samples and oxygen consumption calorimetry. The measured thermal combustion properties include the heat of complete combustion of the pyrolysis gases per unit mass of original solid  $h_c^0$  (J/g), the maximum specific heat release rate  $Q_{max}$  at heating rate  $\beta$ , and the temperature at maximum pyrolysis rate  $T_{max}$  ( $^{\circ}\text{C}$ ), which are all measurable in the MCC. For polymers that thermally decompose to fuel gases and possibly char in a single step, as measured by TGA, the pyrolysis temperature interval is  $\Delta T_p = eRT_{max}^2 / E_a$ , where  $E_a$  (J/mol) is the global activation energy for pyrolysis,  $e$  is the natural number, and  $R$  is the gas constant. These combustion properties define a heat release capacity  $\eta_c$  as shown in equation 24.

The heat release capacity is the maximum potential of the material to release combustion heat in a fire or flame [22,34,141]. As a combination of material properties,  $\eta_c$  itself is a material property as measured in the MCC [141,142].

## 5.2 FLAMING COMBUSTION

### 5.2.1 Steady Burning

In contrast to MCC, flaming combustion is a highly coupled, non-equilibrium process because of chemical kinetics and diffusion (mass or heat) in the gas and condensed phases and is highly dependent on test conditions. The incomplete nature of flaming combustion is evidenced in flame tests as incomplete pyrolysis in the condensed phase and incomplete combustion in the diffusion flame (gas phase) both of which reduce the apparent flammability of the material relative to complete combustion, e.g., as measured in MCC. Thus, a model for the incomplete process of flaming combustion that accommodates the thermal combustion properties measured by MCC must be

developed to use MCC to screen flame-retardant plastics for flammability. The simplest model for flaming combustion is one-dimensional steady burning for which the heat release rate HRR (W/m<sup>2</sup>) of the solid is [47,143]

$$HRR = \chi \frac{H_c^0}{L_g} (q''_{flame} - q''_{loss} + q''_{ext}) \quad (58)$$

In equation 59  $HRP = EHC / L_g = \chi H_c^0 / L_g$  is the heat release parameter, which is the dimensionless ratio of the effective heat of combustion of the fuel gases  $EHC = \chi H_c^0$  (J/g) to the heat required to gasify a unit mass of volatile fuel,  $L_g = h_g / (1 - \phi)$  (J/g), where  $h_g$  is the heat of gasification per unit initial mass of solid. The driving force for HRR is the difference between the heat flux to the surface from the flame  $q''_{flame}$  (W/m<sup>2</sup>) and any external sources flame  $q''_{ext}$  (e.g., radiant heater or fire) and the heat losses from the surface to the environment  $q''_{loss}$ . Defining a limiting heat release rate at zero external heat flux,  $HRR_0 = HRP(q''_{flame} - q''_{loss})$ , the HRR in flaming combustion (equation 58) can be written in linear form [47,143]

$$HRR = HRR_0 + HRP q''_{ext} \quad (59)$$

where  $HRR_0$  is the limiting heat release rate at  $q''_{ext} = 0$ . Thus, a plot of HRR versus  $q''_{ext}$  has slope  $HRP$  and intercept  $HRR_0$ .  $HRR_0$  is the heat release rate of the material where the radiation from the flame,  $q''_{flame}$ , is sufficient to sustain burning. The heat release parameter can be written with equation 59, as the ratio of specific quantities

$$HRP = \chi \frac{H_c^0}{L_g} = \chi \frac{h_c^0}{h_g} = \chi \frac{h_c^0 / \Delta T_p}{h_g / \Delta T_p} = \frac{\eta_c}{\eta_g} \quad (60)$$

The term  $\eta_g = h_g / \chi \Delta T_p$  in equation 60 is a normalizing parameter that contains thermal combustion properties and the flaming (gas phase) combustion efficiency  $\chi$ . If the condensed phase heat/mass transfer efficiency  $\theta$  is included in  $\eta_g$ , this becomes

$$\eta_g = \frac{h_g / \Delta T_p}{\chi \theta} \quad (61)$$

The denominator  $\chi\theta$  of  $\eta_g$  in equation 61 has the character of a macroscopic ‘‘burning efficiency.’’ At the large external heat fluxes that can occur in fires or fire calorimeters,  $q''_{ext} \gg q''_{flame} - q''_{loss}$ , and from equations 59-61,

$$HRR = HRR_0 + HRPq''_{ext} \approx HRPq''_{ext} = \eta_c \frac{q''_{ext}}{\eta_g} = \eta_c \left( \frac{\chi\theta}{h_g/\Delta T_p} \right) q''_{ext}. \quad (62)$$

Equation 62 shows that the HRR in forced flaming combustion at high external heat flux, which is thought to be the best indicator of fire hazard [1], should be roughly proportional to  $\eta_c$ , assuming all other factors ( $\eta_g, q''_{ext}$ ) remain unchanged.

### 5.2.2 Unsteady Burning

Transient or unsteady burning is an aspect of flammability that relates to the tendency of a thin strip of material to resist ignition by a small flame or burner, i.e., flame resistance. The most common flame resistance tests are the Underwriters Laboratory test for flammability of plastic materials UL94 [144] and the limiting oxygen index (LOI) test [145]. In these tests, the specimen is briefly exposed to a small flame and the time to extinction is recorded. At the start of the test when the flame is removed  $q''_{ext} = 0$  at  $t = 0$ . If a minimum (critical) heat release rate  $HRR^*$  is the criterion for sustained flaming combustion [47,143,146,147], then according to equations 58-60 flame extinction in these tests should occur when  $HRR_0 < HRR^*$ , or

$$HRP \leq \frac{HRR^*}{q''_{flame} - q''_{loss}} \text{ (macroscale)} \quad (63)$$

$$\eta_c \leq \eta_g \frac{HRR^*}{q''_{flame} - q''_{loss}} \text{ (microscale)} \quad (64)$$

Equations 63 and 64 are chemical criteria for flame extinction in the UL94 and LOI tests in terms of HRP (macroscale) or  $\eta_c, h_g, \Delta T_p$ , and the burning efficiency parameters,  $\chi$  and  $\theta$ , of the polymer/additive compound (microscale).

A thermal criterion for flame extinction states that a minimum net heat flux is required to pyrolyze the solid and generate sufficient fuel for sustained combustion, i.e.,  $q''_{flame} \leq q''_{loss}$ . Assuming that heat losses from the flaming surface are loss by re-radiation only, because that is what prevents a material from further degrading, and the burning and ignition temperatures are similar and approximately equal to  $T_{max}$  [146-148], then the critical heat flux  $CHF$  for self-sustained burning is

$$q''_{loss} = CHF = \varepsilon\sigma(T_{max}^4 - T_a^4) \approx \varepsilon\sigma T_{max}^4 \quad (65)$$

where  $T_a$  is the ambient temperature,  $\varepsilon$  is the surface emissivity, and  $\sigma$  is the Boltzmann radiation constant. Assuming,  $q''_{flame} \approx 30 \text{ kW/m}^2$  [146,147] and  $\varepsilon = 1$ , the critical heat flux criterion for self-sustained burning is equivalent to

$$T_{max} \geq \left( \frac{q''_{flame}}{\varepsilon\sigma} \right)^{1/4} \approx \left( \frac{30 \text{ kW/m}^2}{(1)(5.7 * 10^{-8} \text{ Wm}^{-4} \text{ K}^{-4})} \right)^{1/4} = 852 \text{ K} = 579^\circ \text{C} \quad (66)$$

Equations 65 and 66 are thermal criteria for flame extinction in standard tests in terms of a single thermal combustion property  $T_{max}$  measured in the MCC.

### 5.3 FLAMMABILITY

The propensity for vertical and horizontal burning under ambient conditions was measured on plastic samples according to standard methods [144,149]. The minimum concentration of oxygen in the environment that would support candle-like combustion of plastics (limiting oxygen index / LOI) was measured according to a standard method [145]. Generic values for flame resistance as measured in the UL94 and LOI tests were obtained from a handbook [143] for commercial polymers/ plastics at 3 mm thickness. The heat release rate in forced flaming combustion was measured on 100 x 100 x 6.4 mm<sup>3</sup> samples in a horizontal orientation at a radiant heat flux  $q''_{ext} = 50 \text{ kW/m}^2$  using an edge frame sample holder according to a standard method [36].

### 5.3.1 UL94

Table 33 lists the average  $T_{max}$  from three separate laboratories and the  $CHF$  calculated from  $T_{max}$  using equation 65 for some common plastics. Also listed in Table 33 are handbook values [143] for the UL94 rating, HRP, and the measured CHF for these polymers. Reasonable agreement is observed between the CHF estimated from  $T_{max}$  and the  $CHF$  measured directly for hydrocarbon polymers. However, the thermal criteria for flame extinction (equations 65 and 66),  $CHF \geq 30 \text{ kW/m}^2$  or  $T_{max} \geq 579^\circ\text{C}$ , are poor predictors of UL94 rating for heteroatom (PPS) and halogen-containing polymers (PVC, PVDF, FEP) that burn with low combustion efficiency because of chemical inhibition of the flame. For these plastics, the chemical criterion (equation 63) of a critical  $HRP \approx 5$  is a better predictor of self-sustained ignition than a critical (ignition) temperature [146,150].

Table 33. UL94 rating of plastics,  $HRP$ ,  $T_{max}$ , and critical heat flux ( $CHF$ ).

Plastic	UL94 Rating	HRP	$T_{max}$ (°C)	$CHF$ (kW/m <sup>2</sup> )	
				Equation 65	Reference 143
PMMA	HB	14	401 ± 8	11-12	6-23
POM	HB	6	409 ± 10	11-13	13
HIPS	HB	14	463 ± 10	15-17	15
ABS	HB	13	467 ± 12	16-18	9-15
PET	HB	13	471 ± 12	16-18	10-19
PA6.6	HB	18	482 ± 11	17-19	15-21
PVC	V-0	3	478 ± 8	17-18	15-28
PP	HB	22	493 ± 10	18-20	15-16
HDPE	HB	18	514 ± 10	20-22	15-20
PVDF	V-0	2	510 ± 2	21	30-50
PC	V-2	9	556 ± 9	25-28	15-20
PPS	V-0	4	551 ± 18	24-28	35-38
PEI	V-0	6	576 ± 10	28-31	25-40
FEP	V-0	2	600 ± 10	31-34	38-50

Figure 49 is a plot of  $\eta_c$  and the UL94 rating of 1.6 mm-thick samples of the glass fiber-reinforced plastics (GFRP) polycaprolactam (PA6), polybutyleneterephthalate (PBT), polycarbonate (PC), and polyphenylenesulfide (PPS) versus the fiberglass loading level of these GFRP [151]. The data in figure 49 show that  $\eta_c$  decreases in approximate proportion to the mass fraction of combustibles,  $1 - \phi$ , following an initial rise at low fiberglass fraction  $v$ . This rule-of-mixtures effect of inert fiberglass loading on  $\eta_c$  translates into relatively small improvement in the UL94 rating up to levels as high as 30% by weight. Thus, inert additives such as mineral fillers or fiberglass are relatively inefficient on a weight basis at reducing flammability.

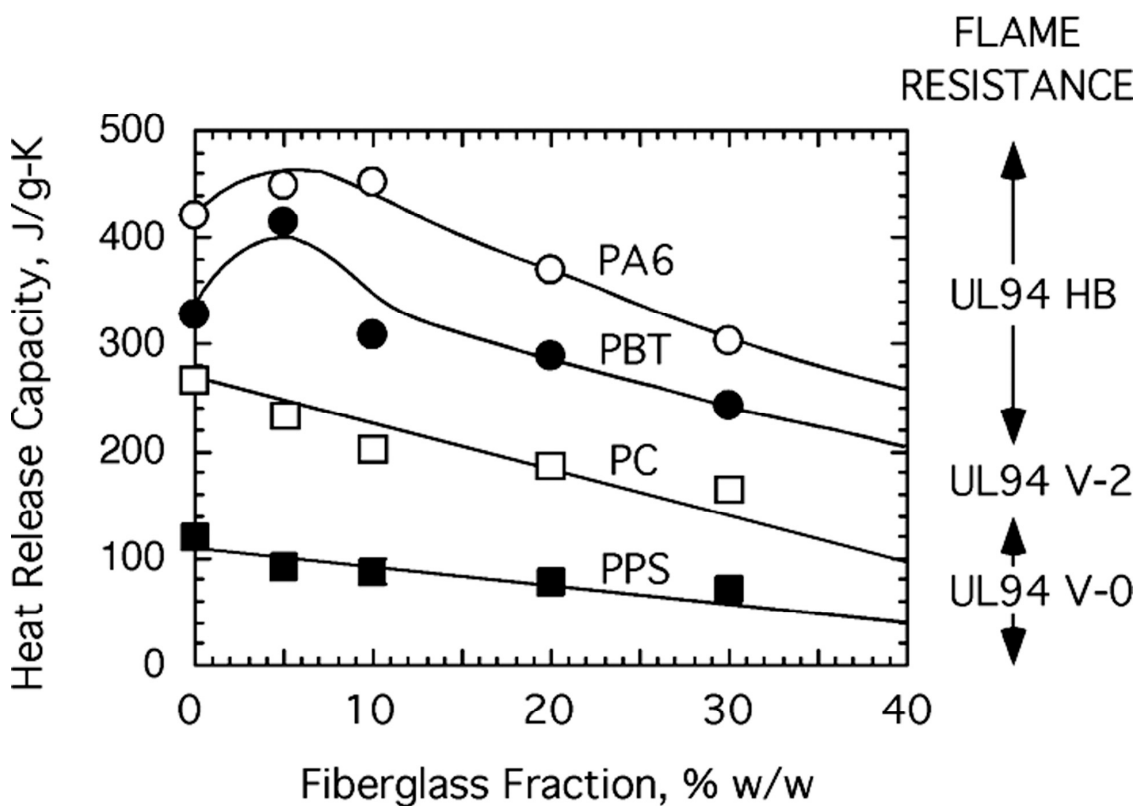


Figure 49. Flammability ( $\eta_c$  and UL 94 rating) of glass fiber-reinforced plastics versus fiberglass weight fraction.

Figure 50 shows experimental data for self-extinguishing tendency in a 45-degree Bunsen burner ignition test [149] and  $\eta_c$  on the right and left ordinate, respectively, versus phosphorus concentration on the abscissa for an aerospace epoxy containing various amounts of reactive phosphorus-compounds in the form of aromatic glycidyl ethers and aromatic amines [152]. Figure 50 shows that phosphorus is very efficient on a weight basis at improving flame resistance, and that the efficacy (negative slope of  $\eta_c$

versus % P) increases with the number of oxygen atoms bound to phosphorus in the starting compound. Self-extinguishing behavior is observed at phosphorus concentrations as low as 1% by weight, whereas fiberglass (an inert filler) at 30% by weight (w/w) does not render polycarbonate self-extinguishing / V-0 (figure 49).

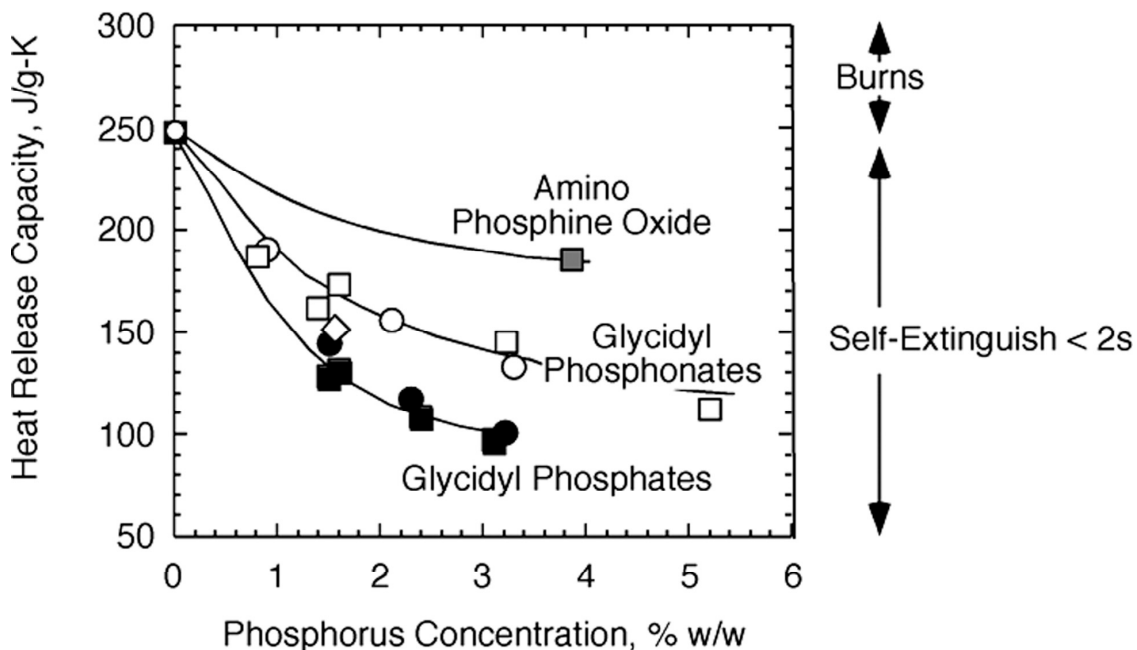


Figure 50. Flammability ( $\eta_c$  and flame resistance) of aerospace epoxy versus phosphorus concentration for reactive phosphorus compounds.

Figure 51 is a plot of  $\eta_c$  and the heat of complete combustion of the volatiles for diglycidylether of bisphenol-A (DGEBA) cured with 2,4-ethylmethyimidazole (4% by weight) and co-reacted with brominated-DGEBA (DER 542, Dow Chemical) or blended with tetrabromobisphenol-A (TBBA) to obtain the bromine concentrations plotted along the abscissa [153]. The heat of combustion per unit mass of hydrocarbon fuel gases plotted on the right ordinate was calculated by subtracting the mass of bromine and char from the original sample mass. The data in figure 51 indicate that  $\eta_c$  decreases in rough proportion to the combustible (non-bromine) fuel fraction and solid-state reactions are relatively unimportant. Likewise, the heat of combustion of the volatile hydrocarbons is unaffected by bromine concentration, indicating that gas-phase combustion / oxidation inhibition is absent under the standard conditions [48] of the MCC test. These observations show that bromine acts simply as an inert additive in the MCC with little condensed-phase activity and no gas-phase activity [153,154], under standard conditions, because pyrolysis and combustion are forced to completion. Tests

performed in the MCC at lower combustor temperatures have shown gas phase inhibition with the addition of bromine, but are not presented here.

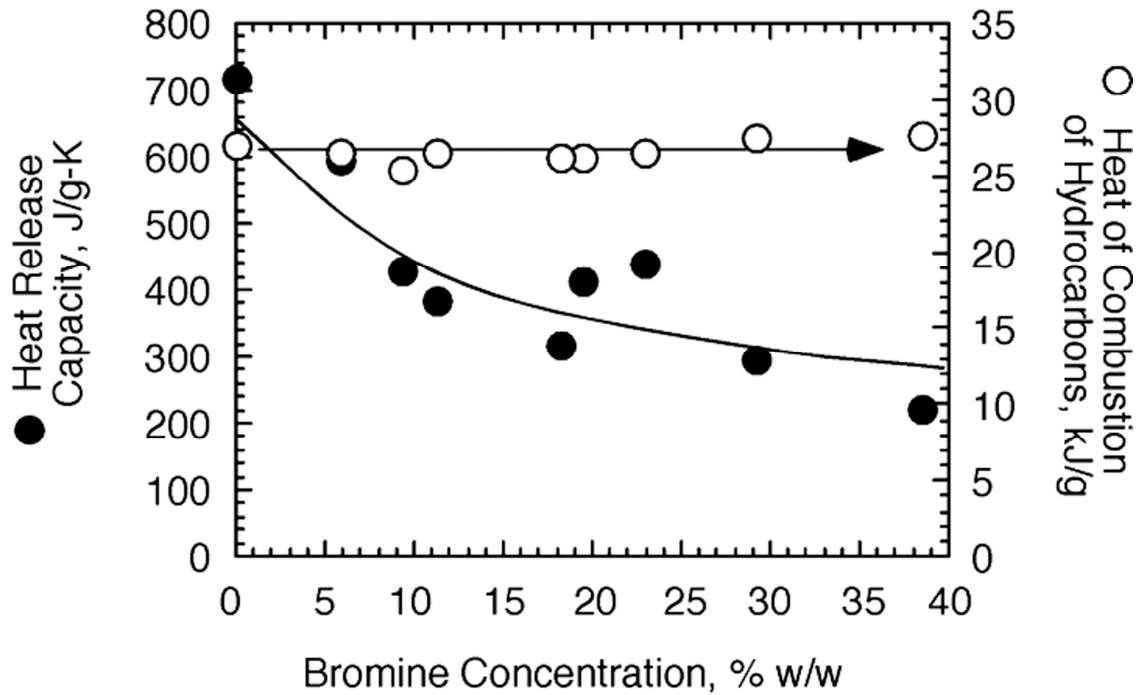


Figure 51. Heat release capacity,  $\eta_c$ , and heat of combustion of hydrocarbon volatiles versus bromine concentration for DGEBA epoxy.

Figure 52 compares UL94 test results for polymers, copolymers, polymer blends, and plastics with (FR) and without (natural) flame-retardant additives plotted versus the heat release capacity  $\eta_c$  measured in the MCC. The samples whose data are plotted in figure 52 span a wide range of chemical structure and thermal stability and range in thickness from 1.6 to 3.2 mm. This range of thickness can account for a variation of one UL94 classification on the ordinate. Figure 52 shows that the threshold for self-sustained burning (UL 94 V rating) is about 200 J/g-K but occurs over the broad range,  $\eta_c = 200$ –700 J/g-K for polymers (natural plastics) as well as plastics containing bromine (gas phase active) and phosphorus (condensed phase active) flame-retardant additives. The data in figure 52 can be described using the microscale extinction model (equations 64 and 65) as follows. Evaluating equation 61 for natural plastics exhibiting typical properties,  $h_g = 2$  kJ/g and  $\Delta T_p = 50$  K,

$$\eta_g = \frac{h_g / \Delta T_p}{\chi \theta} \approx \frac{40 \text{ J/g-K}}{\chi \theta} .$$

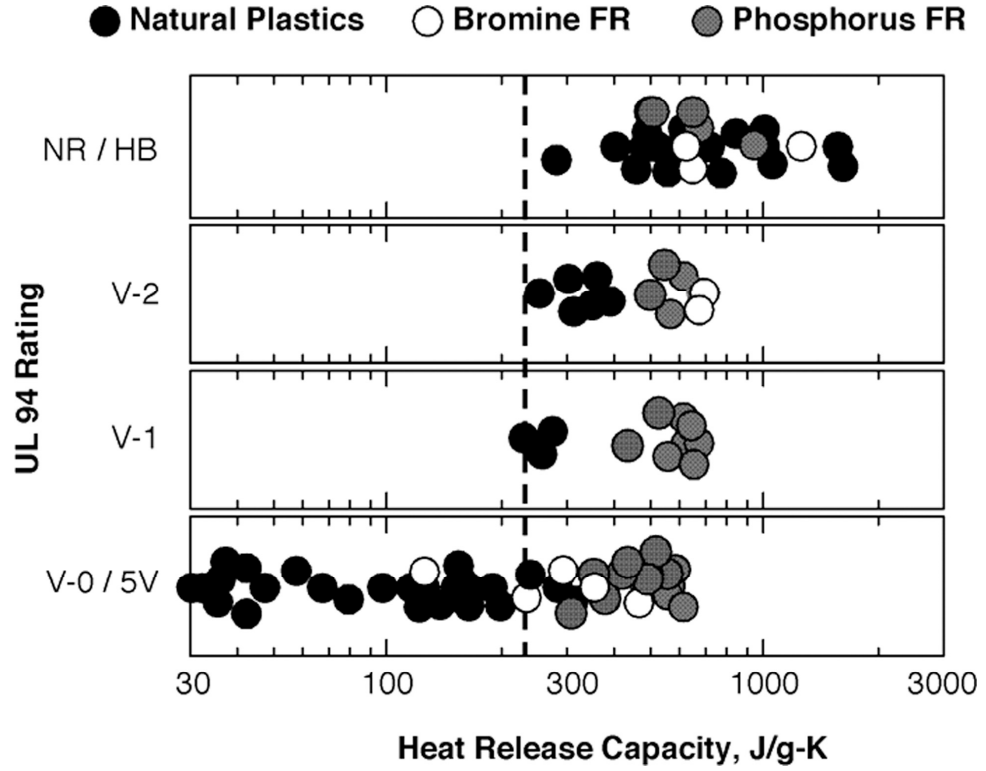


Figure 52. UL 94 rating versus heat release capacity  $\eta_c$  of polymers (NR = no rating in vertical test). The lower threshold for self-sustained ignition,  $\eta_c \approx 200$  J/g-K is shown as a vertical dashed line.

The critical heat release rate for burning of a condensed phase with a diffusion flame in air is  $HRR^* \approx 60$  kW/m<sup>2</sup> [146,147] and the flame heat flux is  $q''_{flame} \approx 30$  kW/m<sup>2</sup> [147]. Assuming,  $q''_{loss} \approx CHF$  (see table 34) =  $\epsilon\sigma T_{max}^4$ , the extinction condition for plastics with  $\epsilon = 1$  in the UL94 test is obtained from equations 64 and 65,

$$\eta_c \leq \frac{\eta_g HRR^*}{(q''_{flame} - \epsilon\sigma T_{max}^4)} \approx \frac{67 J/g-K}{\chi\theta(1 - 1.9 * 10^{-12} K^{-4} T_{max}^4)} \quad (67)$$

Coupling between the gas phase and condensed phase processes of flaming combustion is implicit in equation 67, which predicts an inverse relationship between  $\eta_c$  at flame extinction and the burning efficiency  $\chi\theta$  and thermal stability of the plastic.

Figure 53 is a graphical representation of equation 67 showing that  $\eta_c$  for flame extinction ( $\eta^*$ ) increases with  $T_{max}$  and  $\chi\theta$  as expected because the amount of heat

entering the plastic from the flame is reduced by incomplete gas phase combustion ( $\chi$ ) and by attenuated mass/heat transport across the surface due to charring/swelling ( $\theta$ ). Figure 53 shows that polymers having  $T_{max} \approx 460^\circ\text{C}$  such as HIPS, ABS, and PET can exhibit flame resistance / extinction at  $\eta_c$  ranging from 150 to 750 J/g-K as  $\chi\theta$  decreases from 1 to 0.2 with the incorporation of gas phase-active flame retardants, char promoters, intumescent (swelling) compounds, inert fillers or some combination of these. Thus, the same range of  $\chi\theta$  that correlates the HRR in forced flaming combustion also correlates the flame resistance data in figure 53 as per the flame extinction model (equations 64 and 65).

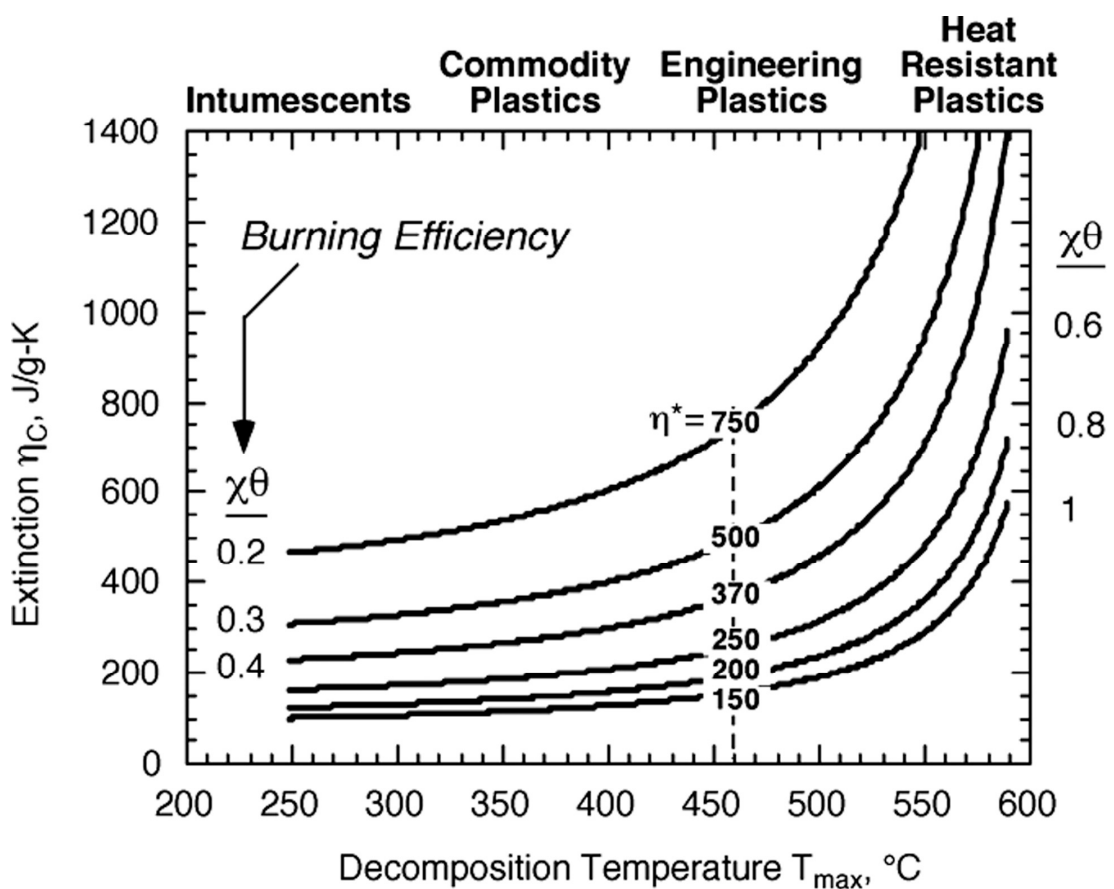


Figure 53. Flame resistance diagram showing the heat release capacity for flame extinction versus decomposition temperature. Upper abscissa indicates decomposition temperature range for generic plastics.

The deterministic model of flame extinction (equations 64 and 65) requires *a priori* knowledge of  $\chi$  and  $\theta$  or additional experiments to determine these parameters to predict flame resistance from MCC data. A statistical model circumvents these

problems by calculating a probability of flame extinction. Logistic regression [155] is a statistical procedure that is widely used in the medical, social, and physical [156] sciences to relate the unconditional probability  $p$  of a binary dependent variable (e.g., burn / no burn) to independent explanatory variables using an equation of the form

$$\ln\left[\frac{p}{1-p}\right] = \alpha_0 + \alpha_1\chi_1 + \alpha_2\chi_2 + \dots \quad (68)$$

where  $\alpha_i$  are fitting parameters with the significance of likelihood coefficients and  $x_i$  are independent explanatory variables, e.g.,  $\eta_c$ ,  $h_0$ ,  $T_{max}$ ,  $\mu$ , etc. For a single explanatory variable  $x = \eta_c$

$$p = \frac{e^{\alpha_0 + \alpha_1\eta_c}}{1 + e^{\alpha_0 + \alpha_1\eta_c}} \quad (69)$$

The probabilistic model was applied to flame resistance in the present study by assuming that  $\eta_c$  is the sole explanatory variable for the 100 UL94 ratings in figure 52 and assigning a numerical value to each rating: HB, No Vertical Rating = 3; V-2 rating = 2; V-1 rating = 1; V-0, 5V rating = 0. The probability of self-sustained ignition was assumed equal to one-third of the numerical UL rating, so that the burning probability ranges from 0.0 (V-0/5V) to 1.0 (NR or HB) as illustrated in figure 54. The solid line in figure 54 is equation 69 for  $p = p(\eta_c)$  with  $\alpha_0 = -6$  and  $\alpha_1 = 1/67$ .

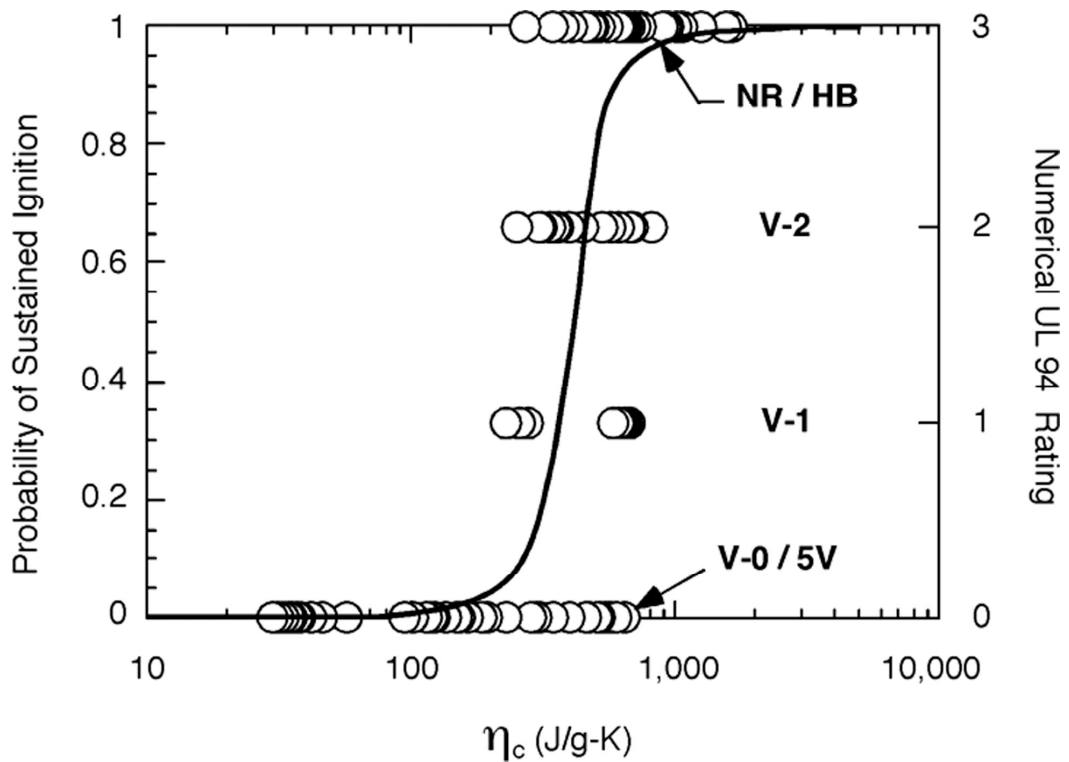


Figure 54. Probability of sustained ignition in UL94 test versus  $\eta_c$ ; solid line is equation 69 with  $\alpha_0 = -6$  and  $\alpha_1 = 1/67$ .

The probability of obtaining a UL94 V-0 rating is  $P(0) = 1 - p$  and the associated 68% confidence interval is  $C = p \pm [p(1 - p)/n]^{1/2} [(N - n)/(N - 1)]^{1/2}$  for  $n = 5$  specimens drawn from the  $N = 100$  tests plotted in figure 54. Figure 55 shows these calculations for  $P(0)$  and  $C$  as black and gray lines, respectively. Figure 55 shows that there is a 95% probability ( $P_0 = 0.95$ ) of obtaining a V-0 or 5V rating for  $\eta_c \leq 205$  J/g-K. This result agrees with the lower threshold for burning approximated by the vertical dashed line in figure 52. Figure 55 shows that a plastic having  $\eta_c = 400$  J/g-K has between a 30 and 73% chance of obtaining a UL 94 V-0 rating.

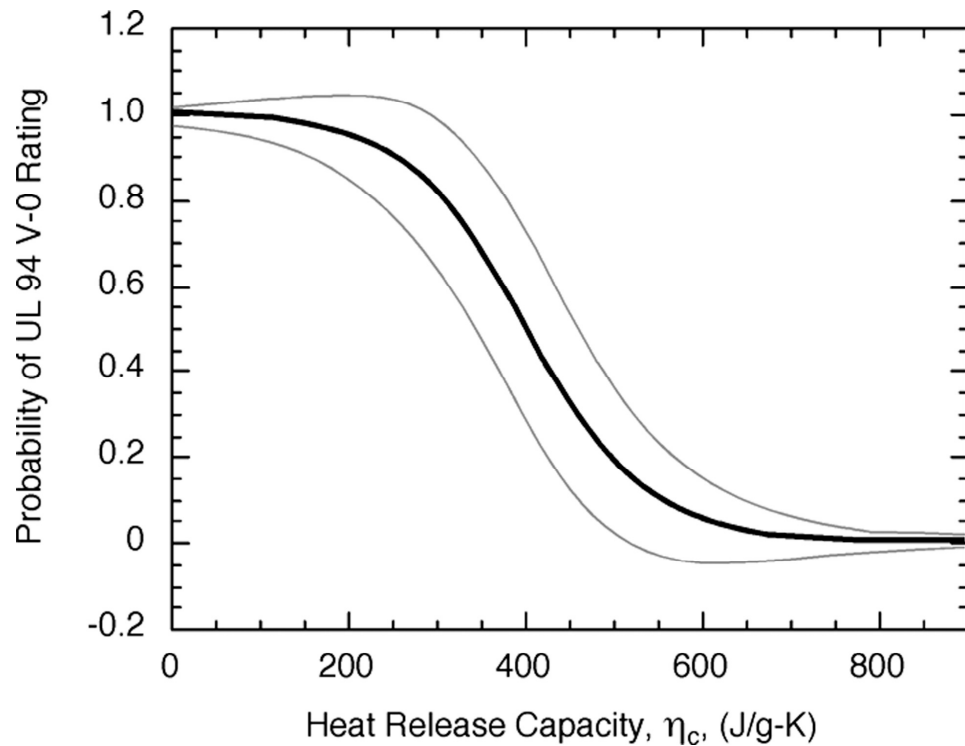


Figure 55. The probability (black line) and 68% confidence interval (gray lines) of a UL 94 V-0 rating versus heat release capacity.

The UL 94 rating system accommodates only four discrete burning probabilities 0, 0.33, 0.67, and 1.0, corresponding to V-0 / 5V, V-1, V-2, and HB / NR, respectively. An alternative approach is to use the after-flame times or the burn length [156] as the continuous dependent variable in the probabilistic analysis and calculate a spectrum of burning probabilities from these data.

### 5.3.2 Oxygen Index

The deterministic flame extinction model can also correlate the LOI test with MCC data as follows. The heat flux from a flame to the surface of a combustible condensed phase (solid or liquid) has been shown [157] to be proportional to the volume fraction of oxygen  $[O_2]$  in the atmosphere, i.e.  $q''_{flame} \propto [O_2] = b[O_2]$ . Empirically, it is found that  $b = 1.40 \text{ kW/m}^2 - \%[O_2]$  [157], so the critical heat release rate for extinction can be written in terms of the oxygen concentration in the LOI test atmosphere and the burning temperature of the plastic using equations 64 and 65,

$$LOI = [O_2]^* = \frac{h_g HRR^* / b \Delta T_p}{\eta_c \chi \theta} + \frac{\sigma}{b} T_{max}^4 \quad (70a)$$

Using the same properties as for equation 67 and evaluating terms

$$LOI = \left( \frac{(2kJ/g)(60kW/m^2)}{(1.4kW/m^2 - \%O_2)(50K)} \right) \frac{1}{\eta_c \chi \theta} + \left( \frac{5.7 * 10^{-8} Wm^{-2} K^{-4}}{1.4kW/m^2 - \%O_2} \right) T_{max}^4 \quad (70b)$$

$$LOI = \frac{1.7 * 10^3 \%O_2 J/g - K}{\eta_c \chi \theta} + \{4.1 * 10^{-11} \%O_2 / K^4\} T_{max}^4 \quad (70c)$$

Figure 56 is a plot of equation 70 as LOI of 3.2-mm-thick samples versus  $\eta_c$  for  $\chi\theta = 1$  and  $T_{max} = 250, 450, 550,$  and  $650^\circ\text{C}$ . Experimental data for hydrocarbon and halogen-containing plastics is also plotted in figure 56, which demonstrates that heat resistance/thermal stability can have a large effect on LOI at a given value of  $\eta_c$ . Figure 57 is a plot of LOI versus  $\eta_c$  for  $\chi\theta = 0.2, 0.4, 0.6, 0.8,$  and  $1.0$  at a typical (see table 33)  $T_{max} = 450^\circ\text{C}$ .

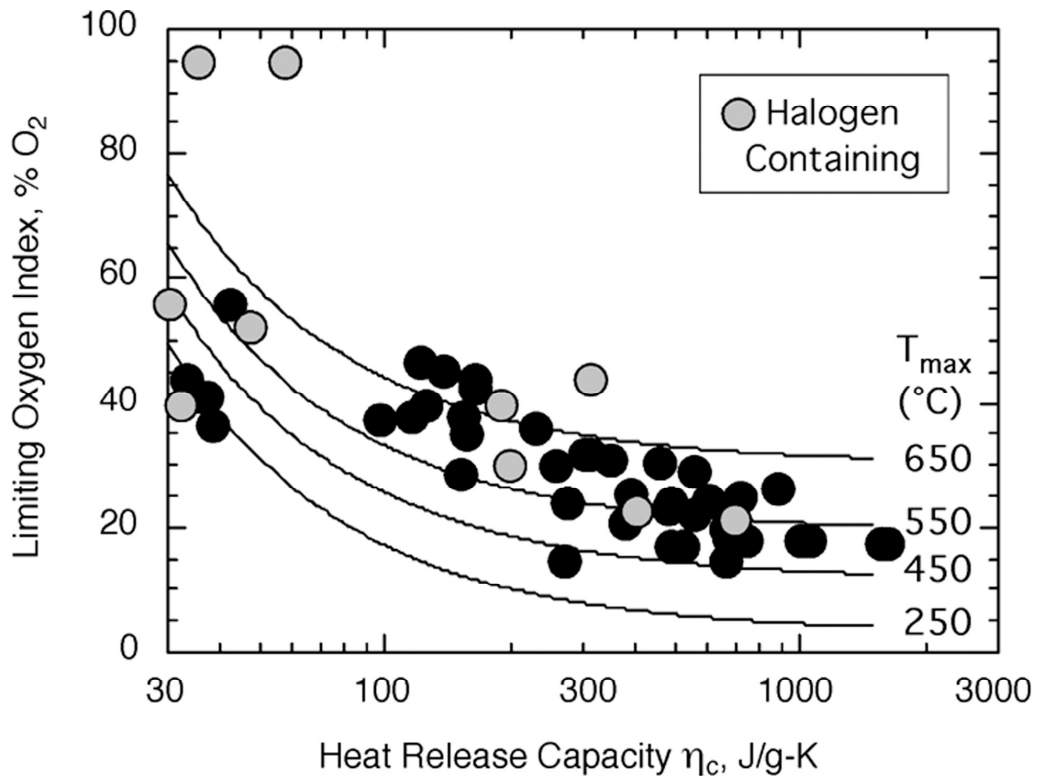


Figure 56. LOI versus  $\eta_c$  for  $\chi\theta = 1$  and various  $T_{max}$ .

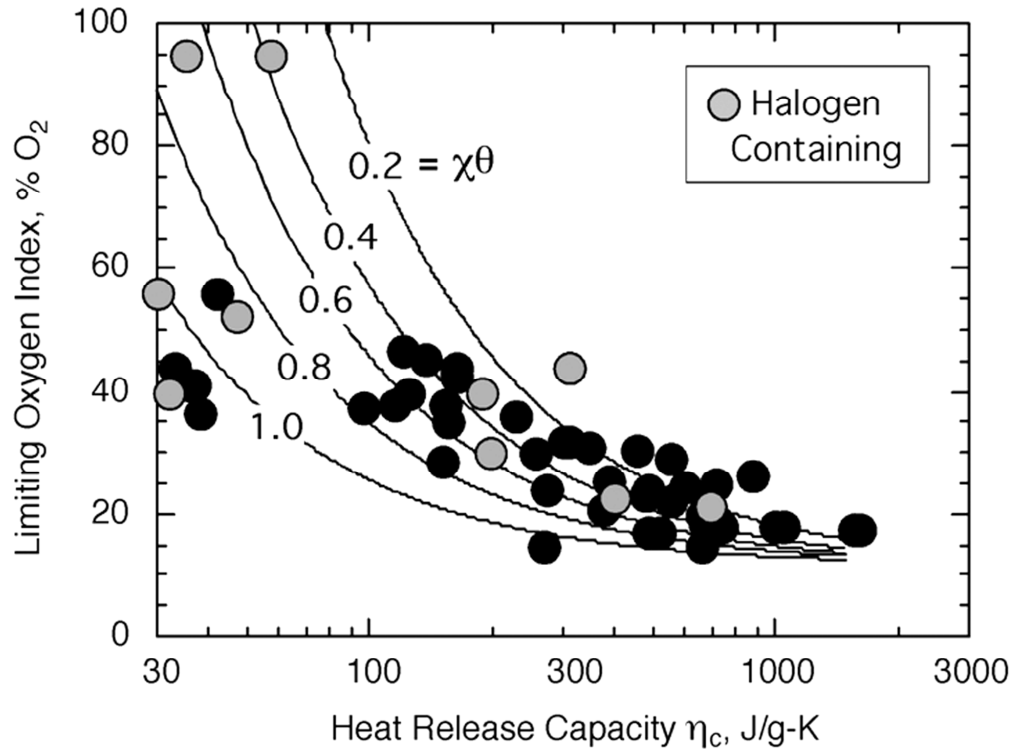


Figure 57. LOI versus  $\eta_c$  for  $T_{max} = 450^\circ\text{C}$  and various  $\chi\theta$ .

Equation 70 shows that the LOI asymptote at high  $\eta_c$  for a typical  $T_{max}$  is LOI = 11%  $\text{O}_2$ , in agreement with theory [156]. Because of the variation in  $\chi\theta$ , a broad range of LOI is associated with a broad range of  $\eta_c$ , but LOI  $\geq 30$  is likely for  $\eta_c < 200$  /g-K. Thus,  $\eta_c$  measured in the MCC is not a unique criterion for flame extinction of plastics in either the UL 94 or LOI tests as demonstrated by the data in figures 52-57. Instead, a critical HRR (a test-dependent quantity) is the criterion for flame extinction and it is related to the burning potential  $\eta_c$ , the burning efficiency  $\chi\theta$ , and the thermal stability/heat resistance  $T_{max}$  of the plastic through an extinction model (equations 64 and 65). Because flame extinction is a critical phenomenon, a slight variation in any of the terms or parameters describing extinction can have a large effect on flame resistance. As combustion is necessarily incomplete at extinction, while  $\eta_c$  is a complete combustion parameter, the relationship of  $\eta_c$  to flame resistance is inherently uncertain but amenable to analysis.

In contrast,  $\eta_c$  correlates closely ( $R = 0.9$ ) with the peak HRR in forced flaming combustion (fire conditions) because the gas-and condensed-phase processes are relatively efficient. As the potential (rather than the actual) capacity of a plastic to

release heat in a fire,  $\eta_c$  is a conservative estimate of fire hazard. Consequently, additives that impart flame resistance to plastics with high  $\eta_c$  in standardized fire tests may have little [158] or no [159] effect on their reaction to performance due to complete combustion in the MCC.

#### 5.4 FIRE RESPONSE

The single best parameter characterizing the fire hazard of a polymer is its HRR ( $\text{W}/\text{m}^2$ ) in flaming combustion [1]. However, HRR is difficult to quantify in fire calorimeters because the test results depend on the external heat flux (heating rate), sample thickness, sample orientation, edge conditions, ventilation rate, etc. In contrast, the heat release capacity measured by PCFC using controlled pyrolysis and complete combustion of the fuel gases depends only on the material being tested. The HRR of a solid polymer in flaming combustion is characterized by a heat of gasification  $L_g$  and an effective heat of combustion of the fuel gases (HOC), which is related to  $h_{c,v}^0$  by the combustion efficiency in the flame,  $\chi = \text{HOC} / h_{c,v}^0$ .

At an external heat flux  $q''_{ext} = 50 \text{ kW}/\text{m}^2$ , typical of a large fire such that  $\text{HRR}_0 \ll \text{HRP}$   $q''_{ext}$ , equation 63 predicts that for typical polymers having a normalizing parameter  $\eta_g = L_g/\chi\Delta T_{p,0} \approx (2 \text{ MJ}/\text{kg})/((0.8)(50\text{K})) = 50 \text{ kJ}/\text{kg}\text{-K}$

$$\text{HRR} = \frac{q''_{ext}}{\eta_g} \eta_c \approx \frac{50 \text{ kW} / \text{m}^2}{50 \text{ kJ} / \text{kg} - \text{K}} \eta_c = 1 \frac{\text{kg} - \text{K}}{\text{m}^2 - \text{s}} \eta_c$$

In other words, the  $\text{HRR}$  in flaming combustion at large external heat flux should be roughly proportional to  $\eta_c$  with slope  $1 \text{ kg}\text{-K}/\text{m}^2\text{-s}$  at  $q''_{ext} = 50 \text{ kW}/\text{m}^2$ . Figure 58 is a plot of the peak HRR in flaming combustion measured in a fire calorimeter at  $q''_{ext} = 50 \text{ kW}/\text{m}^2$  according to a standard method [36] versus  $\eta_c$  measured in the PCFC for the same or similar polymers. The solid line through the data has the expected slope  $1 \text{ kg}\text{-K}/\text{m}^2\text{-s}$  and describes the trend reasonably well, considering it represents an average value of  $\eta_g$ .

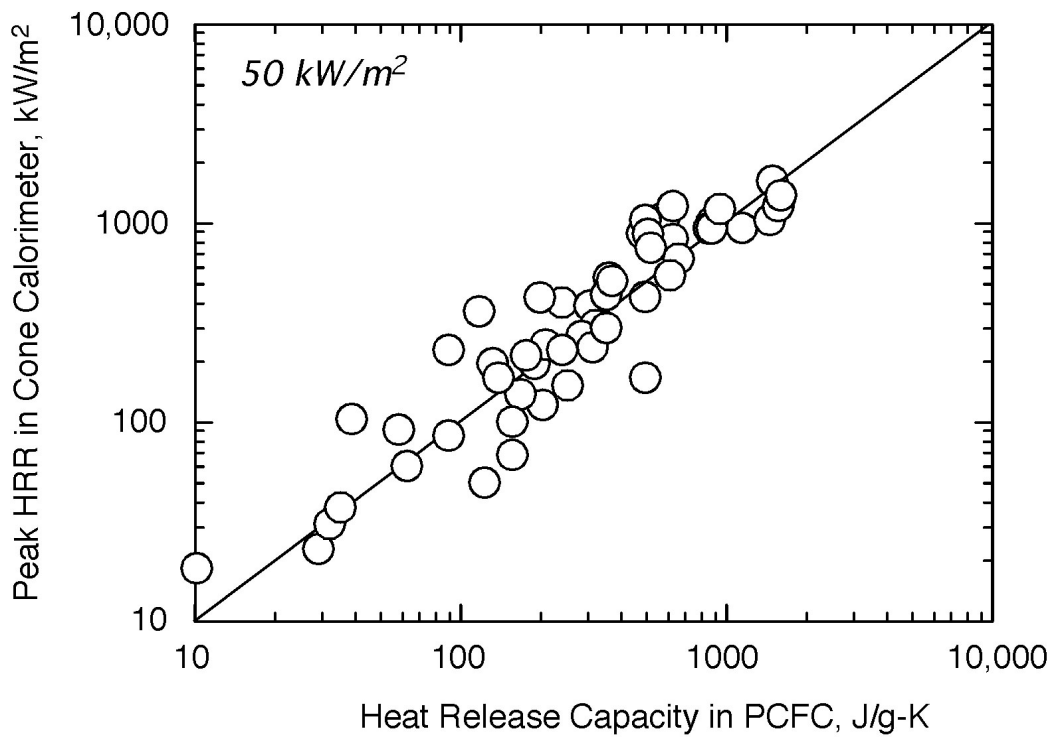


Figure 58. Peak HRR in cone calorimeter at  $50 \text{ kW/m}^2$  external flux versus heat release capacity in PCFC shows there is a definite trend.

Figure 59 is a plot of the maximum/peak value of the HRR measured in an OSU fire calorimeter that operates on the sensible enthalpy method [160] versus the heat release capacity  $\eta_c$  of the material. The horizontal dashed line at  $\text{HRR} = 65 \text{ kW/m}^2$  is the maximum HRR value allowed during the standard 5-minute HRR test [160] by Title 14 Code of Federal Regulations Part 25.853(a-1) for large area materials in commercial aircraft cabins. In general, it is seen that peak HRR for these thin materials in the OSU increases with  $\eta_c$ , and the data is roughly approximated ( $R = 0.64$ ) by a power law,  $\text{HRR} (\text{kW/m}^2) = 8\eta_c^{1/2}$ . The relatively few data in the range of  $\eta_c < 100 \text{ J/g-K}$  is a consequence of the fact that only fluoroplastics and research polymers exhibit this low level of flammability and the latter are available in limited quantities.

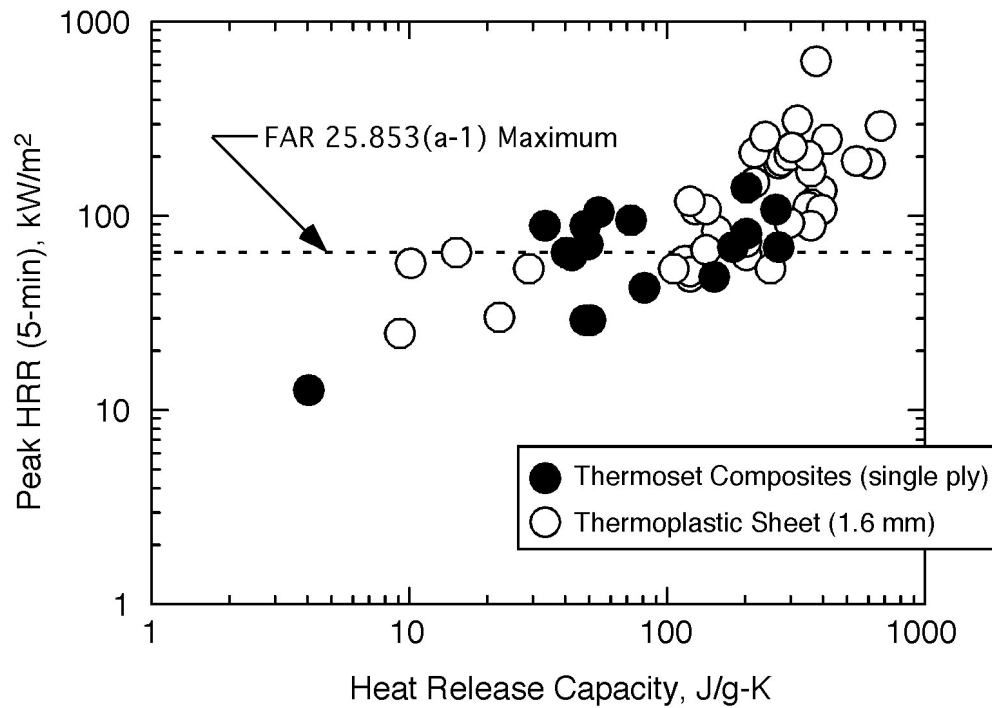


Figure 59. Peak HRR in OSU versus heat release capacity in PCFC.

## 5.5 FIRE MODELLING

A model of burning of two widely-used charring and intumescent polymers, bisphenol A polycarbonate and polyvinylchloride, was developed and validated. The modelling was performed using a flexible computational framework called ThermaKin. ThermaKin solves time-resolved energy and mass conservation equations describing a one-dimensional material object subjected to external heat. Most of the model parameters were obtained from direct property measurements. The model was validated against the results of cone calorimetry experiments performed under a broad range of conditions.

A quantitative understanding of the processes that take place in the condensed phase of a burning material is critical for prediction of ignition and growth of fires. ThermaKin [161,162] was used to simulate cone calorimetry tests. This one [163], focused on non-charring polymers (polymethylmethacrylate, high-impact polystyrene and high density polyethylene). The results of both studies indicate that a combination of material properties describing energy transport and thermally-induced gasification reactions defines polymer burning behavior in a wide range of conditions.

ThermaKin solves energy and mass conservation equations describing a one dimensional material object subjected to external heat. Only a brief description of the framework is given here; a complete description can be found in earlier publications [161,162]. In this framework, the material is represented by a mixture of components, which may interact chemically and physically. The components are assigned individual properties and categorized as solids, liquids or gases. The governing equations can be summarized as follows:

$$\sum_c^{comp} \xi_c C_c \frac{\partial T}{\partial t} = \frac{\partial}{\partial x} \left( k_M \frac{\partial T}{\partial x} \right) + \sum_r^{react} r_r h_r - \sum_g^{gases} J_g \frac{\partial}{\partial x} \left( \int_0^T c_g dT \right) + \alpha_M I \left( 1 - \frac{\sigma T^4}{I_s} \right) \quad (71)$$

$$\frac{\partial \xi_c}{\partial t} = \sum_r^{react} \theta_r^s r_r - \frac{\partial J_g}{\partial x} \quad (72)$$

$$r_r = A_r \exp\left(-\frac{E_r}{RT}\right) \xi_r \quad (73)$$

$$J_g = -\rho_g \lambda_M \frac{\partial}{\partial x} \left( \frac{\xi_g}{\rho_g} \right) \quad (74)$$

Equation 71 is the energy conservation statement; equation 72 is the mass balance for a gaseous component. Equation 73 is an expression of the first order reaction rate,  $r$  (second order reactions between components can also be defined within the ThermaKin framework). Equation 74 is the definition of a gaseous component mass flux ( $J$ ). Only gaseous components are assumed to be mobile, which means that, for a liquid or solid component, the last right-hand-side term in the mass balance equation is 0.

$\xi$ ,  $c$  and  $\rho$  are concentration, heat capacity and density of a component.  $T$  is temperature;  $t$  is time; and  $x$  is the Cartesian coordinate.  $h$  is the heat of reaction;  $\theta$  is a stoichiometric coefficient, which is negative when the corresponding component is a reactant and positive when it is a product.  $A$  and  $E$  are the Arrhenius parameters; and  $R$  is the gas constant.  $k$ ,  $\lambda$  and  $\alpha$  are thermal conductivity, gas transfer and radiation absorption coefficients.  $I_s$  is the flux of infrared radiation from an external source incident onto the material surface.  $I$  is the flux of the radiation inside the material,

which is computed using a generalized form of Beer–Lambert law and corrected for the material reflectivity.  $\sigma$  is the Stefan–Boltzmann constant. Subscript or superscript  $g$  is used to refer to a gaseous component; subscript  $c$  is used for all types of components (including gaseous). Subscript  $r$  is used to refer to a reaction and the corresponding reactant. Subscript  $M$  indicates a property of mixture (rather than that of an individual component). The material’s volume is defined as a sum of component masses divided by the corresponding densities. The volumetric contribution of gaseous components can be scaled by a user defined factor (which can be related to the local composition). The boundary conditions are defined separately for the two surfaces of the material object. These definitions include radiative ( $I_s$ ) and convective ( $H_s$ ) heat fluxes. The convective heat flux into the material is expressed as:

$$H_s = \nu(T_A - T_s) \quad (75)$$

where  $\nu$  is the convection coefficient;  $T_s$  is the material surface temperature; and  $T_A$  is the temperature outside of material. Both  $I_s$  and  $T_A$  can be defined as a piecewise linear function of time. The radiative and convective heat fluxes can also be related to gaseous component fluxes out of the material ( $-J_s$ ). These relations are based on the following criterion:

$$CI = \sum_g^{\text{gases}} \frac{-J_s^g}{\zeta_g} \quad (76)$$

where  $\zeta_g$  are critical mass fluxes specified for gaseous components. When  $CI$  reaches 1, a constant value can be added to  $I_s$  and the values of  $\nu$  and  $T_A$  can be reset. These relations are used to simulate the effects of appearance of flame on the material surface.

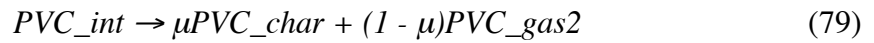
The system of equations is solved numerically by subdividing the material object into finite elements and computing changes in the element temperature and composition in small time steps. All calculations were performed using 0.05 mm element size and 0.005 second time step (the only exception was thermogravimetric analysis modelling, which was performed using 0.01 mm element size). Increasing or reducing these integration parameters by a factor of 2 did not produce any significant changes in the results of the calculations.

### 5.5.1 Model Parameterization

The results of the TGA experiments shown in figure 60 were used to parameterize polymer decomposition kinetics. The thermal decomposition of PC was represented by a single first order reaction:



In the case of PVC, a sequence of two first order reactions was employed to reflect the presence of two peaks in the TGA curves:



Here  $PC_{pol}$  and  $PVC_{pol}$  are the components representing non-degraded polymers.  $PC_{char}$ ,  $PVC_{int}$  and  $PVC_{char}$  represent condensed-phase products of the polymer decomposition.  $PC_{char}$  and  $PVC_{char}$  are the final decomposition products (also referred to as char);  $PVC_{int}$  is an intermediate.  $PC_{gas}$ ,  $PVC_{gas1}$  and  $PVC_{gas2}$  represent the gaseous decomposition products.  $\mu$  is used to designate the yields of the condensed-phase products. The values of  $\mu$  were determined directly from the TGA data by calculating the fractional mass remainder at the minimum between the two  $MLR_{TGA}$  peaks or at the end of decomposition, which was assumed to be complete when the temperature reaches 1050 K. The yields showed no significant dependence on b; their values are listed in table 34. The uncertainties in  $\mu$  and other parameters discussed below are expressed as  $\pm 2$  standard errors.

Table 34. Reaction parameters for polycarbonate and polyvinylchloride decomposition.

Reaction #	$A$ ( $s^{-1}$ )	$E$ (J/mol)	$\mu$	$H$ (J/kg)	$HCC_g$ (J/kg)
77	$(1.9 \pm 1.1) \times 10^{18}$ [ $4.5 \times 10^{24}$ ]*	$(2.95 \pm 0.06) \times 10^5$ [ $4.01 \times 10^5$ ]*	$0.21 \pm 0.01$	$-(8.3 \pm 1.4)$ $\times 10^5$	$(2.6 \pm 0.13)$ $\times 10^7$
78	$(1.4 \pm 0.8) \times 10^{33}$ [ $9.5 \times 10^{20}$ ]*	$(3.67 \pm 0.04) \times 10^5$ [ $1.92 \times 10^5$ ]*	$0.44 \pm 0.01$	$-(1.7 \pm 1.7)$ $\times 10^5$	$(2.7 \pm 0.3)$ $\times 10^6$
79	$(3.5 \pm 2.1) \times 10^{12}$ [ $5.5 \times 10^{11}$ ]*	$(2.07 \pm 0.06) \times 10^5$ [ $4.01 \times 10^5$ ]*	$0.47 \pm 0.01$	$-(1.2 \pm 0.9)$ $\times 10^5$	$(3.65 \pm 0.18)$ $\times 10^7$

\* Arrhenius parameters obtained by fitting 0.5 K/s TGA data.

The Arrhenius parameters describing the decomposition reactions were obtained by fitting the experimental TGA curves with the ThermaKin model. The model was set up to simulate an idealized TGA experiment, where a sample is heated uniformly at a specified heating rate. The uniform heating was achieved by using a very thin (0.05 mm) material object, which initially consisted of *PC\_pol* or *PVC\_pol*. The object was heated convectively at both boundaries. The convective heat flow was defined by  $\nu = 1 \times 10^5 \text{ W/m}^2\text{-K}$  and  $T_A = 400 + \beta t \text{ K}$  (the high value of the convection coefficient was used to insure that the sample temperature always follows the programmed temperature ramp). All component properties were set as specified below. Under these conditions, the mass fluxes of gaseous components out of the object depended only on the Arrhenius parameters (provided that the  $\mu$  values were fixed) and were insensitive to other material properties. These parameters were adjusted incrementally until the calculated mass loss rates showed a good agreement with the experimental TGA curves (the quality of the agreement was determined on the basis of a visual inspection).

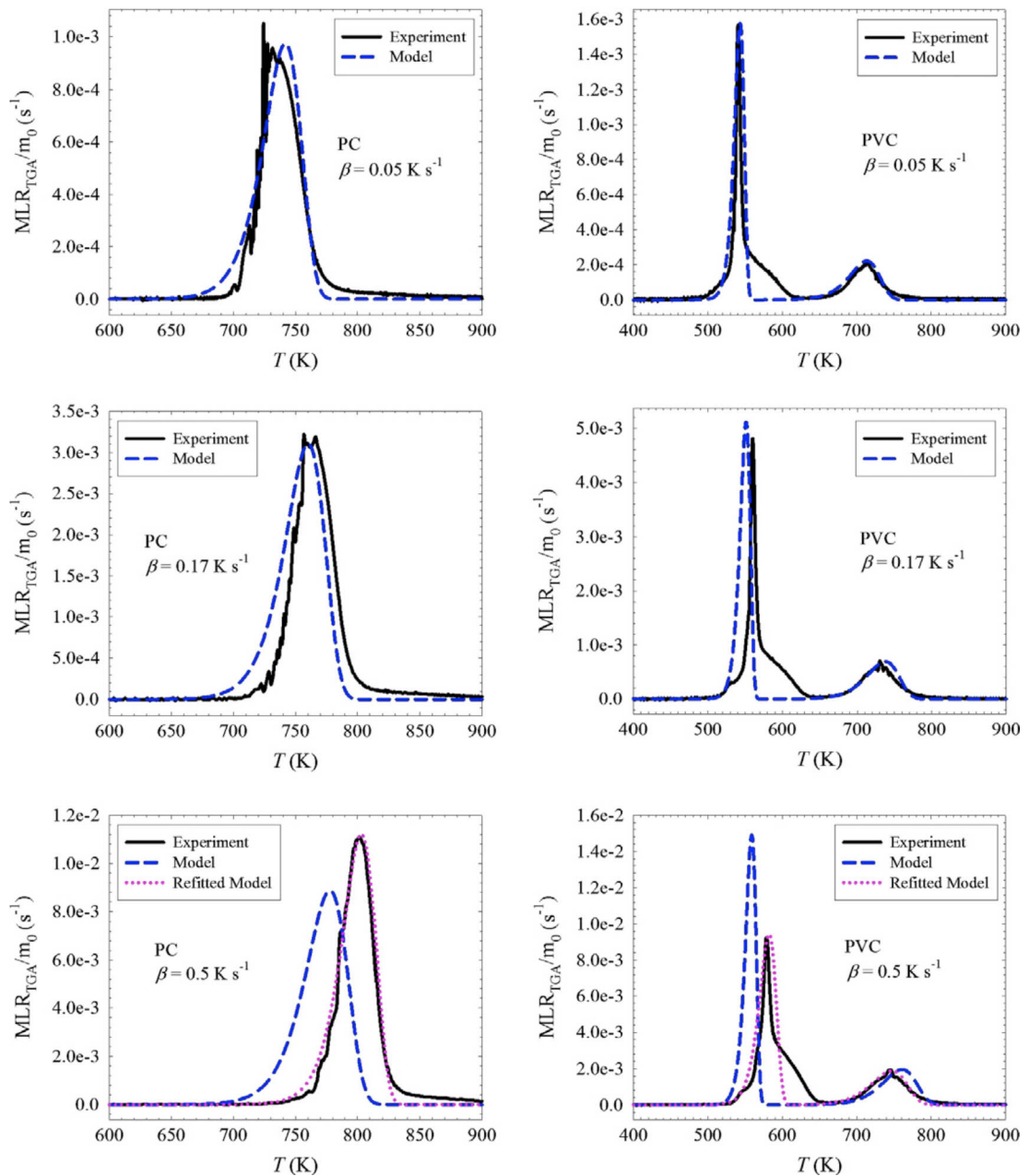


Figure 60. Results of TGA experiments and decomposition reaction modelling. The mass loss rates are normalized by the initial sample mass.

The results of TGA experiments performed at  $\beta = 0.05$  K/s (3 K/min) were used as a fitting target because the experimental conditions were expected to be the closest to the modeled uniform heating. The fitted Arrhenius parameters are listed in table 34; the calculated mass loss rates are depicted in figure 60. Modelling of the 0.17 K/s (10 K/min) TGA curves using these parameters produced a fair agreement with the experiments (see figure 60). However, in the case of 0.5 K/s (30 K/min) heating rate, the agreement is rather poor. Non-uniform heating of the sample in the high heating

rate experiments is a likely reason for the disagreement. To examine potential effects of the heating-rate-related variation in the measured kinetics on the cone calorimetry modelling, 0.5 K/s TGA data were refitted. The resulting Arrhenius parameters are listed in table 34 in square brackets. While these parameters are significantly different from those obtained from the low heating rate experiments, it will be shown below that these differences have little effect on simulated HRR cone calorimeter profiles.

The heats of the decomposition reactions were measured in a previous study [164] using DSC. These heats, which were renormalized for PVC to reflect the stoichiometry of reactions 78 and 79, are listed in table 34. Table 34 also contains HCC values for the gaseous decomposition products. These values were obtained by numerically integrating the  $HRR_{MCC}$  peaks shown in figure 60 and re-normalizing the integrated values by the mass lost in each decomposition step (determined from the TGA data). It was assumed that the two lowest temperature (overlapping) peaks of the PVC  $HRR_{MCC}$  curve correspond to the lowest temperature peak of the TGA curves. It appears that it contributes relatively little to heat release.

Physical properties of material components were obtained from measurements and analyses of literature data [63,164]. The property information is summarized in table 35.

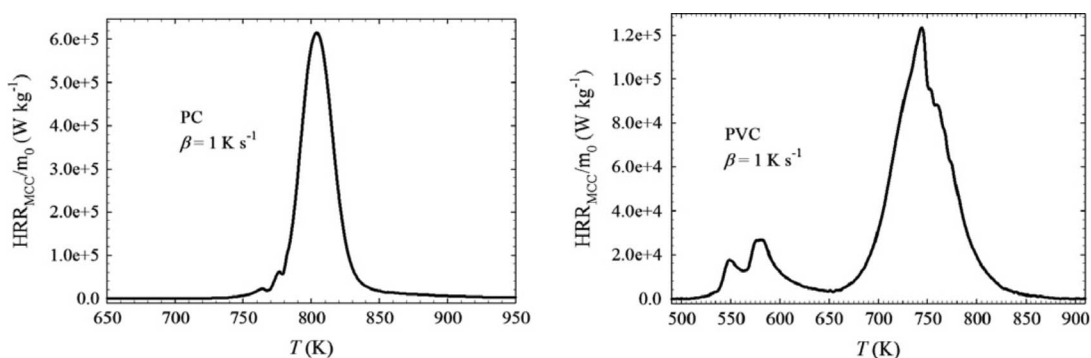


Figure 61. Heat release results of MCC experiments. The heat release rates are normalized by the initial sample mass ( $m_0$ ).

Table 35. Physical properties of polycarbonate and polyvinylchloride material components.

Component	Density (kJ/m <sup>3</sup> )	Heat Capacity (J/kg-K)	Thermal Conductivity (W/m-K)	Reflectivity	Absorption Coefficient (m <sup>2</sup> /kg)
<i>PC_pol</i>	1180 ± 60	1900 ± 300	0.22 ± 0.03	0.10 ± 0.05	1.5 ± 0.5
<i>PC_char</i>	See text	1700 ± 170	See text	0.15 ± 0.05	≈100
<i>PC_gas</i>	-	≈1000	-	-	≈1.5
<i>PVC_pol</i>	1430 ± 70	1550 ± 250	0.17 ± 0.01	0.10 ± 0.05	1.5 ± 0.5
<i>PVC_int</i>	See text	≈1550	≈0.17	≈0.10	See text
<i>PVC_char</i>	See text	1720 ± 170	See text	0.15 ± 0.05	≈100
<i>PVC_gas1</i>	-	840 ± 150	-	-	≈1.5
<i>PVC_gas2</i>	-	≈1000	-	-	≈1.5

In most ThermaKin simulations performed in this study, the gaseous components (*PC\_gas*, *PVC\_gas1* and *PVC\_gas2*) were specified not to contribute to the material's volume. Therefore, their densities, thermal conductivities and reflectivities (where contributions are weighted by the component volumetric fractions) are irrelevant and were not defined. The absorption coefficients of these components were assumed be the same as those of the unreacted polymers. The heat capacity of *PVC\_gas1* was assigned temperature-averaged (500–1100 K) heat capacity of hydrogen chloride, 840 J/kg-K [165], because of substantial evidence indicating that HCl represents more than 80 wt.% of the gaseous products released during the first step of PVC degradation [11]. The quantitative compositions of *PC\_gas* and *PVC\_gas2* are not known; their heat capacities were assumed to be 1000 J/kg-K.

### 5.5.2 Model Set Up

The one-dimensional objects that were used to model cone calorimetry experiments consisted of two layers. The top layer, which represented a polymer sample, was initially composed of *PC\_pol* or *PVC\_pol*. The initial thickness of this layer was taken to be equal to the initial sample thickness. The bottom layer consisted of component *KB* that represented the Kaowool blanket used in the experiments. This component was assigned the physical properties of the blanket,  $\rho = 48 \text{ kg/m}^3$ ,  $c = 800 \text{ J/kg-K}$  and  $k =$

0.08 W/m<sup>2</sup>-K, which were obtained from the manufacturer. The *KB* layer was specified to be 15 mm thick; increasing this thickness by a factor of 2 made no significant impact on the results of the simulations. In most of the simulations, the gas transfer coefficient was set sufficiently high,  $2 \times 10^{-5}$  m<sup>2</sup>/s for all components representing polymer samples. This was done to ensure that the fluxes of gaseous components evolved out of a material object were always equal to the rates of their production inside the object. In other words, the mass transfer was made so fast that it had no effect on mass loss or heat release rates. To simulate the presence of aluminum foil between the sample and insulating blanket, the *KB* layer was specified to be impenetrable to gas flow and external radiation ( $\gamma = 1$ , where  $\gamma$  is the reflectivity). The initial temperature of the objects was always set at 305 K (a few degrees above the room temperature) to take into account a slight heating caused by the flux penetrating the cone heater shutter.

Before ignition, the top surface of the objects was subjected to radiative heat and convective cooling. The incident external radiative heat flux (*EHF*) was specified to be equal to the experimental heat flux set point. The convection was defined by  $\nu = 10$  W/m<sup>2</sup>-K and the ambient temperature  $T_A = 300$  K. The value of the convection coefficient is the mean of the values calculated (8.2 W/m<sup>2</sup>-K and measured (11 W/m<sup>2</sup>-K) in previous studies [163,166]. After ignition, a time dependent correction (*EHF<sub>t</sub>*) was added to the initial value of *EHF* (*EHF<sub>0</sub>*) to account for the sample surface movement towards the heater (details are provided below). The convective cooling was turned off and an additional 15 kW/m<sup>2</sup> of incident radiative heat flux was applied to the surface to simulate the presence of flame. This heat flux is the mean of the values obtained from direct [167] and indirect [163] measurements performed on several polymeric materials. These measurements indicate that, for the horizontal cone calorimetry configuration, the flame heat flux is relatively insensitive to *EHF* and chemical nature of the polymer. The top surface of the objects was specified to have no resistance to the outward gas flow. The bottom surface was defined to be completely impenetrable to energy and mass. The gaseous component critical mass fluxes, which define ignition, were determined from the cone calorimetry data as described below.

During the cone calorimetry experiments, both polymers produced intumescent char. At the end of tests, the volumes of PC and PVC samples increased approximately 10 and 7 times, respectively. The end of test was declared 30 seconds after flame out. In a

few cases where the samples were left under the heater after the end of test, they continued to smolder and release heat (at a fairly steady rate) for extended periods of time. The images of the chars are shown in figure 62. While these images are representative, even when the tests were performed under identical conditions, the char shapes and superficial structural features were found to differ significantly from test to test. These shape fluctuations are probably related to a relatively poor repeatability of the tests performed at  $EHF_0 = 75 \text{ kW/m}^2$  on 6 mm thick samples, the results of which are shown in figure 63. During two of these tests (one of PC and the other of PVC), the char was punctured multiple times using a thin (1.5 mm in diameter) stainless steel spear. The punctures had no significant effect on the  $HRR_{cone}$ , which indicates the absence of large pockets of pressurized gases inside the pyrolyzing materials. This observation is consistent with the assumption that the mass transport is not the rate limiting step of the pyrolysis processes.



Figure 62. Six millimeter thick samples of PC (left) and PVC (right) burnt in the cone calorimeter at  $EHF_0 = 75 \text{ kW/m}^2$ . Both tests were stopped at about 200 seconds: the samples were removed from under the cone and photographed.

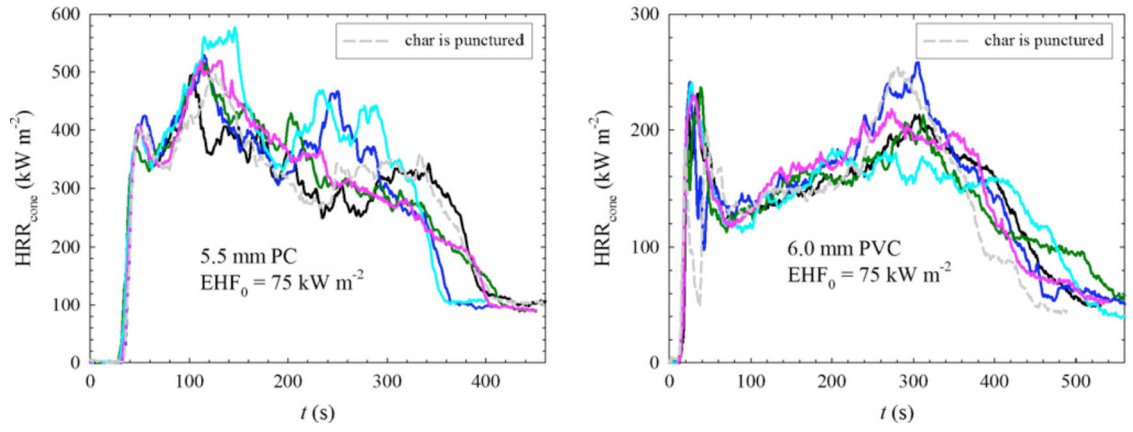


Figure 63. Results of 6 cone calorimetry experiments performed on each polymer under identical conditions at a heat flux of  $75 \text{ kW/m}^2$ .

The test results shown in figure 63 were used to determine the efficiency of the cone calorimetry combustion ( $CE_{cone}$ ). First, the effective heats of combustion of gaseous pyrolysis products were computed by dividing the total heat released by the total mass lost in each cone test. Subsequently, the mean effective heat values were divided by the total heats released in the corresponding MCC experiments (which were also normalized by the total lost mass) to obtain  $CE_{cone}$ . For PC, the value of  $CE_{cone}$  was found to be  $0.84 \pm 0.03$ ; for PVC, the value is notably lower,  $0.75 \pm 0.03$ . These values were used to convert the surface mass fluxes calculated by ThermaKin to heat release rate:

$$HRR_{cone} = CE_{cone} \sum_g^{gases} HCC_g (-J_S^g) \quad (80)$$

They were also used to specify the critical mass fluxes:

$$\zeta_g = \frac{CHR}{CE_{cone} HCC_g} \quad (81)$$

where  $CHR$  is the critical heat release rate.  $CHR$  was used to define ignition in the model and calculate the time to ignition ( $TTI$ ) from experimental  $HRR_{cone}$  curves. It was set at  $20 \text{ kW/m}^2$  because this value gave the best agreement between the  $TTI$  determined from experimental  $HRR_{cone}$  and the corresponding times of appearance of a sustained flame recorded by an operator. In essence, using the  $CHR$  value to define ignition in the model is equivalent to stating that a stable flame appears over the material surface if the

gases flowing through the surface are capable of producing at least 20 kW/m<sup>2</sup> upon combustion.

To account for the effects of sample expansion on  $EHF$ , the times of char surface reaching half and full distances to the cone heater bottom were recorded. At  $EHF_0 = 75$  kW/m<sup>2</sup>, PC samples reached the cone bottom at about 75 s. At 50 kW/m<sup>2</sup> and 92 kW/m<sup>2</sup>, it took 150 and 50 seconds, respectively. The expansion occurred after ignition and was very rapid. Therefore, for PC,  $EHF_t$  was specified to be a step function that increased from 0 to  $0.15 \times EHF_0$  (in accordance with the heat flux measurements described above) at these times. It should be noted that, after reaching the heater bottom, PC char entered the heater and, in some cases, came into direct contact with parts of the heating element. The heat flux inside the heater was found to be highly non-uniform and difficult to measure. Therefore, no additional corrections were applied to account for this behavior. In the case of PVC, the sample expansion also occurred after ignition; however, it was much more gradual. At  $EHF_0 = 75$  kW/m<sup>2</sup>, it took about 300 s for the samples to reach the heater bottom. At 50 kW/m<sup>2</sup> and 92 kW/m<sup>2</sup>, it took 450 and 250 seconds, respectively. The thin ( $3 \times 10^{-3}$  m) sample only reached half the distance to the bottom of the heater (in half the time). Thus, for PVC,  $EHF_t$  was specified to increase linearly from 0 to  $0.15 \times EHF_0$  (to  $0.075 \times EHF_0$  in the case of thin sample) between  $TTI$  and the times indicated above. After that, the  $EHF_t$  value was held steady.

To complete the model formulation, a sub-model describing intumescent chars needs to be defined. In this study, two approaches to defining intumescence were considered. In the first approach, material expansion was formulated to be a result of retention of gaseous decomposition products by  $PC\_char$  and  $PVC\_char$ . However, it was found that the number of unknown parameters associated with this approach was too large and these parameters were too interdependent to carry physical sense. Therefore, a simpler approach where the chemical reactions (equations 77-79) define the expansion was adopted. In this approach, gaseous components were chosen not to contribute to material's volume. Instead,  $PC\_char$  and  $PVC\_char$  were assigned the densities that produce experimentally observed sample expansion. This approach was further simplified by observing that the heat flow through the char-representing component layers is defined by the product of their density,  $\rho$ , and thermal conductivity,  $k$  (because the densities are inversely proportional to the layer thicknesses). Computationally

expensive simulations of the actual expansion were avoided by specifying  $\rho_{PC\_char} = 248 \text{ kg m}^{-3}$ ,  $\rho_{PVC\_int} = 629 \text{ kg/m}^3$  and  $\rho_{PVC\_char} = 296 \text{ kg/m}^3$ , which defined a constant volume for the decomposing samples. To relate the values of  $k_{PC\_char}$  and  $k_{PVC\_char}$  used in these simulations to the thermal conductivities of the actual chars, the simulation values were multiplied by the corresponding experimental sample expansion factors (10 for PC and 7 for PVC).

Two heat transfer modes inside *PC\_char* and *PVC\_char* were considered. These components were assumed to transfer heat either through conduction or radiation. The radiative transfer was described using the radiative diffusion approximation [168]:

$$k = \omega T^3 \quad (82)$$

Representative experimental heat release curves obtained at  $EHF_0 = 75 \text{ kW/m}^2$  for 6 mm thick samples were used to determine  $k$  for the conductive chars and  $\omega$  for the radiative chars. The results of fitting these curves with the heat transfer parameters are shown in figure 64. The conductivities of *PC\_char* and *PVC\_char* were found to be 0.37 and 0.26 W/m-K. The values of the radiative heat transfer coefficient,  $\omega$ , were determined to be  $4.9 \times 10^{-10}$  and  $3.5 \times 10^{-10} \text{ W/m-K}^4$ , respectively. Taking into account significant uncertainties in the experimental data (see figure 63), the model describes the experiments reasonably well. The end parts of the experimental curves, which are not captured by the model, represent transition from flaming combustion to smoldering – the process that was not included in the current model formulation.

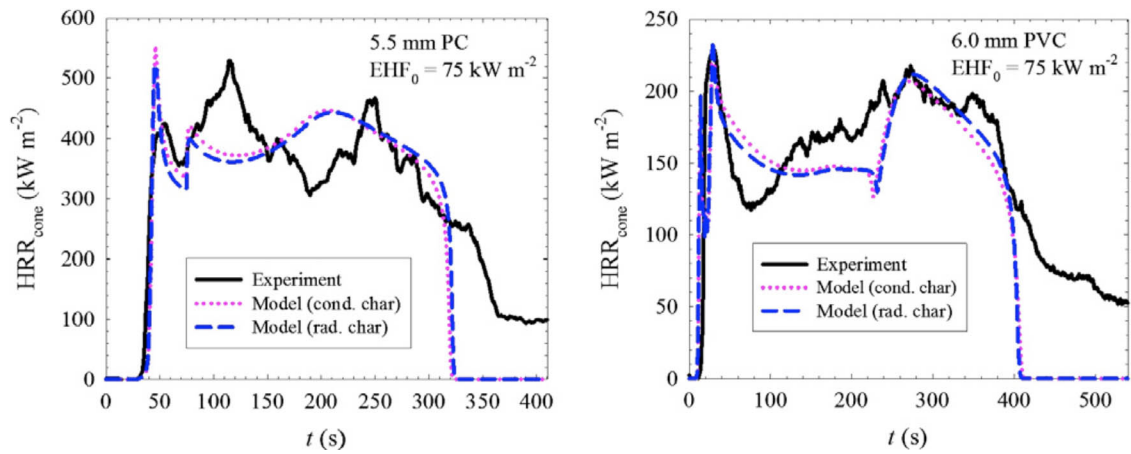


Figure 64. Results of fitting experimental heat release rates in cone calorimeter with *PC\_char* and *PVC\_char* heat transfer parameters.

The conductive and radiative char sub-models produce almost identical results. However, when the conductivity values are recalculated to the actual char dimensions, they appear to be too high (3.7 and 1.8 W/m-K) to be consistent with the char structures, which contain at least 85 vol.% of gas-filled void (based on the assumption that the solid in the char has the density of graphite, 2200 kg/m<sup>3</sup> [169]). Therefore, the radiative char sub-model was used in all further calculations. It should be noted that, for PVC, the absorption coefficient of *PVC\_int* was also adjusted during the fitting procedure to be 3.9 m<sup>2</sup>/kg. The only feature of the  $HRR_{cone}$  curve that was found to be sensitive to this coefficient was the height of the second (from the left) narrow maximum.

The predictive power of the fully parameterized models of PC and PVC was examined by simulating a series of cone calorimetry tests, which were performed under the conditions considerably different from those used in the parameterization. A comparison of the simulation results with the experiments is shown in figure 65. All  $HRR_{cone}$  curves (including those shown in figure 64) were characterized by calculating *TTI* and the average heat release rate (*AHRR*). *TTI* was defined as the time when the heat release rate exceeds the *CHR* value for the first time. *AHRR* was determined by calculating the mean heat release rate for the time interval between the initial rise of  $HRR_{cone}$  above significant heat release threshold and final drop below the threshold. The value of the threshold was set at 200 kW/m<sup>2</sup> for PC and 100 kW/m<sup>2</sup> for PVC. The peak heat release parameter, which is frequently employed in the characterization of  $HRR_{cone}$  curves, was not used in the current case because it was not clear which of the multiple peaks present in each curve contributes most to the development of a large scale fire.

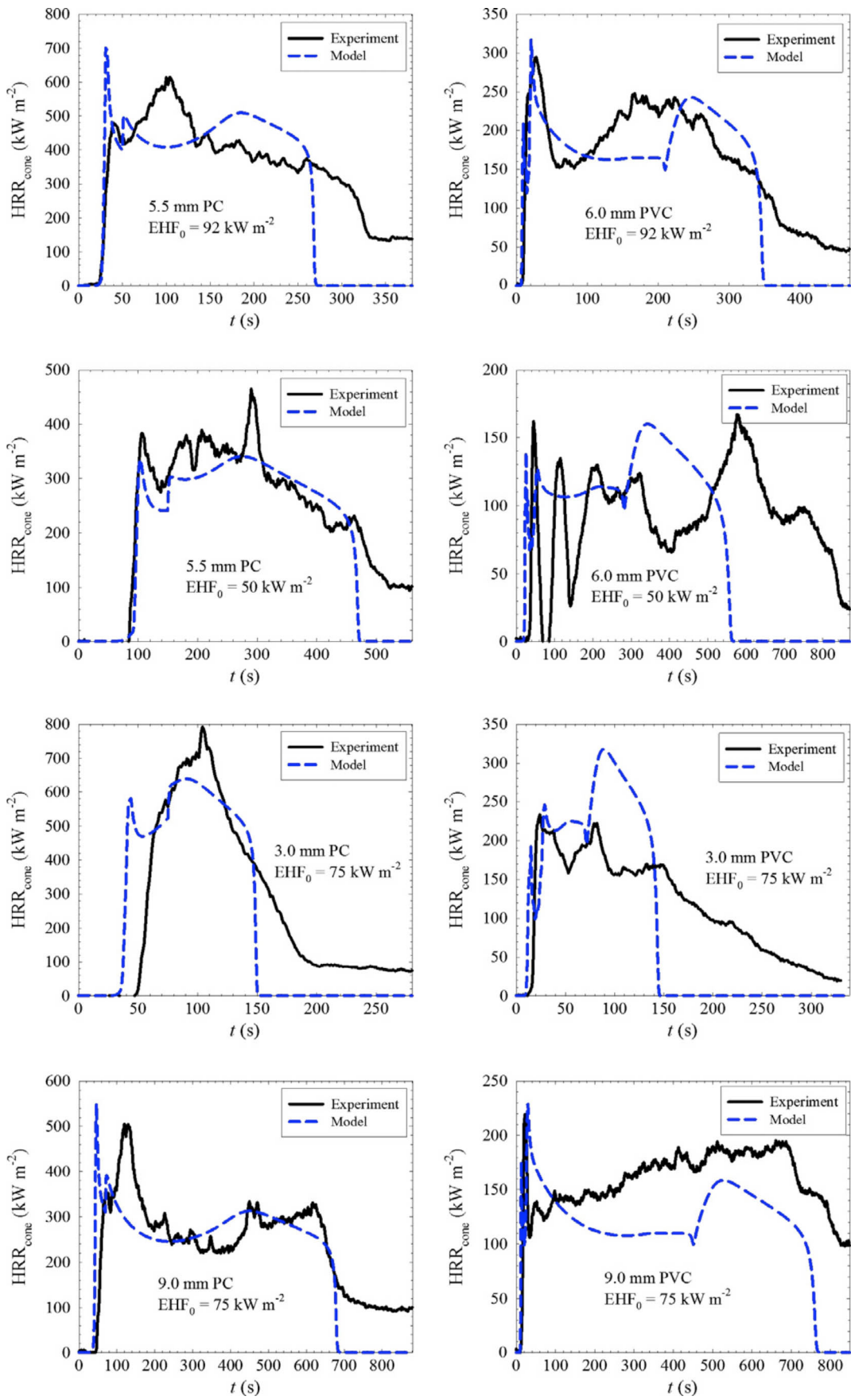


Figure 65. Comparison of model predictions with the results of cone calorimetry experiments performed at  $EHF_0 = 50 - 92 \text{ kW/m}^2$  on 3 - 9 mm thick samples.

The calculated *TTI* and *AHRR* are reported in table 36. For most tests, the differences between the experimental and simulated values are less than or comparable to experimental uncertainties. These uncertainties were estimated from the results obtained at  $EHF_0 = 75 \text{ kW/m}^2$  for 6 mm thick samples (see figure 63) to be  $\pm 15\%$  (for both *TTI* and *AHRR*). In addition, only the absolute differences in *TTI* that exceed the  $HRR_{cone}$  signal time resolution, which was estimated to be 4 s, were considered to be significant. For 1 PC test and 2 PVC tests, the simulated *AHRR* and/or *TTI* (which are marked by asterisks in table 36) significantly deviate from the corresponding experimental values. In the case of the PVC test performed at  $EHF_0 = 50 \text{ kW/m}^2$ , the discrepancies can be explained by the difficulties in maintaining a sustained flame during the experiment. As evident from the data shown in figure 65, the sample self-extinguished multiple times and had to be re-ignited. The sources of discrepancies observed for 3 mm samples of PC and PVC are less clear. One possible behavioral feature that may have contributed to these discrepancies is a notable warping of the samples, which was observed before and after ignition.

Table 36. Summary of results of cone calorimetry experiments and simulations for PC and PVC.

Polymer	$EHF_0$ (kW/m <sup>2</sup> )	Thickness (mm)	Exp. <i>TTI</i> (s)	Mod. <i>TTI</i> (s)	Exp. <i>AHRR</i> (kW/m <sup>2</sup> )	Mod. <i>AHRR</i> (kW/m <sup>2</sup> )
PC	75	5.5	35	39	370	390
	92	5.5	25	26	410	450
	50	5.5	86	93	310	290
	75	3.0	51	36*	510	550
	75	9.0	47	39	290	280
PVC	75	6.0	15	11	170	160
	92	6.0	11	8	190	190
	50	6.0	37	22*	100	120*
	75	3.0	17	11*	170	240*
	75	9.0	14	11	160	130

\* The result of modelling that significantly deviate from the corresponding experimental values.

The results of this study demonstrate that a one-dimensional numerical pyrolysis model can be used to predict the outcome of cone calorimetry experiments performed on a charring and intumescent polymer. The predictions require the knowledge of the thermal and optical properties of the polymer and a quantitative description of the kinetics and thermodynamics of its decomposition. All this information can be obtained from direct mg and g scale measurements or existing structure–property correlations. The predictions also require the knowledge of the properties of the decomposition products, in particular, of those products that comprise intumescent char. Due to fragility and inhomogeneity, a direct characterization of the char (at least of those observed in this work) appears to be very difficult. However, according to our results, a simple sub-model based on the properties of graphite and a single adjustable heat transfer parameter, the value of which is determined using the results of one cone calorimetry experiment, provides a reasonable approximation to the carbonaceous char description.

## 5.6 SUMMARY AND CONCLUSIONS

Correlations between different fire and flammability tests were examined. Steady burning equations that define the parameters that influence the rate were identified. Unsteady burning and how it relates to different small-scale tests that indicate ignition and flame resistance was examined. Geometries and function of flammability tests such as oxygen index and UL94 were characterized. Material properties, measured using PCFC, were plotted versus material ratings from UL94 and LOI tests. Empirical correlations showed definite trends in the data that were used to predict material performance and probabilities of ratings in the small scale flammability tests.

Bench-scale fire tests, OSU and cone calorimeters, were also compared to PCFC measurements. Empirical relationships were shown that attempt to correlate the non-flaming PCFC measurements to the flaming heat release rates from the cone and OSU calorimeters.

The ultimate goal for the measurements that are made, using the small- and bench-scale tests, is to be able to predict and model the fire response of an object in a fire scenario. Thermakin is used in an early attempt at predicting fire behavior for TGA and cone calorimeter tests. Materials that burn steadily and do not char can be modeled easily.

However, materials that decompose in several steps, swell, and leave a carbonaceous char have proven to be more difficult. The decomposition reactions were defined and parameters for polycarbonate and polyvinylchloride were defined. Those parameters were then used to recreate the mass loss rates from a TGA. The physical properties and material components were added to describe the burning behavior in a cone calorimeter. Data from the cone was fitted to back out heat transfer characteristics of char forming, intumescent samples. Those parameters were then used to predict the burning behavior in the cone calorimeter at different heat fluxes. Calculated values for time to ignition and average heat release rates were in good agreement with the measured values.

## CHAPTER 6

### CONCLUSIONS & FUTURE WORK

## 6.1 CONCLUSIONS

A new technology called PCFC was envisioned. Thermal analysis and flammability were two different fields that were brought together to explain what makes things burn and how fast. Using test methods that are well characterized, behaved, repeatable, and reproducible are key in assessing the performance of materials. The MCC was developed as a stand-alone piece of equipment that could separate the thermal and fire processes and recombine them in a robust and reproducible manner. Heating a sample like other thermal analysis techniques and adding evolved gas analysis proved to be an invaluable tool for assessing flammability. Measurements are made and the math to explain the processes derived (not necessarily in that order). Values measured using PCFC are rooted in the chemical make-up of a material. Thermodynamic constants and material properties equate the fire properties measured directly in the MCC.

The development of the MCC was an iterative process. All volatile thermal decomposition products had to be transferred without condensation. This was a challenge when approached from working with existing equipment. Once new equipment was fabricated, heated interfaces, transfer lines, and mathematical routines for correcting analyzer response and mixing of the gases were eliminated, the rest fell into place.

The combustor had several iterations before converging on a design that was practical and functional. The rate of the combustion reaction was measured and the time needed to oxidize volatile decomposition products determined. This enabled shorter residence times, and therefore, smaller geometries for the combustor. Combining what worked from experimentation, with an effective transfer mechanism, enabled the quantitative evaluation of the fuel value of volatile material decomposition products. Further development lead to optimization of several parameters. Sample size, gas flow rates, heating rates converged into a system that produced high quality data rapidly with a minimal sample size.

The MCC was designed to generate flammability data that has a significance greater than, and not tied to, the physical attributes of a sample. Material properties are the foundation to material characterization. Measurement of these values leads to better predictive capabilities and understanding of the materials. Accurate thermal properties

as well as combustion properties are essential for characterizing and predicting how materials decompose and burn. The measurements made with thermal analyzers quantitatively determine the processes and associated energies for heating a material to temperature, melting it and volatilizing it. All of the heats associated with the decomposition of a material are measured in a DSC and summed to yield the heat of gasification. Other fire parameters are calculated from series of tests in the cone calorimeter. Trends in the fire-response and observed and ignition criteria calculated.

Knowledge of the heat of combustion and the heat of combustion of evolved gases from thermal decomposition leads to the heat of combustion of the char. The heat of combustion is the fuel value for materials. Heats of combustion are determined in a bomb calorimeter. This represents the total possible heat a sample can release in a fire. The heat of complete combustion was the basis for the calculation of the E value used extensively in fire science. Other thermo-chemical calculations based on the heats of formation were developed to predict fuel values and flammability of materials. Molar group contribution theory was developed as a simple way to directly calculate the heat of combustion of polymers and small molecules. This theory was expanded to include the newly developed heat release capacity.

Other aspects of materials must be considered for commercially viable materials. Materials must be facile and easily processed. High temperature and high performance materials usually have high temperature processing routes. Materials that are drop-in replacements for existing processing routes are abandoned due to public perception and misconceptions about the environmental impact of halogenated materials. Many studies have been performed to demonstrate the improved fire performance of these materials. Reaction chemistries have been examined for high performance epoxy and cyanate ester systems. Some of these systems are already inherently thermally stable, but the substitution of hydrocarbon moieties for halogenated versions makes them ultra-fire resistant.

Thermal analysis has been performed to evaluate the cure chemistry and energies as well as the thermal stability and decomposition chemistry. The chemistry of decomposition, as it relates to fire, has examined the volatile decomposition products as well as the residuals. Chemistries have been identified that produce volatiles that are non-flammable or do not have much fuel value. Also, when a material is degraded, an

alternate route to flame resistance is to boost char formation. Conjugated and aromatic structures tend to stay in the char. The flammability of materials that are inherently fire resistant has been evaluated using fire calorimeters and the MCC. Fuel values have been measured for many polymers with varying chemical structures and heteroatom inclusion. The use of additives can completely change the performance of materials for good or bad (also considering environmental aspects).

Modelling work has been done to explain and predict burning behavior. These models use results from small- and medium-scale tests along with material properties to simulate large-scale scenarios. Comparisons between the various fire tests can be used to make predictions. Simple models take values from tests that make measurements and predict performance in pass / fail tests. Other models predict a probability of a material to receive a ranking in a test.

Established correlations between tests has shown that reasonable estimates of performance can be made. More advanced modelling involves quantifying the energy to heat a material through melting and decompose it and volatilize the decomposition products. Materials that char introduce more parameters. So far thermal decomposition of polymers (like in a TGA) has been modeled. This model has been applied to charring materials successfully. Preliminary work has been done to predict burning of a sample in the cone calorimeter. Eventually the goal is to predict full-scale performance in a real-life scenario.

## 6.2 FUTURE WORK

MCC technology can be developed further by coupling techniques and adding capabilities to existing technologies. Additional measurements can be made at the sample. Adjacent thermocouples can be used to control and monitor processes that occur in the sample and furnace. This could possibly yield heat flow results that could provide insight into the energy required to gasify a material.

Temperatures of gas phase flame retardant activity need to be evaluated for materials that exhibit fire extinguishing capabilities. Future work could include examining incomplete combustion to quantify gas phase combustion reaction rates. Correlations between the cone calorimeter and MCC can be made when examining the CO / CO<sub>2</sub>

ratios and combustion efficiencies. Reaction rates, flame geometries and velocities can be used to evaluate the effectiveness and efficiency of gas phase additives. This could help to identify synergies and optimal loadings of additives.

These additional measurements will hopefully provide better data that can be used for modelling and a better understanding of what makes things burn.

## REFERENCES

1. V. Babrauskas and R.D. Peacock, "Heat Release Rate: The Single Most Important Variable in Fire Hazard," *Fire Safety Journal*, 18, pp. 255-272, 1992.
2. C.P. Sarkos and R.G. Hill, "Evaluation of Aircraft Interior Panels Under Full Scale Cabin Fire Conditions," *Proceedings of the AIAA 23rd Aerospace Sciences Meeting*, Reno, NV, January 14-17, 1985.
3. J.G. Quintiere, V. Babrauskas, L. Cooper, M. Harkelroad, K. Steckler, and A. Tewarson, "The Role of Aircraft Panel Materials in Cabin Fires and Their Properties," *DOT/FAA/CT-84/30*, June 1985.
4. V. Babrauskas, "From Bunsen Burner to Heat Release Rate Calorimeter," in *Heat Release in Fires*, V. Babrauskas and S. Grayson, eds., Elsevier Applied Science, New York, pp. 7-29, 1992.
5. M. Janssens, "Calorimetry," in *SFPE Handbook of Fire Protection Engineering*, 2nd Edition, Chapter 3.2, Society of Fire Protection Engineers, Boston, MA, 1995.
6. M.J. Scudamore, P.J. Briggs, and F.H. Prager, "Cone Calorimetry—A Review of Tests Carried out on Plastics for the Association of Plastic Manufacturers in Europe," *Fire and Materials*, 15, pp. 65-84, 1991.
7. V. Babrauskas, "Comparative Rates of Heat Release from Five Different Types of Test Apparatuses," *Journal of Fire Sciences*, 4,2, pp. 148-158, 1986.
8. T. Kashiwagi and T.G. Cleary, "Effects of Sample Mounting on Flammability Properties of Intumescent Polymers," *Fire Safety Journal*, 20, pp. 203-225, 1993.
9. A. Tewarson, "Generation of Heat and Chemical Compounds in Fires," in *SFPE Handbook of Fire Protection Engineering*, 2nd Edition, Chapter 3-4, Society of Fire Protection Engineers, Boston, MA, 1995.
10. N. Grassie, "Products of Thermal Degradation of Polymers," in *Polymer Handbook*, Third Edition, J. Brandrup and E.H. Immergut, eds., Third Edition, Chapter II, John Wiley & Sons, NY, pp. 365-386, 1989.

11. CF Cullis, MM Hirschler, *The Combustion of Organic Polymers*, Oxford, England: Claredon Press, 1981.
12. R.A. Susott, "Characterization of the Thermal Properties of Forest Fuels by Combustible Gas Analysis," *Forest Sciences*, 28, 2, pp. 404-420, 1982.
13. D.W. Van Krevelen, *Properties of Polymers*, Elsevier, Amsterdam, pp. 627-653, 1990.
14. R.N. Walters and R.E. Lyon, "A Microscale Combustion Calorimeter for Determining Flammability Parameters of Materials," presented at NIST Annual Conference on Fire Research, Gaithersburg, MD, October 30, 1996.
15. R.N. Walters and R.E. Lyon, "A Microscale Heat Release Rate Device," presented at Society of Plastics Engineers Annual Technical Conference (ANTEC 96), Indianapolis, IA, May 5-9, 1996.
16. T.V. Inguilizian, "Correlating Polymer Flammability Using Measured Pyrolysis Kinetics," Masters Thesis, University of Massachusetts (Amherst), January 1999.
17. W. Thornton, *The Relation of Oxygen to the Heat of Combustion of Organic Compounds*, *Philosophical Magazine and J. of Science*, 33, 196, 1917.
18. R.A. Susott, F. Shafizadeh, and T.W. Aanerud, "A Quantitative Thermal Analysis Technique for Combustible Gas Detection," *Journal of Fire and Flammability*, 10, pp. 94-104, 1979.
19. C. Huggett, "Estimation of Rate of Heat Release by Means of Oxygen Consumption Measurements," *Fire and Materials*, 4, 2, p. 61, 1980.
20. V. Babrauskas, "Heat of Combustion and Potential Heat," in *Heat Release in Fires*, V. Babrauskas and S.J. Grayson, eds., Chapter 8, Elsevier Applied Science, New York, pp. 207-232, 1992.

21. R.E. Lyon, "Solid-State Thermochemistry of Flaming Combustion," in *Fire Retardancy of Polymeric Materials*, A.F Grand and C.A. Wilkie, eds., Marcel Dekker, Inc., New York, NY, pp. 391-447, 2000.
22. R.E. Lyon, "Heat Release Kinetics," *Fire and Materials*, 24, pp. 179-186, 2000.
23. R.E. Lyon, "Heat Release Capacity," *Proceedings of the Fire and Materials Conference*, San Francisco, CA, January 22-24, 2001.
24. D.W. Van Krevelen, "Some Basic Aspects of Flame Resistance of Polymeric Materials," *Polymer*, 16, pp. 615-620, 1975.
25. P. Carty and W. White, "The Importance of Char Forming Reactions in Thermoplastic Polymers," *Fire and Materials*, 18, pp. 151-166, 1994.
26. R.E. Lyon, "Pyrolysis Kinetics of Char Forming Polymers," *Polymer Degradation and Stability*, 6, 2, pp. 201-210, 1998.
27. B. Moghtaderi, V. Novozhilov, D. Fletcher, and J.H. Kent, "An Integral Model for the Transient Pyrolysis of Solid Materials," *Fire and Materials*, 21, pp. 7-16, 1997.
28. J. Quintiere, and N. Iqbal, "An Approximate Integral Model for the Burning Rate of a Thermoplastic-Like Material," *Fire and Materials*, 18, pp. 89-98, 1994.
29. Y. Chen, M.A. Delichatsios, and V. Motevalli, "Material Pyrolysis Properties, Part I: An Integral Model for One-Dimensional Transient Pyrolysis of Charring and Non-Charring Materials," *Combustion Science and Technology*, 88, pp. 309-328, 1993.
30. J.E.J. Staggs, R.H. and Whiteley, "Modelling the Combustion of Solid-Phase Fuels in Cone Calorimeter Experiments," *Fire and Materials*, 23, pp. 63-69, 1999.
31. J.E.J. Staggs, and M.I. Nelson, "A Critical Mass Flux Model for the Flammability of Thermoplastics," *Combustion Theory and Modelling*, 5, pp. 399-427, 2001.

32. J.E.J. Staggs, "Modelling Thermal Degradation of Polymers Using Single-Step First-Order Kinetics," *Fire Safety Journal*, 32, pp. 17-34, 1999.
33. A. Bucsi, and J. Rychly, "A Theoretical Approach to Understanding the Connection Between Ignitability and Flammability Parameters of Organic Polymers," *Polymer Degradation and Stability*, 38, pp. 33-40, 1999.
34. R.E. Lyon, R.N. Walters and S.I. Stoliarov, "A Thermal Analysis Method for Measuring Polymer Flammability," *Journal of ASTM International*, 3, 4, pp. 1-18, 2006.
35. M.L. Janssens and W.J. Parker, "Oxygen Consumption Calorimetry," *Heat Release in Fires*, V. Babrauskas, S. Grayson, eds., Elsevier Applied Science, pp. 31-59, 1992.
36. Standard Test Method for Heat and Visible Smoke Release Rates for Materials and Products Using an Oxygen Consumption Calorimeter, ASTM E 1354, American Society for Testing and Materials, West Conshohocken, PA, 2013.
37. Standard Test Method for Measurement of Synthetic Polymer Material Flammability Using a Fire Propagation Apparatus (FPA), ASTM E 2058, American Society for Testing and Materials, West Conshohocken, PA, 2006.
38. R.E. Lyon and R.N. Walters, "Pyrolysis-Combustion Flow Calorimetry," *J. Analytical and Applied Pyrolysis*, 71, pp. 27-46, 2004.
39. C.F. Cullis, "The Role of Pyrolysis in Polymer Combustion and Flame Retardance," *Journal of Analytical and Applied Pyrolysis*, 11, pp. 451-463, 1987.
40. R.E. Lyon, "A New Method for Measuring Polymer Flammability," *Flame Retardants 2002*, London, England, February 5-6, 2002.
41. R.E. Lyon, and R.N. Walters, "Heat Release Capacity: A Molecular Level Fire Response Parameter," *Proceedings of the 7th International Symposium on Fire Safety Science*, Intl. Assoc. for Fire Safety Science, Worcester, MA, pp. 1167-1168, 2003.

42. R.N. Walters, and R.E. Lyon, "Molar Group Contributions to Polymer Flammability," *Journal of Applied Polymer Science*, 87, pp. 548-563, 2003.
43. J. Bicerano, *Prediction of Polymer Properties*, 2nd Edition, Marcel Dekker, New York, NY, 1996.
44. R.N. Walters, "Molar Group Contributions to the Heat of Combustion," *Fire and Materials*, 26, pp. 131-145, 2002.
45. M. Le Bras, G. Camino, S. Bourbigot, and R. Delobel, Eds., *Fire Retardancy of Polymers: The Use of Intumescence*, The Royal Society of Chemistry, Cambridge, UK, 1998.
46. A. Casu, G. Camino, M. De Giorgi, D. Flath, A. Laudi, and V. Morone, "Effect of glass fibres and fire retardant on the combustion behaviour of composites, glass fibres–poly(butylene terephthalate)," *Fire and Materials*, 22, 7, 1998.
47. R.E. Lyon and M.L. Janssens, "Polymer Flammability," in *Encyclopedia of Polymer Science and Engineering* (on-line edition), Wiley, New York, 2005.
48. Standard Test Method for Determining Flammability Characteristics of Plastics and Other Solid Materials Using Microscale Combustion Calorimetry, ASTM D 7309-07, American Society for Testing and Materials (International), West Conshohocken, PA, 2007.
49. R.A. Susott, "Thermal Behavior of Conifer Needle Extractives," *Forest Sciences*, 26, 3, pp.147-160, 1980.
50. Standard Test Method for Heat of Combustion of Hydrocarbon Fuels by Bomb Calorimeter (High Precision Method), ASTM-D238, American Society for Testing of Materials, Philadelphia, PA, 1988.

51. T.B. Brill, P.J. Brush, K.J. James, J.E. Shepherd, and K.J. Pfeiffer, "T-Jump / FT-IR Spectroscopy: A New Entry into the Rapid, Isothermal Pyrolysis Chemistry of Solids and Liquids," *Applied Spectroscopy*, 46, 6, pp. 900-911, 1992.
52. M.E. Brown (ed.), *Handbook of Thermal Analysis and Calorimetry*, Elsevier: Amsterdam, Vol. 1, 1998.
54. T. Hatakeyama and F.X. Quinn, *Thermal Analysis. Fundamentals and Applications to Polymer Science*, John Wiley & Sons: Chichester, England, 1999.
54. R.P. Hunter, *Automated Process Control Systems. Concepts and Hardware*, Prentice-Hall: Englewood Cliffs, NJ, 1978.
55. LabVIEW Professional Development System 7.0 for Windows, National Instruments Corporation.
56. J.P. Holman, *Heat Transfer*, Ninth Edition, McGraw-Hill: Boston, MA, 133-135, 2002.
57. V. Babrauskas, W.J. Parker, G. Mulholland, and W.H. Twilley, "The Phi Meter: A Simple, Fuel-Independent Instrument for Monitoring Combustion Equivalence Ratio," *Review of Scientific Instruments*, 65, 7, pp. 2367-2375, 1994.
58. W.M. Heffington, G.E. Parks, K.G.P. Sulzmann, and S.S. Penner, "Studies of Methane Oxidation Kinetics," *Proceedings of the Sixteenth Symposium (International) on Combustion*, the Combustion Institute, pp. 997-1010, 1976.
59. S.M. Reshetnikov, and I.S. Reshetnikov, "Oxidation Kinetic of Volatile Polymer Degradation Products," *Polymer Degradation and Stability*, 64, pp. 379-385, 1999.
60. R.N. Walters, S.M. Hackett, and R.E. Lyon, "Heats of Combustion of High Temperature Polymers," *Fire and Materials*, 24, pp. 245-252, 2000.
61. A. Schoemann, P.R. Westmoreland, H. Zhang, R.J. Farris, R.N. Walters, and R.E. Lyon, "A Pyrolysis/GC-MS Method for Characterizing Flammability and Thermal

Decomposition of Polymers,” Proc. 4th Joint Meeting of the U.S. Sections of the Combustion Institute, Philadelphia, PA, March 21-23, 2005.

62. P.R. Westmoreland, T. Inguilzian, K. and Rotem, “Flammability Kinetics From TGA/DSC/GCMS, Microcalorimetry and Computational Quantum Chemistry,” *Thermochimica Acta* 67, pp. 401-405, 2001.

63. J. Brandrup, E.H. Immergut, E.A. Grulke, A. Abe, D.R. Bloch, eds., “Polymer Handbook,” Fourth Edition, John Wiley & Sons, New York, 1999.

64. C.A. Harper, ed., “Modern Plastics Handbook,” McGraw-Hill, New York, 2000.

65. W.J. Frederick, C.C. Mentzer, “Determination of Heats of Volatilization for Polymers by Differential Scanning Calorimetry,” *Journal of Applied Polymer Science*, vol. 19, pp. 1799-1804, 1975.

66. P.R. Bevington, D.K. Robinson, “Data Reduction and Error Analysis for the Physical Sciences,” Second Edition, WCB/McGraw-Hill, Boston, 1992.

67. A. Tewarson, R.F. Pion, “Flammability of Plastics – I. Burning Intensity,” *Combustion and Flame*, vol. 26, pp. 85-103, 1976.

68. V. Babrauskas, “The Cone Calorimeter,” in *The SFPE Fire Protection Engineering* (2nd Ed.), Section 3, Chapter 3, pp. 37-52, Society of Fire Protection Engineers, Boston, MA, 1995.

69. F.D. Rossini, ed., *Experimental Thermochemistry*, Interscience, NY, 1956.

70. S.W. Benson, *Thermochemical Kinetics*, “Methods for the Estimation of Thermochemical Data and Rate Parameters,” John Wiley, New York, NY, 1968.

71. M.M. Coleman, J.F. Graf, and P.C. Painter, “Specific Interactions and the Miscibility of Polymer Blends,” Technomic Publishing Co., Inc., Lancaster, PA, 1991.

72. M. Janssens and W.J. Parker, "Oxygen Consumption Calorimetry," in Heat Release in Fires, V. Babrauskas, S.J. Grayson, eds., Chapter 3, pp. 31-59, Elsevier Applied Science, London, 1992.
73. F.Y. Hsieh, "Predicting Heats of Combustion and Lower Flammability Limits of Organosilicon Compounds," Fire and Materials, 23, 1999.
74. R.L. Cardozo, "Prediction of the Enthalpy of Combustion of Organic Compounds," AIChE Journal, Vol. 32, No. 5, pp. 844-848, 1986.
75. K. Wang, Q. Li, "A New Method for Predicting the Heat of Combustion of Liquid Alkanes by Using the Group-Bond Contribution Method," Journal of Ningxia University (Natural Science Edition), Vol. 21, No. 3, 2000.
76. M.M. Hirschler, "Heat Release in Fires," V. Babrauskas and S. Grayson, Eds., pp. 207-232; Elsevier Applied Science, New York, 1992.
77. J.W. Gilman and T. Kashiwagi, "Nanocomposites: Radiative Gasification and Vinyl Polymer Flammability," Proc. 6th European Meeting of Fire Retardancy of Polymeric Materials, Lille, France, September 24-26, 1997.
78. R.N. Walters and R.E. Lyon, "A Microscale Combustion Calorimeter for Determining Flammability Parameters of Materials," Proceedings 42nd International SAMPE Symposium and Exhibition, 42, 2, 1335-1344, 1997.
79. R.E. Lyon and R.N. Walters, U.S. Patent 5981290, Microscale Combustion Calorimeter, 11/09/1999.
80. R.N. Walters and R.E. Lyon, "Molar Group Contributions to Polymer Flammability," PMSE Preprints, 83, 86, ACS National Meeting, Washington, D.C., 2000.
81. R.N. Walters and R.E. Lyon, "Calculating Polymer Flammability from Molar Group Contributions," Proc. BCC Conference on Flame Retardancy of Polymeric Materials, Stamford, CT, May 22-24, 2000.

82. C.F. Cullis, and M.M. Hirschler, "The Significance of Thermoanalytical Measurements in the Assessment of Polymer Flammability," *Polymer*, 24, 7, pp. 834-840, 1983.
83. M.M. Hirschler, "Chemical Aspects of Thermal Decomposition of Polymeric Materials," in *Fire Retardancy of Polymeric Materials*, A.F. Grand and C.A. Wilkie, eds., Marcel Dekker, New York, pp. 28-75, 2000.
84. A. Factor, "Char Formation in Aromatic Engineering Polymers," *Fire and Polymers*, G.L. Nelson, ed., ACS Symposium Series 425, American Chemical Society, Washington, D.C., pp. 274-287, 1990.
85. I. Hamerton, ed., *Chemistry and Technology of Cyanate Ester Resins*, Blackie Academic & Professional (Chapman & Hall), London, 1994.
86. R.N. Walters, S. Gandhi, and R.E. Lyon, "Flammability of Cyanate Ester Resins," FAA International Aircraft Fire and Cabin Safety Research Conference, 1998.
87. R.N. Walters, S. Gandhi, and R.E. Lyon, "Flammability of Cyanate Ester Resins," NIST Annual Conference on Fire Research, 1998.
88. R.E. Lyon, R.N. Walters, and S. Gandhi, "Combustibility of Cyanate Ester Resins," 43rd Int'l SAMPE Symposium and Exhibition, Anaheim, CA, May 31-June 4, 1998.
89. S. Gandhi, R.N. Walters, and R.E. Lyon, "Cone Calorimeter Study of Cyanate Esters for Aircraft Applications," 27th International Conference on Fire Safety, San Francisco International Airport, CA, January 11-15, 1999.
90. M. Ramirez, R.N. Walters, E.P. Savitski, and R.E. Lyon, "Thermal Decomposition of Cyanate Ester Resins," FAA Report DOT/FAA/AR-01/32, September 2001.
91. "Epoxy Resin Manual," Industry Edition, Dow Chemical, 1988.

92. C.A. May and Tanaka, Y. ed. Epoxy Resins: Chemistry and Technology, Marcel Dekker, Inc, New York, 1973.
93. R.N. Walters, Fire Resistant Cyanate-Epoxy Blends, Proc. 46th Intl. SAMPE Symposium, Long Beach, CA, May 6-10, 2001.
94. M. Bauer, and J. Bauer, " Networks from cyanic acid esters and glycidyl ethers," Macromolekulare Chemie, Macromolecular Symposia, 30, 1, pp. 1-11, 1989.
95. B. Lin, "Cyanate Esters with Improved Fire Resistance," Proc. 44th Intl. SAMPE Symposium, Long Beach, CA, Vol. 2, pp. 1421-1430, 1999.
96. B. Lin, "Cyanate Esters with Improved Fire Resistance," Proc. ACUN-2: Intl. Composites Conference, Composite s Transportation Industry , 1, pp. 368-374, 2000.
97. M.L. Ramirez, Thermal Decomposition Mechanism of 2,2-bis(hydroxy-phenyl)-1,1-dichloroethylene-based Polymers, Final Report DOT/FAA/AR-00/42, February 2001.
98. S. Das, D.C. Prevorsek, and B.T. DeBona, Modern Plastics, 72, Feb. 1990.
99. F.E. Arnold Jr., R.E. Lyon, J. Rodrgiguez-Arnold, A.M. Granville, and S. Das, "Fire Resistant Triazine Resins," Int'l Conference on Fire Retardant Polymers, Salford, England, September 4-6, 1995.
100. E. Grigat, and R. Putter, Angewandt Chemie (International Edition), 6 ,3, pp 207, 1967.
101. S. Das, Polymeric Materials Science and Engineering, 66, pp 506, 1992.
102. S. Das, D.C. Prevorsek, and B.T. DeBona, 21st Inter. SAMPE Technical Conference, pp. 972, 1989.

103. S. Das, Amer. Composites International Conference. Orlando, FL, May 6-8, 1992.
104. M. Bauer, J. Bauer, and G. Kuhn, *Acta Polymerica*, 37, 218, 1986.
105. R.F. Cozzens, P. Walter, A.W. Snow, *J. Applied Polymer Sci.*, 34, pp. 601, 1987.
106. P. Penczek, B. Szczepaniak, & J. Rejdch, "Synteza Oligomerow Epoksydowo-Oksazolidonowych," *Polimery – Tworzywa Wielkocząsteczkowe*, 1986.
107. Lonza product brochure, Cyanate Ester Resins – Primaset™ Resins.
108. D.A. Schimp, F.A. Hudock and S.J. Ising, International SAMPE Symposium, 33, pp. 754, 1988.
109. D.A. Shimp, J.R. Christenson, and S.J. Ising, 34th International SAMPE Symposium, 34, pp. 222, 1989.
110. J. Galy, J.F. Gerard and J.P. Pascault, *Reactivity of Cyanate Ester Resins and Characterization of Polycyanurate Networks, Polyimides and Other High-Temperature Polymers*, Elsevier Science Publishers, B.V., Amsterdam 1991.
111. J. Vogt, "Thermoset Matrices for Structural Adhesives," *J. Adhesion*, 22, pp. 139-151 1987.
112. F. Ricciardi, W.A. Romanchick, and M.M. Joullie, "Mechanism of Imidazole Catalysis in the Curing of Epoxy Resins," *Journal of Polymer Science*, 21, pp. 1475-1490, 1983.
113. V. Jisova, "Curing Mechanism of Epoxides by Imidazoles," *Journal of Applied Polymer Science*, 34, pp. 2547-2558, 1987.
114. A. Osei-Owusu and G.C. Martin, "Analysis of the Curing Behavior of Cyanate Ester Systems," *Polymer Engineering and Science*, 31, 22, 1991.

115. A.Osei-Owusu and G.C. Martin, "Catalysis and Kinetics of Cyclotrimerization of Cyanate Ester Resin Systems," *Polymer Engineering and Science*, 32, 8, 1992.
116. H. Lee and K. Neville, *Handbook of Epoxy Resins*, McGraw-Hill, Inc., 1967.
117. ASTM D 790-95a, "Standard Test Methods for Flexural Properties of Unreinforced and Reinforced Plastics and Electrical Insulating Materials," Philadelphia, American Society of Testing and Materials, 1996.
118. M. Ramirez, *Thermal Degradation Mechanism of Chloral-Based Polymers*, Masters Thesis, University of Puerto Rico (Mayaguez), January 2000.
119. A. Factor, Char Formation in Aromatic Engineering Polymers, in: *Fire and Polymers: Hazards Identification and Prevention*, ACS Symposium Series 425, G.L. Nelson, Ed., American Chemical Society, Washington, D.C., Chapter 19, pp. 274-287, 1990.
120. A. Factor and C. M. Orlando, "Polycarbonates from 1,1,-Dichloro-2,2-Bis(4-Hydroxyphenyl ethylene and Bisphenol A: A Highly Flame Resistant Family of Engineering Polymers," *J. Polym. Sci: Polym. Chem. Ed.*, 18, pp. 579-592, 1980.
121. J.R. Stewart, "Synthesis and Characterization of Chlorinated Bisphenol-based Polymers and Polycarbodiimides as Inherently Fire Safe Polymers," FAA Report, DOT/FAA/AR-00/39, August 2000.
122. I. Glassman, *Combustion*, 3rd Edition, Academic Press, San Diego, CA, pp. 567-573, 1977.
123. R.N. Walters and R.E. Lyon, "Calculating Polymer Flammability From Molar Group Contributions," FAA Report DOT/FAA/AR-01/31, September 2001.
124. V. V. Korshak, P.N. Gribkova, A.V. Dmitrienko and S.V. Vinogradova. *Vysokomol Soed*, A16, 14, 1974.

125. V.V. Korshak, V.A. Pandratov, A.G. Puchin, S.A. Pavlova, I.V. Zhuravleva, V.G. Danilov, and S.V. Vinogradova, " Effect of the structure of polycyanates prepared by polycyclotrimerization of aryl dicyanates on their thermal stability," Polym.Sci. USSR, 17,3, pp. 554-559, 1975.
126. V.V. Korshak, S.A. Pavlova, P.N. Gribkova, M.V. Tsiirghiladze, V.A. Pankratov, S.V. Vinogradova, P.D. Tsiskarishvili, and G.S. Papava, Izv. Akad. Nauk. Grz. USSR, Ser. Khim., 3, 1, pp. 7-15, 1977.
127. D.A. Shimp, Private Communication, August 26, 1996.
128. D.A. Shimp and S.J. Ising, American Chemical Society National meeting PMSE Division. San Francisco California. ACS Press. Washington, D.C., April 1992.
129. A.S. Politou, C. Morterra, and M.J. D. Low. "Infrared Studies of Carbons; The Formation of Chars From Polycarbonate", Carbon, 28, 4, pp. 529-538, 1990.
130. E.M. Smolin and L. Rapoport, "The Chemistry of Heterolytic Compounds," A. Weissberger, ed., 13, "s-Triazines and Derivatives," Interscience, New York, pp. 17-48, 1959.
131. Z. Linhard, Anorg. Allgem. Chem., 236, pp. 200, 1938.
132. FAR 25.853, Heat Release Test for Cabin Materials, Aircraft Materials Fire Test Handbook, DOT/FAA/AR-00/12, 2000.
133. R.E. Lyon, "Fire-Resistant Materials: Research Overview," FAA Report DOT/FAA/AR-97/99, December 1997.
134. R.E. Lyon, "Fire-Safe Aircraft Cabin Materials," Fire & Polymers II, Chapter 38, p. 618, American Chemical Society, Washington DC, 1995.
135. U. Sorathia, G. Long, M. Blum, J. Ness, and T. Gracik, "Performance Requirements for Fire Safety of Materials in U.S. Navy Ships and Submarines,"

SAMPE Symposium & Exhibition, Long Beach, CA, May 6-10, 46, pp. 1683-1694, 2001.

136. MIL-STD-2031, "Fire and Toxicity Test methods and Qualification Procedure for Composite Materials Systems Used in Hull, Machinery, and Structural Applications Inside Naval Submarines," 1991.

137. J. Koo, B. Muskopf, G. McCord, P. VanDine, B. Spencer, U. Sorathia, and S. Venumbaka, "Characterization of Fire Safe Polymer Matrix Composites for Naval Applications," SAMPE Symposium & Exhibition, Long Beach, CA, May 6-10, 46, pp. 2170-2182, 2001.

138. W.J. Parker, "Development of a Model for the Heat Release Rate of Wood," NBISR 85-3163, 1985.

139. D. Drysdale, "An Introduction to Fire Dynamics," John Wiley and Sons, New York, 1996.

140. P. VanDine and U. Sorathia, "Developments in Fire Proof Composites," Proc. 46th Intl. SAMPE Symposium & Exhibition, Long Beach, CA, May 6-10, 2001.

141. R.E. Lyon, R.N. Walters, and S.I. Stoliarov, "Thermal Analysis of Polymer Flammability," J. Therm. Anal. Calorimetry, 89, 2, pp. 441-448, 2007.

142. R.N. Walters and R.E. Lyon, "Molar Group Contributions to Polymer Flammability," J. Appl. Polym. Sci., 87, pp. 548-563, 2003.

143. R.E. Lyon, "Plastics and Rubber," in Handbook of Building Materials for Fire Protection, C. A. Harper, ed., McGraw-Hill, New York, NY, Chapter 3, pp. 3.1-3.51, 2004.

144. Flammability of Plastic Materials, UL 94 Section 2 (Horizontal: HB) and Section 3 (Vertical: V-0/1/2), Underwriters Laboratories, Northbrook, IL, 1991.

145. Standard Test Method for Measuring the Minimum Oxygen Concentration to Support Candle-Like Combustion of Plastics (Oxygen Index), D 2863, American Society for Testing and Materials, West Conshohocken, PA, 2006.
146. R.E. Lyon, "Piloted Ignition of Combustible Solids," in Society for the Advancement of Materials and Process Engineering (SAMPE) International Conference, Long Beach, CA, May 2–5, 2005.
147. J.G. Quintiere and A.S. Rangwala, "A Theory for Flame Extinction Based on Flame Temperature," *Fire and Materials*, 28, pp. 387-402, 2004.
148. Standard Guide for Obtaining Data for Deterministic Fire Models, ASTM E 1591, American Society for Testing and Materials, West Conshohocken, PA, 2000.
149. Standard Test Method for Materials Response to Flame-458 (For Aerospace Vehicles), ASTM F 1103, American Society for Testing and Materials, West Conshohocken, PA, 1993.
150. V. Babrauskas, *Ignition Handbook*, Fire Science, Issaquah, WA, 2003.
151. R.E. Lyon, "Flammability of Glass Fiber Reinforced Plastics," in Society for the Advancement of Materials and Process Engineering SAMPE International Conference, Long Beach, CA, April 30–May 4, 2006.
152. P.M. Hergenrother, C.M. Thompson, J.G. Smith Jr., J.W. Connell, J.A. Hinkley, R.E. Lyon, and R. Moulton, "Flame Retardant Aircraft Epoxy Resins Containing Phosphorus," *Polymer* 46, pp. 5012-5024, 2005.
153. S.I. Stoliarov, Q. Williams, S. Crowley, R.N. Walters, and R.E. Lyon, "Analysis of Flammability of Brominated Epoxies," Presented at the 15th Annual BCC Conference on Flame Retardancy of Polymeric Materials, Stamford, CT, June 7–9, 2004.

154. B. Scharrel, K.H. Pawlowski, and R.E. Lyon, " Pyrolysis Combustion Flow Calorimeter: A Tool to Assess Flame Retarded PC / ABS Materials?," *Thermochimica Acta*, 462, pp. 1-14, 2007.
155. D.W. Hosmer and S. Lemeshow, *Applied Logistic Regression*, 2nd ed., Wiley, New York, 2000.
156. M.D. Pedley, J.H. Pao, L. Bamford, R.E. Williams, and B. Plante, *Ignition of Contaminants by Impact of High-Pressure Oxygen, Flammability and Sensitivity of Materials in Oxygen-Enriched Atmospheres*, Vol. 3, ASTM STP 986, D.W. Schroll, Ed., American Society for Testing and Materials, Philadelphia, PA, 1987.
157. A. Tewarson, J.L. Lee, and R.F. Pion, "The Influence of Oxygen Concentration on Fuel Parameters for Fire Modelling," Presented at the Eighteenth Symposium (International) on Combustion, The Combustion Institute, Pittsburgh, PA, 563, 1981.
158. S. Hong, J. Yang, A. Sunghee, M. Yongik, and G. Lee, " Flame Retardant Performance Of Various UL94 Classified Materials Exposed To External Ignition Sources," *Fire and Materials*, 28, pp. 25-31, 2004.
159. M. Bundy and T. Ohlemiller, *Bench-Scale Flammability Measures for Electronic Equipment*, NIST IR 7031, National Institute of Standards and Technology, Gaithersburg, MD, 2003.
160. Heat Release Rate Test for Cabin Materials as per Federal Aviation Regulation 25.853, "Aircraft Materials Fire Test Handbook," Section 5, FAA Final Report DOT/FAA/AR-00/12, April 2000.
161. S.I. Stoliarov and R.E. Lyon, "Thermo-Kinetic Model of Burning," Federal Aviation Administration Technical Note, DOT/FAA/AR-TN08/17, 2008.
162. S.I. Stoliarov, R.E. Lyon, "Thermo-kinetic model of burning for pyrolyzing materials," *Proceedings of the Ninth International Symposium on Fire Safety Science*, pp. 1141–1152, 2009.

163. S.I. Stoliarov, S. Crowley, R.E. Lyon, G.T. Linteris, "Prediction of the burning rates of non-charring polymers," *Combustion and Flame* 156, pp. 1068–1083, 2009.
164. S.I. Stoliarov, R.N. Walters, Determination of the heats of gasification of polymers using differential scanning calorimetry, *Polymer Degradation and Stability*, 93, pp. 422–427, 2008.
165. M.W. Chase Jr., NIST-JANAF Thermochemical Tables, fourth ed., (J. Phys. Chem. Ref. Data, Monograph 9), pp. 1–1951, 1998.
166. J.G. Quintiere, X. Liu, "Flammability Properties of Clay–Nylon Nanocomposites," Federal Aviation Administration Technical Report DOT/FAA/AR-07/29, 2007.
167. P.A. Beaulieu, N.A. Dembsey, "Effect of Oxygen On Flame Heat Flux In Horizontal And Vertical Orientations," *Fire Safety Journal*, 43, pp. 410–428, 2008.
168. R. Siegel, J. Howell, *Thermal Radiation Heat Transfer*, fourth ed., Taylor & Francis, New York, NY, 2002.
169. J.P. Holman, *Heat Transfer*, ninth ed., McGraw-Hill, Boston, MA, 2002.

APPENDIX A

COMBUSTION DATA FOR POLYMERIC MATERIALS

Values for the gross heat of combustion,  $Q_c$ , were determined experimentally. Values for the net heat of combustion,  $\Delta h_c$ , were calculated from the measured gross heat of combustion corrected for the latent heat of vaporization of water produced during the reaction. The  $E$  value,  $\Delta h_c/r_o$ , was calculated from the net heat of combustion and the amount of oxygen required to completely oxidize the repeat unit structure. An average value of  $E = 13.10 \pm 0.78 \text{ kJ/g-O}_2$  was found for the net heat of combustion per gram of diatomic oxygen consumed in this study.

	Material (abbreviated name), [CAS Registry Number]	Trade Name, Manufacturer/ Supplier	Repeat Unit Composition	$Q_c$ (kJ/g)	$\Delta h_c$ (kJ/g)	$\Delta h_c/r_o$ (kJ/g-O <sub>2</sub> )
1	Poly(oxymethylene) (POM) [9002-81-7]	Aldrich Chemical Company, Inc.	CH <sub>2</sub> O	17.39 ± 0.13	15.93	14.93
2	Polytetrafluoroethylene (PTFE) [9002-84-0]	Aldrich Chemical Company, Inc.	C <sub>2</sub> F <sub>4</sub>	6.68	6.68	10.44
3	Polyvinylalcohol (≥99%) (PVOH) [9002-89-5]	Aldrich Chemical Company, Inc.	C <sub>2</sub> H <sub>4</sub> O	23.31 ± 0.54	21.31	11.72
4	Polyethylene (PE) [9002-88-4]	LDPE Polysciences, Inc.	C <sub>2</sub> H <sub>4</sub>	47.74	44.60	13.01
5	Poly(dimethylsiloxane) (PDMS) [9016-00-6]	Dow Corning 346	C <sub>2</sub> H <sub>6</sub> OSi	19.53 ± .74	17.75	13.68
6	Polypropylene (PP) [25085-53-4]	Polysciences, Inc.	C <sub>3</sub> H <sub>6</sub>	45.80 ± 0.48	42.66	12.44
7	Poly(methylmethacralate) (PMMA) [9011-14-7]	Aldrich Chemical Company, Inc.	C <sub>5</sub> H <sub>8</sub> O <sub>2</sub>	26.75 ± 0.14	24.99	13.02
8	Poly(methylmethacrylate) (PMMA) [9011-14-7]	Polycast acrylic (black)	C <sub>5</sub> H <sub>8</sub> O <sub>2</sub>	26.86 ± .61	25.10	13.07
9	Poly(1,4-phenylenesulfide) (PPS) [9016-75-5]	Aldrich Chemical Company, Inc	C <sub>6</sub> H <sub>4</sub> S	29.62 ± 0.71	28.81	13.89
10	Poly(phenylenesulfide) (PPS) [9016-75-5]	KETRON PPS™ DSM Engineering	C <sub>6</sub> H <sub>4</sub> S	28.39 ± .37	27.58	13.30
11	Poly(2,6-dimethyl-1,4-phenyle neoxide) (PPO) [25134-01-4]	Noryl 0.4 IV™ virgin General Electric	C <sub>8</sub> H <sub>8</sub> O	34.21 ± 0.36	32.75	12.93
12	Polystyrene (PS) [9003-53-6]	Polysciences, Inc.	C <sub>8</sub> H <sub>8</sub>	43.65	41.96	13.64
13	Polyethyleneterephthalate (PET) [25038-59-9]	Polysciences, Inc.	C <sub>10</sub> H <sub>8</sub> O <sub>4</sub>	24.13 ± 0.39	23.22	13.93
14	Epoxy Novolac, catalytic cure (phenoxy-N) [028064-14-4]	DEN-438™ Dow Chemical	C <sub>10</sub> H <sub>11</sub> O	31.37 ± .14	29.73	11.15

	Material (abbreviated name), [CAS Registry Number]	Trade Name, Manufacturer/ Supplier	Repeat Unit Composition	$Q_c$ (kJ/g)	$\Delta h_c$ (kJ/g)	$\Delta h_c/r_o$ (kJ/g-O <sub>2</sub> )
15	Poly(1,4-phenyleneethersulfone) (PES) [25667-42-9]	BASF Ultron™ E1010/ Natural	C <sub>12</sub> H <sub>8</sub> O <sub>3</sub> S	25.42 ± 0.55	24.66	14.30
16	Poly(1,4- butanediolterephthalate) (PBT) [26062-94-2]	Polysciences, Inc.	C <sub>12</sub> H <sub>12</sub> O <sub>4</sub>	27.91	26.71	14.13
17	Poly(hexamethyleneadiapamide) (nylon 66) [32131-17-2]	Polysciences, Inc.	C <sub>12</sub> H <sub>22</sub> O <sub>2</sub> N <sub>2</sub>	30.90 ± 0.15	28.76	12.31
18	Poly(etherketone) (PEK) [27380-27-4]	P22 (virgin) Victrex USA	C <sub>13</sub> H <sub>8</sub> O <sub>2</sub>	31.07 ± 0.70	30.17	13.20
19	Poly(benzoyl-1,4-phenylene)	POLYX- 1000™ MAXDEM, Inc.	C <sub>13</sub> H <sub>8</sub> O	38.35	37.37	14.50
20	Poly(p- phenylenebenzobisoxazole) (PBO) [852-36-8]	PBO DOW Chemical Co.	C <sub>14</sub> H <sub>6</sub> O <sub>2</sub> N <sub>2</sub>	29.18 ± 0.21	28.62	14.43
21	Poly(m-phenylene isophthalamide)	Nomex™ Dupont	C <sub>14</sub> H <sub>10</sub> O <sub>2</sub> N <sub>2</sub>	26.45 ± 0.09	25.53	12.25
22	Aramid-arylester copolymer	Aramid Z- 200™ Dupont	C <sub>14</sub> H <sub>10</sub> O <sub>2</sub> N <sub>2</sub>	25.27 ± 0.81	24.35	11.68
23	Poly(p-phenylene terephthalamide)	KEVLAR™ Dupont	C <sub>14</sub> H <sub>10</sub> O <sub>2</sub> N <sub>2</sub>	26.92 ± 0.54	26.00	12.48
24	Polyamideimide (PAI)	TORLON 4203L™ Amoco	C <sub>15</sub> H <sub>8</sub> O <sub>3</sub> N <sub>2</sub>	24.97 ± 0.13	24.31	12.94
25	Poly(acrylonitrilebutadiene- styrene) (ABS) [9003-56-9]	Polysciences, Inc.	C <sub>15</sub> H <sub>17</sub> N	39.84	38.07	13.04
26	Bisphenol-E Cyanate Ester [47073-92-7]	AroCy L-10™ Ciba Specialty Chemicals	C <sub>16</sub> H <sub>12</sub> O <sub>2</sub> N <sub>2</sub>	29.38 ± 0.06	28.38	13.01
27	Polycarbonate of bisphenol-A (PC) [24936-68-3]	Polysciences Inc. 32-36K mol.wt.	C <sub>16</sub> H <sub>14</sub> O <sub>3</sub>	31.53 ± 0.88	30.32	13.37
28	Polycarbonate of bisphenol-A (PC) [24936-68-3]	LEXAN 141™ General Electric	C <sub>16</sub> H <sub>14</sub> O <sub>3</sub>	31.06 ± 0.08	29.85	13.16
29	Hexafluorobisphenol-A Cyanate Ester [32728-27-1]	AroCy F-10™ Ciba Specialty Chemicals	C <sub>17</sub> H <sub>8</sub> O <sub>2</sub> N <sub>2</sub> F <sub>6</sub>	18.71 ± 0.03	18.25	12.23
30	Bisphenol-A Cyanate Ester [1156-51-0]	AroCy B-10™ Ciba Specialty Chemicals	C <sub>17</sub> H <sub>14</sub> O <sub>2</sub> N <sub>2</sub>	29.92 ± 0.27	28.81	12.84
31	Bisphenol-A Epoxy, catalytic cure (Phenoxy-A) [001675-54- 3]	DER-332™ Dow Chemical	C <sub>21</sub> H <sub>24</sub> O	32.50 ± 0.15	30.94	11.40
32	Poly(etheretherketone) (PEEK) [29658-26-2]	450F™ Victrex USA	C <sub>19</sub> H <sub>12</sub> O <sub>3</sub>	31.07 ± 0.53	30.16	13.24
33	Poly(etheretherketone) (PEEK) [29658-26-2]	KETRON PEEK 1000™ DSM	C <sub>19</sub> H <sub>12</sub> O <sub>3</sub>	31.48 ± 0.44	30.57	13.42

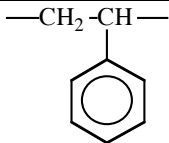
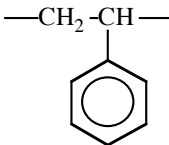
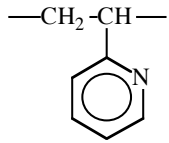
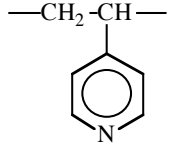
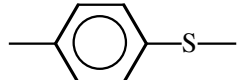
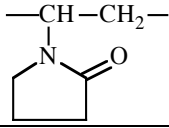
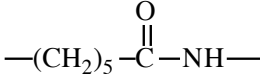
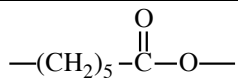
	Material (abbreviated name), [CAS Registry Number]	Trade Name, Manufacturer/ Supplier	Repeat Unit Composition	$Q_c$ (kJ/g)	$\Delta h_c$ (kJ/g)	$\Delta h_c/r_o$ (kJ/g-O <sub>2</sub> )
34	Tetramethylbisphenol F Cyanate Ester [101657-77-6]	AroCy M-10™ Ciba Specialty Chemical	C <sub>19</sub> H <sub>18</sub> O <sub>2</sub> N <sub>2</sub>	31.23 ± 0.05	29.94	12.72
35	Poly(etherketoneketone) (PEKK)	G040™ (virgin flake) Dupont	C <sub>20</sub> H <sub>12</sub> O <sub>3</sub>	31.15 ± 0.17	30.27	13.20
36	Polybenzimidazole (PBI) [25928-81-8]	CELAZOLE™ PBI Hoechst Celanese	C <sub>20</sub> H <sub>12</sub> N <sub>4</sub>	31.65 ± 0.35	30.79	12.90
37	Polyimide (PI) [26023-21-2]	Aldrich Chemical Company, Inc.	C <sub>22</sub> H <sub>10</sub> O <sub>5</sub> N <sub>2</sub>	26.03 ± 0.77	25.45	13.81
38	Novolac Cyanate Ester [P88-1591]	AroCy XU-371™ Ciba Specialty Chemical	C <sub>23</sub> H <sub>15</sub> O <sub>3</sub> N <sub>3</sub>	28.61 ± 0.53	27.77	12.99
39	Novolac Cyanate Ester [P88-1591]	Primaset PT-30™ Allied Signal	C <sub>23</sub> H <sub>15</sub> O <sub>3</sub> N <sub>3</sub>	30.65 ± 0.05	29.81	13.95
40	Bisphenol-M Cyanate Ester [127667-44-1]	AroCy XU-366™ Ciba Specialty Chemical	C <sub>26</sub> H <sub>24</sub> O <sub>2</sub> N <sub>2</sub>	34.39 ± 0.15	33.06	13.20
41	Polysulfone of bisphenol-A (PSF) [25135-57-7]	Aldrich Chemical Company, Inc.	C <sub>27</sub> H <sub>22</sub> O <sub>4</sub> S	30.28 ± 0.47	29.19	13.22
42	Polysulfone of bisphenol-A (PSF) [25135-57-7]	UDEL™ Amoco	C <sub>27</sub> H <sub>22</sub> O <sub>4</sub> S	30.63 ± 0.35	29.54	13.38
43	Polybenzoxazine of bisphenol-A/aniline (b-a benzoxazine)	Case Western Reserve University	C <sub>31</sub> H <sub>30</sub> O <sub>2</sub> N <sub>2</sub>	34.89 ± 0.19	33.46	12.88
44	Arylether of hexafluorobisphenol -A and triphenylphosphine oxide	6F-ETPP™ DAYCHEM	C <sub>33</sub> H <sub>21</sub> O <sub>3</sub> F <sub>6</sub> P	26.50 ± 0.25	25.74	13.35
45	Polyetherimide (PEI) [61128-46-9]	Polysciences, Inc.	C <sub>37</sub> H <sub>24</sub> O <sub>6</sub> N <sub>2</sub>	29.59 ± 0.28	28.70	13.27
46	Polyetherimide (PEI) [61128-46-9]	ULTEM 1000, General Electric	C <sub>37</sub> H <sub>24</sub> O <sub>6</sub> N <sub>2</sub>	29.06 ± .06	28.17	13.03
47	Polyester of hydroxybenzoic and hydroxynaphthoic acids [70679-92-4]	VECTRA C LCP™ (virgin/unfilled) Hoechst Celanese	C <sub>39</sub> H <sub>22</sub> O <sub>10</sub>	26.54 ± 0.39	25.80	13.27
48	Polyethylenenaphthylate (PEN)	Eastman Chemical Company	C <sub>14</sub> H <sub>10</sub> O <sub>4</sub>	25.92 ± 0.09	25.01	13.06
49	Dicyclopentadienyl bisphenol	XU-71787™ Dow Chemical	C <sub>17</sub> H <sub>17</sub> NO	33.64 ± 0.24	32.14	11.88

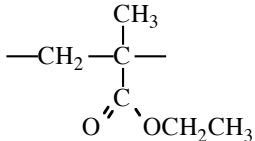
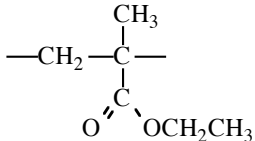
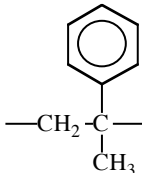
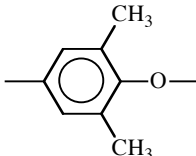
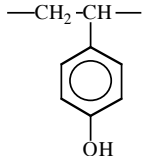
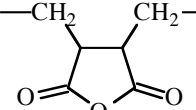
APPENDIX B

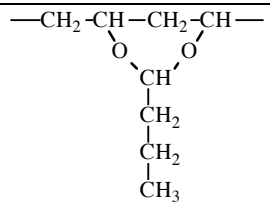
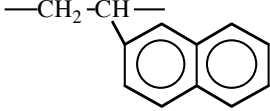
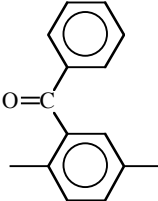
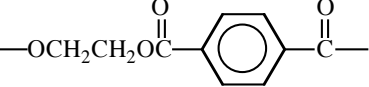
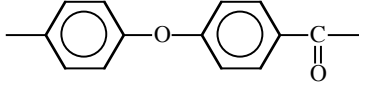
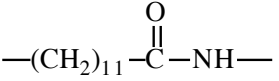
HEAT RELEASE VALUES FROM MICROSCALE COMBUSTION  
CALORIMETER

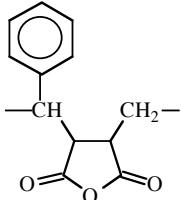
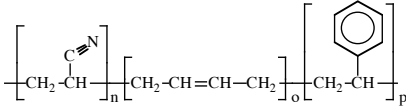
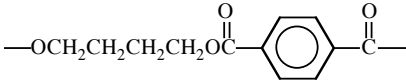
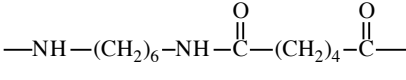
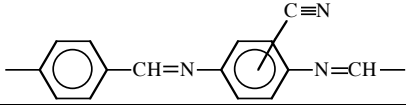
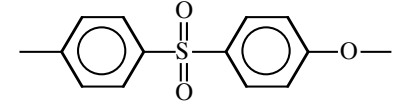
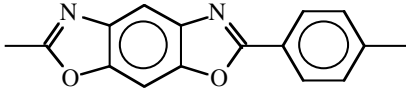
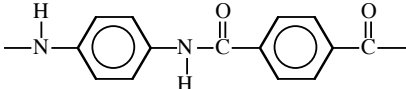
Material and Abbreviated Name	Trade Name, Manufacturer / Supplier	CAS Number	Repeat Unit Composition	Repeat Unit Structure	HR Capacity (J/g-K)	Total HR (kJ/g)	Char (%)	MW (g/mol)
Polyethylene PE	LDPE Polysciences, Inc.	[9002-88-4]	C <sub>2</sub> H <sub>4</sub>	—CH <sub>2</sub> -CH <sub>2</sub> —	1676	41.6	0	28.06
Polyoxymethylene POM	Polysciences, Inc.	[9002-81-7]	CH <sub>2</sub> O	—CH <sub>2</sub> -O—	169	14	0	30.03
Polypropylene PP	Polysciences, Inc.	[25085-53-4]	C <sub>3</sub> H <sub>6</sub>	—CH <sub>2</sub> -CH—   CH <sub>3</sub>	1571	41.4	0	42.08
Polyvinylalcohol (≥99%) PVOH	Aldrich Chemical Company, Inc.	[9002-89-5]	C <sub>2</sub> H <sub>4</sub> O	—CH <sub>2</sub> -CH—   OH	533	21.6	3.3	44.03
Polyethyleneoxide	Polysciences, Inc.	[25322-68-3]	C <sub>2</sub> H <sub>4</sub> O	—CH <sub>2</sub> -CH <sub>2</sub> -O—	652	21.6	1.7	44.05
Polyisobutylene	Aldrich	[9003-27-1]	C <sub>4</sub> H <sub>8</sub>	—CH <sub>2</sub> -C—   CH <sub>3</sub>	1002	44.4	0	56.11
Polyvinylchloride	PVC	[9002-86-2]	C <sub>2</sub> H <sub>3</sub> Cl	—CH <sub>2</sub> -CH—   Cl	138	11.3	15.3	62.48
Polyvinylidene fluoride	PVDF MW:120000 Polysciences	[24937-79-9]	C <sub>2</sub> H <sub>2</sub> F <sub>2</sub>	—CH <sub>2</sub> -C—   F	311	9.7	7	64.02
Polyacrylamide	Polysciences, Inc.	[9003-05-8]	C <sub>3</sub> H <sub>5</sub> NO	—CH <sub>2</sub> -CH—   C(=O)NH <sub>2</sub>	104	13.3	8.3	71.08
Polyacrylic Acid	Polysciences	[9003-01-4]	C <sub>3</sub> H <sub>4</sub> O <sub>2</sub>	—CH <sub>2</sub> -CH—   C(=O)OH	165	12.5	6.1	72.06

Material and Abbreviated Name	Trade Name, Manufacturer / Supplier	CAS Number	Repeat Unit Composition	Repeat Unit Structure	HR Capacity (J/g-K)	Total HR (kJ/g)	Char (%)	MW (g/mol)
Polyvinylacetate PVAc	Polysciences, Inc.	[9003-20-7]	C <sub>4</sub> H <sub>6</sub> O <sub>2</sub>	$\begin{array}{c} \text{---CH}_2\text{---CH---} \\   \\ \text{O} \\   \\ \text{C} \\ / \quad \backslash \\ \text{O} \quad \text{CH}_3 \end{array}$	313	19.2	1.2	86.09
Polymethacrylic Acid	MW:100000 Polysciences	[25087-26-7]	C <sub>4</sub> H <sub>6</sub> O <sub>2</sub>	$\begin{array}{c} \text{CH}_3 \\   \\ \text{---CH}_2\text{---C---} \\   \\ \text{C} \\ / \quad \backslash \\ \text{O} \quad \text{OH} \end{array}$	464	18.4	0.5	86.09
Polychloroprene	Neoprene Polysciences	[9010-98-4]	C <sub>4</sub> H <sub>5</sub> Cl	$\begin{array}{c} \text{---CH}_2\text{---} \quad \text{C}=\text{C} \quad \text{---CH}_2\text{---} \\ / \quad \backslash \\ \text{Cl} \quad \text{H} \end{array}$	188	16.1	12.9	88.54
Polytetrafluoroethylene PTFE	Aldrich Chemical Company, Inc.	[9002-84-0]	C <sub>2</sub> F <sub>4</sub>	$\text{---CF}_2\text{---CF}_2\text{---}$	35	3.7	0	100.02
Polymethyl methacralate PMMA	Aldrich Chemical Company, Inc.	[9011-14-7]	C <sub>5</sub> H <sub>8</sub> O <sub>2</sub>	$\begin{array}{c} \text{CH}_3 \\   \\ \text{---CH}_2\text{---C---} \\   \\ \text{C} \\ / \quad \backslash \\ \text{O} \quad \text{OCH}_3 \end{array}$	514	24.3	0	100.12
Polymethyl methacralate PMMA	Polysciences MW: 75000	[9011-14-7]	C <sub>5</sub> H <sub>8</sub> O <sub>2</sub>	$\begin{array}{c} \text{CH}_3 \\   \\ \text{---CH}_2\text{---C---} \\   \\ \text{C} \\ / \quad \backslash \\ \text{O} \quad \text{OCH}_3 \end{array}$	461	23.2	0	100.12
Polyethylacrylate	Polysciences MW:70000	[9003-32-1]	C <sub>5</sub> H <sub>8</sub> O <sub>2</sub>	$\begin{array}{c} \text{---CH}_2\text{---CH---} \\   \\ \text{C} \\ / \quad \backslash \\ \text{O} \quad \text{OCH}_2\text{CH}_3 \end{array}$	323	22.6	0.3	100.12
Polymethacrylamide	Polysciences	[25014-12-4]	C <sub>4</sub> H <sub>7</sub> NO <sub>2</sub>	$\begin{array}{c} \text{CH}_3 \\   \\ \text{---CH}_2\text{---C---} \\   \\ \text{C} \\ / \quad \backslash \\ \text{O} \quad \text{ONH}_2 \end{array}$	103	18.7	4.5	101.1

Material and Abbreviated Name	Trade Name, Manufacturer / Supplier	CAS Number	Repeat Unit Composition	Repeat Unit Structure	HR Capacity (J/g-K)	Total HR (kJ/g)	Char (%)	MW (g/mol)
Polystyrene PS	Polysciences, Inc.	[9003-53-6]	C <sub>8</sub> H <sub>8</sub>		927	38.8	0	104.15
Isotactic Polystyrene	Questra	[25086-18-4]	C <sub>8</sub> H <sub>8</sub>		880	39.9	0	104.15
Poly-2-vinylpyridene	Polysciences MW:200000-400000	[25014-15-7]	C <sub>7</sub> H <sub>7</sub> N		612	34.7	0	105.14
Poly-4-vinylpyridene	Polysciences MW:300000	[25232-41-1]	C <sub>7</sub> H <sub>7</sub> N		568	31.7	0	105.14
Poly-1,4-Phenylene Sulfide PPS	Aldrich Chemical Company, Inc	[9016-75-5]	C <sub>6</sub> H <sub>4</sub> S		165	17.1	41.6	108.16
Poly-n-vinylpyrrolidone	Polysciences	[9003-39-8]	C <sub>6</sub> H <sub>9</sub> NO		332	25.1	0	111.14
Polycaprolactam	Nylon 6	[25038-54-4]	C <sub>6</sub> H <sub>11</sub> NO		487	28.7	0	113.16
Polycaprolactone	Polysciences, Inc.	[24980-41-4]	C <sub>6</sub> H <sub>10</sub> O <sub>2</sub>		526	24.4	0	114.14

Material and Abbreviated Name	Trade Name, Manufacturer / Supplier	CAS Number	Repeat Unit Composition	Repeat Unit Structure	HR Capacity (J/g-K)	Total HR (kJ/g)	Char (%)	MW (g/mol)
Polyethyl methacrylate	Polysciences MW:250000	[9003-42-3]	C <sub>6</sub> H <sub>10</sub> O <sub>2</sub>		470	26.4	0	114.14
Polyethyl methacrylate	Aldrich MW:850000	[9003-42-3]	C <sub>6</sub> H <sub>10</sub> O <sub>2</sub>		380	26.8	0	114.14
Poly α Methyl styrene	Aldrich	[52014-31-7]	C <sub>9</sub> H <sub>10</sub>		730	35.5	0	118.18
Poly-2,6-dimethyl-1,4-phenyleneoxide PPO	Noryl 0.4 IV virgin General Electric	[25134-01-4]	C <sub>8</sub> H <sub>8</sub> O		409	20	25.5	120.15
Poly-4-vinylphenol	Polysciences MW:22000	[24979-70-2]	C <sub>8</sub> H <sub>8</sub> O		261	27.6	2.8	120.15
Polyethylenemaleic anhydride	Polysciences	[9002-26-2]	C <sub>6</sub> H <sub>6</sub> O <sub>3</sub>		138	12.1	2.8	126.11

Material and Abbreviated Name	Trade Name, Manufacturer / Supplier	CAS Number	Repeat Unit Composition	Repeat Unit Structure	HR Capacity (J/g-K)	Total HR (kJ/g)	Char (%)	MW (g/mol)
Polyvinylbutyral	Polysciences MW:100000-150000	[63148-65-2]	C <sub>8</sub> H <sub>14</sub> O <sub>2</sub>		806	26.9	0.1	142.1
Poly-2-vinylnaphthalene	Aldrich MW:175000	[28406-56-6]	C <sub>12</sub> H <sub>10</sub>		834	39	0	154.21
Polybenzoyl-1,4-Phenylene	POLYX-1000, MAXDEM, Inc.	[NA]	C <sub>13</sub> H <sub>8</sub> O		41	10.9	65.2	180.21
Polyethylene Terephthalate PET	Polysciences, Inc.	[25038-59-9]	C <sub>10</sub> H <sub>8</sub> O <sub>4</sub>		332	15.3	5.1	192.17
Polyetherketone PEK	P22 (virgin), Victrex USA	[27380-27-4]	C <sub>13</sub> H <sub>8</sub> O <sub>2</sub>		124	10.8	52.9	196.2
Polylauro lactam	Nylon 12 Polysciences, Inc.	[25030-74-8]	C <sub>12</sub> H <sub>23</sub> O		743	33.2	0	197.32

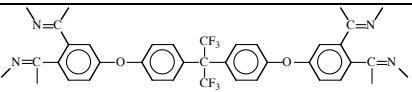
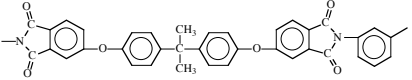
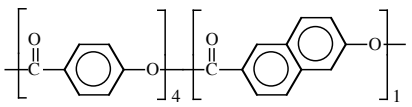
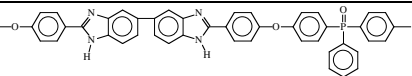
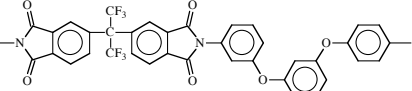
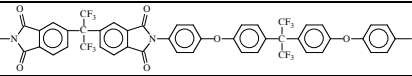
Material and Abbreviated Name	Trade Name, Manufacturer / Supplier	CAS Number	Repeat Unit Composition	Repeat Unit Structure	HR Capacity (J/g-K)	Total HR (kJ/g)	Char (%)	MW (g/mol)
Polystyrene maleicanhydride	Polysciences	[9011-13-6]	$C_{12}H_{10}O_3$		279	23.3	2.2	202.21
Polyacrylonitrile Butadiene-Styrene ABS	ABS Polysciences, Inc.	[9003-56-9]	$C_{15}H_{17}N$		669	36.6	0	211.31
Poly-1,4-butanediol Terephthalate PBT	Polysciences, Inc.	[26062-94-2]	$C_{12}H_{12}O_4$		474	20.3	1.5	220.22
Polyhexamethylene Adiapamide	Nylon 6/6 Polysciences, Inc.	[32131-17-2]	$C_{12}H_{22}O_2N_2$		615	27.4	0	226.32
Polyazomethine	UMASS	[NA]	$C_{15}H_9N_3$		36	8.7	77.8	231.26
Poly-1,4-Phenylene Ethersulfone PES	BASF Ultrason E1010/ Natural BASF	[25667-42-9]	$C_{12}H_8O_3S$		115	11.2	29.3	232.26
Poly-p-Phenylene Benzobisoxazole PBO	PBO, DOW Chemical Co.	[852-36-8]	$C_{14}H_6O_2N_2$		42	5.4	69.5	234.21
Poly(p-phenylene Terephthalamide)	Kevlar Dupont	[308069-56-9]	$C_{14}H_{10}O_2N_2$		302	14.8	36.1	238.25

Material and Abbreviated Name	Trade Name, Manufacturer / Supplier	CAS Number	Repeat Unit Composition	Repeat Unit Structure	HR Capacity (J/g-K)	Total HR (kJ/g)	Char (%)	MW (g/mol)
Poly(m-Phenylene Isophthalamide)	Nomex Dupont	[24938-60-1]	$C_{14}H_{10}O_2N_2$		52	11.7	48.4	238.25
Polyethylene naphthylate PEN	Eastman Chemical Company	[24968-11-4]	$C_{14}H_{10}O_4$		309	16.8	18.2	242.23
Dicyclopentadienyl Bisphenol	XU-71787 Dow Chemical	[1355-71-0]	$C_{17}H_{17}NO$		493	20.1	27.1	251.32
Polycarbonate of Bisphenol-A PC	Polysciences Inc., 32-36K MW	[24936-68-3]	$C_{16}H_{14}O_3$		359	16.3	21.7	254.28
Polyphosphazine	Eypel-A Rice University	[NA]	$C_{14}H_{14}PNO_3$		204	21.9	20	259.24
Polydiphenylether Chloral	Rice University MW:9350	[NA]	$C_{14}H_8OCl_2$		16	5.2	57.1	263.12
Cyano-Substituted Kevlar	UMASS	[NA]	$C_{15}H_9N_3O_2$		54	9.1	58.3	263.26

Material and Abbreviated Name	Trade Name, Manufacturer / Supplier	CAS Number	Repeat Unit Composition	Repeat Unit Structure	HR Capacity (J/g-K)	Total HR (kJ/g)	Char (%)	MW (g/mol)
Bisphenol-E Cyanate Ester	AroCy L-10 Ciba Specialty Chemicals	[47073-92-7]	$C_{16}H_{12}O_2N_2$		316	14.7	41.9	264.28
Bisphenol-A Cyanate Ester	AroCy B-10 Ciba Specialty Chemicals	[1156-51-0]	$C_{17}H_{14}O_2N_2$		283	17.6	36.3	278.31
Polyhexamethylene Sebacamide	Nylon 6/10 Polysciences	[9008-66-6]	$C_{16}H_{30}O_2N_2$		878	35.7	0	282.43
Polyetheretherketone PEEK	450F Victrex USA	[29658-26-2]	$C_{19}H_{12}O_3$		155	12.4	46.5	288.3
PSA	General Electric	[NA]	$C_{18}H_{18}SiO_2$		119	15.7	60.1	294.42
Polyetherketone ketone PEKK	G040 (virgin flake), Dupont	[74970-25-5]	$C_{20}H_{12}O_3$		96	8.7	60.7	300.31
Tetramethylbisphenol-F Cyanate Ester	AroCy M-10, Ciba Specialty Chemical	[101657-77-6]	$C_{19}H_{18}O_2N_2$		280	17.4	35.4	306.36
Bisphenol-C Polycarbonate	BPCPC General Electric	[NA]	$C_{15}H_8O_3Cl_2$		29	3.0	50.1	307.13
Polybenzimidazole PBI	CELAZOLE PBI, Hoechst Celanese	[25928-81-8]	$C_{20}H_{12}N_4$		36	8.6	67.5	308.34

Material and Abbreviated Name	Trade Name, Manufacturer / Supplier	CAS Number	Repeat Unit Composition	Repeat Unit Structure	HR Capacity (J/g-K)	Total HR (kJ/g)	Char (%)	MW (g/mol)
Polyhexamethylene Dodecanediamide	Nylon 6/12 Polysciences, Inc.	[26098-55-5]	$C_{18}H_{34}N_2O_2$		707	30.8	0	310.48
Bisphenol-C Cyanate Ester	BPCCE Ciba Specialty Chemicals	[NA]	$C_{16}H_8O_2Cl_2$		24	4.2	53.3	331.16
Bisphenol-A Epoxy, Catalytic cure Phenoxy-A	DER-332 Dow Chemical	[001675-54-3]	$C_{21}H_{24}O_4$		657	26.0	3.9	340.42
Phenolphthalein Polycarbonate	Dow Chemical	[NA]	$C_{21}H_{12}O_5$		28	8	49.8	344.32
Polyamideimide PAI	TORLON 4203L, Amoco	[42955-03-3]	$C_{15}H_8O_3N_2$		33	7.1	53.6	354.36
Novolac Cyanate Ester	Primaset PT-30 Allied Signal XU-371 Ciba	[173452-35-2] [30944-92-4]	$C_{23}H_{15}O_3N_3$		122	9.9	51.9	381.39
Polyimide PI	Aldrich Chemical Company, Inc.	[26023-21-2]	$C_{22}H_{10}O_5N_2$		25	6.6	51.9	382.33
Hexafluorobisphenol-A Cyanate Ester	AroCy F-10, Ciba Specialty Chemicals	[32728-27-1]	$C_{17}H_8O_2N_2F_6$		32	2.3	55.2	386.25

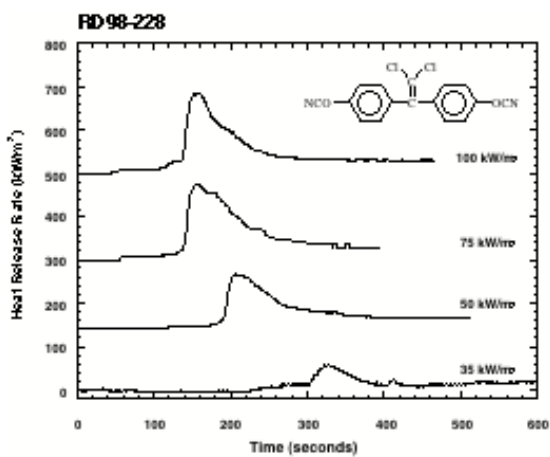
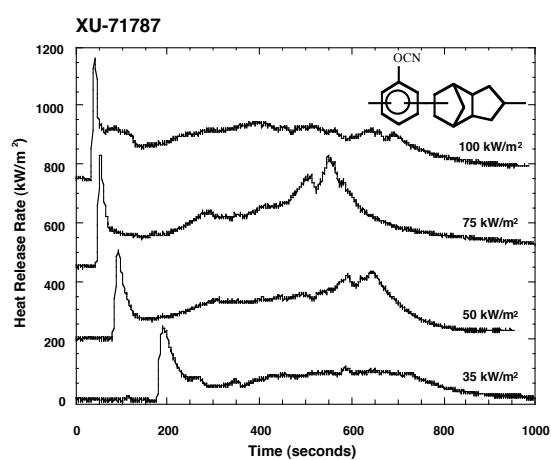
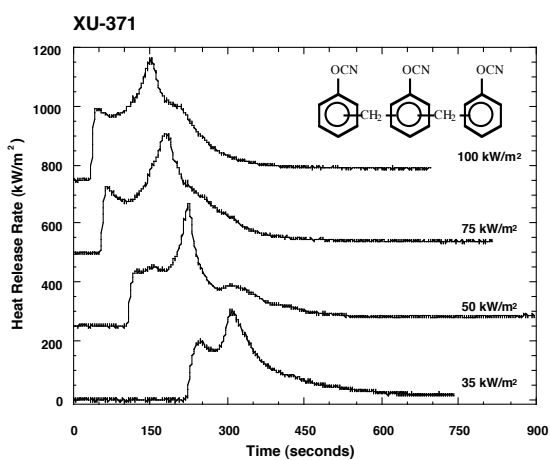
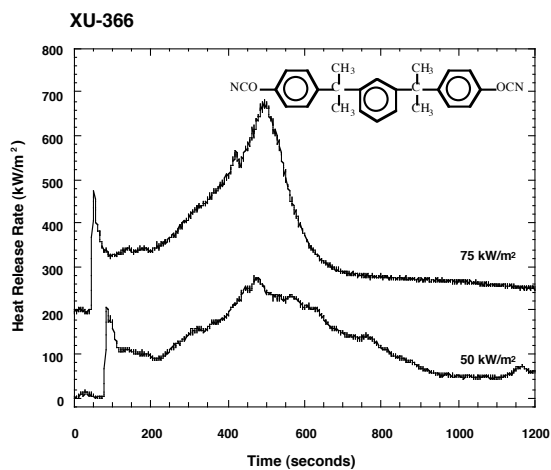
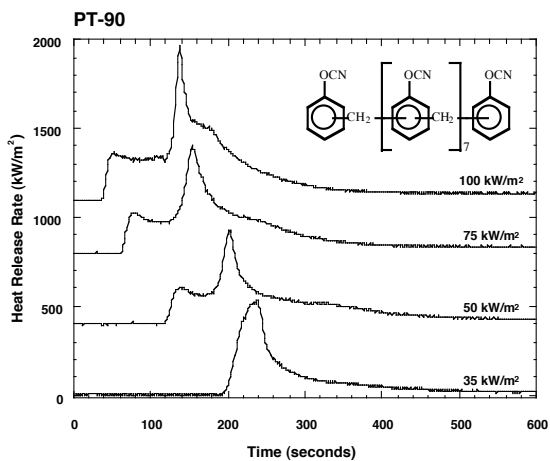
Material and Abbreviated Name	Trade Name, Manufacturer / Supplier	CAS Number	Repeat Unit Composition	Repeat Unit Structure	HR Capacity (J/g-K)	Total HR (kJ/g)	Char (%)	MW (g/mol)
Bisphenol-C Epoxy	BPCE	[NA]	$C_{20}H_{18}O_4Cl_2$		506	10	36	393.26
Bisphenol-M Cyanate Ester	AroCy XU-366, Ciba Specialty Chemicals	[127667-44-1]	$C_{26}H_{24}O_2N_2$		239	22.5	26.4	396.49
Polyphenylsulphone	Radel R5200 Amoco	[25839-81-0]	$C_{24}H_{16}SO_4$		153	11.3	38.4	400.45
Bisphenol-C Polyarylate	BPCPA UMass	[NA]	$C_{22}H_{12}O_4Cl_2$		21	7.6	42.7	411.02
Biphenol Phthalonitrile	Navy	[NA]	$C_{28}H_{14}N_4O_2$		15	3.5	78.8	438.44
Polysulfone of Bisphenol-A PSF	Udel Amoco	[25135-57-7]	$C_{27}H_{22}O_4S$		345	19.4	28.1	442.53
LaRC-1A	NASA Langley	[105030-42-0]	$C_{28}H_{14}N_2O_6$		38	6.7	57	474.43
Epoxy Novolac, Catalytic Cure Phenoxy-N	DEN-438, Dow Chemical	[028064-14-4]	$C_{10}H_{11}O$		246	18.9	15.9	474.55
Bisphenol-A Phthalonitrile	Navy	[NA]	$C_{31}H_{20}N_4O_2$		40	5.9	73.6	480.52
Technora	UMASS	[NA]	$C_{34}H_{24}N_4O_5$		131	15.3	41.8	568.59

Material and Abbreviated Name	Trade Name, Manufacturer / Supplier	CAS Number	Repeat Unit Composition	Repeat Unit Structure	HR Capacity (J/g-K)	Total HR (kJ/g)	Char (%)	MW (g/mol)
Bisphenol-A6F Phthalonitrile	Navy	[NA]	$C_{31}H_{14}N_4O_2F_6$		9	2.8	63.8	588.46
Polyetherimide PEI	Ultem 1000, General Electric	[61128-46-9]	$C_{37}H_{24}O_6N_2$		121	11.8	49.2	592.61
Polyester of Hydroxybenzoic and Hydroxynaphthoic Acids	Vectra C LCP (virgin/unfilled) Hoechst Celanese	[70679-92-4]	$C_{39}H_{22}O_{10}$		164	11.1	40.6	650.6
TOR	NASA Langley	[191985-77-0]	$C_{44}H_{29}N_4O_3P$		135	11.7	63	692.71
LaRC-CP2	NASA Langley	[79062-55-8]	$C_{37}H_{18}N_2O_6F_6$		14	3.4	57	700.55
LaRC-CP1	NASA Langley	[87186-94-5]	$C_{46}H_{22}N_2O_6F_{12}$		13	2.9	52	926.66

APPENDIX C

HEAT RELEASE HISTORIES FOR CYANATE ESTERS AT INDICATED HEAT  
FLUXES





APPENDIX D

CONTRIBUTION TO SCIENCE AND UNDERSTANDING IN THE PROPOSED  
AREA USING EACH PAPER

**Manuscript 1 (MS 1):** R.N. Walters, R.E. Lyon and S.M. Hackett, "Heats of Combustion of High Temperature Polymers," *Fire and Materials*, 24, pp. 245-252, 2000.

In MS 1, the constant used for the calculation of heat release rates based upon oxygen consumption measurements [1-3] was re-evaluated using commodity, engineering, and high performance plastics. In addition, the heat of combustion for these materials was calculated using the molar group additivity of the heats of formation of the combustion products and reactants [4]. The polymers examined were thermally stable, char forming thermoplastics and thermoset resins containing a significant degree of aromaticity and hetero-atoms including nitrogen, sulfur, phosphorus, silicon, and oxygen in linear and heterocyclic structures. The gross heats of combustion for these polymers of known chemical structure were determined using an oxygen bomb calorimeter according to standard methods [5]. The net heats of combustion, which account for the heat of vaporization of water that is formed, were determined mathematically from the hydrogen in the sample [6]. In MS 1, data for forty nine samples were evaluated in the oxygen bomb calorimeter where the gross and net heats of combustion were obtained and presented. The experimental results were compared to thermochemical calculations of the net heat of combustion from oxygen consumption and the gross heat of combustion from group additivity tables of the heats of formation, where available. The results from MS 1 show gross and net heats of combustion calculated from polymer enthalpies of formation and oxygen consumption thermochemistry were within 5 % of the experimental values from oxygen bomb calorimetry. The heat released by combustion per gram of diatomic oxygen consumed in the present study was  $E = 13.10 \pm 0.78$  kJ/g-O<sub>2</sub> for polymers tested. This value is indistinguishable from the universal value  $E = 13.1$  kJ/g-O<sub>2</sub> used in oxygen consumption (combustion) calorimetry [2,3].

**Manuscript 2 (MS 2):** R.E. Lyon, L.M. Castelli and R.N. Walters, "A Fire-Resistant Epoxy," DOT/FAA/AR-01/53, FAA Technical Report August 2001.

The flammability, thermomechanical properties, and fire response of the diglycidylether of 1,1-dichloro-2,2-bis(4-hydroxyphenyl)ethylene (DGEBC) cured with several hardeners were examined and compared to diglycidylether of bisphenol-A (DGEBA) systems. The DGEBC and DGEBA were cured with triethylenetetramine,

methylenedianiline, the parent phenol (BPC or BPA), catalytic amounts of 2-ethyl-4-methylimidazole (EMI-24), and the dicyanate of bisphenol-C as recommended by the literature [7,8]. The heat of reaction for each of the epoxy systems was measured using differential scanning calorimetry. The extent of the reaction, to ensure samples were completely reacted, was determined using infrared spectroscopy by monitoring the CH overtone band at  $4535\text{ cm}^{-1}$  [7,8]. Cured samples were measured for thermal stability, strength, modulus, flame resistance limiting oxygen index (LOI) [9], UL-94 [10], flaming heat release rate [11,12], and heat release capacity [13]. The mechanical properties [14] of the DGEBC and DGEBA systems were equivalent but the DGEBC systems exhibited superior flame resistance and 50% lower heat release rate and heat release capacity than the corresponding DGEBA system. Thermogravimetric analysis showed a 20 to 30 % higher char yield for the DGEBC systems due to the decomposition mechanism liberating HCl and forming a thermally stable aromatic char structure [15]. The DGEBC cured with methylenedianiline had an LOI of 30-31, exhibited UL 94 V-0/5V behavior and easily passed the Federal Aviation Administration heat release requirement Federal Aviation Regulation 25.853 (a-1) [10] as a single-ply glass fabric lamina.

**Manuscript 3 (MS 3):** R.E. Lyon and **R.N. Walters**, “A Microscale Combustion Calorimeter,” FAA Technical Report, DOT/FAA/AR-01/117, 2002.

A development of the second generation microscale combustion calorimeter equipment and method for measuring the heat release rate of milligram-sized samples is described in this manuscript. Other small scale laboratory tests and methods developed by others are reviewed and discussed [17-22]. The method of pyrolysis-combustion flow calorimetry (PCFC) separately reproduces the solid-state and gas phase processes of flaming combustion in a non-flaming test. The principle of operation, based on oxygen consumption calorimetry [1-3,23], is derived and related to mass loss rates and heats of combustion. In practice, rapid controlled pyrolysis of a sample in an inert gas stream followed by high-temperature oxidation (combustion) of the pyrolyzate in excess oxygen is performed to simulate conditions in a fire. The rate at which the sample releases fuel, and hence its heat of combustion, is calculated from the oxygen consumption history. Integrating the heat release rate over the duration of the test yields a heat of combustion for the volatiles. A char yield is obtained by weighing the sample

before and after the test. The peak heat release rate is normalized for the test conditions by dividing by the heating rate during the test which yields a material property for flammability called the heat release capacity [24]. This heat release capacity has been found to correlate with average heat release rates in flaming combustion tests.

The manuscript details measurements made on the components to optimize the method parameters. Tests on the pyrolyzer included the optimization of the sample size coupled with the heating rate and interface temperature. These tests ensured the fuel pulse was repeatable and the mass transfer was efficient. The combustion furnace was designed to provide a high residence time to ensure the complete oxidation of the gaseous decomposition products [25]. The temperature of this furnace was mapped and tested with methane and acetylene, a soot forming gas, to ensure complete combustion at the temperatures being used [26].

Since the microscale combustion calorimeter was a new test the data had to be validated by another test method. A thermogravimetric analyzer coupled with a gas chromatogram – mass spectrometer was used for the validation [27]. In these tests, samples were degraded and the decomposition products identified and quantified. The heats of combustion of the components were summed and multiplied by the instantaneous mass loss rate to effect a heat release rate. The heat release rate was normalized for sample weight and heating rate and compared to the results from the microscale combustion calorimeter. The two test methods were found to be within 9 % for a set of 14 polymers.

This study showed that pyrolysis-combustion flow calorimetry (PCFC) is a reproducible, calibrated technique for measuring dynamic and static combustion parameters of materials, that provides a convenient methodology for estimating the fire hazard potential of a material using only milligram samples.

**Manuscript 4 (MS 4):** M. Ramirez, **R.N. Walters**, E.P. Savitski, and R.E. Lyon, “Thermal Decomposition of Cyanate Ester Resins,” *Polymer Degradation and Stability*, 78, pp. 73-82, 2002.

In this manuscript, the thermal stability and decomposition mechanism of a family of thermoset cyanate ester resins was examined. Polycyanurate networks were prepared by thermal polymerization of cyanate ester monomers containing two or more cyanate ester ( $-O-C\equiv N$ ) functional groups [28]. The thermal decomposition chemistry of nine different polycyanurates was studied by thermogravimetry and infrared analysis. Analysis of the gases evolved during pyrolysis using infrared spectroscopy and gas chromatography-mass spectrometry was also performed. It was found that the thermal stability of the polycyanurates was essentially independent of monomer chemical structure with the major mass loss occurring at about 450°C for all materials, which agrees with the literature [28-31]. Analysis of the solid-state and gas phase thermal degradation chemistry indicates a thermal decomposition mechanism for polycyanurates, which begins with hydrocarbon chain scission and crosslinking at temperatures between 400-450°C with negligible mass loss, followed by decyclization of the triazine ring at 450°C which liberates volatile cyanate-ester decomposition products [32-34]. Further decomposition of residue above 500°C proceeds with the elimination of alkenes and hydrogen leaving a carbonaceous char. The solid residue after pyrolysis increases with the aromatic content of the polymer and incorporates about two thirds of the nitrogen and oxygen present in the original material.

**Manuscript 5 (MS 5): R.N. Walters**, “Molar Group Contributions to the Heat of Combustion,” *Fire and Materials*, 26, pp. 131-145, 2002.

Experimental results for the gross heat of combustion of over 140 commercial and developmental polymers and small molecules of known chemical structure [6,35-37] were used to derive additive molar group contributions to the heat of combustion. The materials examined contained carbon, hydrogen, oxygen, nitrogen, phosphorous, sulfur, chlorine, fluorine, and silicon in linear, branched and cyclic structures. Additive molar contributions to the gross heat of complete combustion for 37 structural groups have been determined from data for 66 polymers [35,36] and 78 small molecules [6,37]. In practice, the molar groups that comprise the molecular structure of a material have contribution values that are summed and divided by the molecular weight of the molecule or polymer repeat unit to yield the gross heat of combustion as determined by oxygen bomb calorimetry [5]. The present group contribution method improves upon previous molar group [38], atomic bond [39-41] and heat of formation [4,42]

calculation techniques. This new method provides an accurate single step method for calculating the heat of combustion of chemical compounds. The average relative error of the calculated gross heats of combustion is 2.8 percent. In addition, this manuscript provides a large database of molecular structures and heat of combustion values.

**Manuscript 6 (MS 6): R.N. Walters** and R.E. Lyon, “Molar Group Contributions to Polymer Flammability,” *Journal of Applied Polymer Science*, 87, pp. 548-563, 2003.

In MS 6, a database of molecular structures and heat release values obtained in the microscale combustion calorimeter (MCC) [43,44] was compiled and examined. Specific heat release rate is the molecular-level fire response of a burning polymer. The MCC obtains the specific heat release rate of milligram samples by analyzing the oxygen consumed by complete combustion of the pyrolysis gases during a linear heating program. Dividing the specific heat release rate (W/g) by the rate of temperature rise (K/s) gives a material fire parameter with the units (J/g-K) and significance of a heat (release) capacity [45].

The heat release rate in forced flaming combustion is the primary indicator of a fire hazard [37,46]. The heat release capacity was found to be proportional to this value as measured in a cone calorimeter [47]. The heat release capacity was also found to correlate with flammability tests such as UL 94 [10] and limiting oxygen index (LOI) [9]. The UL 94 test does not provide a quantitative measure of flammability, but a rating of the propensity to burn. Values of the heat release capacity indicate whether a material will produce enough energy to sustain and propagate burning or self-extinguish in the UL 94 test [48]. The LOI increases the energy feedback and temperature with an increase in oxygen concentration. There is an inverse relationship between literature values for the oxygen index [49] and measured heat release capacities because materials with a high heat release capacity do not require elevated oxygen (more energy) to sustain burning.

The heat release capacity appears to be a true material property that is rooted in the chemical structure of the polymer and is calculable from additive molar group contributions. The structure of the polymer repeat unit was analyzed and broken into structural groups that comprise the molecule. Those structural groups were then

assigned a value for heat release through empirical methods. Hundreds of polymers of known chemical composition have been tested to date, providing over 40 different molar group contributions to the heat release capacity. Measured and calculated heat release capacities for over 80 polymers agree to within  $\pm 15\%$ , suggesting a new capability for predicting flammability from polymer chemical structure. The proposed methodology for predicting the fire behavior and flammability of polymers from their chemical structure allows for the molecular-level design of ultra-fire-resistant polymers without the expense of synthesizing and testing new materials.

**Manuscript 7 (MS 7): R.N. Walters** and R. E. Lyon, "Fire Resistant Cyanate Ester-Epoxy Blends," *Fire and Materials*, 27, pp. 183-194, 2003.

The cure chemistry, thermal stability, and fire behavior in a series of fire-resistant cyanate ester-epoxy blends were examined in this manuscript. The di-cyanate and di-epoxide of 1,1-dichloro-2,2-bis(4-hydroxyphenyl)ethylene (bisphenol-C, BPC) were combined in various molar ratios and the reaction chemistry was monitored using Fourier Transform Infrared Spectroscopy (FT-IR) and differential scanning calorimetry (DSC). The DSC was used to determine melting temperature, heat of reaction and temperatures needed to completely react the blended resins. One peak was obtained for each of the neat resins and two peaks were obtained for each of the blends. Two large exotherms were observed for the BPC blends in the DSC, and infrared spectroscopy was used to assign reactions to the measured heat flow. It was found that the cyanate ester reacts first to form the six-membered triazine ring. This reaction proceeds at a much lower temperature than the neat cyanate ester. This is due to  $-OH$  groups formed by the ring opening of the epoxy which catalyzes the cyanate reaction [50,51]. Once the triazine is generated, it reacts with the epoxy to form the five-membered oxazoline [28,52,53]. The maximum rate of epoxy consumption was observed after almost all of the cyanate ester had been consumed.

Fire behavior of the BPC cyanate-epoxy blends was studied in flaming and non-flaming combustion using pyrolysis-combustion flow calorimetry (PCFC) and fire calorimetry (OSU). The PCFC showed a dramatic reduction in the peak heat release rate of the BPC epoxy with the addition of as little as 20% BPC cyanate ester. Further reductions in the peak and total heat release rates were observed as the BPC cyanate ester

concentration was increased. Similar trends were observed in the OSU with a factor of 2 reduction in the measured peak and total heat release rates as the BPC cyanate ester concentration increased. Low fuel content, high char yields, and halogen inclusion in the polymer structure all contribute to the low heat release rate of these materials.

**Manuscript 8 (MS 8):** R. Lyon and R. Walters, “Pyrolysis Combustion Flow Calorimetry,” *Journal of Applied Pyrolysis*, 71, pp. 27-46, 2004.

In MS 8, a method for evaluating the combustibility of samples using milligram quantities is described. Previous methods have been developed (1-10) [18-22,25,54-57], but have failed to provide an accurate indication of material flammability. The evolution of the theory and operation of a small-scale flammability test that recreates the events that occur in a fire has been developed [58]. Pyrolysis-combustion flow calorimetry (PCFC) separately reproduces the solid state and gas phase processes of flaming combustion in a non-flaming test by controlled pyrolysis of the sample in an inert gas stream, followed by high temperature oxidation of the volatile pyrolysis products. Oxygen consumption calorimetry [3,23] is used to measure the heat of combustion of the pyrolysis products. The maximum amount of heat released per unit mass per degree of temperature ( $J/g-K$ ) is a material property that appears to be a good predictor of flammability.

The construction of the instrument, characterization of the components, and development of the test method are described. Since the maximum heat release rate is divided by the heating rate during the experiment, the pyrolyzer has to be able to heat the sample at a constant rate throughout its decomposition. The volatile decomposition products must stay gaseous while being transferred to the high temperature combustion furnace where oxygen is added to the gas stream. The combustor was designed to provide a long residence time to oxidize all gaseous decomposition products and any soot that may have formed [25]. A data acquisition system was used to control the gas flow rates and monitor the oxygen concentration and temperatures. Software was written to display all of the measured signals and perform the heat release rate calculations.

A database of polymer heat release rates was generated. Polymer heat release capacities span two orders of magnitude and suggests that it is a reliable indicator of fire hazard.

**Manuscript 9 (MS 9):** R.E. Lyon, **R.N. Walters**, and S. Gandhi, “Combustibility of Cyanate Ester Resins,” *Fire and Materials*, 30, pp. 89-106, 2006.

Flaming and non-flaming combustion studies were conducted on a series of polycyanurates to examine the effect of chemical composition and physical properties on the fire behavior of these polymers. Polycyanurates are thermoset polymers that are crosslinked through the cyclotrimerization reaction of three cyanate ester ( $-\text{O}-\text{C}\equiv\text{N}$ ) groups to form oxygen-linked triazine rings (cyanurates) [28]. Polymerization (curing) occurs via a thermally-activated addition reaction which produces no volatiles so that void-free castings and fiber reinforced composites with good surface finish can be obtained.

Heats of complete combustion of the polymer and fuel gases were determined by oxygen bomb calorimetry [5] and pyrolysis-combustion flow calorimetry [59]. Fire calorimetry experiments were conducted to measure the heat released, the rate of heat release, and the smoke generation in flaming combustion. The effects of chemical composition were evidenced in the ignitability and burning behavior in the flame. Aromatic polycyanurates thermally decompose by a common mechanism which begins with thermolytic cleavage of the resin backbone between 300–450°C and culminates with decyclization of the cyanurate rings at  $450 \pm 8^\circ\text{C}$  to produce a variety of volatile fuel species and significant char [60].

Fire response parameters derived from the data include the thermal inertia, heat of gasification, effective heat of combustion, and combustion efficiency [61]. Halogen-containing polycyanurates exhibited extremely low heat release rate in flaming combustion compared to the hydrocarbon resins yet produced significantly less smoke and comparable levels of carbon monoxide and soot [61].

**Manuscript 10 (MS 10):** R.E. Lyon, **R.N. Walters**, and S.I. Stoliarov, "A Thermal Analysis Method for Measuring Polymer Flammability", *Journal of ASTM International*, 3, 4, pp. 1-17, 2006.

A thermal analysis method is presented in which controlled heating of polymer samples and complete combustion of the evolved gases are used to separately reproduce the condensed and gas phase processes of flaming combustion in a single laboratory test [43,59,62,63]. The condensed phase model describes how materials thermally decompose to produce fuel gases and carbonaceous char. Mass loss rates, as determined by thermogravimetric analysis (TGA) [64], are used to derive kinetic parameters [65] that can be used to model thermal decomposition. The heat release capacity [66] is derived using these kinetic parameters along with the heat of complete combustion for materials that decompose in a single step. The gas phase model assumes complete combustion of the gaseous fuel and is uniquely related to its composition. Oxygen consumption calorimetry [1-3,23], applied to the combustion gas stream, gives the heat release rate history of the sample as a function of its temperature. The maximum rate of heat release, and the temperature at which it occurs, are polymer characteristics related to fire performance and flame resistance [67]. Experiments were performed using TGA, several variations of pyrolysis-combustion flow calorimetry (PCFC) [68,69], oxygen bomb calorimetry [36,70], and thermal oxidation of fuel gases. TGA results at several heating rates were compared to values calculated using the mass loss kinetics, and were in good agreement. Gas phase combustion experiments were performed to determine the time and temperatures required to completely oxidize all fuel gases without the use of catalysts [26,56]. The heats of combustion of methane and several non-charring polymers were compared to the total heat released as measured by PCFC, and were found to be within 1% of each other. PCFC heat release capacity results were compared to values calculated from TGA experiments were also in good agreement. Oxidative pyrolysis experiments in the PCFC were performed on charring polymers so any carbonaceous char residue could also be oxidized to provide a complete combustion value comparable to oxygen bomb data.

**Manuscript 11 (MS 11):** R.E. Lyon, **R.N. Walters** and S.I. Stoliarov, "Screening Flame Retardants for Plastics Using Microscale Combustion Calorimetry," *Polymer Engineering and Science*, 47, 10, pp. 1501-1510, 2007.

Microscale combustion calorimetry (MCC) [71] was evaluated as a screening test for efficacy of flame-retardant additives in polymers. The MCC method separately reproduces the gas and condensed phase processes of flaming combustion in a non-flaming laboratory test and forces them to completion to obtain intrinsic/material combustion properties. The non-flaming MCC data was compared to flaming combustion tests [9,10,12]. Steady burning in the cone calorimeter [12] was measured and described with a simple one-dimensional model [72] where the external heat flux was much greater than the minimum heat flux for sustained ignition. This value is thought to be the best indicator of fire hazard [46]. A good correlation was found between the two data sets at the peak heat release rate in the cone calorimeter when the flaming combustion is at its highest efficiency. Unsteady burning was characterized in the UL94 [10] and limiting oxygen index (LOI) [9] tests. These tests measure ignition resistance to a small flame and time to extinction after the ignition source is removed [73]. Threshold values of heat release capacity from the MCC were found to correlate with the UL94 ratings for natural plastics. Samples containing bromine and phosphorous did not follow the same trend due to gas phase inhibition in the flame and forced complete combustion in the MCC [74]. Trends between the heat release capacity and oxygen index values were also found. Materials with a high LOI tend to have a low heat release capacity. This is due to the low heat release capacity materials needing higher heat fluxes to sustain ignition which is achieved at elevated oxygen concentrations [75].

At flame extinction, MCC combustion properties are comparable in magnitude and effect to the extrinsic factors (sample size and orientation), physical behavior (dripping, swelling), and chemical processes (flame inhibition, charring) associated with flame retardancy. Consequently, MCC properties by themselves cannot correlate flame resistance of plastics over a broad range of flame-retardant chemical composition. However, the thermal combustion property, heat release capacity, is probably the best single indicator of the fire hazard of a material.

**Manuscript 12 (MS 12):** S.I. Stoliarov, **R.N. Walters** and R.E. Lyon, "A Method for Constant-Rate Heating of Milligram Sized Samples," *Journal of Thermal Analysis and Calorimetry*, 89, 2, pp. 367-371, 2007.

MS 12 details the derivation of an algorithm to control the heating rate of a small heater. Heating a small (1-10 mg) sample of material at a constant heating rate (typically, 0.1-1.0 °C/s) is a technique that is used widely in thermal analysis and pyrolysis experiments [76,77]. The constant-rate heating is usually achieved by employing a furnace equipped with a resistive heating element. The temperature of the element is monitored by a thermocouple and controlled by a proportional integral derivative (PID) controller [76,78]. The controller manipulates electric power supplied to the element in order to keep its temperature as close as possible to the programmed temperature, which is a linear function of time. A separate thermocouple is used to monitor the temperature of a sample, which is usually placed in the middle of the furnace.

Here we present a new method for constant-rate heating that is based on a semi-empirical mathematical expression relating sample temperature, heating rate, and electric power supplied to the furnace. In this method, a single thermocouple is used to monitor the temperature of a sample and control its heating rate. According to the comparative analysis, the linearity of the sample temperature versus time curves obtained using this method in combination with a simple furnace setup is the same as the linearity of the curves generated by modern commercial thermogravimetric analyzers. The algorithm described in this manuscript is employed in the microscale combustion calorimeter for pyrolyzing small samples at a controlled, constant heating rate [63,79].

**Manuscript 13 (MS 13):** R.E. Lyon, **R.N. Walters** and S.I. Stoliarov, "Thermal Analysis of Flammability," *Journal of Thermal Analysis and Calorimetry*, 89, 2, pp. 441-448, 2007.

A thermal analysis method for laboratory determination of flammability parameters of materials is presented in this manuscript. The method separately reproduces the condensed phase (pyrolysis) and gas phase (oxidation) processes of flaming combustion in a single, non-flaming combustion test. Decoupling the pyrolysis and combustion processes in this way, and forcing them to completion, isolates the thermochemistry of the condensed phase and provides the maximum potential (capacity) of the material to release heat in fires.

The condensed phase model describes the fuel generation rate with single-step, first-order decomposition kinetics [80] measured using thermogravimetry. The gas phase model is derived from the stoichiometry of the complete combustion reaction of fuels with known composition [6] and is measured using oxygen consumption calorimetry [3]. Combustion kinetics were determined for fuel gases [56] using pyrolysis-combustion flow calorimetry (PCFC) [63] to ensure complete combustion was attained. Data from PCFC was compared to flammability measurements of ignitability, fire response, and flame resistance. It was found that PCFC is not a good predictor of ignitability due to ignition temperatures being much higher than maximum fuel generation rate temperatures [72]. Fire response was found to correlate better with PCFC because it is a measure of heat release rate which is a good indicator of fire hazard [46]. Good correlations between the peak heat release rates in fire calorimeters [12,81] and the heat release capacity from PCFC were demonstrated. Flame resistance of materials is characterized in tests such as UL94 [10] and limiting oxygen index (LOI) [9]. UL94 measures the propensity of a material to resist upward flame spread [82]. PCFC showed that materials with a low heat release capacity tend to self-extinguish (V0 rating), materials with high heat release capacities burn readily (HB or no rating), and heat release capacities in between exhibit mixed behavior (V1 and V2 ratings) in the UL94 test. The LOI is a measure of downward flame spread where the oxygen concentration is adjusted until flame extinction occurs. The intensity of the flame and its thermal feed-back into the sample is related to the oxygen concentration [75]. Materials with a low heat release capacity need a more intense flame to propagate the reaction, materials with a high heat release capacity burn more readily and do not.

In this manuscript it was shown that a simple burning model with a critical heat release rate for extinction provides a physical basis for the observed correlation between flammability tests and the results of PCFC. Physical and chemical phenomena such as melting, dripping, heat distortion, swelling, charring, intumescence and incomplete combustion are not captured by milligram samples in the PCFC test, but can have a real effect on flame and fire test results.

**Manuscript 14 (MS 14):** S.I. Stoliarov and **R.N. Walters**, “Determination of Heats of Gasification of Polymers Using Differential Scanning Calorimetry,” *Polymer Degradation and Stability Journal* 93, pp. 422-427, 2008.

In this manuscript, the heats of gasification of a set of ten common plastics and engineering polymers was determined using differential scanning calorimetry (DSC). The heat of gasification is thermodynamic quantity equal to the amount of energy required to gasify unit mass of material and is one of the key properties that define its ignition resistance and fire response. Knowledge of this property is necessary to assess a material’s fire hazard in a particular fire scenario. Nevertheless, even for the most common polymers, the values of this property are not well established. In this work, the heat of gasification has been defined as a function of the initial and final temperatures of the gasification process. A method for determining parameters of this function using power-compensation differential scanning calorimetry has been developed and applied to a set of non-charring and charring polymers. The heat capacity, heat of melting, degree of crystallinity, and heat of decomposition were all determined using DSC. The results of the measurements have been verified against literature data [83-86]. These parameters were used to obtain integral values of the heats of gasification for heating materials from room temperature through their decomposition. For most of the studied polymers, the contributions to the integral heats from heat capacity and melting were found to be approximately equal to the contributions from decomposition and vaporization.

**Manuscript 15 (MS 15):** **Richard N. Walters** and Richard E. Lyon, “Flammability of Polymer Composites,” FAA Report DOT/FAA/AR-08/18 May 2008.

The flammability and mechanical properties of fiber-reinforced thermoset resin structural composites were evaluated. The processing characteristics, thermal stability, and flammability of the neat resins were measured using rheology, thermogravimetry (TGA), and pyrolysis-combustion flow calorimetry (PCFC), respectively. Structural laminates were fabricated from liquid resins and woven glass fabric by vacuum-assisted resin transfer molding. Single-layer specimens (lamina) were prepared for fire testing using a hand lay-up technique. The mechanical properties of the laminates were measured in a three-point bending test [87]. Fire behavior of the lamina and laminates

was measured according to Title 14 Code of Federal Regulations 25.853(a-1) [16] and cone calorimeter [12] testing as described in Military Standard MIL-STD-2031 [88]. The results for flammability, fire performance, and mechanical properties of these composites are compared and presented in this report.

Several thermosetting epoxy and cyanate ester (CE) resin systems containing bisphenol-A (4,4 dihydroxy-2,2-diphenyl propane, BPA) [8] and bisphenol-C (1,1-dichloro-2,2-bis(4-hydroxyphenyl)ethane, BPC) [89] were examined. The rheology showed the experimental liquid BPC resins had viscosities within the reported range for BPA epoxies [90]. The thermal stability and flammability of the neat resins was evaluated using TGA and PCFC where the experimental BPC resins were found to be more thermally stable, have higher char yields and lower heat release than the BPA analogues. Flexural strengths of the BPC composites were comparable to the BPA composites. Fire calorimetry results showed the BPC epoxy and cyanate esters had reduced flammability when tested in single ply laminates and multiple layered structural composite configurations.

It has been demonstrated that high flexural strengths, similar to those of epoxies, can be achieved with the bisphenol-C cyanate ester (BPCCE) when prepared using vacuum-assisted resin transfer molding. This study showed the BPCCE glass fiber-reinforced laminates had comparable mechanical properties to epoxy resin laminates in contrast to previous results. The BPCCE resin satisfies the fire performance requirements for both large surface area decorative panels in commercial aircraft and structural polymer composites for United States Navy ships and submarines as an unmodified resin containing no fillers or additives to reduce flammability, improve mechanical properties, or enhance processing characteristics.

**Manuscript 16 (MS 16):** S.I. Stoliarov, S. Crowley, **R.N. Walters** and R.E. Lyon, "Prediction of the Burning Rate of Charring Polymers, Combustion and Flame," 157, 11, pp. 2024-2034, 2010.

A quantitative understanding of the processes that take place in the condensed phase of a burning material is critical for prediction of ignition and growth of fires. In this manuscript, a model of burning for two widely-used charring and intumescent

polymers, bisphenol A polycarbonate and poly(vinyl chloride), was developed and validated. The modelling was performed using a framework called ThermaKin [91,92]. ThermaKin is a flexible computational framework that solves energy and mass conservation equations describing a one-dimensional material object subjected to external heat. Most of the model parameters were obtained from direct property measurements using thermogravimetric analysis (TGA), microscale combustion calorimetry, and cone calorimetry. The TGA mass loss rates were modeled for several heating rates. Under ideal conditions (uniform heating of the sample) the model worked well, but at high heating rates the model had to be adjusted to account for temperature gradients within the sample. The one-dimensional numerical pyrolysis model was validated against the results of cone calorimetry experiments performed under a broad range of conditions (external heat flux and sample thickness). Potential sources of uncertainties [93] in the model parameterization were analyzed. The uncertainties had a limited effect on most of the parameters generated in the model. The largest discrepancies came from the sample intumescing and the flaming combustion switching to smoldering at the end of the test. The agreement between the model predictions and experiments performed in this study is worse than that achieved for non-charring polymers [94]. One possible reason for the discrepancies is a low accuracy of decomposition thermochemistry (especially that of PVC). It is also possible that the discrepancies arise from the inability of a one-dimensional model to capture three-dimensional processes. Both flame and char structures observed in the cone calorimetry experiments are clearly non-one-dimensional. Availability of a three-dimensional pyrolysis model may help achieve a better agreement. However, significant char shape and heat release profile fluctuations detected in the experiments suggest that the predictive power of the current model is already approaching the limit dictated by chaotic elements of the processes under study.

## References

1. W. Thornton, "The Role of Oxygen to the Heat of Combustion of Organic Compounds," *Philosophical Magazine and J. of Science*, 33, 196, 1917.
2. C. Hugget, "Estimation of Rate of Heat Release by Means of Oxygen Consumption Measurements," *Fire and Materials*, 4, 2, 1980.

3. M. Janssens and W.J. Parker, "Oxygen Consumption Calorimetry," in Heat Release in Fires, V. Babrauskas, S.J. Grayson, eds., Chapter 3, pp. 31-59, Elsevier Applied Science, London, 1992.
4. D.W. Van Krevlen, "Thermochemical Properties: Calculation of the Free Enthalpy of Reaction from Group Contributions," in Properties of Polymers, 3rd Ed., Chapter 20, pp. 629-639, Elsevier, Amsterdam, 1990.
5. "D2382-88: Standard Test Method for Heat of Combustion of Hydrocarbon Fuels by Bomb Calorimeter (High Precision Method)," ASTM Fire Test Standards, 3rd Edition, pp. 230-238, American Society for Testing of Materials, Philadelphia, PA, 1990.
6. V. Babrauskas, "Heat of Combustion and Potential Heat," in Heat Release in Fires, V. Babrauskas, S.J. Grayson, eds., Chapter 8, pp. 207-223, Elsevier Applied Science, London, 1992.
7. H. Lee and K. Neville, Handbook of Epoxy Resins, McGraw-Hill, Inc., 1967.
8. C.A. May and Tanaka, Y. ed., Epoxy Resins: Chemistry and Technology, Marcel Dekker, Inc, New York, 1973.
9. Standard Test Method for Measuring the Minimum Oxygen Concentration to Support Candle-Like Combustion of Plastics (Oxygen Index), D 2863, American Society for Testing and Materials, West Conshohocken, PA, 2006.
10. Standard for Tests for Flammability of Plastic Materials for Parts in Devices and Appliances, Underwriters Laboratory: UL 94, 4th edition, Underwriters Laboratories, Inc., Research Triangle Park, NC, 1991.
11. V. Babrauskas, "Heat Release Rate: The Single Most Important Variable in Fire Hazard," Fire Safety Journal, 18, pp. 255-272, 1992.
12. Standard Test Method for Heat and Visible Smoke Release Rates for Materials and Products Using an Oxygen Consumption Calorimeter, ASTM E 1354, American Society for Testing and Materials, West Conshohocken, PA 2004.
13. R. E. Lyon and R. N. Walters, "A Pyrolysis-Combustion Flow Calorimeter Study of Polymer Heat Release Rate," Ninth Annual BCC Conference on Flame Retardancy, Stamford, CT, June 1-3, 1998.
14. Standard Test Method for Compressive Properties of Rigid Cellular Plastics, (ASTM D1621-94), American Society for Testing of Materials, Philadelphia, PA, 2000.
15. M. Ramirez, "Thermal Degradation Mechanism of Chloral-Based Polymers," Masters Thesis, University of Puerto Rico (Mayaguez), January 2000.

16. "Aircraft Material Fire Test Handbook, Section 5: Heat Release Rate Test for Cabin Materials," DOT/FAA/AR-00/12, April 2000.
  17. R.A. Susott, F. Shafizadeh, and T.W. Aanerud, "A Quantitative Thermal Analysis Technique for Combustible Gas Detection," *Journal of Fire and Flammability*, 10, pp. 94-104, 1979.
  18. R.A. Susott, "Thermal Behavior of Conifer Needle Extractives," *Forest Sciences*, 26, 3, pp.147-160, 1980.
  19. R.A. Susott, "Characterization of the Thermal Properties of Forest Fuels by Combustible Gas Analysis," *Forest Sciences*, 28, 2, pp. 404-420, 1982.
- W.J. Parker, "Prediction of the Heat Release Rate of Wood," Ph.D. Thesis, The George Washington University, April 1988.
20. W.J. Parker, "Determination of the Input Data for a Model of the Heat Release Rate of Wood," in *Mathematical Modelling of Fires*, ASTM STP 983, J.R. Mchaffey, ed., American Society for Testing and Materials, Philadelphia, PA, pp. 105-115, 1987.
  21. T.D. Gracik and G.L. Long, "Heat Release and Flammability of a Small Specimen Using Thermoanalytical Techniques," in *Fire Calorimetry*, proceedings from the 50th Calorimetry Conference, R.E. Lyon and M.M. Hirschler eds., Gaithersburg, MD, DOT/FAA/CT-95/46, p. 101, 1995.
  22. T.D. Gracik, G.L. Long, U.A.K. Sorathia, and H.E. Douglas, "A Novel Thermogravimetric Technique for Determining Flammability Characteristics of Polymeric Materials," *Thermochimica Acta*, pp. 212, pp. 209-217, 1992.
  23. M. L. Janssens, "Measuring Heat Release by Oxygen Consumption," *Fire Technology*, 27, pp. 234, 1991.
  24. R.E. Lyon, "Heat Release Capacity," presented at the Fire and Materials Conference, San Francisco, CA, January 22-24, 2001.
  25. V. Babrauskas, W.J. Parker, G. Mulholland, and H. Twilley, "The Phi Meter: A Simple, Fuel-Independent Instrument for Monitoring Combustion Equivalence Ratio," *The Review of Scientific Instruments*, 65, 7, pp. 2367-2375, 1994.
  26. W.M. Heffington, G.E. Parks, K.G.P. Sulzmann, and S.S. Penner, "Studies of Methane Oxidation Kinetics," *Proceedings of the Sixteenth Symposium (International) on Combustion*, the Combustion Institute, pp. 997-1010, 1976.
  27. T.V. Inguilizian, "Correlating Polymer Flammability Using Measured Pyrolysis Kinetics," Masters Thesis, University of Massachusetts (Amherst), January 1999.
  28. I. Hamerton, ed., *Chemistry and Technology of Cyanate Ester Resins*, Blackie Academic & Professional (Chapman & Hall), London, 1994.

29. V. V. Korshak, P.N. Gribkova, A.V. Dmitrienko and S.V. Vinogradova. *Vysokomol Soed.*, A16, 14, 1974.
30. V.V. Korshak, V.A. Pandratov, A.G. Puchin, S.A. Pavlova, I.V. Zhuravleva, V.G. Danilov, and S.V. Vinogradova, *Polym.Sci. USSR*, 17,3, 554-559, 1975.
31. V.V. Korshak, S.A. Pavlova, P.N. Gribkova, M.V. Tsirghiladze, V.A. Pankratov, S.V. Vinogradova, P.D. Tsiskarishvili, and G.S. Papava, *Izv. Akad. Nauk. Grz. USSR, Ser. Khim.*, 3, 1, 7-15, 1977.
32. Shimp, D.A., Private Communication, August 26, 1996.
33. Shimp, D.A.; Christenson, J.R., and Ising, S. J., 34th International SAMPE Symposium, 34, pp. 222, 1989.
34. D. A. Shimp and S.J. Ising. 1992. American Chemical Society National meeting PMSE Division. San Francisco California. ACS Press. Washington, D.C., April 1992.
35. R.E. Lyon, S.M. Hackett, and R.N. Walters, "Heats of Combustion of High-Temperature Polymers," DOT/FAA/AR-TN97/8, 1998.
36. R.N. Walters, R.E. Lyon, and S.M. Hackett, "Heats of Combustion of High-Temperature Polymers," *Fire and Materials*, 24, 2000.
37. M.M. Hirschler, "Heat Release From Plastic Materials," in *Heat Release in Fires*, V. Babrauskas and S. Grayson, eds., Elsevier Applied Science, New York, pp. 207-232, 1992.
38. Wang Ke-qiang, Li Qin, "A New Method for Predicting the Heat of Combustion of Liquid Alkanes by Using the Group-Bond Contribution Method," *Journal of Ningxia University (Natural Science Edition)*, 21, 3, September 2000.
39. S.W. Bensen, "Methods for the Estimation of Thermochemical Data and Rate Parameters," *Thermochemical Kinetics*, John Wiley, New York, NY, 1968.
40. Jozef Bicerano, *Prediction of Polymer Properties*, 2nd Edition, Marcel Dekker, Inc., New York, NY, 1996.
41. F.Y. Hshieh, "Predicting Heats of Combustion and Lower Flammability Limits of Organosilicon Compounds," *Fire and Materials*, 23, 1999.
42. R.L. Cardozo, "Prediction of the Enthalpy of Combustion of Organic Compounds," *AIChE Journal*, 32, 5, pp. 844-848, May 1986.
43. U.S. Patent 5981290, "Microscale Combustion Calorimeter," R.E. Lyon and R.N. Walters, 11/09/1999.
44. R.N. Walters and R.E. Lyon, "A Microscale Combustion Calorimeter for Determining Flammability Parameters of Materials," *Proceedings 42nd International SAMPE Symposium and Exhibition*, 42,2, pp. 1335-1344, 1997.

45. R.E. Lyon, "Heat Release Capacity," Proceedings of the 7th International Conference on Fire and Materials, San Francisco, CA, pp. 285-300, 2001.
46. V. Babrauskas and R.D. Peacock, "Heat Release Rate: The Single Most Important Variable in Fire Hazard," Fire Safety Journal, 18, pp. 255-272, 1992.
47. M.J. Scudamore, P.J. Briggs, and F.H. Prager, "Cone Calorimetry—A Review of Tests Carried Out on Plastics for the Association of Plastic Manufacturers in Europe," Fire and Materials, 15, pp. 65-84, 1991.
48. "Plastics Digest, Ranked Properties Reference Index," Flammability, 17,1, pp. 773-889, D.A.T.A. Business Publishing, Englewood, CO, 1996.
49. C.J. Hilado, Flammability Handbook for Plastics, 5th edition, Technomic Publishing Co., Lancaster, Pennsylvania, 1998.
50. A. Osei-Owusu and G.C. Martin, "Analysis of the Curing Behavior of Cyanate Ester Systems," Polymer Engineering and Science, 31, 22, 1991.
51. A. Osei-Owusu and G.C. Martin, "Catalysis and Kinetics of Cyclotrimerization of Cyanate Ester Resin Systems," Polymer Engineering and Science, 32, 8, 1992.
52. Lonza product brochure, Cyanate Ester Resins—Primaset TM Resins
53. D.A. Schimp, F.A. Hudock, and S.J. Ising, International SAMPE Symposium, 33, pp. 754, 1988.
54. T.D. Gracik, G.L. Long, "Prediction of Thermoplastic Flammability by Thermogravimetry," Thermochimica Acta 212, pp. 163–170, 1992.
55. W.J. Parker, "Prediction of the heat release rate of wood," Ph.D. Thesis, The George Washington University, April 1988.
56. Reshetnikov, S. M. and Reshetnikov, I. S., "Oxidation Kinetic of Volatile Polymer Degradation Products," Polymer Degradation and Stability, 64, pp. 379–385, 1999.
57. S.M. Reshetnikov, G.A. Prevozchikov, USSR 285663, 01/02/1998.
58. R.N. Walters, R.E. Lyon, "A microscale combustion calorimeter for determining flammability parameters of materials," presented at NIST Annual Conference on Fire Research, Gaithersburg, MD, October 30, 1996.
59. Lyon, R. E. and Walters, R. N., "A Microscale Combustion Calorimeter," Final Report DOT/FAA/ AR-01/117, February 2002.
60. M. Ramirez, R.N. Walters, E.P. Savitski, and R.E. Lyon, "Thermal Decomposition of Cyanate Ester Resins," DOT/FAA/AR-01/32, September 2002.

61. A. Tewarson, in *SFPE Handbook of Fire Protection Engineering*, 2nd Edition, Chapters 3-4, "Generation of Heat and Chemical Compounds in Fires," Society of Fire Protection Engineers, Boston, MA, 1995.
62. R.E. Lyon, "Heat Release Rate Calorimeter for Milligram Samples," U.S. Patent 6,464,391, October 15, 2002.
63. R.E. Lyon, and R.N. Walters, "Pyrolysis Combustion Flow Calorimetry," *J. Anal. Appl. Pyrolysis*, 71, 1, pp. 27–46, 2004.
64. ASTM Standard E 2008, Test Method for Volatility Rate by Thermogravimetry, ASTM International, West Conshohocken, PA, 1999.
65. Standard E 1641, Test Method for Decomposition Kinetics by Thermogravimetry, ASTM International, West Conshohocken, PA, 2012.
66. R.E. Lyon, and R.N. Walters, "Heat Release Capacity: A Molecular Level Fire Response Parameter," *Proceedings of the 7th International Symposium on Fire Safety Science*, Intl. Assoc. for Fire Safety Science, Worcester, MA, pp. 1167–1168, 2003.
67. D.W. Van Krevelen, "Some Basic Aspects of Flame Resistance of Polymeric Materials," *Polymer*, 16, pp. 615–620, 1975.
68. A. Schoemann, P.R. Westmoreland, H. Zhang, R.J. Farris, R.N. Walters, and R.E. Lyon, "A Pyrolysis/GC-MS Method for Characterizing Flammability and Thermal Decomposition of Polymers," *Proceedings 4th Joint Meeting of the U.S. Sections of the Combustion Institute*, Philadelphia, PA, March 21-23, 2005.
69. P.R. Westmoreland, T. Inguilzian, and K. Rotem, "Flammability Kinetics from TGA/DSC/GCMS, Microcalorimetry and Computational Quantum Chemistry," *Thermochimica Acta* 67, pp. 401–405, 2001.
70. ASTM Standard D 2015, Test Method for Gross Calorific Value of Coal and Coke by the Adiabatic Bomb Calorimeter, ASTM International, West Conshohocken, PA, 2000.
71. Standard Test Method for Determining Flammability Characteristics of Plastics and Other Solid Materials Using Microscale Combustion Calorimetry, ASTM D 7309-07, American Society for Testing and Materials (International), West Conshohocken, PA, 2007.
72. R.E. Lyon and M.L. Janssens, "Polymer Flammability," *Encyclopedia of Polymer Science & Engineering* (on-line edition), John Wiley & Sons, New York, NY, October 2005.

73. R.E. Lyon, "Piloted Ignition of Combustible Solids," in Society for the Advancement of Materials and Process Engineering SAMPE International Conference, Long Beach, CA, May 2–5, 2005.
74. S.I. Stoliarov, Q. Williams, S. Crowley, R.N. Walters, and R.E. Lyon, "Analysis of Flammability of Brominated Epoxies," Presented at the 15th Annual BCC Conference on Flame Retardancy of Polymeric Materials, Stamford, CT, June 7–9, 2004.
75. A. Tewarson, J.L. Lee, and R.F. Pion, "The Influence of Oxygen Concentration on Fuel Parameters for Fire Modelling, Eighteenth Symposium (International) on Combustion," The Combustion Institute, Pittsburgh, PA, pp. 563-570, 1981
76. M. E. Brown (ed.), Handbook of Thermal Analysis and Calorimetry, Elsevier: Amsterdam, 1, 1998.
77. T. Hatakeyama and F. X. Quinn, Thermal Analysis. Fundamentals and Applications to Polymer Science, John Wiley & Sons: Chichester, England, 1999.
78. R.P. Hunter, Automated Process Control Systems. Concepts and Hardware, Prentice-Hall: Englewood Cliffs, NJ, 1978.
79. R.E. Lyon, R.N. Walters, S.I. Stoliarov, Journal of ASTM International, 3, 2006.
80. R.E. Lyon, Heat Release Kinetics, Fire & Materials, 24, 4, pp. 179-186, 2000.
81. Title 14 of the Code of Federal Regulations (CFR), Chapter 1, Federal Aviation Administration, Department of Transportation, Part 25, Airworthiness Standards: Transport Category Airplanes.
82. R.E. Lyon, Fire & Flammability, Fire Risk & Hazard Assessment Research Symposium, Fire Protection Research Foundation, Baltimore, MD, July 9-11, pp. 22-32, 2003.
83. J. Brandrup, E.H. Immergut, E.A. Grulke, A. Abe, D.R. Bloch, editors. Polymer Handbook. 4th ed. New York: John Wiley and Sons; 1999.
84. Frederick WJ, Mentzer CC. Determination of heats of volatilization for polymers by differential scanning calorimetry. Journal of Applied Polymer Science, 19, pp. 179-804, 1975.
85. Tewarson A, Pion RF. Flammability of plastics e I. Burning intensity. Combustion and Flame, 26, pp. 85-103, 1976.
86. Harper CA, editor. Modern Plastics Handbook. New York: McGraw-Hill; 2000.
87. ASTM D 790-95a, "Standard Test Methods for Flexural Properties of Unreinforced and Reinforced Plastics and Electrical Insulating Materials," American Society of Testing and Materials, Philadelphia, PA, 1996.

88. MIL-STD-2031, "Fire and Toxicity Test Methods and Qualification Procedure for Composite Materials Systems Used in Hull, Machinery, and Structural Applications Inside Naval Submarines," 1991.
89. A.L. Rusanov, "Condensation Polymers Based on Chloral and Its Derivatives," *Prog. Polym. Sci.*, 19, pp. 589-662, Elsevier Science Ltd., Great Britain, 1994.
90. "Epoxy Resin Manual," Industry Edition, Dow Chemical, 1988.
91. S.I. Stoliarov, R.E. Lyon, Thermo-Kinetic Model of Burning, Federal Aviation Administration Technical Note, DOT/FAA/AR-TN08/17, 2008.
92. S.I. Stoliarov, R.E. Lyon, "Thermo-Kinetic Model Of Burning For Pyrolyzing Materials," *Proceedings of the Ninth International Symposium on Fire Safety Science*, pp. 1141–1152, 2009.
93. S.I. Stoliarov, N. Safronava, R.E. Lyon, "The Effect Of Variation In Polymer Properties On The Rate Of Burning," *Fire and Materials*, 33, pp. 257–271, 2009.
94. S.I. Stoliarov, S. Crowley, R.E. Lyon, G.T. Linteris, "Prediction Of The Burning Rates Of Non-Charring Polymers," *Combustion and Flame*, 156, pp. 1068–1083, 2009

APPENDIX E

RICHARD WALTERS CONTRIBUTION TO EACH MANUSCRIPT TO FORM THE  
PhD THESIS (by Publication)

1. **R.N. Walters**, R.E. Lyon and S.M. Hackett, "Heats of Combustion of High Temperature Polymers," *Fire and Materials Journal*, 24, pp. 245-252, 2000.

I did 50% of the experimental work using the oxygen bomb calorimeter, analyzing the data, performed many of the calculations, and provided significant contribution to manuscript write up. Stacey Hackett did the other 50% of the experimental work. Edward Savitski showed us how to do the thermochemical calculations and Richard Lyon wrote the bulk of the manuscript.

2. R.E. Lyon, L.M. Castelli and **R.N. Walters**, "A Fire-Resistant Epoxy," DOT/FAA/AR-01/53, FAA Technical Report August 2001.

I did 100% of the experimental work using the FT-IR, DSC, rheometer, and OSU calorimeter and 50% of the experimental work formulating samples using the MCC and TGA. I performed many of the calculations, assisted with analyzing the data, and provided significant contribution to manuscript write up. Richard Lyon wrote the bulk of the manuscript. Lauren Castelli did the other 50% of the formulation and experimental work and Sean Crowley and Michael Mazzoni did the LOI and UL94 testing.

3. R.E. Lyon and **R.N. Walters**, "A Microscale Combustion Calorimeter," FAA Technical Report, DOT/FAA/AR-01/117, 2002.

I did 100% of the experimental work building and using the MCC along with characterizing and optimizing the MCC components in the FAA labs. I also analyzed the data, performed many of the calculations, and provided significant contribution to manuscript write up. Taline Inguilizian, Huiqing Zhang, and Stanislav Stoliarov did additional work at the University of Massachusetts to validate the work done in the FAA labs. Richard Lyon derived the theory and wrote the bulk of the manuscript.

4. M. Ramirez, **R.N. Walters**, E.P. Savitski, and R.E. Lyon, "Thermal Decomposition of Cyanate Ester Resins," *Journal of Polymer Degradation and Stability*, 78, 73-82, 2002.

I did a most of the experimental work preparing samples, using the FT-IR, DSC and TGA. I also provided a significant contribution to the manuscript data analysis and write up, prepared all of the figures for the report, and took it through to publication in the journal. Edward Savitski did some of the initial work characterizing the cyanate ester resins. Michael Ramirez performed FT-IR analysis, pyrolysis-GC-MS, and wrote the bulk of the report. Richard Lyon provided some minor editorial additions. David Esral performed char forming tendency calculations.

5. **R.N. Walters**, “Molar Group Contributions to the Heat of Combustion,” Fire and Materials Journal, 26, pp. 131-145, 2002.

I did 100% of the derivation of the theory and background research. The experimental work was done previously in MS 1 and obtained from the literature. I did >90% of the data analysis. Stanislav Stoliarov helped with the analysis by showing me the optimization routine in Excel. I wrote all (>95%) of the manuscript with some minor editorial changes by Richard Lyon.

6. **R.N. Walters** and R.E. Lyon, “Molar Group Contributions to Polymer Flammability,” Journal of Applied Polymer Science, 87, pp. 548-563, 2003.

I did 100% of the experimental work building and using the MCC. I derived the group contribution theory with some notation help from Richard Lyon. I did >90% of the data analysis. Stanislav Stoliarov helped with the analysis by performing some group contribution calculations in parallel to what I was doing and showing me the optimization routine in Excel. I wrote all (>85%) of the manuscript with some minor analysis and editorial additions by Richard Lyon.

7. **R.N. Walters** and R. E. Lyon, “Fire Resistant Cyanate Ester - Epoxy Blends,” Fire and Materials Journal, 27, pp. 183-194, 2003.

I did 100% of the experimental work, data analysis, and write up with guidance and minor editorial changes from Richard Lyon.

8. R. Lyon and **R. Walters**, “Pyrolysis Combustion Flow Calorimetry,” Journal of Applied Pyrolysis, 71, pp. 27-46, 2004.

I did 100% of the experimental work including equipment construction and characterization. I also analyzed the data, performed many of the calculations, and provided significant contribution to manuscript write up. Taline Inguilizian, Huiqing Zhang, and Stanislav Stoliarov did additional work at the University of Massachusetts to validate the work done in the FAA labs. Richard Lyon derived the theory and wrote the bulk of the manuscript.

9. R.E. Lyon, **R.N. Walters**, and S. Gandhi, "Combustibility of Cyanate Ester Resins," *Fire and Materials Journal*, 30, pp. 89-106, 2006.

I performed 100% of the cone and MCC testing. I performed the data analysis and prepared the figures for the manuscript and assisted in the write up. Sanjeev Gandhi oversaw the cone testing and provided a significant contribution to the manuscript write up. Sean Crowley assisted with bomb calorimeter testing. Richard Lyon derived the theory and wrote the bulk of the manuscript.

10. R.E. Lyon, **R.N. Walters**, and S.I. Stoliarov, "A Thermal Analysis Method for Measuring Polymer Flammability", *Journal of ASTM International*, 3, 4, 2006.

I performed most of the most of the testing and data analysis for this manuscript. Lauren Castelli and Qadir Williams provided data from the 2nd generation MCC. Richard Lyon derived the theory and wrote the bulk of the manuscript.

11. R.E. Lyon, **R.N. Walters** and S.I. Stoliarov, "Screening Flame Retardants for Plastics Using Microscale Combustion Calorimetry," *Polymer Engineering & Science*, 47, 10, pp. 1501-1510, 2007.

I did the experimental work using the MCC and cone calorimeter previously described in other manuscripts. Richard Lyon wrote the bulk of the manuscript with contributions from me and Stanislav Stoliarov.

12. S.I. Stoliarov, **R.N. Walters** and R.E. Lyon, "A Method for Constant-Rate Heating of Milligram Sized Samples," *Journal of Thermal Analysis and Calorimetry*, 89, 2, pp. 367-371, 2007.

I did 100% of the experimental work performed at the FAA for this manuscript. I also constructed the experimental apparatus and performed some of the analysis. Marc Nyden and Richard Harris from NIST performed additional TGA experiments to compliment our research. Stanislav Stoliarov derived the theory and wrote the bulk of the manuscript with minor editorial additions from me and Richard Lyon.

13. R.E. Lyon, **R.N. Walters** and S.I. Stoliarov, "Thermal Analysis of Flammability," *Journal of Thermal Analysis and Calorimetry*, 89, 2, pp. 441-448, 2007.

I performed 100% of the experimental work that was not obtained from the literature for this manuscript. Richard Lyon wrote the bulk of the manuscript with contributions from me and Stanislav Stoliarov.

14. S.I. Stoliarov and **R.N. Walters**, "Determination of Heats of Gasification of Polymers Using Differential Scanning Calorimetry," *Polymer Degradation and Stability Journal* 93, pp. 422-427, 2008.

I performed 100% of the experimental work for this manuscript. Stanislav Stoliarov derived the theory and collaborated on the method development and I performed all of the analysis. Stanislav Stoliarov wrote the bulk of the manuscript with minor editorial additions from me.

15. **Richard N. Walters** and Richard E. Lyon, "Flammability of Polymer Composites," FAA Report DOT/FAA/AR-08/18 May 2008.

I did 100% of the experimental work, data analysis, and write up with guidance and minor editorial changes from Richard Lyon.

16. S.I. Stoliarov, S. Crowley, **R.N. Walters** and R.E. Lyon, "Prediction of the Burning Rate of Charring Polymers," *Combustion and Flame*, 157, 11, pp. 2024-2034, 2010.

I performed 100% of the TGA, DSC and MCC experiments and analysis and assisted Sean Crowley with the cone calorimeter testing. Stanislav Stoliarov derived the theory

and wrote the bulk of the manuscript. Myself and Richard Lyon provided minor editorial additions.

APPENDIX F

BACKGROUND / LITERATURE REVIEW

Some of the early work that has been done to characterize materials for flammability is presented here. The physical test methods along with the theoretical assumptions are discussed. The extrapolation of technology and coupling of the previous works, along with more development, provided the basis for the present embodiment of the microscale combustion calorimeter.

Over the past few decades several small (milligram) scale flammability tests that try to correlate fire performance for organic materials have been developed. Thermogravimetric techniques have been attempted [1] with some success. Onset of decomposition, peak mass loss temperature, and char yields are derived from these tests. Although these properties are important for characterizing the flammability of materials, thermogravimetry results by themselves are not enough to predict the burning behavior of materials. Oxygen bomb calorimetry [2] can be coupled with mass loss rates to approximate the heat release of materials but that does not take into account differing composition of the decomposition products throughout transient heating, or the incomplete combustion occurring in real fires.

Oxygen consumption calorimetry has been useful for characterizing the burning rate of organic materials (ASTM oxygen bomb calorimeter standard methods; D240, D4809, D5865, D1989, D5468, E711 etc.). It was discovered that there is a constant amount of heat released per unit of oxygen consumed [3]. This value was derived from sets of materials with known composition and the total heat released as measured in the oxygen bomb calorimeter. This theory has been examined for purely hydrocarbon materials as well as materials containing hetero-atoms such as oxygen, sulfur, phosphorous, nitrogen, silicon, and halogens, etc. The value has been determined to be 13.1 kJ per gram of oxygen consumed [4,5]. Although the value varies slightly for materials of varying composition, this number is a good approximation of heat when the composition of a fuel is unknown. This value has been the enabling factor for the development of several of fire and flammability test methodologies and equipment [6]. In particular, it allows real fire conditions to be simulated with approximately natural ventilation - a very different scenario to the 25 atmospheres of pure oxygen in a bomb calorimeter.

Other milligram sized tests have been developed using controlled heating and evolved gas analysis. An early way of looking at the effectiveness of flame retardants utilized a

thermal evolution analyzer [7]. In this method, samples were degraded and the volatilized decomposition products were run through a flame ionization detector to determine total carbon, which was proportional to the total fuel value of a sample. Susott et al. developed a pyrolytic method to measure the heat of combustion of forest products [8]. A total heat release was measured by the amount of oxygen consumed using a reaction coulometer. This method yielded qualitative dynamic data and gave quantitative total heats of combustion to within 4%. Gracik et al. developed a thermogravimetric technique that calculated heat release rates from CO and CO<sub>2</sub> measurements using infrared sensors [9]. It was shown that there was a correlation between thermogravimetric data, specifically char values, and oxygen index [1]. These methods are lacking as flammability tests because they do not provide a dynamic measure of a heat release rate. The fuel generation rate is observed but not addressed - only the integrated values of total heat released are determined.

A flow calorimeter was developed [10] where a combustible fuel gas was metered into a controlled air stream. The mixture was then run through a high temperature catalytic reactor where the fuel gases were completely oxidized. The amount of oxygen consumed in the reaction was measured. Correlations were made between the calorific value of the fuel and the amount of oxygen required to burn the fuel. A high temperature catalytic reaction is preferred over a flaming combustion reaction because the latter is not as efficient and there is a possibility of incomplete combustion products remaining. Complete combustion is necessary to provide the total possible fuel value of a material which is representative of its maximum potential fire threat.

A multi-instrument technique, thermogravimetric analysis / differential scanning calorimetry - gas chromatography – mass spectrometry (TGA/DSC-GC-MS) has been used to measure the heat release rate of small samples [11]. The pyrolyzer in these experiments, a thermogravimetric analyzer, was used to degrade samples and measure the fuel generation rate. The gas chromatograph separated the evolved species and the mass spectrometer identified and quantified them. The heat of combustion of the evolved species was then determined from the literature and summed. This information, coupled with the mass loss rate data, was used to generate a heat release rate for polymeric materials. Reproducible, quantitative dynamic heat release rates were generated from these experiments. This has been used as an independent method

for validating the results from the microscale combustion calorimeter but is not practical for running routine analyses on materials.

There are many bench scale laboratory fire tests [6,12,13]. These tests are often qualitative in nature and are dependent on the sample geometry. Larger bench scale tests are available that utilize oxygen consumption calorimetry. These tests require a large amount of sample and are expensive to operate. The cone calorimeter is one such bench scale calorimeter. This test was developed at the National Institute of Standards and Technology (NIST) [14]. In practice a sample is placed under a radiant heat flux, which is used to degrade the sample in air, or other environments [15]. The volatilized sample is ignited by a spark igniter when the fuel to air ratio is sufficient to sustain combustion. In general, the sample then burns at a rate that is proportional to the incident heat flux. Many factors can influence this proportionality, such as sample composition, additives, charring, etc.. Also, at high heat fluxes this relationship becomes non-linear. Oxygen concentration along with CO and CO<sub>2</sub> concentrations are measured. In addition, the mass loss rate and smoke generation rate are measured.

Originally, a goal was to create a test that provided information like that of the cone calorimeter. An objective of this research was to develop a technique that could provide meaningful data using oxygen consumption calorimetry from a milligram sized sample. This effort was undertaken to develop new fire-resistant materials in a cost effective manner by enabling material screening early in their development, since large amounts of such samples are not usually available for analysis. In the end, a test that provides data that is more meaningful than the cone calorimeter was created. This was achieved by uncoupling the physical properties of the samples and providing measures of flammability that are material properties.

Materials that are inherently fire-resistant have this material property rooted in their chemical structure. Group additivity methods have been used to calculate material properties from empirical correlations derived from the molecular structures of materials [16,17,18]. This theory can be applied to flammability properties. Van Krevelen derived relationships for a multitude of polymer properties [16]. Of particular interest in the field of flammability are the predictive and group additivity methods for heat capacity, enthalpy, glass transition, crystalline melting, thermal conductivity, thermal degradation, and char formation. These methods are useful for estimating

properties of new materials for modelling when materials are not available for testing. Also, this work provides the foundation for group additivity methods for predicting other flammability properties of polymers, such as the heat of combustion and flammability [19,20]. The relationship of structure to material properties aids the design of new materials. Theoretical values of interest can be estimated before the material is even synthesized. This approach can save on development costs by eliminating poor candidates when synthesizing families of new materials.

In summary, the development of the microscale combustion calorimeter was facilitated by the previous works, as described above, and the derivation of the theory that relates it to other fire tests and flammability properties. [21]. The evolution of the equipment, along with the data, created a new measure of flammability that is a material property. This material property measurement will aid in the understanding of flammability and fire scenarios by providing a value that is not coupled with the physical attributes of a specimen.

1. T.D. Gracik and G.L. Long, "Prediction of Thermoplastic Flammability by Thermogravimetry," *Thermochimica Acta*, 212, pp. 163-170, 1992.
2. ASTM D2382-88: Standard Test Method for Heat of Combustion of Hydrocarbon Fuels by Bomb Calorimeter (High Precision Method), *ASTM Fire Test Standards*, 3rd Edition, pp. 230-238, American Society for Testing of Materials, Philadelphia, PA, 1990.
3. W.M. Thornton, *Philosophical Magazine*, 33, 196, 1917.
4. C. Huggett, "Estimation of Rate of Heat Release by Means of Oxygen Consumption Measurements," *Fire and Materials*, 4, 2, pp. 61, 1980.
5. R.N. Walters, S.M. Hackett, and R.E. Lyon, "Heats of Combustion of High-Temperature Polymers," *Fire and Materials*, 24, pp. 245-252, 2000.
6. V. Babrauskas, "From Bunsen Burner to Heat Release Rate Calorimeter," in *Heat Release in Fires*, V. Babrauskas and S. Grayson, Eds., Elsevier Applied Science, New York, pp. 7- 29, 1992.
7. E.W. Kifer and L.H. Leiner, "Thermal Evolution Analysis of Some Organic Materials, Analytical Calorimetry," Plenum Press, NY, 1974.
8. R.A. Susott, F. Shafizadeh, and T.W. Aanerud, "A Quantitative Thermal Analysis Technique for Combustible Gas Detection," *J. Fire & Flammability*, 10, pp. 94-104, 1979.

9. T.D. Gracik, G.L. Long, U.A.K. Sorathia and H.E. Douglas, "A Novel Thermogravimetric Technique for Determining Flammability Characteristics of Polymeric Materials," *Thermochimica Acta*, 212, pp. 209-217, 1992.
10. T.L. Bohl, R.E. Pockock, S.L. Zimmerlin, Calorimeter, United States Patent, 4,433,922, Feb. 28, 1984.
11. T.V. Inguilizian, "Correlating Polymer Flammability Using Measured Pyrolysis Kinetics," Master of Science Thesis, University of Massachusetts, Amherst, January, 1999.
12. M.L. Janssens, "Calorimetry," in *SFPE Handbook of Fire Protection Engineering*, 2nd Edition, Chapter 3.2, Society of Fire Protection Engineers, Boston, MA, 1995.
13. R.E. Lyon and M.L. Janssens, Polymer Flammability, FAA Report DOT/FAA/AR-05/14, May 2005.
14. V. Babrauskas, "Development of the Cone Calorimeter—A Bench-Scale Heat Release Rate Apparatus Based on Oxygen Consumption," *Fire and Materials*, 8, pp. 81–95, 1984.
15. V. Babrauskas, "The Cone Calorimeter," in *Heat Release in Fires*, V. Babrauskas and S. Grayson, Eds., Elsevier Applied Science, New York, pp. 61-91, 1992.
16. D.W. Van Krevelen, *Properties of Polymers*, 3rd edition, Elsevier, Amsterdam, 1990.
17. J. Bicerano, *Prediction of Polymer Properties*, 2nd edition, Marcel Dekker, Inc., New York, NY, 1996.
18. S.W. Benson, *Thermochemical Kinetics, Methods for the Estimation of Thermochemical Data and Rate Parameters*, John Wiley, New York, NY, 1968.
19. R.N. Walters, "Molar Group Contributions to the Heat of Combustion," *Fire & Materials Journal*, 26, pp. 131-145, 2002.
20. R.N. Walters and R.E. Lyon, "Molar Group Contributions to Polymer Flammability," *Journal of Applied Polymer Science*, 87, pp. 548-563, 2003.
21. R.E. Lyon, R.N. Walters and S.I. Stoliarov, "Thermal Analysis of Flammability," *Journal of Thermal Analysis and Calorimetry*, 89, 2, pp. 441-448, 2007.

## PUBLISHED WORKS